

IRIDIUM CATALYZED C-H BORYLATION: IMPROVED SELECTIVITY
THROUGH CATALYST DESIGN AND THE VALUE OF SPECTROSCOPY UNDER
CATALYTICALLY RELEVANT CONDITION

By

Behnaz Ghaffari

A DISSERTATION

Submitted to
Michigan State University
in partial fulfillment of the requirements
for the degree of

Chemistry – Doctor of Philosophy

2016

ABSTRACT

IRIDIUM CATALYZED C-H BORYLATION: IMPROVED SELECTIVITY THROUGH CATALYST DESIGN AND THE VALUE OF SPECTROSCOPY UNDER CATALYTICALLY RELEVANT CONDITION

By

Behnaz Ghaffari

In homogeneous transition metal catalysis, the precatalyst usually needs to undergo a series of rearrangements or changes in the coordination sphere to form the active catalyst, which is responsible for the desired transformation. Isolation of these active intermediates along with mechanistic studies would provide greater insight to how the transformation works and would be extremely beneficial for modifying and designing a new catalyst/ligand system.

In Ir-catalyzed C-H activation/borylation, 5-coordinate iridium boryl species are reported to be the active catalytic species. Despite the initial report for utilizing phosphine ligands in thermal catalytic aromatic C-H borylation, bidentate nitrogen donor ligands have been used more frequently due to their higher reactivity.¹ To analyze the origin of this difference, we studied a previously reported 5-coordinate iridium trisboryl complex stabilized by a bidentate phosphine ligand, which reacts directly with sp^2 C-H bonds, providing a rare opportunity for examining the fundamental step in C-H borylation. Previously, this complex had been shown to react stoichiometrically at room temperature, but under catalytic conditions elevated temperatures were required.

We have found that the 16 electron 5-coordinate trisboryl complex and HBpin are in equilibrium with generating a six-coordinate borylene complex, which is the dominant species at the outset of the reaction. As borylation commences during the catalytic

reaction, the H₂ produced from C–H activation converts the borylene to a series of intermediates. These intermediates represent multiple resting states of C–H borylation catalyst, which operate in parallel catalytic cycles. The complexes were isolated and characterized by ³¹P and ¹H NMR, and X-ray crystallography, making this the most fully characterized catalytic system for C–H borylation described to date. Insights from these studies are being used to design new bidentate catalysts for sp² and sp³ C–H functionalizations.

In the second part of this dissertation, ortho directed C–H borylation of aromatic compounds will be discussed. In our novel approach without need of installation and removal of directing or protecting group, borylation of benzoates, benzamides, ketones, anisoles, and phenyl pyridines occurs ortho to the functional group. In this systems, 14-electron intermediates likely mediate these processes. We have shown that low-coordinate Ir precatalysts can be obtained by using donor ligands that incorporate pendant silanes. These species are active for directed C–H borylations with a range of substrates. We will discuss mechanisms by which these catalysts operate, present structures that pertain to catalysis, and discuss substrate scope in the context of other methodologies.

To
My family
& those who dedicated their lives to peace and education

“Peace cannot be kept by force; it can only be achieved by understanding.”
~ **Albert Einstein**

ACKNOWLEDGMENTS

I would like to express my sincere and foremost appreciation to my advisor Professor Mitch Smith; I was delighted to work on fascinating chemistry that he discovered in his group; I was fortunate to learn from such a smart, knowledgeable and great scientist. Without his guidance and resolute help, this dissertation would not have been conceivable. I could never thank him enough for what he has done for me, and I'm always indebted to him.

I also like to offer a very genuine appreciation to Professor Rob Maleczka for his important suggestions and remarks during boron collaboration meetings, for his endless support throughout my doctoral studies, and serving as my committee member.

Special and earnest thanks go to my other committee members, Professor Aaron Odom and Professor Thomas Hamann, for all their helpful guidance during my time at Michigan State. I can't thank all my committee members enough for accommodating my defense within a very short notice.

I'm very thankful to professors Gary Blanchard, Babak Borhan and Late professor Greg Baker and all the admission committee that gave me the opportunity to come to Michigan State for graduate study.

In addition, thank you to Dr. Richard Staples and Dr. Daniel Holmes for their valuable help with X-Ray crystallography and NMR studies. Special thanks go to Drs. Shane Krska and Peter Maligres from Merck for their great discussion on MSU-Merck collaborative projects.

I owe many thanks to all my lab mates; Sean, Phil, John, Marie, Hong-tu, Buddha, Don, Kristin, Yu-Ling, Dmitry, Tim, Olivia, Po-Jen, Reza, Ryan and Tyler; I could not have wished for better lab mates than you, I was fortunate to work with great pool of scientists and learn a great deal from everyone. Yu-Ling and Olivia, I appreciate all your help with editing my dissertation, you made my last week of graduate school more pleasant.

Thanks to Hao, Damith, Suzi, Fangyi, Aaron, Ruwi, Gayanthi, and Jonathan for all valuable discussion during the Maleczka-Smith group meeting. I also would like to thank all my friends in Odom, Borhan and Hamann's group for their help and support.

This voyage would not have been possible without the support of my family, thank you Mom and Dad, for cheering me in all of my pursuits and inspiring me to follow my dreams. I always knew that you believed in me and desired the best for me. Special thanks to my brother Omid, my sister Farnaz, my sister-in-law Azadeh and my nephew Artin, your love, support and encouragement was worth more than I can state on paper.

TABLE OF CONTENTS

LIST OF TABLES	ix
LIST OF FIGURES	x
LIST OF ABBREVIATIONS AND SYMBOLS	xvi
CHAPTER ONE – INTRODUCTION	1
<i>General Introduction to Aromatic Functionalization</i>	<i>1</i>
<i>Transition Metal C–H Functionalization.....</i>	<i>5</i>
<i>Boration of Hydrocarbons</i>	<i>9</i>
<i>Regio and Chemoselectivity of Transition Metal CHB Catalysts</i>	<i>14</i>
<i>Regioselectivity Origins in Ir-catalyzed CHBs</i>	<i>18</i>
<i>Electronic Effects in Ir-catalyzed CHBs.</i>	<i>19</i>
<i>Chelate-Directed, ortho selective Ir-catalyzed CHBs.....</i>	<i>20</i>
<i>Relay-Directed, ortho selective, Ir-catalyzed CHBs.</i>	<i>21</i>
<i>Hydrogen-bond directed, ortho selective Ir-catalyzed CHBs.</i>	<i>22</i>
<i>Other ortho-selective CHBs.</i>	<i>22</i>
<i>Meta-Selective CHBs.....</i>	<i>23</i>
<i>Para-Selective CHBs.....</i>	<i>24</i>
REFERENCES.....	25
CHAPTER 2 – REVERSIBLE BORYLENE FORMATION FROM RING- OPENING OF PINACOLBORANE AND OTHER INTERMEDIATES GENERATED FROM 5-COORDINATE TRISBORYL COMPLEXES: IMPLICATIONS FOR CATALYTIC C-H BORYLATION	32
<i>Studies of 5-coordinate boryl catalysts.</i>	<i>32</i>
<i>Results</i>	<i>34</i>
<i>Discussion</i>	<i>45</i>
<i>Conclusions</i>	<i>52</i>
REFERENCES.....	53
CHAPTER 3 – SILYL PHOSPHORUS AND NITROGEN DONOR CHELATES FOR HOMOGENEOUS ORTHO BORYLATION	56
<i>Directed Aromatic Functionalization.....</i>	<i>56</i>
<i>Results</i>	<i>58</i>
<i>Conclusions</i>	<i>68</i>
REFERENCES.....	69
CHAPTER 4 – EXPERIMENTAL	72
<i>General Procedures</i>	<i>72</i>
<i>Analytical Methods.....</i>	<i>72</i>

<i>X-ray Crystallography Details</i>	72
<i>Computational Methods</i>	73
<i>Synthesis of compounds</i>	74
REFERENCES	110
APPENDICES	113
APPENDIX A, NMR Spectra	114
APPENDIX B, Crystal Data and Structure	173
APPENDIX C, Computational Results	178

LIST OF TABLES

<i>Table 1.</i> Comparison of catalyst efficiency for ortho-borylation	60
<i>Table 2.</i> Ortho-borylation of alkylbenzoates. ^a	61
<i>Table 3.</i> Borylations with 15 /[Ir(OMe)(cod)] ₂ catalyst	64
<i>Table 4.</i> Comparison of Silyl Ligands with Pendant P- and N-donors.....	67
<i>Table 5.</i> Comparing reactivity of Ir-catalyzed CHB using ligand 15 and 20	109

LIST OF FIGURES

<i>Figure 1.</i> Nitration of benzene.....	2
<i>Figure 2.</i> Electrophilic aromatic substitution (EAS)	2
<i>Figure 3.</i> Regioselectivities of EAS for disubstituted arene (ortho/para directors shown in blue and meta directors shown in red)	3
<i>Figure 4.</i> Synthesis of 3-bromo-5-chlorophenol	3
<i>Figure 5.</i> Early reports on DoM	4
<i>Figure 6.</i> Regioselectivity of DoM in presence of two directing groups	5
<i>Figure 7.</i> Synthesis of isolated C-H activated organometallic complex by Chatt and Davidson	6
<i>Figure 8.</i> Sterically directed C-H bond activation of aromatics by Ittel	7
<i>Figure 9.</i> Catalytic cyclization of 2,6-xylyl isocyanide.....	8
<i>Figure 10.</i> Meta selective, Rh-catalyzed silylation of <i>meta</i> -xylene.	9
<i>Figure 11.</i> Synthetic utility of arylboron compounds.....	10
<i>Figure 12.</i> Methods for synthesizing C-B bonds.....	12
<i>Figure 13.</i> Thermodynamic calculation of methane C-H bond borylation	12
<i>Figure 14.</i> First thermal catalytic borylation of benzene.....	13
<i>Figure 15.</i> Regio- and chemoselectivity of iridium and rhodium catalyzed borylation of aromatics	14
<i>Figure 16.</i> Iridium catalyzed CHB cycle reported by Smith and Maleczka	16
<i>Figure 17.</i> A proposed catalytic cycle for Ir-catalyzed CHB of arenes, heteroarenes, and alkanes.....	17
<i>Figure 18.</i> First attempt to quantify steric effect in Ir-catalyzed CHBs	18
<i>Figure 19.</i> Correlation between ΔH and aryl-group charge	19

<i>Figure 20.</i> Chelate directed ortho borylation of benzoate using bulky, electron deficient, mono dentate phosphine	20
<i>Figure 21.</i> Solid supported Iridium catalyst for ortho-directed borylation	21
<i>Figure 22.</i> Silyl-Directed, Iridium-Catalyzed ortho-Borylation of Arenes	22
<i>Figure 23.</i> Mechanism for outer-sphere ortho-borylation	22
<i>Figure 24.</i> Selective meta borylation by using a secondary interaction between ligand and the substrate	23
<i>Figure 25.</i> Directed meta C-H borylation by ion pair mechanism	24
<i>Figure 26.</i> Para selective C-H borylation by using the bulky ligand.....	24
<i>Figure 27.</i> Catalytic cycle for iridium catalyzed C-H borylation using bidentate ligand.	33
<i>Figure 28.</i> Proposed mechanism for borylene formation	34
<i>Figure 29.</i> ^{11}B NMR of compound 6 in benzene- d_6	35
<i>Figure 30.</i> Equilibrium between complex 6 with complex 5 and HBpin	36
<i>Figure 31.</i> X-ray structure for compound 8 with thermal ellipsoids calculated at 50% probability levels. The two independent molecules (8a and 8b) are shown with selected angles and distances	38
<i>Figure 32.</i> Calculated structures (M06//SDD/6-31G*) for 8a and 8b (red) overlaid with coordinates from their X-ray structures (blue). Calculated bond distances and angles correspond to the numbering in Figure 31	40
<i>Figure 33.</i> X-ray structure for compound 9 with thermal ellipsoids calculated at 50% probability levels. Hydride ligands are shown and other hydrogens are omitted for clarity. Selected experimental and computational metric parameters are given	41
<i>Figure 34.</i> The calculated structure (red, M06//SDD/6-31G*) is overlaid with crystallographic coordinates	42
<i>Figure 35.</i> X-ray structure for compound 10 with thermal ellipsoids calculated at 50% probability levels. Hydride ligands are shown and other hydrogens are omitted for clarity, selected experimental metric parameters are given	43
<i>Figure 36.</i> The calculated structure (red, M06//SDD/6-31G*) is overlaid with crystallographic coordinates. Selected computational metric parameters are given	44

<i>Figure 37.</i> $^{31}\text{P}\{1\text{H}\}$ NMR spectra showing catalysts evolution during the reaction	44
<i>Figure 38.</i> Putative equilibria for hydride exchange in compound 8	46
<i>Figure 39.</i> ^1H NMR spectrum (500 MHz, toluene- d_8 , -5°C) of the hydride region for compound 10.....	48
<i>Figure 40.</i> Possible structures for compound 7	50
<i>Figure 41.</i> H_2 induced equilibria by H_2 addition to compound 5	50
<i>Figure 42.</i> Parallel catalytic cycles for C–H borylation	51
<i>Figure 43.</i> Chelate assisted mechanism for bulky, electron deficient monodentate phosphine	57
<i>Figure 44.</i> Ortho borylation of phenylpyridine using hemilabile ligand.....	57
<i>Figure 45.</i> General chelate assisted mechanism for homogenous borylation	58
<i>Figure 46.</i> Designing a bidentate, monoanionic ligand.....	58
<i>Figure 47.</i> Designing a bidentate, monoanionic ligand.....	59
<i>Figure 48.</i> Ligand dependent borylation regioselectivity	62
<i>Figure 49.</i> Crystal structure of compound 19 with H atoms omitted	66
<i>Figure 50.</i> Expansion of ^1H NMR in benzene- d_6 for calculation of equilibrium constant	75
<i>Figure 51.</i> Catalytic conversion of 2-methylthiophene with compound 5, using 0.5 equivalents of HBpin	77
<i>Figure 52.</i> Catalytic intermediates for borylation of 2-methylthiophene with compound 5, using 0.5 equivalents of HBpin.....	78
<i>Figure A 1.</i> $^{31}\text{P}\{1\text{H}\}$ NMR of reaction intermediates for catalytic borylation of 2-methylthiophene with compound 5, using 0.5 equivalents of HBpin in cyclohexane- d_{12}	114
<i>Figure A 2.</i> $^{31}\text{P}\{1\text{H}\}$ NMR spectra in cyclohexane- d_{12} at the end of catalytic borylation run of 2-methylthiophene with 0.5 equivalents of HBpin, mainly shows compound 10	115
<i>Figure A 3.</i> ^1H NMR spectra of hydride region in cyclohexane- d_{12} at the end of catalytic run of 2-methylthiophene with 0.5 equivalents of HBpin, mainly shows compound 10	116

<i>Figure A 4.</i> gCOSY spectrum of hydride region in cyclohexane- d_{12} at the end of catalytic run of 2-methylthiophene with 0.5 equivalents of HBpin, mainly shows compound 10	117
<i>Figure A 5.</i> ^1H - ^{31}P HMQC spectrum of hydride region in cyclohexane- d_{12} at the end of catalytic run of 2-methylthiophene with 0.5 equivalents of HBpin, mainly shows compound 10.....	118
<i>Figure A 6.</i> $^{31}\text{P}\{^1\text{H}\}$ NMR of reaction intermediates for early stage of catalytic conversion of 2-methylthiophene with compound 5, using 0.5 equivalents of HBpin...	119
<i>Figure A 7.</i> Hydride region in ^1H NMR spectra of reaction intermediates for early stage of catalytic borylation of 2-methylthiophene with compound 5, using 0.5 equivalents of HBpin in toluene- d_8	120
<i>Figure A 8.</i> ^{31}P NMR spectrum with selective decoupling of aliphatic protons for compound 7 at $-45\text{ }^\circ\text{C}$, ($J = 9.9\text{ Hz}$)	121
<i>Figure A 9.</i> ^{31}P NMR spectrum with selective decoupling of aliphatic protons for compound 9 ($J = 18.3\text{ Hz}$).....	122
<i>Figure A 10.</i> $^{31}\text{P}\{^1\text{H}\}$ NMR of reaction of H_2 with compound 5. 1) Initial spectrum at $-45\text{ }^\circ\text{C}$, 2) At $-15\text{ }^\circ\text{C}$ after 10 sec of shaking the tube, 3) At rt after 15 minutes of shaking the tube.....	123
<i>Figure A 11.</i> Hydride region in ^1H NMR spectra of reaction of H_2 with compound 5 1) Initial ^1H NMR at $-45\text{ }^\circ\text{C}$, 2) At $-15\text{ }^\circ\text{C}$ after 10 sec of shaking the tube, 3) At rt after 15 minutes of shaking the mixture.....	124
<i>Figure A 12.</i> Hydride region in ^1H NMR spectra of compound 10 in toluene d_8 at different temperatures	125
<i>Figure A 13.</i> $^{31}\text{P}\{^1\text{H}\}$ NMR spectra of compound 10 in toluene d_8 at different temperatures	126
<i>Figure A 14.</i> ^1H NMR spectra of thermolysis of compound 10, in toluene d_8 at different temperatures	126
<i>Figure A 15.</i> $^{31}\text{P}\{^1\text{H}\}$ NMR spectra of thermolysis of compound 10, in toluene d_8 at different temperatures	127
<i>Figure A 16.</i> ^1H NMR of compound 15.....	128
<i>Figure A 17.</i> ^{13}C NMR of compound 15.....	129
<i>Figure A 18.</i> ^{31}P NMR of compound 15	130

<i>Figure A 19.</i> ^1H NMR of compound 16b.....	131
<i>Figure A 20.</i> ^{13}C NMR of compound 16b.....	132
<i>Figure A 21.</i> ^1H NMR of compound 16e'	133
<i>Figure A 22.</i> ^{13}C NMR of compound 16e'	134
<i>Figure A 23.</i> ^1H NMR of compound 16f	135
<i>Figure A 24.</i> ^{13}C NMR of compound 16f	136
<i>Figure A 25.</i> ^1H NMR of compound 16i.....	137
<i>Figure A 26.</i> ^{13}C NMR of compound 16i	138
<i>Figure A 27.</i> ^{19}F NMR of compound 16i	139
<i>Figure A 28.</i> ^1H NMR of compound 16k'	140
<i>Figure A 29.</i> ^1H NMR of compound 16k'	141
<i>Figure A 30.</i> ^1H NMR of compound 16l.....	142
<i>Figure A 31.</i> ^{13}C NMR of compound 16l	143
<i>Figure A 32.</i> ^{19}F NMR of compound 16l.....	144
<i>Figure A 33.</i> ^1H NMR of compound 16n	145
<i>Figure A 34.</i> ^{13}C NMR of compound 16n.....	146
<i>Figure A 35.</i> ^1H NMR of compound 16o	147
<i>Figure A 36.</i> ^{13}C NMR of compound 16o.....	148
<i>Figure A 37.</i> ^{19}F NMR of compound 16o	149
<i>Figure A 38.</i> ^1H NMR of compound 18a.....	150
<i>Figure A 39.</i> ^{13}C NMR of compound 18a.....	151
<i>Figure A 40.</i> ^1H NMR of compound 18c	152
<i>Figure A 41.</i> ^{13}C NMR of compound 18c.....	153

<i>Figure A 42.</i> ^1H NMR of compound 18d.....	154
<i>Figure A 43.</i> ^1H NMR of compound 18f.....	155
<i>Figure A 44.</i> ^{13}C NMR of compound 18f	156
<i>Figure A 45.</i> ^1H NMR of compound 18g.....	157
<i>Figure A 46.</i> ^{13}C NMR of compound 18g.....	158
<i>Figure A 47.</i> ^1H NMR of compound 18i.....	159
<i>Figure A 48.</i> ^{13}C NMR of compound 18i	160
<i>Figure A 49.</i> gCOSY NMR of compound 18i	161
<i>Figure A 50.</i> Expansion of gCOSY NMR of compound 18i.....	162
<i>Figure A 51.</i> ^1H NMR of compound 18j'.....	163
<i>Figure A 52.</i> ^{13}C NMR of compound 18j'.....	164
<i>Figure A 53.</i> gCOSY NMR of compound 18j'	165
<i>Figure A 54.</i> Expansion of gCOSY NMR of compound 18j'	166
<i>Figure A 55.</i> ^1H NMR of compound 19.....	167
<i>Figure A 56.</i> ^{13}C NMR of compound 19.....	168
<i>Figure A 57.</i> ^{31}P NMR of compound 19	169
<i>Figure A 58.</i> ^1H NMR of compound 20.....	170
<i>Figure A 59.</i> ^1H NMR of compound 20.....	171
<i>Figure A 60.</i> ^1H NMR of compound 22a.....	172

LIST OF ABBREVIATIONS AND SYMBOLS

Å	Ångstrom
Ac	acetyl
BDE	bond dissociation energy
Bn	benzyl
Boc	butoxycarbonyl
BOX	2,2'-bisoxazoline
Bu	butyl
cat	catecholate
Cp	cyclopentadienyl
Cp*	pentamethylcyclopentadienyl
cod	1,5-cyclooctadiene
coe	cyclooctene
Cy	cyclohexyl
DMG	directed metallating group
dmpe	1,2-bis(dimethylphosphino)ethane
DoM	directed <i>ortho</i> metalation
dcpe	1,2-bis(dicyclohexylphosphino)ethane
dippe	1,2-bis(di- <i>iso</i> -propylphosphino)ethane
dmpe	1,2-bis(dimethylphosphino)ethane
dppe	1,2-bis(diphenylphosphino)ethane
dtbpy	4,4'-di(<i>tert</i> -butyl)-2,2'-bipyridine

E^+	electrophile
EAS	electrophilic aromatic substitution
EDG	electron donating group
EI	electron ionization
equiv	equivalents
ESI	electrospray ionization
Et	ethyl
η	hapticity, denotes how many contiguous atoms of a ligand bind to a metal
EWG	electron withdrawing group
FG	functional group
GC	gas chromatography
gCOSY	gradient-select correlated spectroscopy
HRMS	high-resolution mass spectrometry
Ind	indenyl
kcal mol^{-1}	kilocalorie per mole
κ	kappa, denotes how many, and which atoms of a ligand are binding
K_{eq}	equilibrium constant
$[M]$	metal
$[M]^+$	molecular ion peak
<i>m</i>	<i>meta</i>
Me	methyl
Mes	mesityl

mp	melting point
μ	mu, denotes bridging ligand
NAS	nucleophilic aromatic substitution
NMR	nuclear magnetic resonance
<i>o</i>	<i>ortho</i>
ORTEP	Oak Ridge Thermal Ellipsoid Plot Program
<i>p</i>	<i>para</i>
$P(\text{Ar}^{\text{F}})_3$	tris[3,5-bis(trifluoromethyl)phenyl]phosphine
Ph	phenyl
pin	pinacolate
pK_{a}	acid dissociation constant at logarithmic scale
ppm	parts per million
Pr	propyl
R	remaining attachments
RT	room temperature
sec-	secondary-
SMAP	silicon constrained monodentate phosphine
t-	tertiary-
$t_{1/2}$	half-life
THF	tetrahydrofuran
TNT	2,4,6-trinitrotoluene
TON	turnover number

CHAPTER ONE – INTRODUCTION

General Introduction to Aromatic Functionalization

Rapid development in science and technology over the past several decades has made aromatic hydrocarbons of high value and interest to modern society. Aromatic hydrocarbons are widely used in fuels, various biologically active molecules, agrochemicals and pharmaceuticals, and have also made countless appearances in polymeric materials.¹ Despite the need for a variety of aromatic hydrocarbons, the process of catalytic reforming is currently the major source of aromatic production, supplying raw aromatics including benzene, toluene and xylenes. Additional derivatization is necessary to substitute C-H bonds for other functional groups (FGs) to diversify these basic feedstocks for particular end use.²

The challenges with functionalizing hydrocarbons can be attributed to inherent properties, including their (i) low dipole moments (ii) high pK_a values of C-H bonds and (iii) small polarizabilities. Despite these challenges, chemists have been able to functionalize aromatic C-H bonds by several methods including (1) aromatic substitution (2) deprotonation and (3) transition metal C-H activation.

In 1825, Faraday performed the reaction of benzene with nitric acid (Figure 1).³ A decade later, Mitscherlich determined that nitrobenzene was the product of the reaction, initiating intense research in electrophilic aromatic substitution (EAS), which remains a powerful tool for arene functionalization.⁴

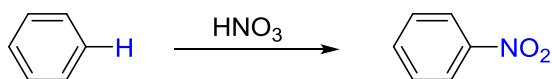


Figure 1. Nitration of benzene

The regioselectivity of these transformations is dictated by the electronic properties of the substituents on the ring. For example, electron donating groups like amine, alkoxides, or halogens result in ortho/para functionalization. Holleman named these substituents as ortho/para directors. A second group of substituents are electron withdrawing through resonance (e.g. NO_2 and $\text{C}(\text{O})\text{R}$) and deactivate the arene toward ortho/para substitutions, which results in meta selectivity. These are called meta directors (Figure 2).⁵

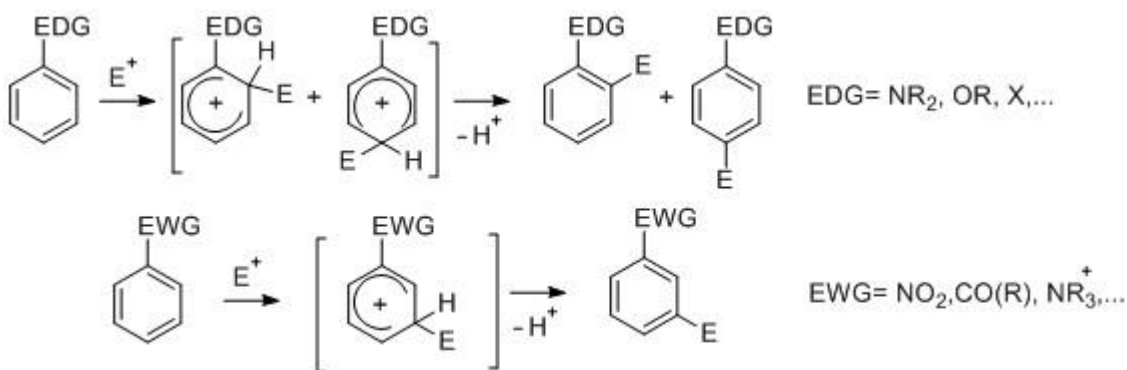


Figure 2. Electrophilic aromatic substitution (EAS)

There are nine regioisomeric permutations for a disubstituted benzene where the substituents are chemically inequivalent. Of all possible combinations of ortho/para and meta directors, only one of them (1,3-disubstituted benzene with both meta director groups) yields a single regioisomer according the selectivity rules for EAS (Figure 3).

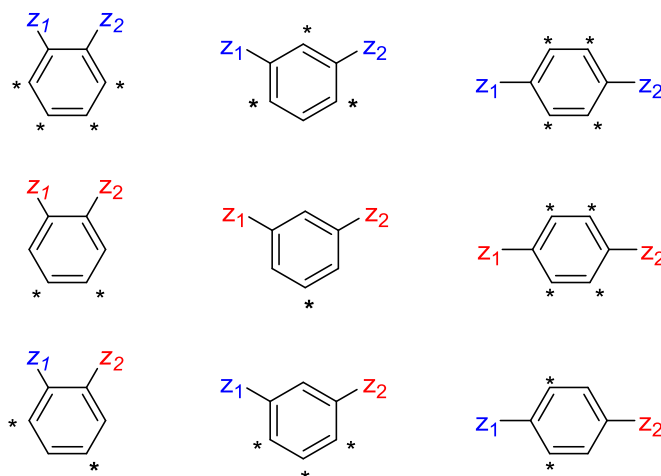


Figure 3. Regioselectivities of EAS for disubstituted arene (ortho/para directors shown in blue and meta directors shown in red)

For polysubstituted aromatics, the selectivities are influenced by combinations of electronic steric effects from all substituents. This makes the preparation of specific regioisomers a daunting task, especially for preparing compounds where meta regiochemistry of ortho/para directing groups is desired. This is illustrated by the preparation of 3-chloro-5-bromophenol using conventional organic chemistry in Figure 4.⁶

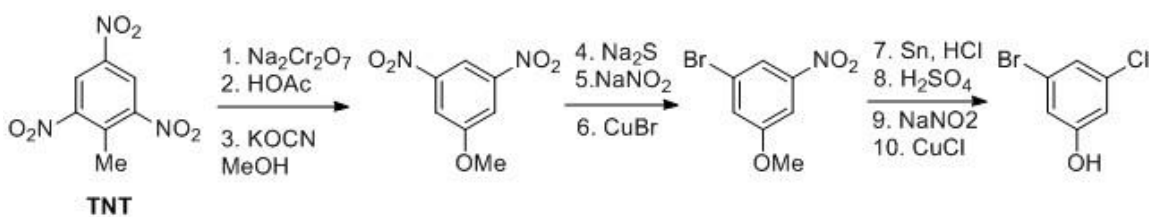


Figure 4. Synthesis of 3-bromo-5-chlorophenol

While aromatic C–H bonds are very weak acids (the pK_a of $C_6H_6 = 37$),⁷ they can be metalated in reactions with Group 1 and 2 metal alkyls and amides. The metalated arene intermediates can be converted to a range of arene products through reactions with electrophiles. Gilman in 1939, reported the deprotonation of a C–H bond in benzene ring

ortho to oxygen in dibenzofuran using lithium and sodium alkyls (Figure 5).⁸ Wittig, Pockels and Dröge were able to isolate *ortho*-methoxy-triphenylcarbinol (68% yield) by adding benzophenone to a mixture of phenyl lithium and anisole, and introduced the concept of the directing metalating group (DMG).⁹ This marked the beginning of directed ortho metalation (DoM), which is now a widely used synthetic method.^{10a-10c}

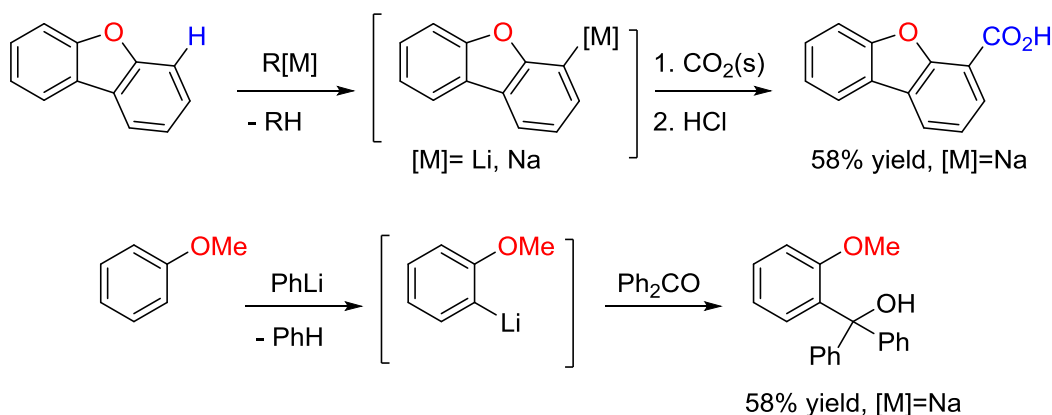


Figure 5. Early reports on DoM

Subsequent research on several classes of substrates revealed that DMGs such as amides, carbamates, protected alcohols and tertiary amines may interact with metal reagents through a heteroatom in the substituted arene and direct the metalation to the ortho position. The deprotonation site can be predicted by considering several factors, including the electronic properties of the ring and the strength of DMG. In cases where two meta-related DMGs share an ortho C–H site, the directing effect is reinforced. Thus, 1,3-DMG-substituted arenes exhibit high DoM selectivity for the 2-position. In contrast, the regioselectivity in 1,2 and 1,4-disubstituted arenes is determined by the relative power of the directing metalation group, which generates a competition for the base, yielding product mixtures (Figure 6).^{10a-10c}

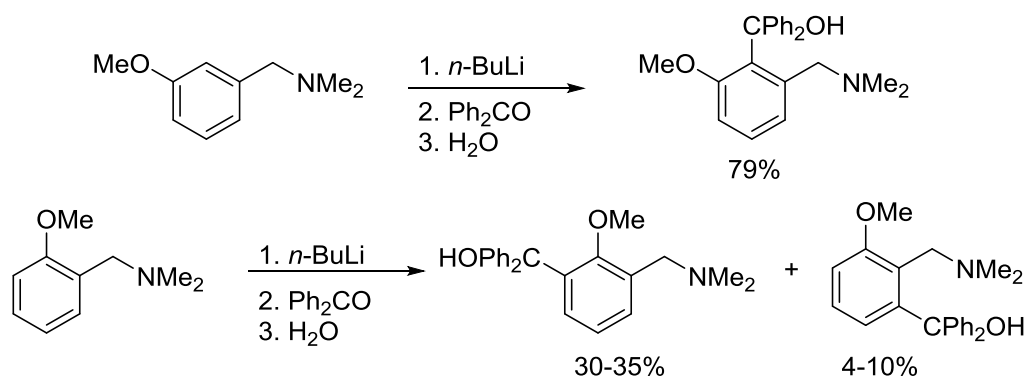


Figure 6. Regioselectivity of DoM in presence of two directing groups

While DoM is a very powerful tool for functionalizing many arenes, there are some drawbacks. These include (1) restricted FG tolerance, (2) a necessity for at least a stoichiometric amount of metal (This increases when FGs are more acidic than the C–H bonds present), and (3) a requirement of cryogenic temperatures. C–H functionalization of hydrocarbons using EAS and DoM prove that the low reactivity of arene C–H bonds toward functionalization can be overcome. Nevertheless, new complementary methods are particularly valuable for diversifying the chemist's synthetic toolbox.¹¹⁻¹³

Transition Metal C–H Functionalization

Due to the shortcomings of previous methods, the direct functionalization of hydrocarbons using organometallic precursors has established a great deal of interest.¹⁴⁻²² The general process can be summarized as converting a C–H bond to a C–FG bond with the aid of a transition metal.

The first example of what was later coined “C–H activation”, appeared in a paper by Chatt and Watson in 1962 that was titled, “Complexes of Zerovalent Transition Metals with the Ditertiary Phosphine, $\text{Me}_2\text{P}\cdot\text{CH}_2\cdot\text{CH}_2\cdot\text{PMe}_2$.”²³ Specifically, the authors stated that for the reduction of metal complexes of the formula $\text{M}(\text{dmpe})_2\text{Cl}_2$, “Sodium

naphthalenide is the most versatile reducing agent we have found but even it gave a hydrido-complex, apparently by taking hydrogen from the naphthalene, in the attempted preparation of $[M(\text{Me}_2\text{P}\cdot\text{CH}_2\cdot\text{CH}_2\cdot\text{PMe}_2)_2]$ ($M = \text{Ru}$ or Os). This reaction is still under investigation.”

The the first example where the product of C–H activation by a transition metal complex was definitely characterized involved the reaction of azobenzene and nickelocene. This was reported by Kleiman and Dubeck in 1963, and the reaction may have been the first example of chelate-directed C–H activation.²⁴

In 1965 Chatt and Davidson published a detailed study of their group’s preliminary observations from 1962.²⁵ When *cis*- $\text{Ru}(\text{dmpe})_2\text{Cl}_2$ was reduced with Na in the presence of benzene, naphthalene, anthracene and phenanthrene, *cis*- $\text{Ru}(\text{dmpe})_2(\text{H})(\text{aryl})$ (aryl = Ph, 2-naphtyl, 2-anthryl, and phenanthryl) compounds were isolated. They proposed that $\text{Ru}(\text{dmpe})_2$, generated from the reduction of *cis*- $\text{Ru}(\text{dmpe})_2\text{Cl}_2$, oxidatively added at the least sterically hindered C–H bond of the arene to give the final product (Figure 7).

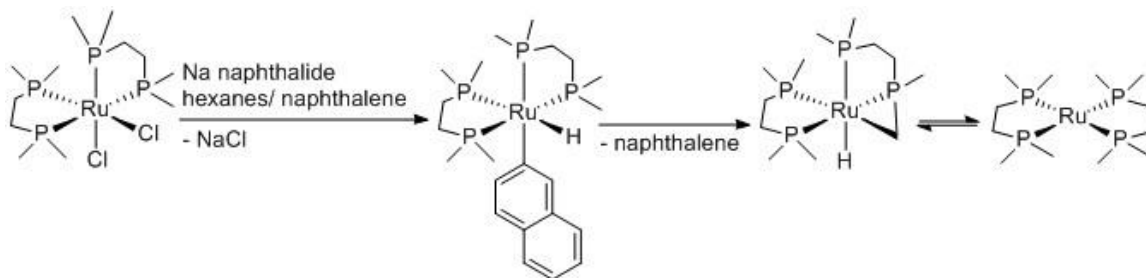


Figure 7. Synthesis of isolated C-H activated organometallic complex by Chatt and Davidson

More than a decade later, Ittel and coworkers reported that C-H oxidative addition for iron analogs of the Chatt *cis*-Ru(dmpe)₂(H)(aryl) compounds was reversible.²⁶ They illustrated that activation of the C-H bonds of toluene takes place with excellent regioselectivity at the least sterically-hindered position with an approximate statistical distribution of meta and *para*-tolyl isomers (Figure 8). This reaction was the earliest evidence that the regioselectivity of transition metal-mediated C-H activation of monosubstituted benzenes could be sterically controlled, and the thermodynamic product arises from reaction of the strongest C-H bonds. Chatt's and Ittel's chemistry illustrated the potential for transition metal C-H functionalizations to complement the selectivities of DoM and EAS.

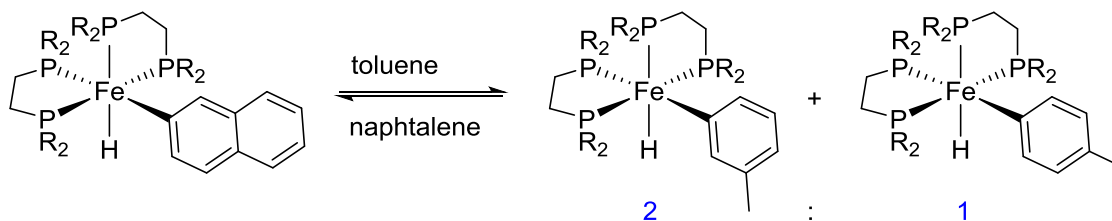


Figure 8. Sterically directed C-H bond activation of aromatics by Ittel

The subsequent functionalization of the M-C bonds that arose from C-H activation in a catalytically compatible fashion proved to be far more challenging than C-H bond activation itself. In 1986, Jones and co-workers reported the first viable catalytic C-H activation/functionalization reaction.²⁷ Using 20 mol% *cis*-Ru(dmpe)₂H₂, they were able to catalytically achieve the formation of 7-methylindole in > 90% yield from 2,6-xylyl isocyanide via an intramolecular cyclization (Figure 9).

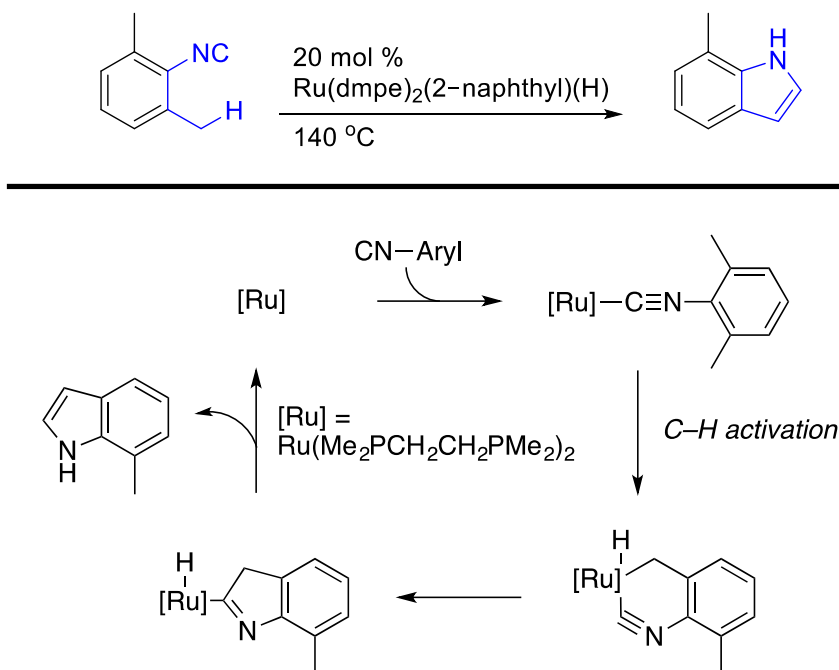


Figure 9. Catalytic cyclization of 2,6-xylyl isocyanide

Their proposed catalytic cycle begins with H_2 reductive elimination from *cis*- $\text{Ru}^{\text{II}}(\text{dmpe})_2\text{H}_2$ to generate 16-electron square planar $\text{Ru}^0(\text{dmpe})_2$. Isocyanide coordination, dissociation of one phosphine arm of dmpe, and C–H oxidative addition of a substrate methyl group affords the C–H activated intermediate. M–C functionalization occurs via formal 1,1-insertion of the isocyanide into the Ru–C bond. Tautomerization gives the *trans*-2-indolyl species, which isomerizes to the *cis*-2-indolyl isomer that forms the product via C–H reductive elimination, regenerating the active catalyst $\text{Ru}^0(\text{dmpe})_2$ to close the cycle.

Despite the numerous intramolecular C–H activation/ functionalization reactions that followed,²⁸ intermolecular C–H activation/functionalization were limited to isotopic labeling with deuterium gas. The first example to expand this narrow scope was reported in 1998 by Berry and co-workers.²⁹ Their dehydrogenative coupling of arenes and trialkylsilanes using a rhodium catalyst and a sacrificial olefin is shown Figure 10.

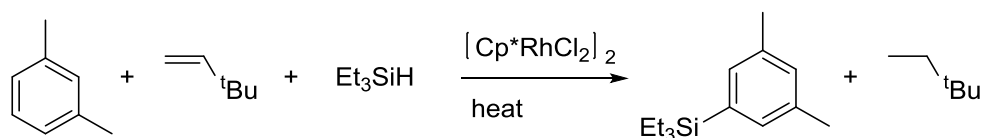


Figure 10. Meta selective, Rh-catalyzed silylation of *meta*-xylene.

This landmark paper showed that sterically selective stoichiometric C–H oxidative additions that had been discovered more than 30 years earlier could be harnessed for catalysis. In particular, meta functionalizations of 1,3-substituted benzenes were possible, as illustrated in Fig. 10. Likewise, *o*-xylene gave a single product. Monosubstituted benzenes gave mixtures of meta and para products. The fact that trifluoromethylbenzene and toluene gave nearly statistical 2:1 meta:para ratios is consistent with steric effects dominating electronic effects on regioselectivity. Their reaction had limited FG tolerance, which may be one reason that this seminal discovery has not been heavily cited.²⁹

Boration of Hydrocarbons

Organoboron reagents are used extensively in synthetic chemistry. These compounds can be easily converted to a broad range of FGs. They often serve as intermediates to access more complex compounds, including pharmaceuticals³⁰ and agrochemicals, as well as fluorescent molecules³¹ and molecular transporters.³²

The importance of organoborones may be best reflected by the fact that their synthesis and applications have been recognized twice by the Nobel committee. In 1979 H. C. Brown shared the Nobel Prize for his group’s efforts in “developing boron-containing compounds into important reagents in organic synthesis.”³³ Thirty-one years later, Akira Suzuki shared the 2010 Nobel Prize for utilizing organoboron compounds in

“palladium-catalyzed cross-couplings in organic synthesis.” Suzuki’s work focused on catalytic C–C bond formation, but aromatic and heteroaromatic boron reagents have much broader synthetic utility as shown in Figure 11, where B–C bonds in organoboron compounds enable C–X (X=halogen),^{34,35} C–O,³⁶⁻³⁹ C–N,^{37,40} C–CN,⁴¹ C–aryl,^{42,43} and other C–C⁴⁴⁻⁴⁶ bond formation. It bears mentioning that many of these transformations can be performed in one-pot.^{38,47}

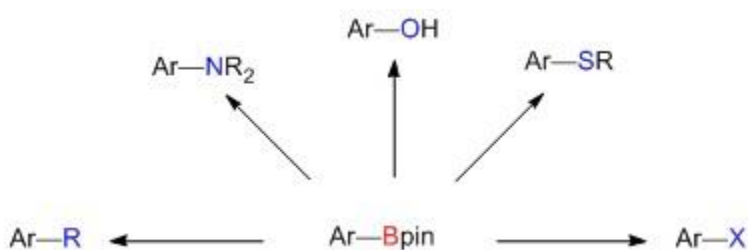


Figure 11. Synthetic utility of arylboron compounds.

Advances in transition metal catalyzed coupling reactions during the past few decades have been heavily represented by reactions between organoboron reagents with carbon electrophiles—the Suzuki coupling reaction being the flagship example.⁴⁸ Catalysts containing Pd^8 and Ni^9 have been particularly effective in making air stable organoboron compounds versatile reagents for the formation of carbon-carbon bonds. Currently, Zn, B, and Sn are commonly used metals in Pd-catalyzed cross-coupling.⁴⁹ The higher air and moisture stability of organoboron reagents relative to organozinc analogs makes the former compounds more popular candidates for coupling reactions. Additionally, the lower toxicity of organoboron compounds relative to organostannanes adds to their appeal.

There are several different routes for preparing of aryl boronic acids and esters. Aryl organoboron compounds are conventionally prepared from corresponding aryl

halides, which are converted to Grignard or organolithium intermediates. These are usually reacted with trialkyl borates and the boronic acids or esters are isolated after hydrolytic workup. These syntheses rely on the availability of aryl halides that are ideally prepared by direct halogenation of aromatic starting materials. The routes also require stoichiometric amounts of metals. From aromatic starting materials, at least two reaction vessels are required, and a stoichiometric metal halide waste stream is unavoidable. It should be noted that commercially available aryl halides are sometimes prepared via multistep processes. Thus, hidden steps from petrochemical or bio-based feedstocks can be associated with their use.

To avoid the requirement of stoichiometric metals, and their associated waste streams, approaches where arylboronates are prepared from aryl halides and borane reagents have been developed. The most commonly used embodiments use transition metal catalysts (e.g. Pd) (Figure 12).⁵⁰ In addition to halides, triflates, diazonium salts⁵¹ and amines⁵² can also be utilized as aryl electrophiles. While this route improves FG tolerance, its regiodiversity is tied to that of available aryl electrophiles. Direct conversion of C–H bond to C–B bonds is potentially the most atom economical approach to their synthesis. These processes offer the potential for accessing regioisomers EAS and DoM cannot. As described below, this can be accomplished with both stoichiometric and catalytic chemistry.^{53,54} More recently, there have been several reports on transition metal free C-B bond formation.⁵⁵⁻⁵⁷



Figure 12. Methods for synthesizing C-B bonds

Fundamental studies regarding the chemistry of transition metal boryl complexes began in the early 1990s. While information on metal-ligand bond energies is vital in understanding what is thermodynamically viable, there was not much data available for boranes and none for transition metal boryl complexes. In 1994, Rablen and Hartwig⁵⁸ reported calculations of B–H and B–C bond dissociation enthalpies to provide the first estimated M–boryl BDE. Using their computational data, and accepted values for C–H and H–H BDEs, the thermodynamic feasibility for the dehydrogenative coupling of C–H and B–H bonds was illustrated.⁵⁸ The reaction seen in Figure 13, is essentially thermoneutral, therefore this transformation is a potentially practical process that required a kinetic solution.⁵⁸⁻⁶⁰

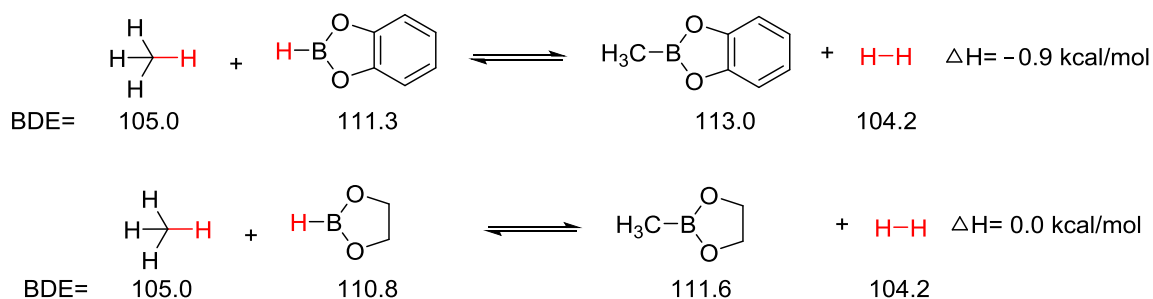


Figure 13. Thermodynamic calculation of methane C-H bond borylation

In 1993, Marder and coworkers synthesized $\text{Ir}(\eta^6\text{-C}_6\text{H}_5\text{Me})(\text{Bcat})_3$, (Bcat = catecholboryl), from $(\eta^5\text{-C}_9\text{H}_7)\text{Ir}(\text{cod})$, (cod = 1,4-cyclooctadiene).⁶¹ Inspection of the GC-MS chromatograms from the supporting information of their paper reveals two species with masses corresponding to $\text{C}_7\text{H}_7\text{Bcat}$ —the formula for toluene C–H borylated products. Four years later, Hartwig reported the first C–H activation/ borylation reactions of aromatics and aliphatic substrates using stoichiometric amounts of $\text{Cp}(\text{OC})_2\text{FeBcat}$, $(\text{OC})_5\text{MnBcat}$ and $(\text{OC})_5\text{ReBcat}$ under photolytic conditions.^{62,63} The metal hydride products in these reactions are not reactive for this transformation and therefore prevented them from being catalytic. Subsequent chemistry from Mankad's group has shown that bimetallic cooperativity makes turnover with Fe possible.⁶⁴

In 1999, Smith and Iverson reported the first thermal catalytic aromatic C–H activation/borylation reaction using $\text{Cp}^*\text{Ir}(\text{PMe}_3)\text{Bpin}(\text{H})$ in the presence of HBpin , (Bpin = pinacolborane) as boron source at 150 °C with 3 turnovers (Figure 14).⁶⁵ While the initial TONs (turn over numbers) were low, this was the first definitive example of thermal, catalytic C–H borylation (CHB) of an arene.

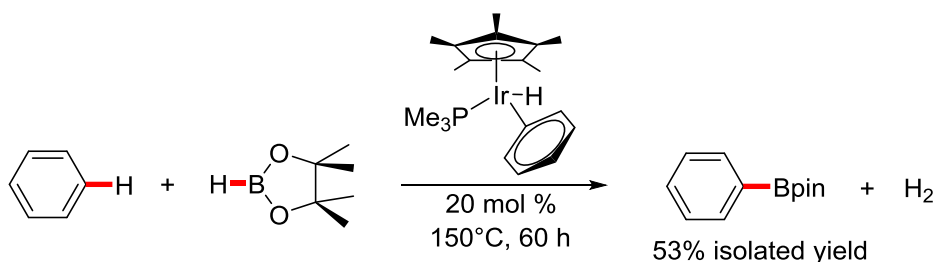


Figure 14. First thermal catalytic borylation of benzene

One year later, Hartwig and coworkers reported CHBs of benzene and terminal methyl groups of alkanes using substoichiometric quantities of $\text{Cp}^*\text{Rh}(\eta^4\text{-C}_6\text{Me}_6)$.⁶⁶ For benzene, CHB reaction temperatures maintained at 150 °C but TONs increased to 328. In

contrast to Berry's Rh-catalyzed silylations, sacrificial olefins were not necessary for catalysis.²⁹

Regio and Chemoselectivity of Transition Metal CHB Catalysts

Comparisons between the two catalytic systems for thermal CHB originally disclosed by Smith and Hartwig revealed differences in their arene selectivities.⁶⁷ While Ir and Rh catalysts borylated the least sterically hindered position, the Ir systems developed by Smith and coworkers offered selectivity advantages, especially for substrates containing aryl C–F or benzylic C–H bonds (Figure 15).⁶⁸

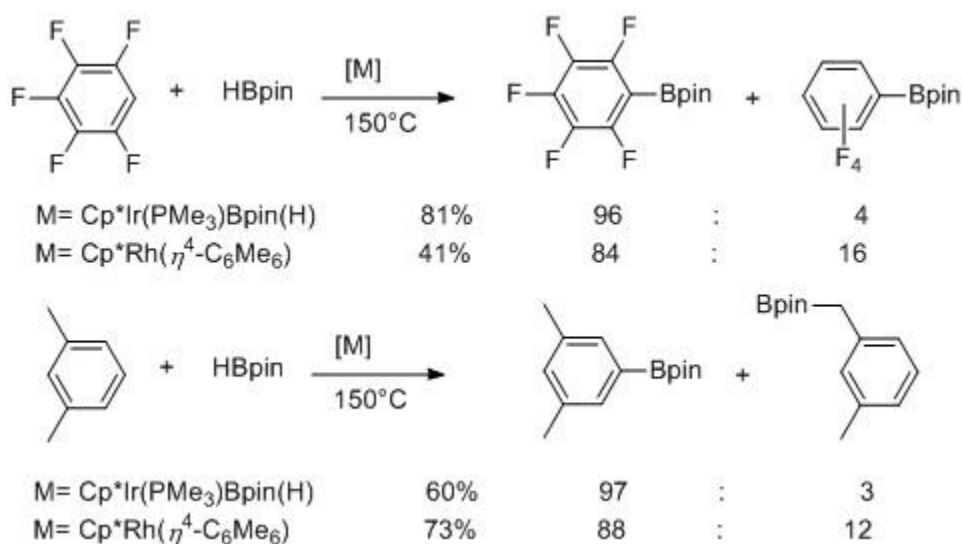


Figure 15. Regio- and chemoselectivity of iridium and rhodium catalyzed borylation of aromatics

Due to better regio- and chemoselectivities of the Ir CHB catalysts, further studies were carried out to better define the Ir catalytic manifold. The stoichiometric reaction of (η^6 -mesitylene)Ir(Bpin)₃ with benzene gave 3 equivalents (equiv) of borylated benzene, but (η^6 -mesitylene)Ir(Bpin)₃ did not catalyze the reaction in the presence of excess HBpin.⁴² The addition of PMe₃ to solutions of HBpin, (η^6 -mesitylene)Ir(Bpin)₃ and

benzene led to catalytic turnover (TON = 50, at 150 °C), a 20 fold improvement relative to $\text{Cp}^*\text{Ir}(\text{PMe}_3)(\text{E})(\text{H})$. Maleczka, Smith, and coworkers performed several experiments to develop their mechanistic hypothesis for the catalytic reaction. The dissociation of PMe_3 from $\text{Cp}^*\text{Ir}(\text{PMe}_3)\text{Bpin}(\text{H})$ was excluded based on the observation that CHB with Cp^*IrH_4 , and the boryl complexes that rapidly form when it reacts with HBpin , is too slow for undetected intermediates generated PMe_3 dissociation from $\text{Cp}^*\text{Ir}(\text{PMe}_3)\text{Bpin}(\text{H})$ to be viable. This was further supported by substantially different regioselectivities for anisole CHB with precatalysts $\text{Cp}^*\text{Ir}(\text{PMe}_3)\text{Bpin}(\text{H})$ and Cp^*IrH_4 .

The evidence for the $\text{Ir}^{\text{III}}/\text{Ir}^{\text{V}}$ cycle that was first proposed by the Maleczka and Smith groups was circumstantial. A remarkable finding of their work was the demonstrated compatibility of aryl halides in Ir-catalyzed CHB. With the Ir(I) precatalyst $[\text{IrCl}(\text{cod})]_2$, aryl C–I bonds did not survive CHB conditions. However, the aryl C–I bonds were retained with the Ir^{III} precatalyst, $(\eta^6\text{-mesitylene})\text{Ir}(\text{Bpin})_3$. This implicated C–I oxidative addition, a well-established reaction for Ir^{I} , as the source of aryl C–I incompatibility when Ir^{I} precatalysts were used. Another observation that favors the $\text{Ir}^{\text{III}}/\text{Ir}^{\text{V}}$ cycle is the stoichiometric reactivity of the Ir^{I} complex $(\text{Ir}(\text{Bpin})(\text{PMe}_3)_4)$ and the Ir^{III} complex (*fac*- $\text{Ir}(\text{Bpin})_3(\text{PMe}_3)_3$) with arenes. Both borylate benzene stoichiometrically. However, stoichiometric CHB for iodobenzene is only found for the Ir^{III} complex. The original catalytic proposed by Cho, et al. is shown in Figure 16.

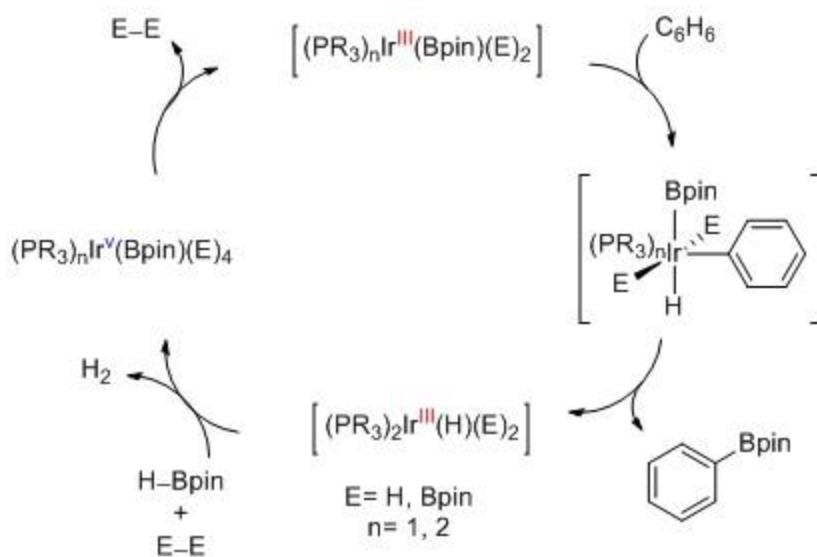


Figure 16. Iridium catalyzed CHB cycle reported by Smith and Maleczka

Other significant findings were reported in the 2002 *Science* article from the Maleczka-Smith collaboration. Due to difficulties in isolating $(\eta^6\text{-mesitylene})\text{Ir}(\text{Bpin})_3$, $(\eta^5\text{-C}_9\text{H}_7)\text{Ir}(\text{cod})$ was tested as a precatalyst for borylation of aromatics since it is the starting material for preparing $(\eta^6\text{-mesitylene})\text{Ir}(\text{Bpin})_3$. Indeed, solutions containing identical concentrations of $(\eta^5\text{-C}_9\text{H}_7)\text{Ir}(\text{cod})$ and bisphosphine ligands efficiently catalyzed CHB of arenes with high TONs and excellent steric selectivity.⁴² They also reported the first catalytic CHB of a heterocycle, the first use of an inert solvent, and a one-pot CHB/Suzuki cross-coupling. This was the first demonstration that the spent Ir CHB catalysts could enable subsequent transformations, including transition metal catalyzed reactions.

On the heels of the Maleczka-Smith report, Hartwig and coworkers disclosed a similar reaction, using an Ir^{I} precatalyst, 2,2'-bipyridine and B_2pin_2 .⁶⁹ While the system's use of an air stable ligand improved this method, most of the substrates still required high temperatures and excess of arene (60 equiv).

Additional experimental^{42,69,70} and computational⁷¹ studies, as well as isolation of the catalyst precursor (dtbpy)Ir(Bpin)₃(coe)⁷² along with independent synthesis of 16-electron (dippe)Ir(Bpin)₃ and (dcpe)Ir(Bpin)₃⁷³ aid in the identification of the active catalytic species and mechanistic cycle (Figure 17).

As depicted in Figure 17, an Ir^I precatalyst, a donor ligand (usually a bidentate ligand like dmpe, dtbpy, or dppe), and HBpin (or B₂pin₂, which is not shown) are proposed to generate the 16-electron intermediate (L₂)Ir(Bpin)₃. This species has been proposed as the intermediate responsible for C–H activation, which is typically rate-determining. The commonly proposed product of C–H activation is an Ir^V intermediate thought to arise from C–H oxidative addition to (L₂)Ir(Bpin)₃. Subsequent reductive elimination of the borylated product from Ir^V affords a 16-electron, Ir^{III} diboryl monohydride. Catalyst regeneration begins with oxidative addition of HBpin to Ir^{III} diboryl monohydride yielding an 18-electron Ir^V species that reductively eliminates H₂ to regenerate (L₂)Ir(Bpin)₃, which closes the catalytic cycle.

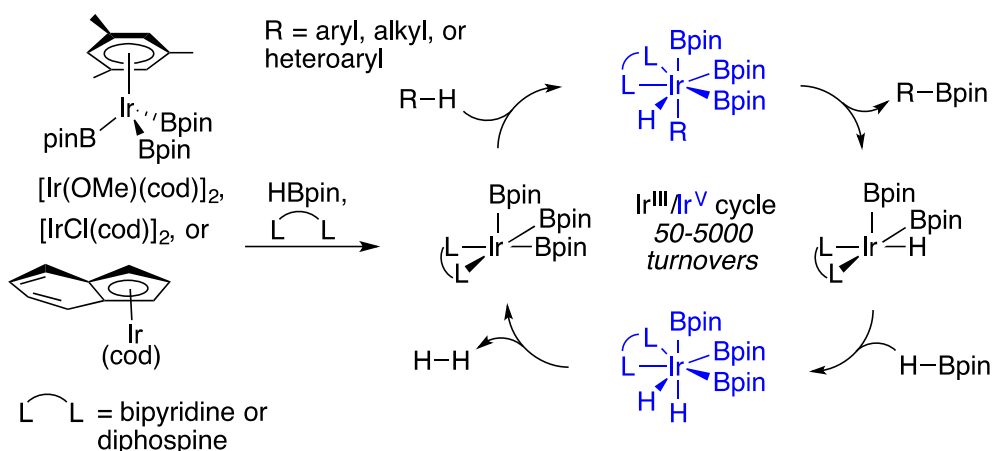


Figure 17. A proposed catalytic cycle for Ir-catalyzed CHB of arenes, heteroarenes, and alkanes

Regioselectivity Origins in Ir-catalyzed CHBs

As described earlier, the Smith group's motivation for exploring metal-catalyzed CHB was to harness steric effects that are significant in the oxidative additions of C–H bonds to transition metal complexes. Indeed, when steric effects dominate, the regioselectivities for Ir-catalyzed CHBs often complement those for DoM and EAS. However, the qualitative “agreement” between selectivities and rationalizations based on steric effects in Ir-catalyzed CHBs is not evidence that electronic effects are unimportant.

The complete separation of steric and electronic effects is impossible. That does not mean that these concepts are useless, and Ir-catalyzed CHB is useful for delineating relative contributions from steric and electronic effects, particularly in cases where regioselectivities are not “perfect”.

The first attempt to quantify steric effects was reported by Smith and coworkers. They attempted to correlate regioselectivities for Ir-catalyzed CHBs of 1,4-disubstituted benzenes (Figure 18). Specifically, the ratios of 2- and 3-borylated isomers were correlated to a slightly modified model. While this work led to selective CHB ortho to nitrile groups, which are weak meta directors in EAS, more detailed studies were clearly warranted.⁷⁴

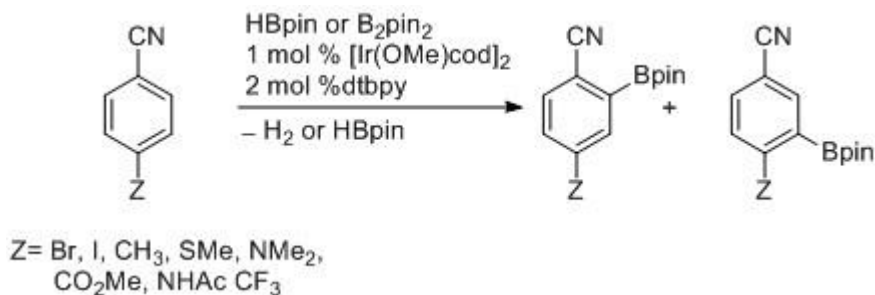


Figure 18. First attempt to quantify steric effect in Ir-catalyzed CHBs

Electronic Effects in Ir-catalyzed CHBs.

Unlike many monosubstituted benzenes, Ir-catalyzed CHB of anisole using $\text{Cp}^*\text{Ir}(\text{PMe}_3)\text{Bpin}(\text{H})$, does not result in a statistical 2:1 ratio of meta and para products. Instead, the observed 4:1 meta:para ratio reflects modest meta selectivity.⁶⁵ This arises from electronic effects associated with the OMe group. Another example of the electronic bias is when the sterically small fluorine FG exists in the molecule. For instance, by modifying the ligand, it is possible to obtain the 2-borylated product starting from 1,3-difluorobenzene.

Maleczka, Singleton and Smith reported a theoretical calculation that the activation barriers (ΔE^\ddagger) for handful of five coordinate Iridium complexes and a very electronically diverse group of substrates and the energy difference between the reactants and products (ΔE) has a strong correlation, they also demonstrated that there is a correlation between the (ΔE) and the charge developed on the aryl group.⁷⁵

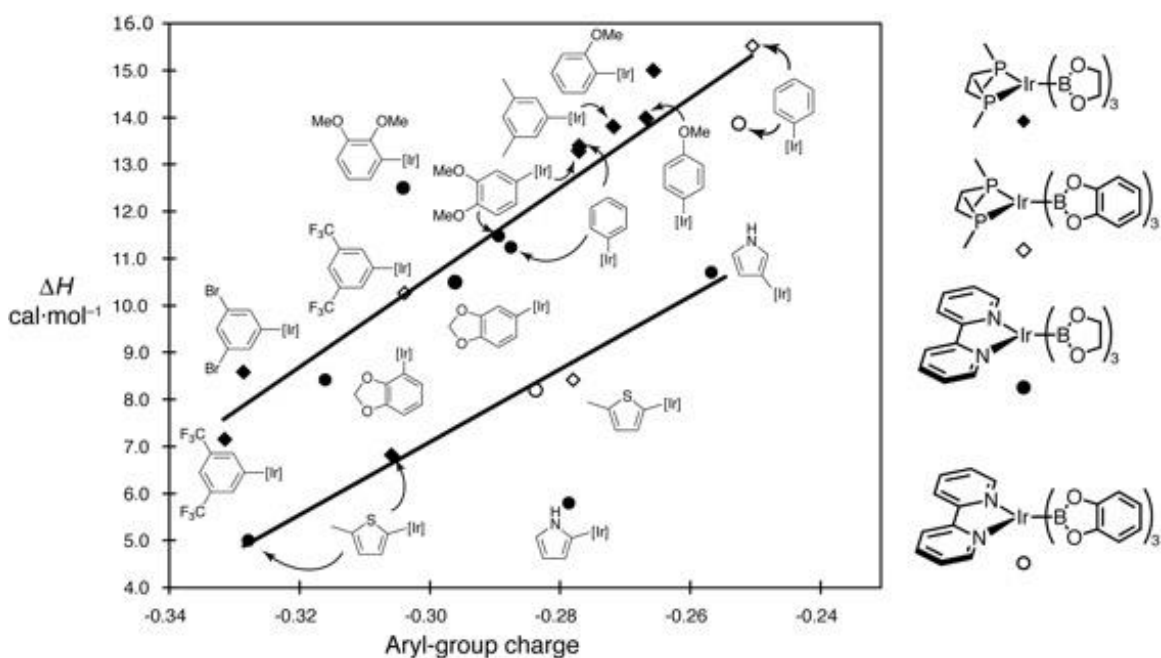


Figure 19. Correlation between ΔH and aryl-group charge

In 2014, Houk and Merlic studied the origin of Ir-catalyzed CHB of mono- and di- substituted arenes using density functional theory. Their computational studies suggest that the regioselectivity of the product is dictated by the interaction energy difference between iridium and arene carbon due to the late nature of the transition state.⁷⁶

Chelate-Directed, ortho selective Ir-catalyzed CHBs.

In 2000, Smith and coworkers first described ortho-selective borylation of benzamide using $\text{Cp}^*\text{Rh}(\eta^4\text{-C}_6\text{Me}_6)$, with ortho: meta: para ratio 4:2:1,⁶⁷ proposing the selectivity arose from chelate direction of a DMG.

The other example of directed ortho borylation is chelate-assisted functionalization; in this method, ortho borylations rely on intrinsic substrate functionality. For instance, Ishiyama and Miyaura described ortho borylation of esters using electron deficient monodentate bulky phosphine (Figure 20).⁷⁷

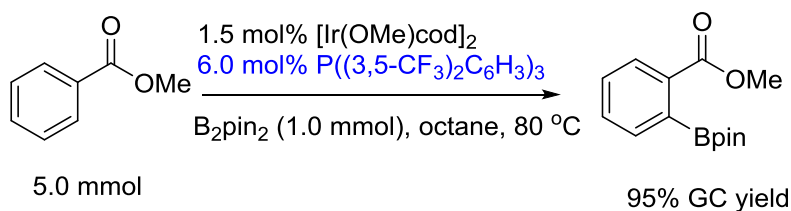


Figure 20. Chelate directed ortho borylation of benzoate using bulky, electron deficient, mono dentate phosphine

Ito and Ishiyama reported ortho borylations of ketones;⁷⁸ Lassaletta reported N-directed ortho-borylations of phenylpyridines using diimine ligands,⁷⁹ and Clark and coworkers developed borylations of benzylamines and phosphines.^{80, 81}

While the substrate scope for homogeneous ortho-directed iridium catalyzed borylation is limited, Sawamura pioneered heterogeneous Ir-catalyzed borylations with a broad scope for ortho directed borylations (Figure 21).⁸²⁻⁸⁵

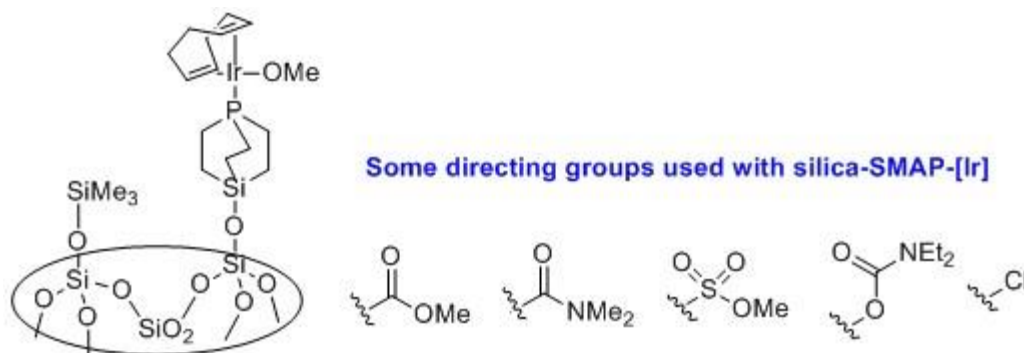


Figure 21. Solid supported Iridium catalyst for ortho-directed borylation

While the surface supported phosphine systems of Sawamura's are highly active, their synthesis can be non-trivial, which makes modification of the phosphine structure challenging.⁸⁶

Relay-Directed, ortho selective, Ir-catalyzed CHBs.

In 2008, Hartwig and Boebel described the first examples of iridium catalyzed ortho borylations using an organosilane moiety as a directing group.⁸⁷ In this "relay directed" method, O–H and N–H bonds need to undergo silane protection to form O–SiR₂H and N–SiR₂H moieties. The Si–H bonds go through formal sigma bond metathesis with Ir–Bpin groups to create Ir–Si bound intermediates that direct functionalization of C–H bonds ortho to O and N groups, but the necessity of a stoichiometric amount of protecting group is the drawback of this system (Figure 22).

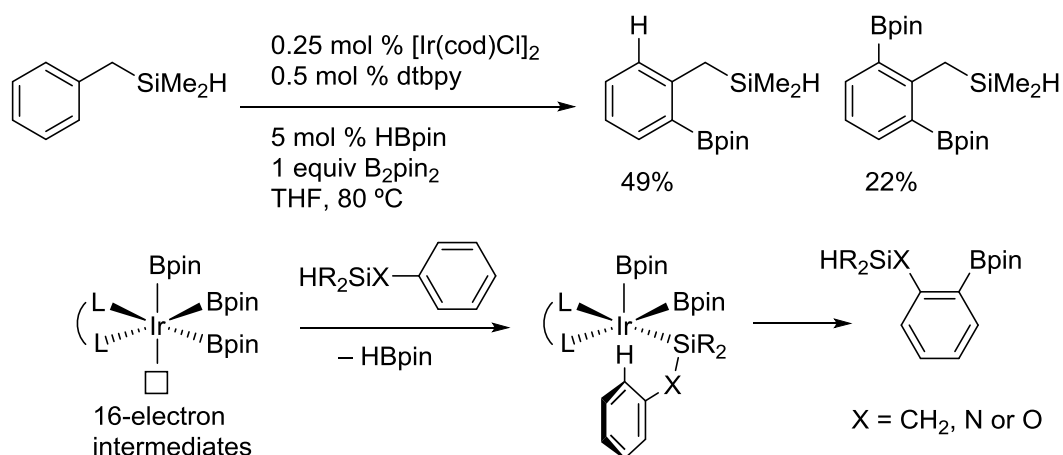


Figure 22. Silyl-Directed, Iridium-Catalyzed ortho-Borylation of Arenes

Hydrogen-bond directed, ortho selective Ir-catalyzed CHBs.

Recently, Maleczka, Singleton, and Smith have proposed that “outer sphere” hydrogen bonding interactions between protected aniline (NBoc or NHBpin) N-H bonds and Bpin O atoms can direct ortho borylations of anilines (Figure 23).^{88,89}

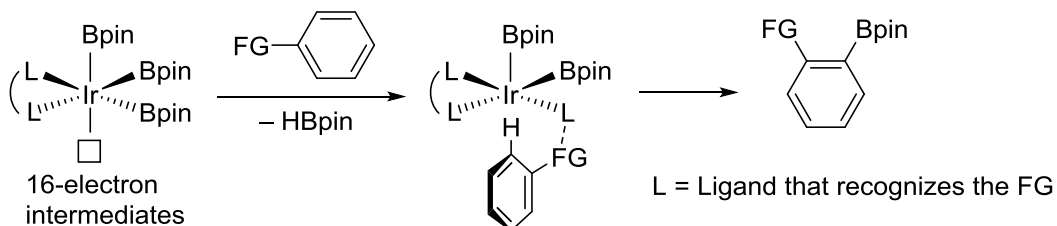


Figure 23. Mechanism for outer-sphere ortho-borylation

Other ortho-selective CHBs.

Diborylation of indole results in substitution first at the 2-position and then at the 7-position.⁹⁰ Several other methods have been reported that use an inner-sphere chelation or outer-sphere hydrogen bonding to perform ortho-borylation (more detailed information on ortho-directed borylation will be discussed in Chapter 3).

Meta-Selective CHBs.

Due to difficulties and challenges for selective meta functionalization, until 2015 the only meta selectivity could be achieved by use of Ir-catalyzed CHB's using 1,3-disubstituted arene. In 2015, Kanai and coworkers reported “A *meta*-selective C–H borylation directed by a secondary interaction between ligand and substrate.”⁹¹ In this method, the bipyridine ligand that coordinates to the iridium center has a pendant urea moiety and all the substrates that have been screened contain a carbonyl group. A secondary interaction between the urea moiety and carbonyl group (hydrogen-bond acceptor) in the substrate seats the metal center in the vicinity to the *meta*-C–H bond and therefore affect the regioselectivity (Figure 24).

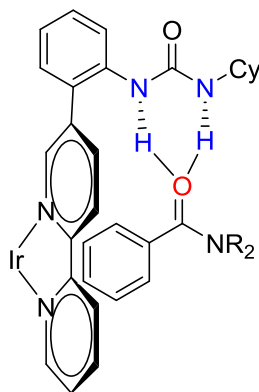


Figure 24. Selective meta borylation by using a secondary interaction between ligand and the substrate

In 2016, Chattopadhyay reported the selective meta borylation of benzaldehydes. In this method, by addition of amine, the aldehyde is protected. The author suggested that an electrostatic interaction and a secondary interaction between the ligand (3,4,7,8-tetramethyl-1,10-phenanthroline) and the substrate are responsible for the high meta selectivity.⁹²

In 2016, Phipps and coworkers reported a new methodology for selective *meta*-C–H bond borylation. They have introduced an ion-pair interaction between an anionic pendant FG on their ligand and the aromatic quaternary ammonium salts in the substrates (Figure 25).⁹³

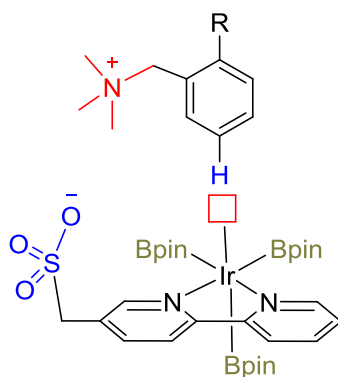


Figure 25. Directed meta C-H borylation by ion pair mechanism

Para-Selective CHBs.

Recently, Itami and coworkers reported the C-H activation of *para*-selective arenes. By means of a very bulky phosphine ligand and bulky substituents on their monosubstituted aromatics, *para*-selectivity up to 91% can be obtained, demonstrating that steric factors between substrate and catalyst play a very important role in achieving the desired regioselectivity (Figure 26).⁹⁴

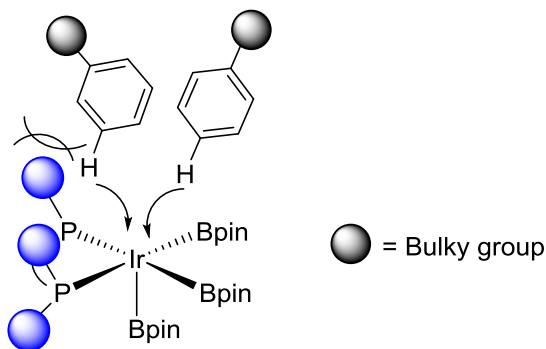


Figure 26. Para selective C-H borylation by using the bulky ligand

REFERENCES

REFERENCES

1. Chenier, P. J. *Derivatives of Basic Aromatics*. In *Survey of Industrial Chemistry*; 3rd ed.; Kluwer Academic: New York, 2002, p 195-203.
2. Chenier, P. J. *Basic Organic Chemicals*. In *Survey of Industrial Chemistry*; 3rd ed.; Kluwer Academic: New York, 2002, p 130.
3. Faraday, M. *Trans. Roy. Soc. (London)* **1825**, *115*, 440.
4. Mitscherlich, E. *Justus Liebigs Ann. Chem.* **1834**, *12*, 308.
5. Holleman, A. F. *Chem. Rev.* **1924**, *1*, 187.
6. Hodgson, H. H.; Wignall, J. S. *J. Chem. Soc.* **1926**, 2077.
7. Butin, K. P.; Beletskaya, I. P.; Kashin, A. N.; Reutov, O. A. *J. Organomet. Chem.* **1967**, *10*, 197.
8. Gilman, H.; Young, R. V. *J. Am. Chem. Soc.* **1934**, *56*, 1415.
9. Wittig, G.; Pockels, U.; Dröge, H. *Ber. Dtsch. Chem. Ges.* **1938**, *71*, 1903.
10. a) Snieckus, V. *Chem. Rev.* **1990**, *90*, 879. b) Chadwick, S. T.; Rennels, R. A.; Rutherford, J. L.; Collum, D. B. *J. Am. Chem. Soc.* **2000**, *122*, 8640. c) Slocum, D. W.; Jennings, C. A. *J. Org. Chem.* **1976**, *41*, 3653.
11. Arndtsen, B. A.; Bergman, R. G.; Mobley, T. A.; Peterson, T. H. *Acc. Chem. Res.* **1995**, *28*, 154.
12. Labinger, J. A.; Bercaw, J. E. *Nature* **2002**, *417*, 507.
13. *Activation and Functionalization of C—H Bonds*; American Chemical Society: Washington, DC, 2004.
14. Shilov, A. E.; Shul'pin, G. B. *Chem. Rev.* **1997**, *97*, 2879.
15. Dyker, G. *Angew. Chem. Int. Ed.* **1999**, *38*, 1699.
16. Crabtree, R. H. *J. Chem. Soc., Dalton Trans.* **2001**, 2437.
17. Ritleng, V.; Sirlin, C.; Pfeffer, M. *Chem. Rev.* **2002**, *102*, 1731.
18. Kakiuchi, F.; Chatani, N. *Adv. Synth. Catal.* **2003**, *345*, 1077.

19. Lersch, M.; Tilset, M. *Chem. Rev.* **2005**, *105*, 2471.
20. Godula, K.; Sames, D. *Science* **2006**, *312*, 67.
21. Herrerias, C. I.; Yao, X. Q.; Li, Z. P.; Li, C. J. *Chem. Rev.* **2007**, *107*, 2546.
22. Giri, R.; Shi, B. F.; Engle, K. M.; Maugel, N.; Yu, J. Q. *Chem. Soc. Rev.* **2009**, *38*, 3242.
23. Chatt, J.; Watson, H. R. *J. Chem. Soc.* **1962**, 2545.
24. Kleiman, P. J.; Dubeck, M. *J. Am. Chem. Soc.*, **1963**, *85*, 1544.
25. Chatt, J.; Davidson, J. M. *J. Chem. Soc.* **1965**, 843.
26. Ittel, S. D.; Tolman, C. A.; English, A. D.; Jesson, J. P. *J. Am. Chem. Soc.* **1976**, *98*, 6073.
27. Jones, W. D.; Kosar, W. P. *J. Am. Chem. Soc.* **1986**, *108*, 5640.
28. Ryabov, A. D. *Chem. Rev.* **1990**, *90*, 403.
29. Ezbiansky, K.; Djurovich, P. I.; LaForest, M.; Sinning, D. J.; Zayes, R.; Berry, D. H. *Organometallics* **1998**, *17*, 1455.
30. Sivaev, I. B.; Bregadze, V. I. *Arkivoc* **2008**, 47.
31. Yoon, J.; Czarnik, A. W. *J. Am. Chem. Soc.* **1992**, *114*, 5874.
32. Westmark, P. R.; Gardiner, S. J.; Smith, B. D. *J. Am. Chem. Soc.* **1996**, *118*, 11093.
33. https://www.nobelprize.org/nobel_prizes/chemistry/laureates/1979/ (Access date: 12/05/2016)
34. Furuya, T.; Ritter, T. *Org. Lett.* **2009**, *11*, 2860.
35. Murphy, J. M.; Liao, X.; Hartwig, J. F. *J. Am. Chem. Soc.* **2007**, *129*, 15434.
36. Norberg, M. A.; Smith, M. R., III; Maleczka, R. E., Jr. *Synthesis* **2011**, 857.
37. Tzschucke, C. C.; Murphy, J. M.; Hartwig, J. F. *Org. Lett.* **2007**, *9*, 761.
38. Shi, F.; Smith, M. R., III; Maleczka, R. E., Jr. *Org. Lett.* **2006**, *8*, 1411.
39. Maleczka, R. E., Jr.; Shi, F.; Holmes, D.; Smith, M. R., III *J. Am. Chem. Soc.* **2003**, *125*, 7792.

40. Murphy, J. M.; Tzschucke, C. C.; Hartwig, J. F. *Org. Lett.* **2007**, *9*, 757.
41. Liskey, C. W.; Liao, X. B.; Hartwig, J. F. *J. Am. Chem. Soc.* **2010**, *132*, 11389.
42. Cho, J. Y.; Tse, M. K.; Holmes, D.; Maleczka, R. E., Jr.; Smith, M. R., III *Science* **2002**, *295*, 305.
43. Kallepalli, V. A.; Sanchez, L.; Li, H.; Gesmundo, N. J.; Turton, C. L.; Maleczka, R. E., Jr.; Smith, M. R., III *Heterocycles* **2010**, *80*, 1429.
44. Robbins, D. W.; Boebel, T. A.; Hartwig, J. F. *J. Am. Chem. Soc.* **2010**, *132*, 4068.
45. Tajuddin, H.; Shukla, L.; Maxwell, A. C.; Marder, T. B.; Steel, P. G. *Org. Lett.* **2010**, *12*, 5700.
46. Boebel, T. A.; Hartwig, J. F. *Tetrahedron* **2008**, *64*, 6824.
47. Holmes, D.; Chotana, G. A.; Maleczka, R. E., Jr.; Smith, M. R., III *Org. Lett.* **2006**, *8*, 1407.
48. a) Miyaura, N.; Suzuki, A. *Chem. Commun.* **1979**, 866. b) Miyaura, N.; Yamada, K.; Suzuki, A.; *Tetrahedron Lett.* **1979**, *20*, 3437. c) Suzuki, A. *Acc. Chem. Res.* **1982**, *15*, 178.
49. Singer, R. D.; Knochel, P. *Chem. Rev.* **1993**, *93*, 2117.
50. Ishiyama, T.; Murata, M.; Miyaura, N. *J. Org. Chem.* **1995**, *60*, 7508.
51. Willis, D. M.; Strongin, R. M. *Tetrahedron Lett.* **2000**, *41*, 8683.
52. Mo, F.; Jiang, Y.; Qiu, D.; Zhang, Y.; Wang, J. *Angew. Chem. Int. Ed.* **2010**, *49*, 1846.
53. Mkhaliid, I. A. I.; Barnard, J. H.; Marder, T. B.; Murphy, J. M.; Hartwig, J. F. *Chem. Rev.* **2010**, *110*, 890.
54. Hartwig, J. F. *Acc. Chem. Res.* **2012**, *45*, 864.
55. Yamamoto, E.; Izumi, K.; Horita, Y.; Ito, H. *J. Am. Chem. Soc.* **2012**, *134*, 19997.
56. Légaré, M. A.; Courtemanche, M. A.; Rochette, É.; Fontaine, F.-G. *Science* **2015**, *349*, 513.
57. Mfuh, A. M.; Doyle, J. D.; Chhetri, B.; Arman, H. D.; Larionov, O. V. *J. Am. Chem. Soc.* **2016**, *138*, 2985.

58. Rablen, P. R.; Hartwig, J. F.; Nolan, S. P. *J. Am. Chem. Soc.* **1994**, *116*, 412.
59. Rablen, P. R.; Hartwig, J. F. *J. Am. Chem. Soc.* **1996**, *118*, 4648.
60. Blanksby, S. J.; Ellison, G. B. *Acc. Chem. Res.* **2003**, *36*, 255.
61. Henk, P. N.; Blom, H. P.; Westcott, S. A.; Taylor, N. T.; Marder, T. B. *J. Am. Chem. Soc.* **1993**, *115*, 9329.
62. Waltz, K. M.; He, X.; Muhoro, C.; Hartwig, J. F. *J. Am. Chem. Soc.* **1995**, *117*, 11357.
63. Waltz, K. M.; Hartwig, J. F. *Science* **1997**, *277*, 211.
64. Mazzacano, T. J.; Mankad, N. P. *J. Am. Chem. Soc.* **2013**, *135*, 17258.
65. Iverson, C. N.; Smith, M. R., III *J. Am. Chem. Soc.* **1999**, *121*, 7696.
66. Chen, H. Y.; Schlecht, S.; Semple, T. C.; Hartwig, J. F. *Science* **2000**, *287*, 1995.
67. Cho, J. Y.; Iverson, C. N.; Smith, M. R., III *J. Am. Chem. Soc.* **2000**, *122*, 12868.
68. Tse, M. K.; Cho, J. Y.; Smith, M. R., III *Org. Lett.* **2001**, *3*, 2831.
69. Ishiyama, T.; Takagi, J.; Ishida, K.; Miyaura, N.; Anastasi, N. R.; Hartwig, J. F. *J. Am. Chem. Soc.* **2002**, *124*, 390.
70. Boller, T. M.; Murphy, J. M.; Hapke, M.; Ishiyama, T.; Miyaura, N.; Hartwig, J. F. *J. Am. Chem. Soc.* **2005**, *127*, 14263.
71. Tamura, H.; Yamazaki, H.; Sato, H.; Sakaki, S. *J. Am. Chem. Soc.* **2003**, *125*, 16114.
72. Ishiyama, T.; Takagi, J.; Ishida, K.; Miyaura, N.; Anastasi, N. R.; Hartwig, J. F. *J. Am. Chem. Soc.* **2002**, *124*, 390.
73. Chotana, G. C.; Vanchura, B. A., II; Tse, M. K.; Staples, R. J.; Maleczka, R. E., Jr; Smith, M. R., III *Chem. Commun.*, **2009**, 5731.
74. Chotana, G. A.; Rak, M. A.; Smith, M. R., III *J. Am. Chem. Soc.* **2005**, *127*, 10539.
75. Vanchura, B. A., II; Preshlock, S. M.; Roosen, P. C.; Kallepalli, V. A.; Staples, R. J.; Maleczka, R. E., Jr; Smith, M. R., III *Chem. Commun.* **2010**, *46*, 7724.
76. Green, A. G.; Liu, P.; Merlic, C. A.; Houk, K. N. *J. Am. Chem. Soc.* **2014**, *136*, 4575

77. Ishiyama, T.; Isou, H.; Kikuchi, T.; Miyaura, N. *Chem. Commun.* **2010**, 159.
78. Itoh, H.; Kikuchi, T.; Ishiyama, T.; Miyaura, N. *Chem. Lett.* **2011**, 40, 1007.
79. Fernandez, R.; Lassaletta, J. M. *Chem. Soc. Rev.* **2014**, 43, 3229.
80. Roering, A. J.; Hale, L. V. A.; Squier, P. A.; Ringgold, M. A.; Wiederspan, E. R.; Clark, T. B. *Org. Lett.* **2012**, 14, 3558.
81. Crawford, K. M.; Ramseyer, T. R.; Daley, C. J. A.; Clark, T. B. *Angew. Chem., Int. Ed.* **2014**, 53, 7589.
82. Kawamorita, S.; Ohmiya, H.; Hara, K.; Fukuoka, A.; Sawamura, M. *J. Am. Chem. Soc.* **2009**, 131, 5058.
83. Kawamorita, S.; Ohmiya, H.; Sawamura, M. *J. Org. Chem.* **2010**, 75, 3855.
84. Kawamorita, S.; Murakami, R.; Iwai, T.; Sawamura, M. *J. Am. Chem. Soc.* **2013**, 135, 2947.
85. Kawamorita, S.; Miyazaki, T.; Ohmiya, H.; Iwai, T.; Sawamura, M. *J. Am. Chem. Soc.* **2011**, 133, 19310.
86. Recently, threefold cross-linked polystyrene-triphenylphosphane hybrid systems have been developed. Their synthesis is simpler and initial studies indicate that these function similar to silica-supported monophosphines.: Iwai, T.; Harada, T.; Hara, K.; Sawamura, M. *Angew. Chem. Int. Ed.* **2013**, 52, 12322.
87. Boebel, T. A.; Hartwig, J. F. *Tetrahedron* **2008**, 64, 6824.
88. Roosen, P. C.; Kallepalli, V. A.; Chattopadhyay, B.; Singleton, D. A.; Maleczka, R. E., Jr.; Smith, M. R., III *J. Am. Chem. Soc.* **2012**, 134, 11350.
89. Preshlock, S. M.; Plattner, D. L.; Maligres, P. E.; Krska, S. W.; Maleczka, R. E., Jr.; Smith, M. R., III *Angew. Chem., Int. Ed.* **2013**, 52, 12915.
90. Paul, S.; Chotana, G. A.; Holmes, D.; Reichle, R. C.; Maleczka, R. E., Jr.; Smith, M. R., III *J. Am. Chem. Soc.* **2006**, 128, 15552.
91. Kuninobu, Y.; Ida, H.; Nishi, M.; Kanai, M. *Nat. Chem.* **2015**, 7, 712.
92. Bisht, R.; Chattopadhyay, B. *J. Am. Chem. Soc.* **2016**, 138, 84.
93. Davis, H. J.; Mihai, M. T.; Phipps, R. J. *J. Am. Chem. Soc.* **2016**, 138, 12759.

94. Saito, Y.; Segawa, Y.; Itami, K. *J. Am. Chem. Soc.* **2015**, *137*, 5193.

CHAPTER 2 – REVERSIBLE BORYLENE FORMATION FROM RING-OPENING OF PINACOLBORANE AND OTHER INTERMEDIATES GENERATED FROM 5-COORDINATE TRISBORYL COMPLEXES: IMPLICATIONS FOR CATALYTIC C- H BORYLATION

Studies of 5-coordinate boryl catalysts.

In homogeneous transition metal catalysis, precatalysts are frequently assembled in situ through reactions with ligands, rearrangements, and/or changes in the coordination sphere. Even then, catalyst resting states often require ligand dissociation to generate more reactive species that carry out the important reactions in a catalytic cycle. Isolation of true intermediates along with mechanistic studies of their reactivity can provide great insights into factors that contribute to reaction rates and catalyst selectivities. This informs the design of improved catalysts.

In Ir-catalyzed CHB, 16-electron 5-coordinate iridium boryl species $L_2Ir(Bpin)_3$ (**1**, Figure 26 where L is a neutral, two-electron donor ligand, and L2 can represent neutral bidentate four-electron donors) are the proposed to mediate C–H cleavage.^{1,2} Reported experimental data and calculations provide support for the cycle shown in Figure 27.

Despite the initial report that utilized phosphine ligands in thermal catalytic aromatic C–H borylation,¹ bidentate nitrogen donor ligands have been used more frequently due to their higher reactivity.² While phosphine ligated catalysts have received less attention, there are some computational studies which predict that the intermediates

that are generated by C–H activation is different from the intermediate generated using bipyridine ligated system and these intermediates are Ir^{III} borane adducts (**2**).³

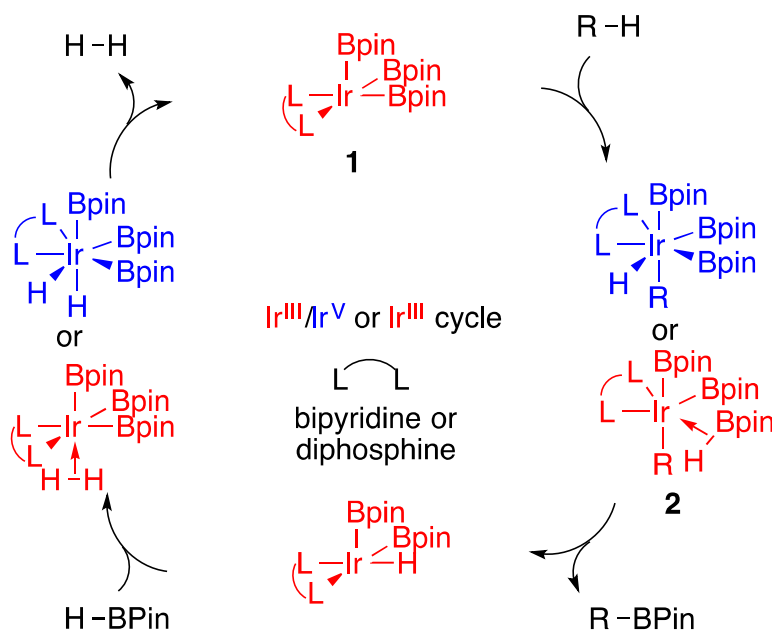


Figure 27. Catalytic cycle for iridium catalyzed C-H borylation using bidentate ligand

The most popular catalytic system for C-H borylation is the dtbpy/[Ir(OMe)-(cod)]₂ ligand/precatalyst combination, where the trisboryl intermediate (dtbpy)Ir(Bpin)₃ (**3**) is proposed to be the active catalyst for C-H activation. Detailed mechanistic studies have been performed using the precatalyst (dtbpy)Ir(Bpin)₃(coe) (**4**). A pre-equilibrium dissociation of coe from compound **4** was proposed to the generation of intermediate **3**, which has eluded detection.¹

To analyze the origin of the reactivity difference between bisphosphine- and bipyridine-ligated systems, we studied our previously reported 5-coordinate iridium trisboryl complexes stabilized by a bidentate phosphine ligand of the general formula (dippe)Ir(boryl)₃, (**5**).⁴ These compounds are rare examples where catalytically relevant

intermediates are isolable.⁴⁻⁶ Compound (**5**) reacts directly with sp^2 C-H bonds, providing a rare opportunity for examining the fundamental step in C-H borylation. Previously, this complex had been shown to react stoichiometrically at room temperature, but elevated temperatures were required to achieve catalytic turnover.

Results

In previous work by Dr. Ghayoor Abbas Chotana,⁷ a color change was observed when HBpin was added to compound **5**, and a new resonance was observed (δ 67.24) in the $^{31}\text{P}\{^1\text{H}\}$ NMR spectrum. The X-ray crystal structure and spectroscopic data indicated that the resulted compound **6** is a borylene diborohydride that formed from ring-opening of HBpin and is presumably is the source of the hydride ligand (Figure 28).⁸ A number of borylene complexes have been reported.⁹⁻¹¹ These are prepared by various synthetic routes, with the H_2 elimination/B-H activation described by Sabo-Etienne and coworkers bearing some similarity to the generation of compound **6** in that borylene formation is reversible and arises from B-H activation.¹² It is noteworthy that compound **6** is the first complex to have both boryl and borylene ligands in the metal coordination sphere.

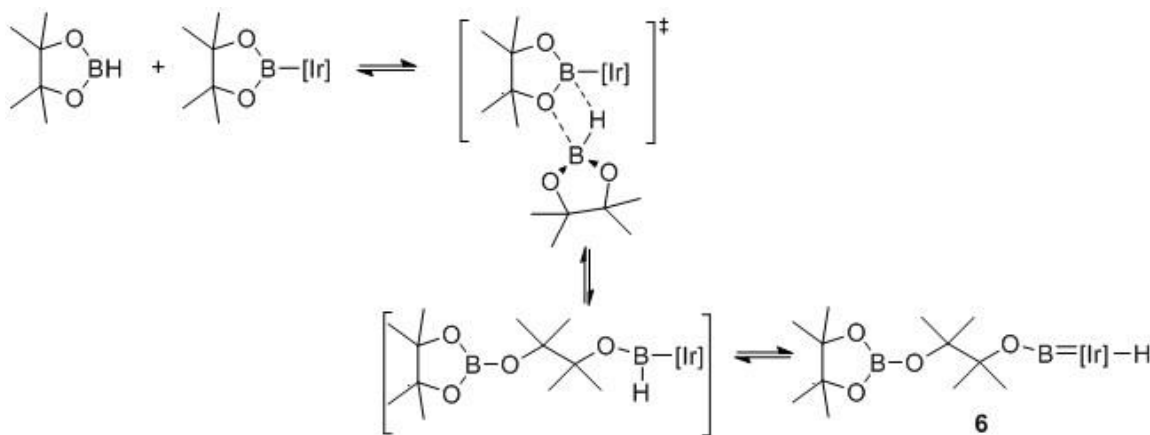


Figure 28. Proposed mechanism for borylene formation

Compound **6** has three different resonances in ^{11}B NMR spectra. The signal for OBpin moiety appears at δ 22.0 which is the most upfield signal among all. The resonance for the two iridium boryl ligands appears at δ 38.8, and the signal for boron atom in borylene is the most downfield resonance δ 54.5 (Figure 28).

The ^1H NMR spectrum confirms the presence of the hydride ligand by a high field triplet signal at δ -11.05 ($|^2J_{\text{PH}}| = 19$ Hz) in the ^1H NMR spectrum. The NMR data including the coupling constant between P and H and also the narrow line will suggest that the hydride does not have any interaction with *cis*-boryl ligands and therefore is a classical hydride.

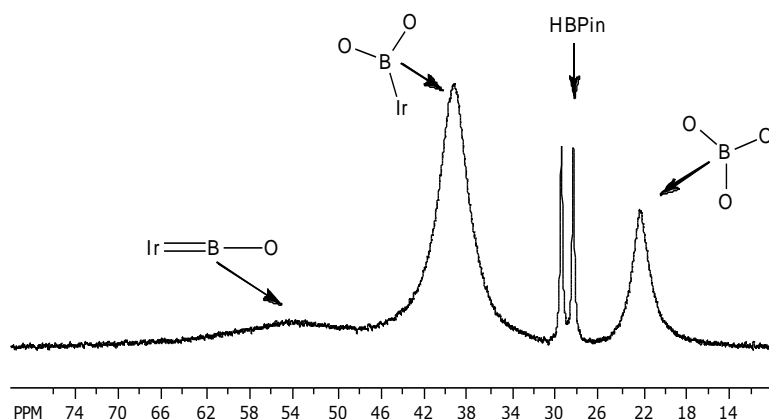


Figure 29. ^{11}B NMR of compound **6** in benzene- d_6

^1H NMR spectrum of compound **6** in benzene- d_6 , showed resonances for HBpin and compound **5**, which suggests that the compound **5** and HBpin are in equilibrium with compound **6** (Figure 30).

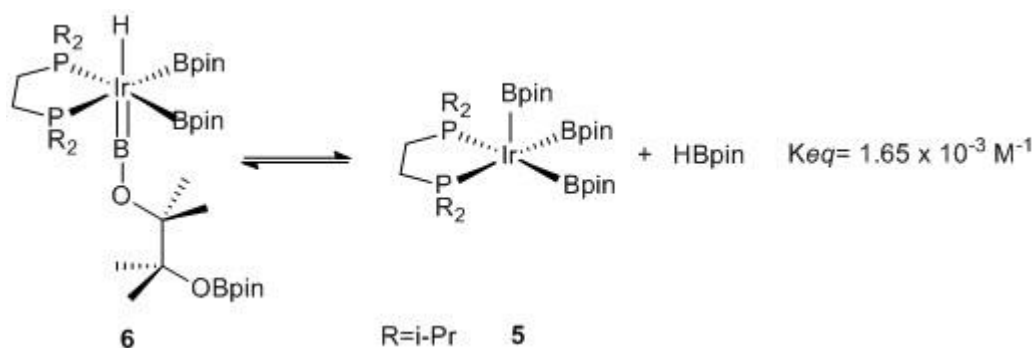


Figure 30. Equilibrium between complex **6** with complex **5** and HBpin

Addition of HBpin to the mixture or placing the mixture under dynamic high vacuum shifts this equilibrium toward compound **6** vacuum removes HBpin and regenerates **5**. Recording the ^1H NMR spectrum we have noticed that methine signal for compound **5** and **6** are well separated so with the aid of the ^1H NMR, we measured the equilibrium constant for this reaction to be $K_{eq} = 1.65 \times 10^{-3} \text{ M}^{-1}$ (see experimental section for the calculation of equilibrium constant).

In catalytic borylation of 2-methylthiophene with compound **5**, the initial $^{31}\text{P}\{^1\text{H}\}$ NMR spectroscopy shows that compound **6** is the major species at the start point of the reaction. Catalytic borylation of 2-methylthiophene does not progress at room temperature, even though the $t_{1/2}$ for stoichiometric borylation by compound **5** at similar concentrations is less than 5 minutes, this would suggest that compound **5** is responsible for borylation, and addition of HBpin shift the equilibrium towards compound **6** which would inhibit catalysis. Upon heating the catalytic reaction mixture at 100 °C, new resonances appears in $^{31}\text{P}\{^1\text{H}\}$ NMR spectra (δ 53.42, 61.22, 66.75, and 77.78 , indicating that compound **6** converts to a series on intermediate, which their relative concentration changes depending on the reaction time, concentration of HBpin and 2-methylthiophene.

Only after heating the reaction for 5 minutes, the intensity of the resonance corresponding to compound **6** (δ 67.24) in the $^{31}\text{P}\{^1\text{H}\}$ NMR spectrum decreases and a new signal appears at δ 53.42. Along with the changes in $^{31}\text{P}\{^1\text{H}\}$ NMR spectrum, a new triplet appears at δ -11.16 ($|J_{\text{PH}}| = 12$ Hz) in ^1H NMR spectrum. The relative integration of signals in $^{31}\text{P}\{^1\text{H}\}$ NMR and ^1H NMR spectrum, suggests that the new species contains two hydrides per dippe ligand. We assign this to a complex with the formula $(\text{dippe})\text{Ir}(\text{H}_2\text{Bpin}_3)$ (**7**). Considering this formulation, compound **7** can be generated independently by adding H_2 to compound **5** (this will be discussed later).

After heating the NMR tube reaction for 10 minutes, the borylene resonances for compound **6** disappear in ^{11}B NMR spectrum but boryl resonance at δ 37.7 are still present, and $^{31}\text{P}\{^1\text{H}\}$ NMR spectrum shows a new resonance at δ 61.22, in addition to the resonance for compound **7**. This is assigned to the complex $(\text{dippe})\text{Ir}(\text{H}_3\text{Bpin}_2)$ (**8**) and a major resonance at δ -11.21 appeared as a broad triplet ($|J_{\text{PH}}| = 6$ Hz) in the ^1H NMR spectrum for compound **8**.

While we were not able to isolate compound **8** in analytically pure form, single crystals were obtained by cooling solutions of compound **5** with a 10-fold excess of HBpin. The structure is depicted in Figure 31.

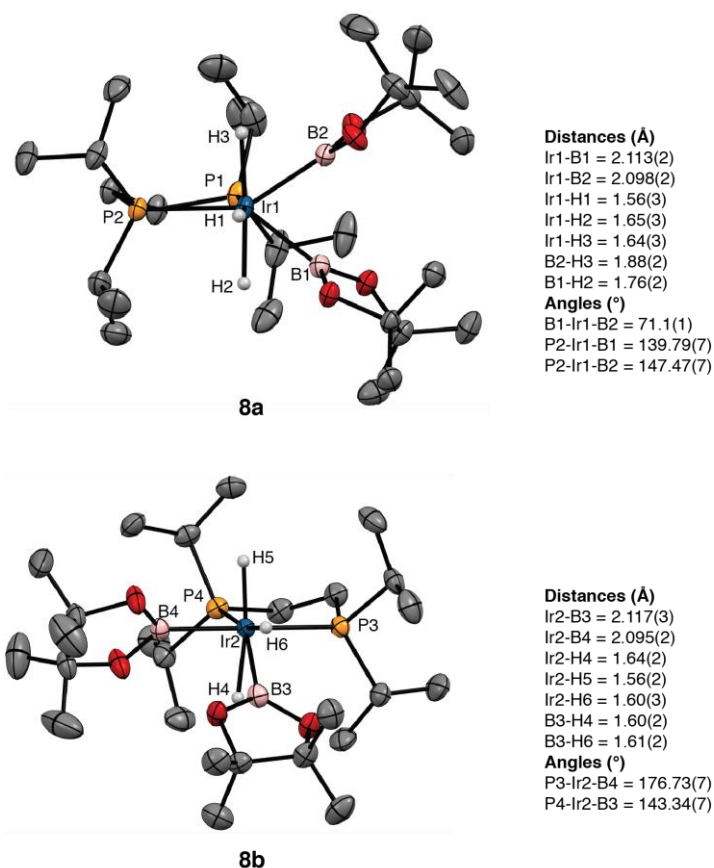


Figure 31. X-ray structure for compound **8** with thermal ellipsoids calculated at 50% probability levels. The two independent molecules (**8a** and **8b**) are shown with selected angles and distances

Two independent molecules appear in the unit cell (Figure 31), and these differ in the relative orientation of the boryl ligands. In independent molecule **8a**, the boryl ligands are both cis to one of the phosphines with the P–Ir vector of the other phosphorus approximately bisecting the B1–Ir1–B2 angle. In the second independent molecule (**8b**), one boryl (B4) is trans to P3 and cis to P4, while the second boryl (B3) is cis to P3 and forms a P4–Ir2–B3 angle of 143.34(7)°. The Ir–B distances range from 2.095(2) to 2.117(3) Å and are slightly longer than the Ir–B bonds trans to phosphines in compound **5** (2.07(1) Å). Electron density was located in regions consistent with hydride ligands and

refined, but the difficulty in locating hydrides bound to Ir prevents definitive characterization of H^{III}B interactions, which contribute to the linewidth of the hydride resonance and the reduced magnitude of $|^1J_{\text{PH}}|$.

The theoretical calculations done by Professor Milton Smith assist us in gaining more insight into the H₃(Bpin)₂ framework. Structures were optimized at an M06//SDD/6-31G* level of theory using the X-ray coordinates as a starting point. Figure 31 shows an overlay of the calculated structures (red) with the coordinates from the X-ray structures (blue). Isomer **8a** is calculated to be 1.5 kcal more stable than isomer **8b**. As can be seen in Figure 23, the calculated coordinates for **8a** are shifted significantly from the experimentally determined ones. Essentially, B1 and B2 swing towards H2 leaving the B1–Ir1–B2 angle unchanged. The shift in the calculated structure allows for a significant B^{III}H interaction (1.48 Å) between B1 and H2 and eliminates any interaction between B2 and H3. The structure is best described as an agostic borane complex of an Ir^{III} dihydridoboryl complex. For structure **8b**, the calculated structure more closely resembles the experimentally determined one. The biggest changes are lengthening of the Ir2–B3 distance and a shortening of the B3–H4 distance. Like **8a**, the calculated structure of **8b** is best represented as an Ir^{III} dihydridoboryl complex.

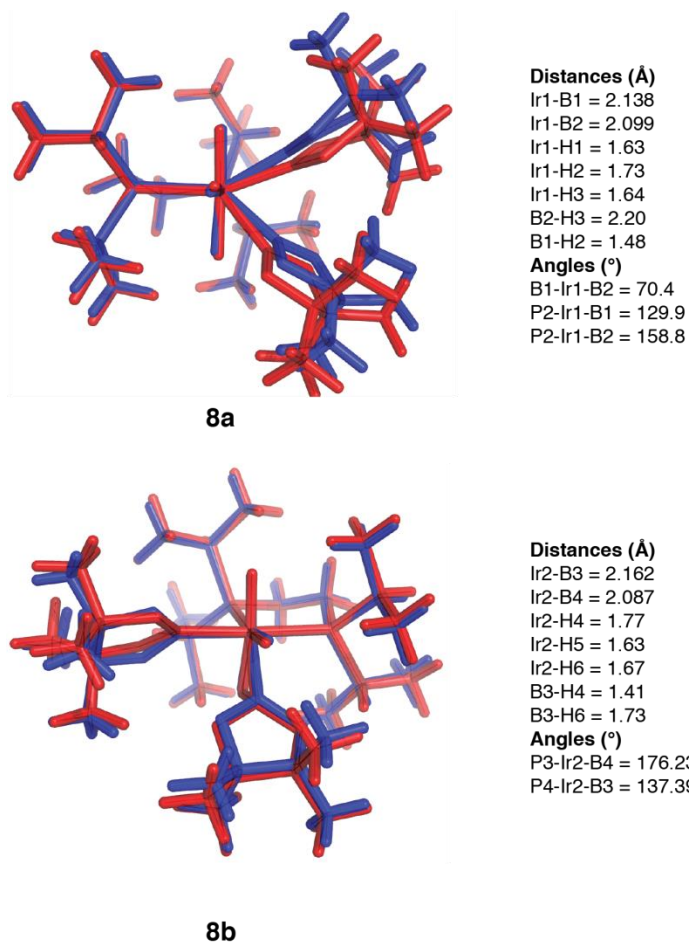


Figure 32. Calculated structures (M06//SDD/6-31G*) for **8a** and **8b** (red) overlaid with coordinates from their X-ray structures (blue). Calculated bond distances and angles correspond to the numbering in Figure 31

By sustained heating of the NMR tube containing the reaction mixture, the signal for compound **7** in the $^{31}\text{P}\{^1\text{H}\}$ NMR spectrum disappears and a new feature at δ 66.75 accompanied the resonance for compound **8**. The ^1H NMR spectrum depicts a new triplet at δ -11.90 ($|J_{\text{PH}}| = 17$ Hz) for compound **9**. By recording the ^{31}P NMR spectrum with selective decoupling of the aliphatic protons while the hydride coupling is preserved, we can find the number of hydrides existing in the structure. The resulting quintet (pentet) evidences that four hydrides are bound to iridium in the structure of compound **9**. This

compound was crystallized by cooling a 1,3-bis(trifluoromethyl)benzene solution containing compounds **6**, **8**, and a 10-fold excess of HBpin to $-30\text{ }^{\circ}\text{C}$. After several weeks crystals formed and X-ray diffraction revealed their structure to be (dippe)Ir(H₄Bpin) (**9**, Figure 33). Compound **9** could be generated independently by exposing a THF solution of compound **5**.

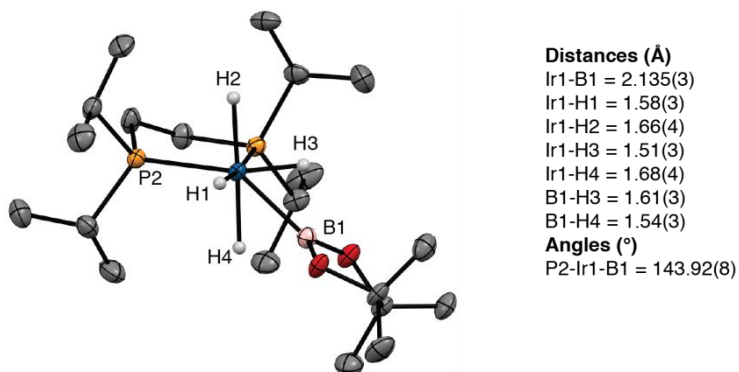


Figure 33. X-ray structure for compound **9** with thermal ellipsoids calculated at 50% probability levels. Hydride ligands are shown and other hydrogens are omitted for clarity.

Selected experimental and computational metric parameters are given

The crystal structure of compound **9** is shown in Figure 33. Hydrides were located and refined, but the usual caveat applies to the certainty of their positions. The Ir1–B1 distance is relatively long compared to the other boryl ligands in this family of complexes and may reflect contributions from agostic borane or borohydride structures. We carried out calculations starting from the X-ray coordinates, and the calculated structure (red) is shown with its overlap to the crystallographic coordinates (blue). There is good agreement between the calculated and experimental structure with the biggest differences being the elongation of the Ir1–B1 bond and B1–H3 distance with a shortening of the B1–H4 distance in the calculated structure, which is best described as a borane adduct of

an Ir^{III} trihydride (Figure 34). Based on the ¹H and ³¹P{¹H} NMR data, the hydride positions are rapidly equilibrating on the NMR time scale.

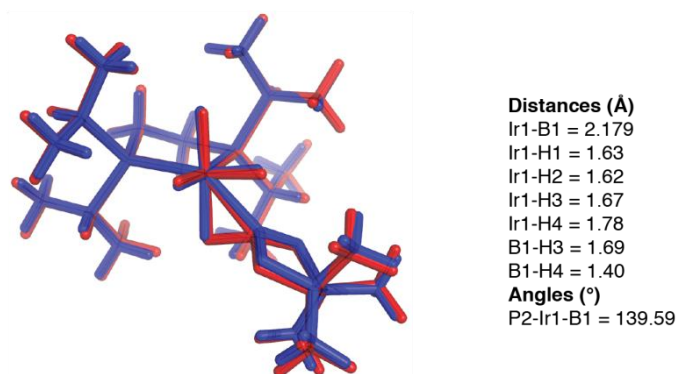


Figure 34. The calculated structure (red, M06//SDD/6-31G*) is overlaid with crystallographic coordinates

With sustained heating of the catalytic reaction mixture, the resonance for compound **9** loses intensity and a new resonance at δ 77.78 appears in the ³¹P{¹H} NMR spectrum. The intensity of the resonance for compound **10** is a maximum at the end of reactions where the initial [HBpin]:[thiophene] = 0.5. Upon cooling the cyclohexane-*d*₁₂ solution of the catalytic reaction to 5 °C the ³¹P{¹H} resonance for compound **10** resolves into four distinct features at δ 78.77, 78.07, 76.52, 76.16. These features are slightly temperature and solvent dependent as the ³¹P{¹H} NMR spectrum in toluene-*d*₈ solution at –68 ° has peaks at δ 77.46, 76.88, 75.79, and 74.96. ¹H NMR spectra at 500 MHz, 5 °C in cyclohexane-*d*₁₂ show a complex pattern in the hydride region with resonances clustered at δ –3.77, –13.23, and –22.55. The three resonances have equal integrations, and a ¹H COSY spectrum indicates that they are all coupled. At 70 °C the two lower-field hydride region vanish and a broad high-field resonance is observed at δ –22.73

We were able to obtain X-ray quality crystals by dissolving the crude reaction mixture in pentane and cooling to –35 °C. The X-ray crystal structure in Figure 35

reveals a dimeric structure **10**, where each Ir center is κ^2 -bound to a dippe ligand. The structure was refined with the constraints of one bridging and two terminal hydrides for each Ir center using distances from the calculated structures. The bridging hydride was fixed with the shorter Ir–H distance. The hydride formulation is consistent with the hydride resonances in the high temperature NMR spectra (vide infra).

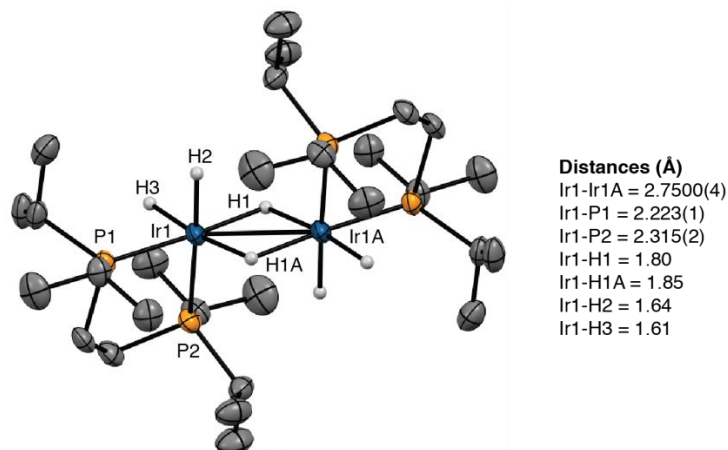


Figure 35. X-ray structure for compound **10** with thermal ellipsoids calculated at 50% probability levels. Hydride ligands are shown and other hydrogens are omitted for clarity, selected experimental metric parameters are given

Calculations starting from the X-ray coordinates refine to a similar structure with a slight elongation of the Ir–Ir distance (Figure 36). Attempts to calculate the structure as $[(\text{dippe})\text{IrH}(\mu\text{-H})]_2$ with one terminal and one bridging hydride gave geometries where the non-hydrogen atoms were shifted significantly from the crystallographically determined positions.

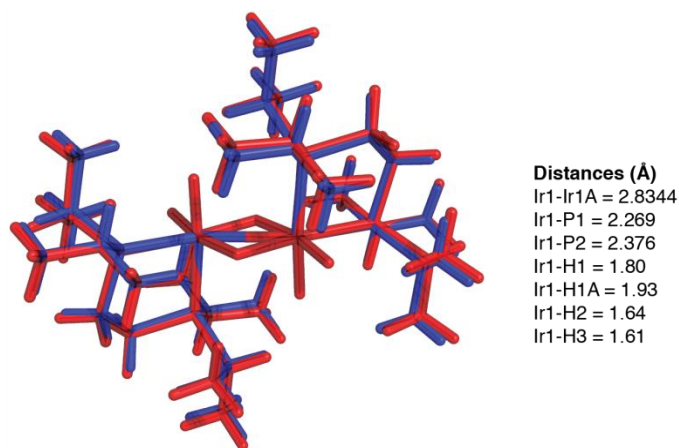


Figure 36. The calculated structure (red, M06//SDD/6-31G*) is overlaid with crystallographic coordinates. Selected computational metric parameters are given

As was discussed before we start the reaction by using compound **5** as catalyst but in the catalytic reaction condition compound **6**, **7**, **8**, **9** and finally **10** will be formed. Figure 37 is demonstrating the $^{31}\text{P}\{^1\text{H}\}$ NMR spectra of catalyst during the course of reaction.

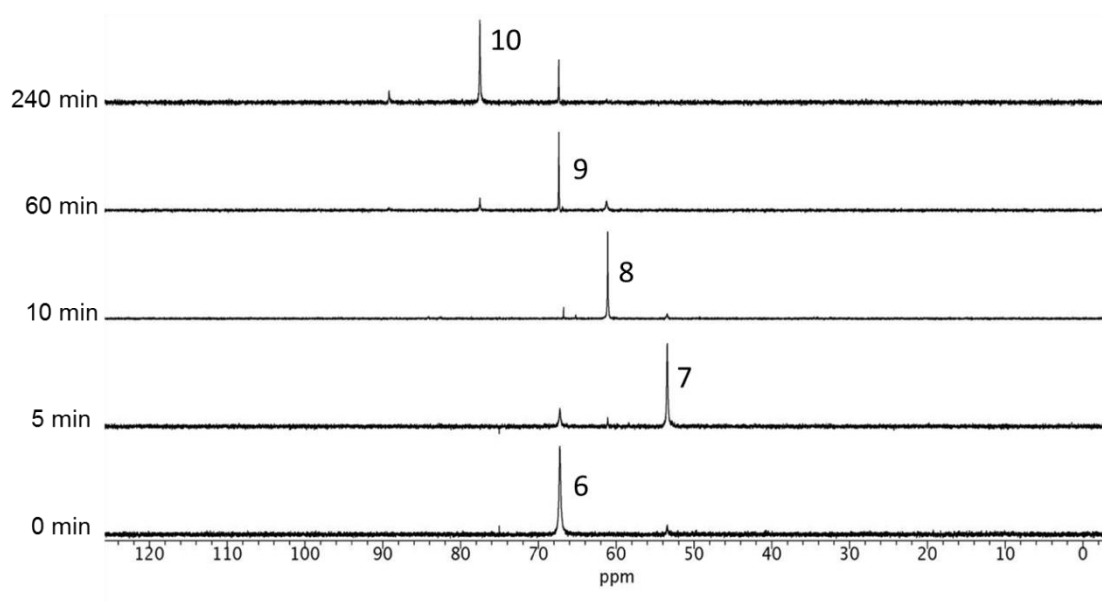


Figure 37. $^{31}\text{P}\{^1\text{H}\}$ NMR spectra showing catalysts evolution during the reaction

To verify the relationship between compounds **5**, **7**, **8**, **9**, and **10**, an independent NMR experiment was performed. When a NMR tube containing a toluene-*d*₈ solution of compound **5** precooled in liquid nitrogen bath and then was briefly exposed to H₂, ³¹P{¹H}, and ¹H NMR spectra at –45 °C show that compound **7** is the major species in solution along with compound **8**. ³¹P NMR spectra with selective decoupling of the aliphatic ¹H region give a broad triplet at δ 53.56, which approves that two high-field Hs are chemically equivalent on the NMR time scale in compound **7**. When the NMR tube was removed from the spectrometer and shaken to dissolve H₂ in the headspace, compound **8** became the dominant species in solution. By repeating this process, compound **8** was transformed to compound **9**. Lastly, equilibration of compounds **8** and **9** with compound **10** was demonstrated by removing the H₂ from an NMR tube where catalytic borylation was complete, leaving compound **10** as the major species. Addition of HBpin to the solution regenerated compounds **8** and **9**.

Discussion

Compound **5** joins a handful of complexes that react directly with C–H bonds without requiring prior ligand dissociation¹³⁻¹⁴ and is a rare example of square pyramidal 16-electron d⁶ complexes.¹⁵ In accord with the tenet that true reactive intermediates are rarely observed under catalytic conditions,¹⁶ compound **5** reacts with HBpin to form a more stable initial resting state in 18-electron borylene compound **6**, and compound **5** is not detected as an intermediate during catalysis. If compound **6** were the only resting state during catalysis and compound **5** were the only C–H activating intermediate, C–H borylation would be inhibited by HBpin since compound **5** is generated from compound **6** by its dissociation. This is not observed experimentally, as the H₂ generated during C–H

borylation sequentially shifts the resting state to 18-electron compounds **7**, **8**, and **9**. Thus, these complexes are more stable than borylene compound **6**.

^1H NMR spectroscopy yields important information about the 18-electron catalytic resting states **7**, **8**, and **9**. Significantly, the inequivalent hydride/borane/boryl positions indicated in the solid state structures of compounds **8** and **9** are exchanging rapidly on the NMR time in solution. In addition, a single methine resonance for the dippe isopropyl groups is observed even though the crystal structures in Figures 30 and 31 feature chemically distinct methine environments. These exchanges are intramolecular, since coupling to ^{31}P is maintained, and exchange with free HBpin is not observed. The dynamic behavior suggests that minima in the potential energy surface are relatively shallow, which is supported by the fact that compound **8** crystallizes with structures where the orientations of the ligands differ significantly. Figure 38 shows a pathway where equilibration of $\sigma\text{-HBpin}$ and $\sigma\text{-H}_2$ intermediates would exchange the hydride ligands in structure **8b**.

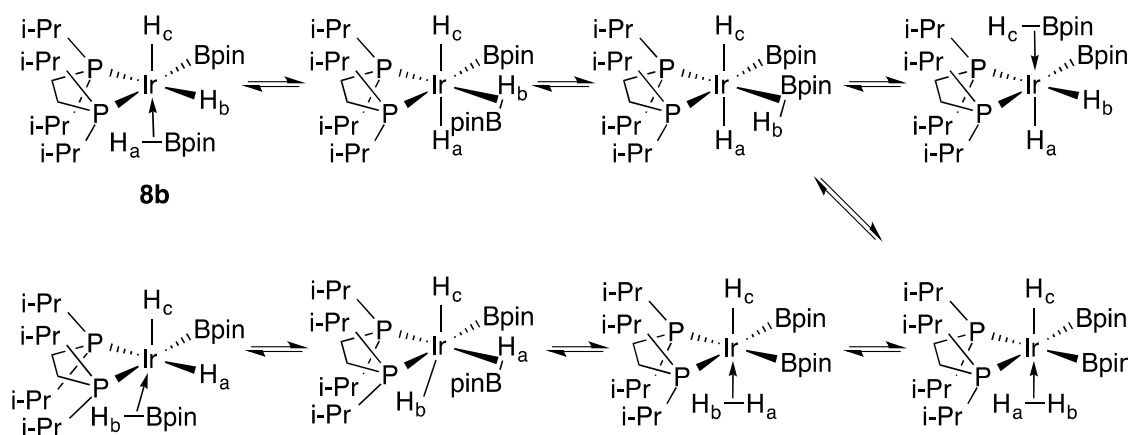


Figure 38. Putative equilibria for hydride exchange in compound **8**

Similar mechanisms have been proposed to account for exchange in $(\kappa^3\text{-C}_6\text{H}_3\text{-1,3-}[\text{OP}(t\text{Bu})_2]_2)\text{IrH}_2(\eta^2\text{-HBpin})$.^{10,17} Calculations support σ -borane complexation in

compounds **8** and **9**, which would account for the broadening of high field resonances in the ^1H NMR spectra of these compounds.

Compound **10** is related to other Ir phosphine complexes with bridging hydrides. The most relevant compound is $[(\text{dfepe})\text{Ir}(\mu\text{-H})(\text{H})_2]_2$ (**11**, $\text{dfepe} = (\text{C}_2\text{F}_5)_2\text{PCH}_2\text{CH}_2\text{P}(\text{C}_2\text{F}_5)_2$).¹⁸ The $[(\text{diphosphine})\text{Ir}]_2$ frameworks of compounds **10** and **11** are very similar, although the latter compound is disordered in the solid state. As in compound **11**, the Ir–P distance in **10** for the phosphorus trans to the terminal hydride (2.315(2) Å) is significantly longer than the distance for the phosphorus trans to the bridging hydride (2.223(1) Å). This is consistent with the strong trans influence for terminal hydrides.

In contrast, the spectroscopic features for compound **10** differ from those for compound **11**. Both ^1H and $^{31}\text{P}\{^1\text{H}\}$ NMR spectra (toluene- d_8 solutions) for compound **10** are more complicated than would be expected for a static structure analogous to that in Figure 35. At 25 °C, the resonances in the hydride and methine regions for compound **10** are relatively broad, suggesting dynamic behavior for compound **10**. At lower temperatures, the hydride resonances sharpen, and at –68 °C, the methine resonance begins to decoalesce with two broad peaks near δ 3.6. At higher temperature, the methine peaks coalesce to a broad resonance at δ 2.5. This implies that a second set of methine resonances should appear near δ 1.4 in the low temperature spectrum, where four methine resonances would be expected for the structure in Figure 35, but these are obscured by other features. At low temperature, the hydride region (Figure 39) is complex—particularly for the feature at $\sim \delta$ –13.

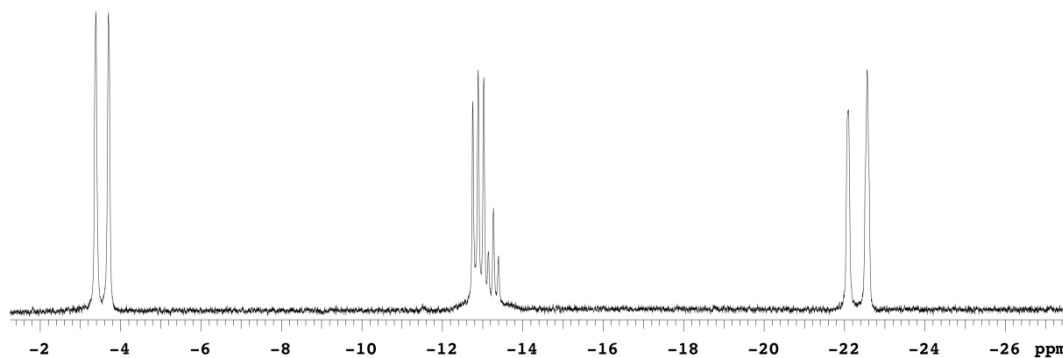


Figure 39. ^1H NMR spectrum (500 MHz, toluene- d_8 , $-5\text{ }^\circ\text{C}$) of the hydride region for compound **10**

We originally questioned whether a trace impurity gives rise to the triplet at $\delta -13.06$, but this feature persisted when compound **10** was prepared independently from compound **9**, generated in situ from compound **5** and H_2 , and 3 equiv of MeOH. At low temperature, the ^{31}P NMR spectrum for compound **10** has four absorptions between δ 78.72 and 76.15 for the phosphorus nuclei, whereas compound **11** has a singlet at δ 84.3. The phosphorus atoms in the crystal structure of compound **10** (Figure 35) are clearly chemically inequivalent. Therefore, P-P coupling would be expected. Because the chemical shift differences are of similar energies to the expected coupling, we considered whether the $^{31}\text{P}\{^1\text{H}\}$ and ^1H NMR spectra reflected second-order coupling. However, the spectra could not be successfully simulated. The ^1H COSY spectrum for compound **10** indicates coupling between the features at $\delta -3.33$, -13.00 , and -22.12 , but selective decoupling of specific hydride resonances did not simplify the other hydride resonances. Thus, H-H couplings are small. Selective ^{31}P decoupling showed that the resonance at $\delta -3.33$ is a doublet ($|^2J_{\text{PH}}| = 166\text{ Hz}$). In contrast, the apparent doublet centered at $\delta -22.12$ did not collapse when the ^{31}P resonances were irradiated, indicating that the two resonances at $\delta -21.83$ and -22.40 represent two hydride environments this is consistent

with the observed spectra arising from two conformations with similar populations and the same formula as compound **10**. From chemical shifts, we assign the resonances for compound **10** at δ -3.33 and -13.00 to terminal hydrides, and the resonances at δ -21.83 and -22.40 to bridging hydrides. This assignment is based on compound **11**, where the terminal hydrides appear as doublet at δ -7.09 ($|^2J_{\text{PH}}| = 149$ Hz)—the approximate the average chemical shift of the two lower field hydride resonances in compound **10**—and the bridging hydrides are assigned to a resonance at δ -21.90.

When the temperature is raised, the hydride resonances in the ^1H NMR spectrum broaden, and at 70 °C the resonances clustered at δ -3.33 and -13.00 vanish, which would be consistent with exchange between these hydrides, as is the case for compound **11**. In addition, the ^{31}P resonances coalesce to a single resonance at δ 76.68. This supports exchange between the conformations observed at lower temperatures. Coalescence of the lower field hydride resonances was not observed, because compound **10** converts to a new species at higher temperatures. This is indicated by a new major ^{31}P NMR peak at δ 87.91 and ^1H NMR peaks at δ -6.80 (dd), -12.33 (br), and -13.01 (br), which integrate as 2:1:2. While it is tempting to assign this as a pentahydride structure of the formula (dippe)IrH₅, it is unclear what the sources of H₂ would be, and there is a broad feature in the ^{31}P NMR spectrum at $\sim \delta$ 63 that we cannot assign. We have insufficient data to definitively assign a structure for this species.

Of the intermediates observed in the catalytic reaction, the ligation of H and Bpin ligands in compound **7** can only be tentatively assigned without a crystal structure. Forms **7a-c** is possible (Figure 40). Access to structures **7a** and **7b** would lead to B-H coupling, which would account for the relatively broad hydride resonance for compound **7**.

Equilibration with structure **7c** allows for exchange if **7a** or **7b** are minimum energy structures. If **7c** is the lowest energy structure, the equivalence of the H positions is directly accounted for. Access to structure **7c** could also be relevant to catalysis (Figure 27), as H₂ dissociation would generate C-H borylation intermediate **5**.

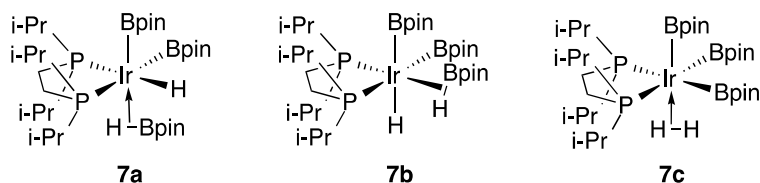


Figure 40. Possible structures for compound **7**

The shift in catalyst resting structures can be understood in terms of equilibria of boryl complexes and H₂, whose concentration increases throughout the reaction. As shown in Figure 41, H₂ equilibration with boryl complexes generates HBpin and hydride intermediates with successive substitution of H for Bpin at the Ir center.

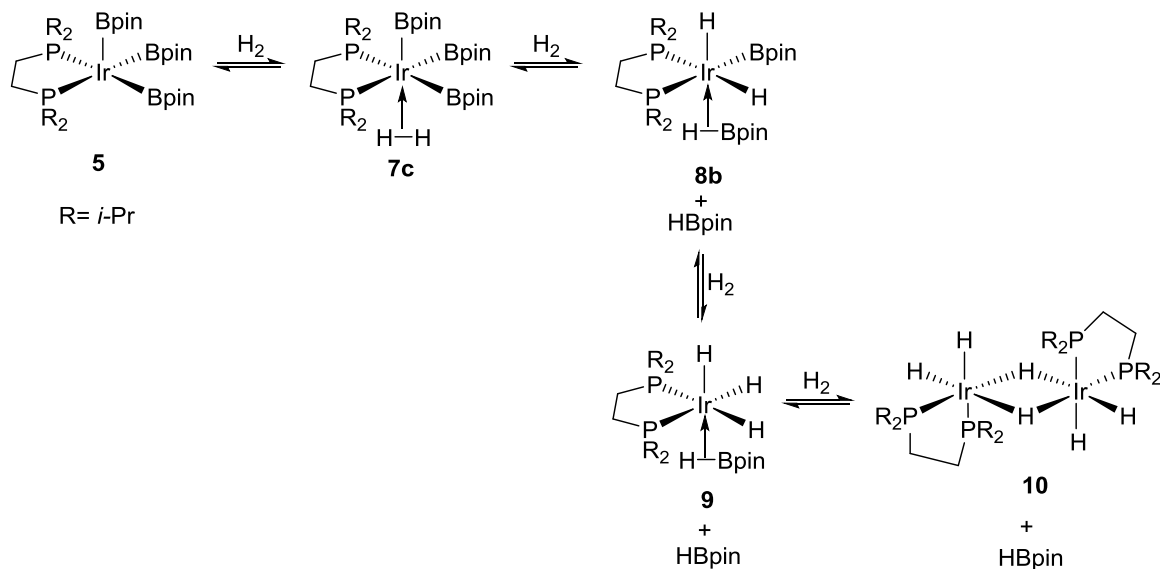


Figure 41. H₂ induced equilibria by H₂ addition to compound **5**

If C–H borylation funnels exclusively through intermediate **5**, H₂ generation would significantly inhibit catalysis. This is not the case as borylation proceeds smoothly until compound **10** is the dominant solution species. Maintenance of borylation activity while compounds **7**, **8** and **9** have significant concentrations can be reconciled if these species are resting states for catalytically competent tris (**5**), bis (**12**), and monoboryl (**13**) intermediates that operate in parallel catalytic borylation cycles, with similar borylation rates, as shown in Figure 42. This behavior is reminiscent of the stoichiometric reactivity of bipyridine-ligated compound **3**, which reacts to generate diborylhydride and monoboryldihydride complexes in reactions with arenes.¹ Potential roles for these complexes in catalysis were not examined, and trihydride complexes were not reported.

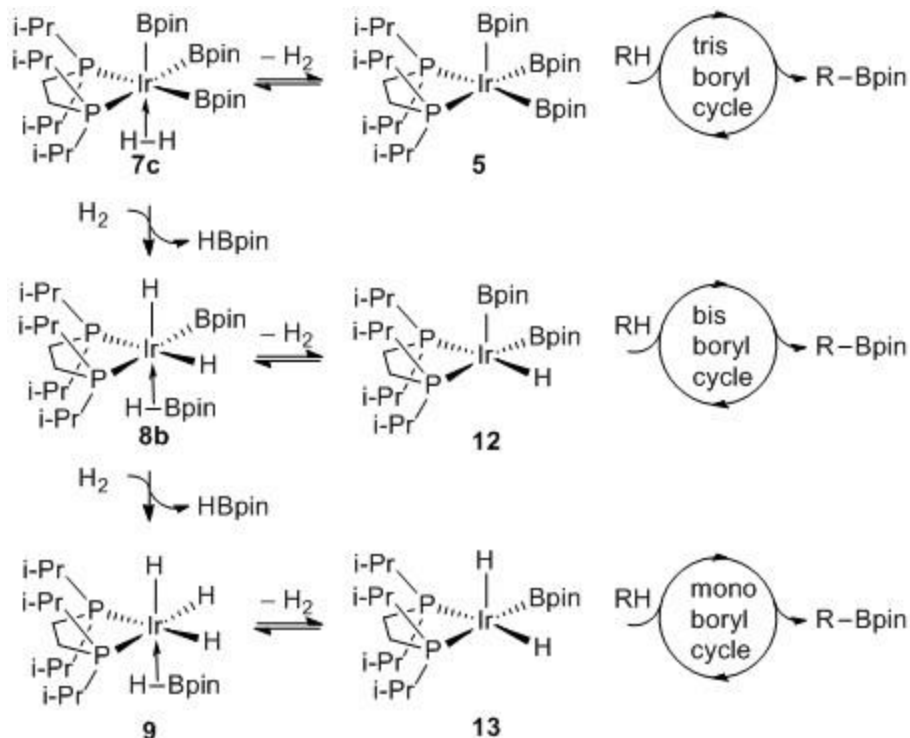


Figure 42. Parallel catalytic cycles for C–H borylation

Conclusions

The fact that compound **5** react directly with $\text{sp}^2\text{-C-H}$ bonds provides a rare opportunity for examining the fundamental step in C-H borylation. The combination of ^{31}P and ^1H NMR spectroscopy, X-ray crystallography, and theory makes it possible to characterize multiple resting states and to assess their roles under catalytically relevant conditions. Although catalysts with bidentate nitrogen donors have been used more extensively, recent chemistry of phosphine-ligated catalysts suggests that they have as yet unrealized potential.¹⁹⁻²¹ The work described herein provides a foundation for understanding catalysis in this family of compounds, which may aid in designing new borylation catalysts.²²

REFERENCES

REFERENCES

1. Cho, J. Y.; Tse, M. K.; Holmes, D.; Maleczka, R. E., Jr.; Smith, M. R., III *Science* **2002**, 295, 305.
2. Boller, T. M.; Murphy, J. M.; Hapke, M.; Ishiyama, T.; Miyaura, N.; Hartwig, J. F. *J. Am. Chem. Soc.* **2005**, 127, 14263.
3. Haines, B. E.; Saito, Y.; Segawa, Y.; Itami, K.; Musaev, D. G. *ACS Catal.* **2016**, 6, 7536.
4. a) Nguyen, P.; Blom, H. P.; Westcott, S. A.; Taylor, N. J.; Marder, T. B. *J. Am. Chem. Soc.* **1993**, 115, 9329. b) Nguyen, P.; Blom, H. P.; Westcott, S. A.; Taylor, N. J.; Marder, T. B. *J. Am. Chem. Soc.* **1993**, 115, 9329. c) Chotana, G. A.; Vanchura, B. A., II; Tse, M. K.; Staples, R. J.; Maleczka, R. E., Jr.; Smith, M. R., III *Chem. Commun.* **2009**, 5731.
5. Iluc, V. M.; Miller, A. J. M.; Anderson, J. S.; Monreal, M. J.; Mehn, M. P.; Hillhouse, G. L. *J. Am. Chem. Soc.* **2011**, 133, 13055.
6. Mindiola, D. J.; Hillhouse, G. L. *J. Am. Chem. Soc.* **2001**, 123, 4623.
7. Ghayoor Abbas Chotana, Iridium Catalyzed Aromatic Borylation and Its Applications in One-Pot Preparations of Substituted Aromatic Building Block, Michigan State University, Ph.D dissertation, **2009**.
8. Britt Andrew Vanchura, Stable Five-coordinate Trisboryl Analogs of Proposed Reactive Intermediates in Ir-Mediated C–H Borylations, Michigan State University, Ph.D dissertation, **2010**.
9. Braunschweig, H.; Dewhurst, R. D.; Gessner, V. H. *Chem. Soc. Rev.* **2013**, 42, 3197.
10. Hebden, T. J.; Denney, M. C.; Pons, V.; Piccoli, P. M. B.; Koetzle, T. F.; Schultz, A. J.; Kaminsky, W.; Goldberg, K. I.; Heinekey, D. M. *J. Am. Chem. Soc.* **2008**, 130, 10812.
11. Braunschweig, H.; Shang, R. *Inorg. Chem.* **2015**, 54, 3099.
12. Alcaraz, G.; Helmstedt, U.; Clot, E.; Vendier, L.; Sabo-Etienne, S. *J. Am. Chem. Soc.* **2008**, 130, 12878.

13. Thompson, M. E.; Baxter, S. M.; Bulls, A. R.; Burger, B. J.; Nolan, M. C.; Santarsiero, B. D.; Schaefer, W. P.; Bercaw, J. E. *J. Am. Chem. Soc.* **1987**, *109*, 203.
14. Watson, P. L. *J. Am. Chem. Soc.* **1983**, *105*, 6491.
15. Lam, W. H.; Shimada, S.; Batsanov, A. S.; Lin, Z.; Marder, T. B.; Cowan, J. A.; Howard, J. A. K.; Mason, S. A.; McIntyre, G. J. *Organometallics* **2003**, *22*, 4557.
16. Halpern, J. *Science* **1982**, *217*, 401.
17. López, A. M.; Mora, M.; Oñate, E. *Organometallics* **2015**, *34*, 941.
18. Schnabel, R. C.; Carroll, P. S.; Roddick, D. M. *Organometallics* **1996**, *15*, 655.
19. Saito, Y.; Segawa, Y.; Itami, K. *J. Am. Chem. Soc.* **2015**, *137*, 5193.
20. Ghaffari, B.; Preshlock, S. M.; Plattner, D. L.; Staples, R. J.; Maligres, P. E.; Krska, S. W.; Maleczka, R. E., Jr.; Smith, M. R., III *J. Am. Chem. Soc.* **2014**, *136*, 14345.
21. Press, L. P.; Kosanovich, A. J.; McCulloch, B. J.; Ozerov, O. V. *J. Am. Chem. Soc.* **2016**, *138*, 9487.
22. This work was previously published as a journal publication. Ghaffari, B.; Vanchura, B. A.; Chotana, G. A.; Staples, R. J.; Holmes, D.; Maleczka, R. E.; Smith, M. R. *Organometallics* **2015**, *34*, 4732.

CHAPTER 3 – SILYL PHOSPHORUS AND NITROGEN DONOR CHELATES FOR HOMOGENEOUS ORTHO BORYLATION

Directed Aromatic Functionalization

As stated in Chapter 1, steric factors control the regioselectivities of products obtained from Ir catalyzed C-H borylation of aromatics. Recently, chemists have been developing the methods that can complement steric direction. There have been several examples where borylation occurs ortho to a carbonyl via inner sphere chelate directed C-H borylation.

In 2000, Smith and coworkers reported borylation of benzamide using $\text{Cp}^*\text{Rh}(\eta^4\text{-C}_6\text{Me}_6)$, with ortho: meta: para ratio 4:2:1.¹ In 2008, Hartwig and Boebel described the first examples of Ir-catalyzed ortho CHB using silyl as a directing group.²

More recently, Maleczka, Singleton, and Smith proposed that hydrogen bonding interactions between protected aniline N-H bonds and Bpin O atoms account for ortho CHB of certain anilines.^{3,4}

Other examples of directed ortho CHB are chelate-assisted functionalizations. The first was reported by Ishiyama and Miyaura where ortho CHB of esters was possible when Ir catalysts were generated with electron deficient monodentate phosphines.⁵ Chelate directed ortho CHBs require two readily accessible metal coordination sites. The DMG coordinates to one of them, while the second vacant site assists in C-H scission. Bulky and electron deficient phosphine undergoes the ligand dissociation to provide the second vacant coordination site and then ortho directed functionalization can occur (Figure 43).

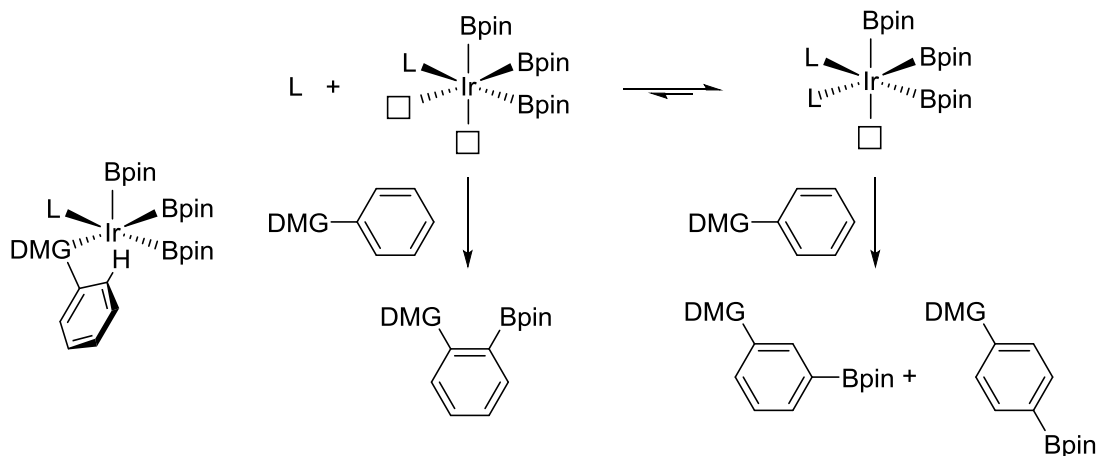


Figure 43. Chelate assisted mechanism for bulky, electron deficient monodentate phosphine

Lassaletta has reported N-directed ortho-borylations of phenylpyridines using diimine ligands, while this system works very well, unfortunately the substrate scope is limited to phenylpyridines (Figure 44).^{6,7}

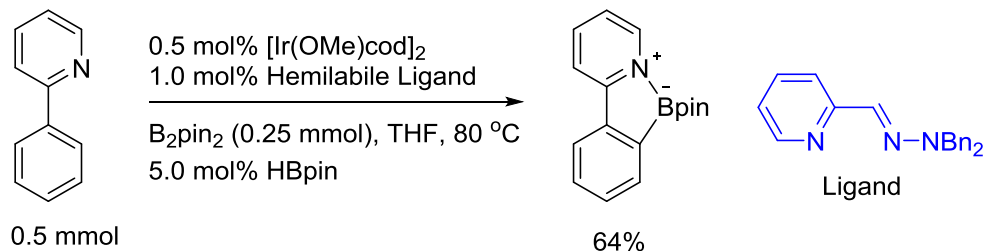


Figure 44. Ortho borylation of phenylpyridine using hemilabile ligand

Ito and Ishiyama have reported ortho borylations of ketones;⁸ and Clark and coworkers have revealed borylations of benzylamines and phosphines.^{9,10} Although detailed kinetic studies have not been reported, mechanism where two coordination sites in the catalyst are available to the substrate, are most probable (Figure 45). One site enables coordination of a directed metalating group (DMG) while the other is necessary to cleave the ortho C–H bond.

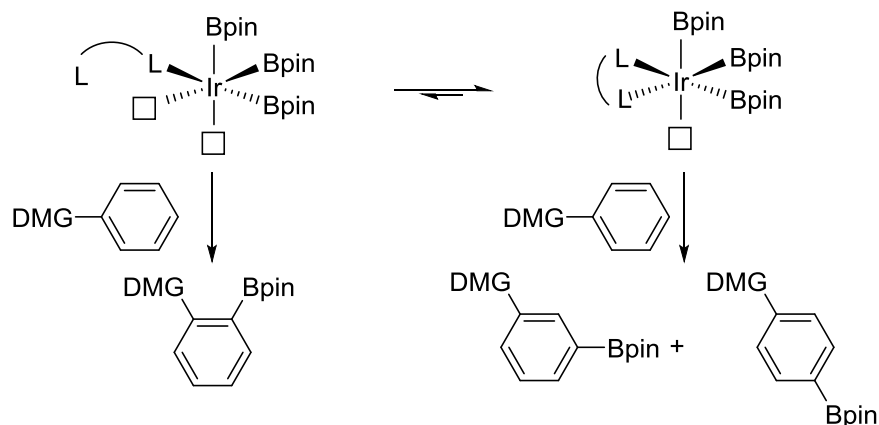


Figure 45. General chelate assisted mechanism for homogenous borylation

While the substrate scope for homogeneous ortho-directed iridium catalyzed borylation is limited, Sawamura pioneered heterogeneous Ir-catalyzed borylations with a broad scope for ortho directed borylations.¹¹⁻¹⁵

Results

Thus, we sought an appropriate ligand framework for homogeneous catalysis that could mimic these heterogeneous catalysts. Given that tridentate PSiP pincer ligands have been utilized in C–H borylation,¹⁶ we were hopeful that bidentate Si–P ligands could generate structures **14**, where the silyl ligand replaces a spectating boryl (Figure 41).

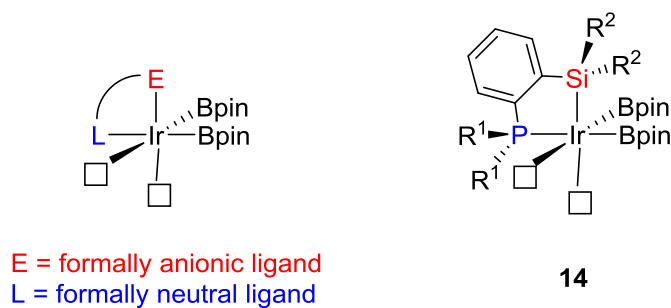


Figure 46. Designing a bidentate, monoanionic ligand.

Silane metathesis with a boryl ligand would steer the phosphine to the metal center to generate intermediates (**14**) with accessible coordination sites. In contrast to other homogeneous approaches where electron deficient ligands are used to achieve coordinative unsaturation, our strategy would create an electron rich framework that facilitates C–H cleavage.¹⁷ If this approach proved to be viable, the ligand framework could be modified in substantive ways. For example, silanes with pendant N-donors (or other basic ligands) could be targeted.

To test our idea, we prepared ligand **15** (Figure 47), using a protocol related to the synthesis of (2-diphenylphosphinophenyl)diphenylsilane.¹⁸ The synthesis is straightforward, modular, and scalable to gram quantities.

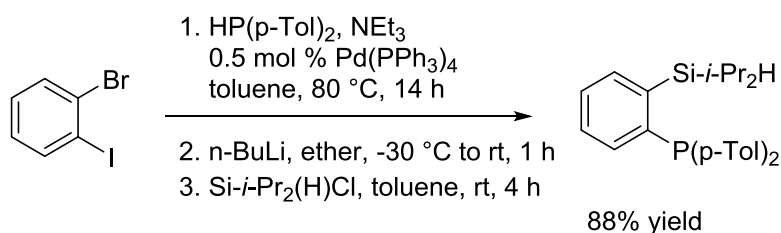


Figure 47. Designing a bidentate, monoanionic ligand

With **15** in hand, we tested it for the C–H borylation of methylbenzoate. Table 1 shows the results compared to those obtained for catalysts generated from $[\text{Ir}(\text{OMe})(\text{cod})]_2$ and $\text{P}(3,5\text{-bis}(\text{trifluoromethyl})\text{phenyl})_3$ (PAr^{F}_3) or triphenylarsine, which have both been used in directed borylations. As can be seen in entry 1, ligand **15** allows for the full conversion of B_2pin_2 and some of the generated HBpin, while the PAr^{F}_3 and AsPh_3 give considerably lower conversions. In contrast, silica-SMAP ligated Ir catalysts are significantly more active.

Table 1. Comparison of catalyst efficiency for ortho-borylation

0.5 mmol

1 equiv B₂pin₂
1.25 mol% [Ir(OMe)(cod)]₂
2.5 mol% ligand

THF, 3h, 80 °C

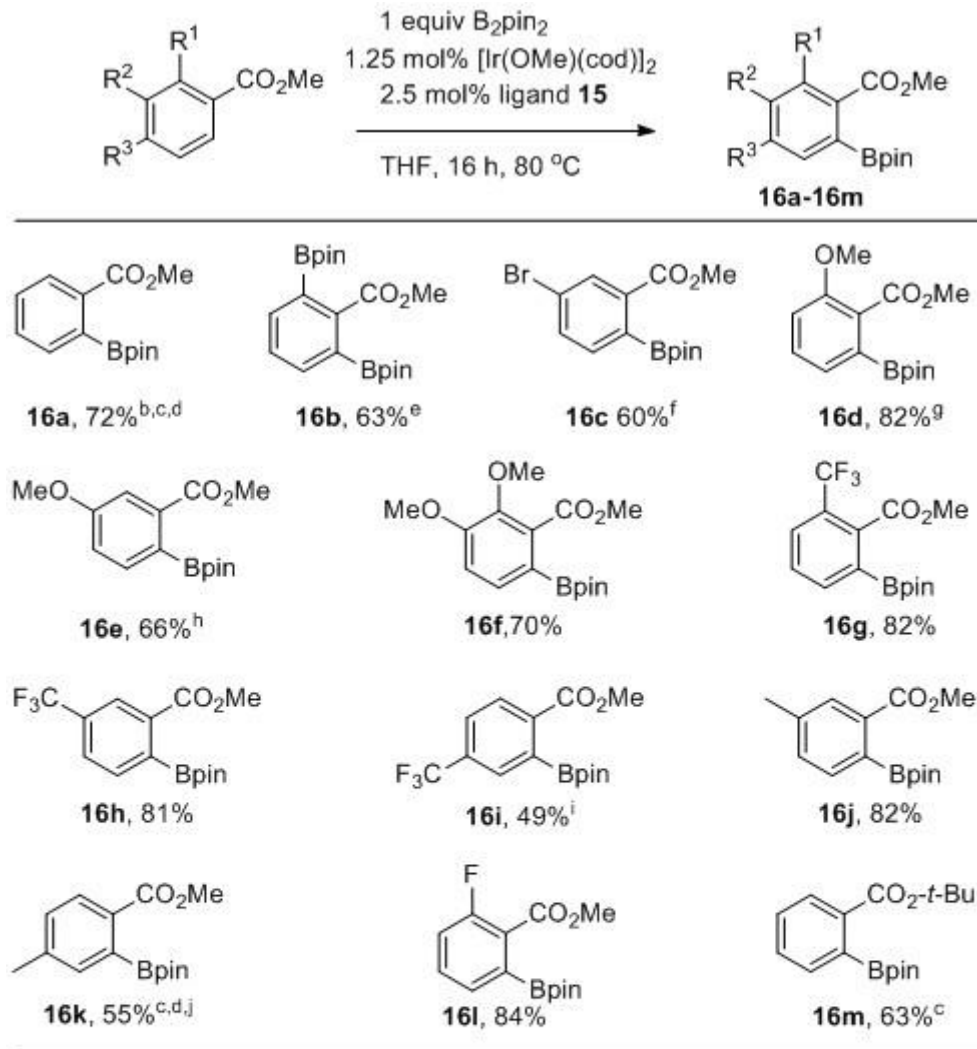
16a + **16b**

Entry ^a	Ligand	% 16a ^b	% 16b ^b	% Conversion ^c
1	SiPbz	63	24	111
2	PArF ₃	2	1	4
3	AsPh ₃	44	3	50
4 ^e	Silica-SMAP	101 ^f	4 ^f	109 ^d

^aReactions run on 0.5 mmol scale in 0.5 mL THF. ^b% Conversions determined by GC integration. ^c% Conversion is calculated as %**16a** + 2(%**16b**) and is based on B₂pin₂ as limiting reagent. ^dConversion exceeds 100% because some of the HBpin generated from B₂pin₂ participates in the borylation. ^eData are from ref. 11. Reaction run at 25 °C with 1 mmol methylbenzoate, 0.5 mmol B₂pin₂, 0.5 mol % silica-SMAP-Ir(OMe)(cod) in 1.5 mL hexane. ^fYields were determined by ¹H NMR spectroscopy.

With promising preliminary data in hand, we explored a number of substituted methyl benzoates these are shown in Table 2. The reactions were performed under identical conditions and reaction times were not optimized.

Table 2. Ortho-borylation of alkylbenzoates.^a



^aReactions were run with 1.0 mmol substrate, 1.0 mmol B₂pin₂, 0.025 mmol **15**, and 0.0125 mmol [Ir(OMe)(cod)]₂ in 1.0 mL THF. Yields are for isolated materials. ^b2.0 mmol substrate was used, 5% diborylated product was isolated. ^c0.5 mol% [Ir(OMe)(cod)]₂ was used. ^dReaction was run at 60 °C. ^e2.0 mmol B₂pin₂, 0.025 mmol [Ir(OMe)(cod)]₂, and 0.050 mmol **5** were used. ^f0.5 mmol substrate was used. ^g1.25 mmol B₂pin₂ was used. ^h5% diborylated material was isolated. ⁱ17% diborylated material was isolated. ^j10% di-borylated material was isolated

Yields range from fair to excellent with the lowest yields corresponding to methylbenzoates that were only substituted at the 4-position. For these substrates, significant amounts of 2,6-diborylated compounds form, which accounts for the diminished yield of monoborylated products **16i** and **16k**. Some diborylation was also observed in the synthesis of **16e**. It is noteworthy that lowering the catalyst loading to 0.5 mol % and reducing the temperature to 60 °C gave a 6% yield increase for **16k**. In addition, diborylation is not observed for *t*-butylbenzoate in contrast to methylbenzoate. Lastly, the selectivity difference for ligand **15** relative to 4,4'-di(*t*-butyl)bipyridine (dtbpy) is highlighted in Figure 48, where different regioisomers are obtained in the borylations of 2-fluoro-4-bromomethylbenzoate.

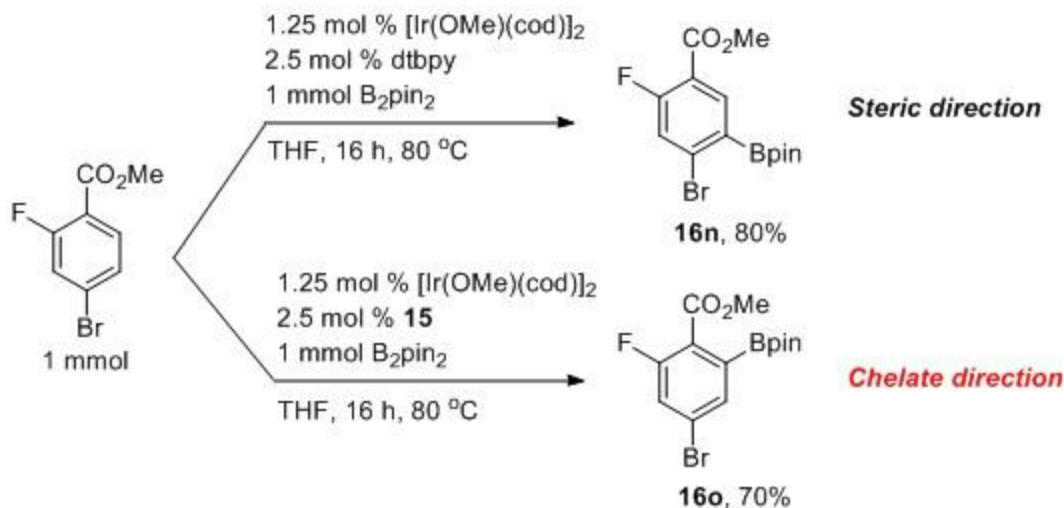
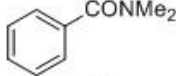
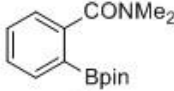
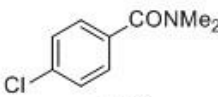
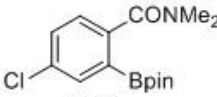
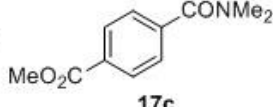
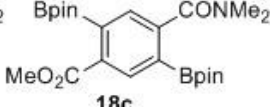
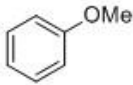
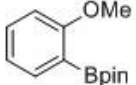
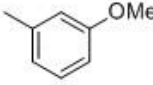
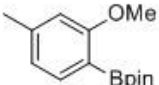
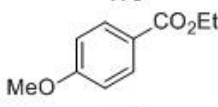
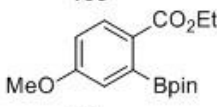
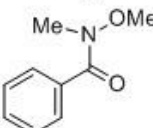
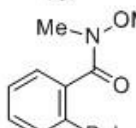
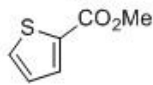
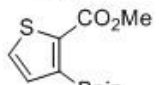
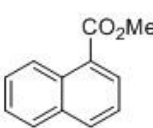
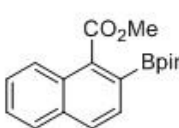
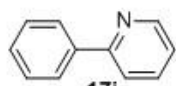
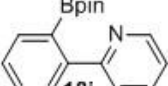


Figure 48. Ligand dependent borylation regioselectivity

Given the results in Table 2, we further explored the scope with respect to substrate and directing group, and the results are given in Table 3. Entry 1 shows that unsubstituted benzamides give excellent conversions to monoborylated substrates without resorting to using excess arene to minimize diborylation as is required for methyl

benzoate. Entry 2 shows that the amide DMG trumps Cl direction. In fact, chlorobenzene does not give ortho borylated product with **15**, contrasting the high ortho selectivity for Ir-SMAP catalysts. In entry 3, diborylated product **18c** was obtained. When 1 equiv B₂pin₂ was used with **17c**, selectivity for borylation ortho to the amide vs. the ester was 4.2:1. Entries 4 and 5 show that OMe can direct borylation to the ortho position, albeit in modest yield. This sets the chemistry of catalysts generated from ligand **15** apart from that of silica-SMAP, where borylation of **17d** gives a 1:1 ratio of *o*:*m*+*p* borylated products. Entry 6 shows that esters are stronger DMGs than OMe, which is in line with SMAP supported catalysts. In entry 7, Weinreb amide **17g** is converted cleanly to ortho-borylated product **18g**. Borylation of 1-methylnaphthoate, **17i**, gives a single isomer where functionalization of the β -C-H bond is favored over the γ -C-H position. Borylation of thiophene substrate **17h** at 60 °C gave slightly better selectivity (14:1) for 3 vs. 5-borylated products than that reported for the borylation with Ir-SMAP catalysts (9:1 at 80 °C). In contrast to the SMAP system, where the Ir catalysts are ineffective for borylation of **17j**, borylation gives the products obtained by Lassaletta using hemilabile N,N ligands.^{8a} Our reaction was performed at a lower temperature (60 vs. 80 °C) and a shorter reaction time (2 vs. 48 h). This was offset by a higher catalyst loading in our study (1.25 mol % vs. 0.5 mol %) and the formation of ~ 15% di-orthoborylated product. With 2.0 equiv B₂pin₂, this was the major product (Table 3).

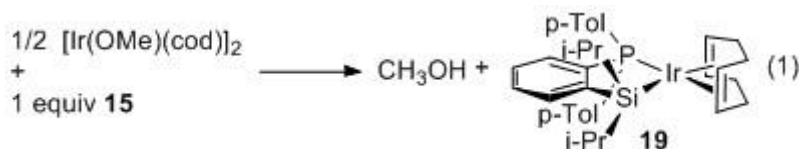
Table 3. Borylations with **15**/[Ir(OMe)(cod)]₂ catalyst

Substrate		1.25 mol% [Ir(OMe)COD] ₂ 2.5 mol% 15, solvent 1 mmol B ₂ pin ₂ , 60-80 °C →		Product	
entry	substrate	product	T(°C)	time (h)	% yield
1	 17a	 18a	80	16	75 ^b
2	 17b	 18b	80	16	85 ^b
3	 17c	 18c	100	16	95 ^{b,c}
4	 17d	 18d	100	12	55 ^{b,d}
5	 17e	 18e	100	12	35 ^b
6	 17f	 18f	80	12	77 ^e
7	 17g	 18g	80	12	84 ^b
8	 17h	 18h	60	1	65 ^e
9	 17i	 18i	80	8	85 ^e
10	 17j	 18j	60	2	65 ^{e,f}

^aTypically reactions were run on 1 mmol scale with equimolar B₂pin₂ and substrate with 2.5 mol% **15**, and 1.25 mol% [Ir(OMe)(cod)]₂. Unless noted, yields are for isolated materials. ^bReaction solvent was THF. ^c2.0 equiv B₂pin₂ was used. ^dGC-conversion with a 6:1:2 ratio of o:m+p:diborylated products. ^eReaction solvent was n-hexane, mixture of 14:1 of 2 and 3-isomer was obtained. ^fApproximately 15% of the crude mixture was the di-orthoborylated compound

The generation of active catalyst from **15**, B₂pin₂, and [Ir(OMe)(cod)]₂ raises interesting questions with regard to how an Ir–Si bond is generated, if it is formed at all. Several literature reports describe the metathesis of M–OR and Si–H bonds to make M–H and Si–OR products. However, silane directed borylations invoke M–B/Si–H metatheses to generate M–Si and B–H bonds. Thus, we considered that initial formation of Ir–Bpin intermediates and subsequent Ir–B/Si–H metathesis could account for the formation of intermediates such as **14**.

Nevertheless, we performed a control experiment where **15** and [Ir(OMe)(cod)]₂ were reacted. ³¹P and ¹H NMR indicate rapid and quantitative conversion to compound **19** and methanol—an unprecedented reaction for a silane with a metal alkoxide (Eq 1).



This is critical for establishing a 1:1 ratio of **15**: Ir, which is the key to creating sites for DMG coordination and C–H activation as posited for structure **14**. The structure of **19** was confirmed by X-ray crystallography and is shown in Figure 49.

Using the centroids of the cod bound carbons as coordinates, the sum of the angles about Ir is 370°, which is close to the value for square-planar Ir^I. The Ir–C and C–C distances for the carbons trans to Si are significantly longer than those for carbons trans to P, which is consistent with strong donation from Si to Ir.

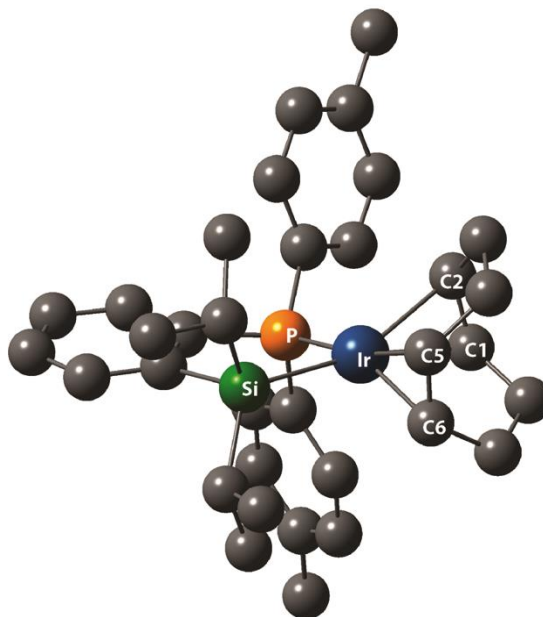


Figure 49. Crystal structure of compound **19** with H atoms omitted

Selected distances (Å) and angles (°): Ir–Si (2.376(2)), Ir–P (2.260(2)), Ir–C1 (2.246(8)), Ir–C2 (2.217(8)), Ir–C5 (2.194(8)), Ir–C6 (2.161(8)), C1–C2 (1.386(12)), C5–C6 (1.357(13)), P–Ir–Si (83.53(6)), P–Ir–centroid_{C1–C2} (96.72), Si–Ir–centroid_{C5–C6} (95.39), centroid_{C1–C2}–Ir–centroid_{C5–C6} (85.25)

Even so, some substrates proved to be challenging for borylations carried out with ligand **15**. For example, carbamates react sluggishly, and ketones give significant amounts of ketone reduction. Since Ir catalysts supported by N-donor ligands in most cases prove to be more reactive than their P-donor counterparts,¹⁹ we reasoned that an N-donor analog of **15** might exhibit better reactivity with carbamates and ketones. Thus, quinoline based ligand **20** was prepared, and Ir catalysis with this ligand was evaluated relative to ligand **15** for compounds **21a** and **21b**.^{20,21}

As shown in Table 4, ligand **20** outperforms its phosphine analog **15** for borylations of **21a** and **21b**. In the case of carbamate **21a**, we see higher conversion, but slightly lower isolated yield to that reported by Sawamura for the related diethylcarbamate substrate. Perhaps more significantly, catalysis with **20** did not yield detectable borylation para to the carbamate, which is a minor byproduct in the silica-SMAP system.

Table 4. Comparison of Silyl Ligands with Pendant P- and N-donors

Substrate	Product	Ligand	T(°C)	Time (h)	% yield
 21a	 22a	15^a	100	16	12
		20	80	4	60 ^b
 21b	 22b	15	80	16	37 ^c
		20	80	1	70

^a2.0 equiv B₂pin₂, 5 mol % **15**, and 2.5 mol % [Ir(OMe)(cod)]₂. ^b93% conversion of starting material was observed by GC. ^cConversion based on GC. 56% conversion to 1-phenylpropan-1-ol was observed

For phenyl ethyl ketone, ligand **15** gave the reduction to the alcohol upon workup as the major product. This unwanted reaction was almost completely eliminated by employing N-donor ligand **20**. When compared to other homogenous catalysts that effect ortho borylation of ketones,⁸ borylations employing **20** had shorter reaction times at considerably lower temperatures.

Furthermore, borylations of *t*-butylbenzoate and benzamide **17a** with ligand **20**, using identical conditions to those used with ligand **15**, gave **16m** in 78% isolated yield after 3 h and **18a** in 80% yield after 4 h, respectively. Significantly, ortho borylation of anisole was not found with ligand **20**. These results show that modification of the silyl ligand framework can dramatically impact reactivity.

Conclusions

In summary, we have shown that Ir catalysts supported by silyl-tethered P- and N-donor ligands are effective for ortho borylation directed by a range of different functional groups. Because the ligands within the coordination sphere are bidentate and electron-rich, the activities are generally superior to homogeneous systems that utilize electron-poor ligands to favor unsaturated intermediates. Exploring effects of varying the ligand framework on the reactivity in other directed C–H functionalizations is of interest.^{22,23}

REFERENCES

REFERENCES

1. Cho, J.-Y.; Iverson, C. N.; Smith, M. R., III *J. Am. Chem. Soc.* **2000**, 122, 12868.
2. Boebel, T. A.; Hartwig, J. F. *J. Am. Chem. Soc.* **2008**, 130, 7534.
3. Preshlock, S. M.; Plattner, D. L.; Maligres, P. E.; Krska, S. W.; Maleczka, R. E., Jr.; Smith, M. R., III *Angew. Chem., Int. Ed.* **2013**, 52, 12915.
4. Roosen, P. C.; Kallepalli, V. A.; Chattopadhyay, B.; Singleton, D. A.; Maleczka, R. E., Jr.; Smith, M. R., III *J. Am. Chem. Soc.* **2012**, 134, 11350.
5. Ishiyama, T.; Isou, H.; Kikuchi, T.; Miyaura, N. *Chem. Commun.* **2010**, 159.
6. Ros, A.; Estepa, B.; Lopez Rodriguez, R.; Alvarez, E.; Fernandez, R.; Lassaletta, J. M. *Angew. Chem., Int. Ed.* **2011**, 50, 11724.
7. López-Rodríguez, R.; Ros, A.; Fernández, R.; Lassaletta, J. M. *J. Org. Chem.* **2012**, 77, 9915.
8. Itoh, H.; Kikuchi, T.; Ishiyama, T.; Miyaura, N. *Chem. Lett.* **2011**, 40, 1007.
9. Roering, A. J.; Hale, L. V. A.; Squier, P. A.; Ringgold, M. A.; Wiederspan, E. R.; Clark, T. B. *Org. Lett.* **2012**, 14, 3558.
10. Crawford, K. M.; Ramseyer, T. R.; Daley, C. J. A.; Clark, T. B. *Angew. Chem., Int. Ed.* **2014**, 53, 7589.
11. Kawamorita, S.; Ohmiya, H.; Hara, K.; Fukuoka, A.; Sawamura, M. *J. Am. Chem. Soc.* **2009**, 131, 5058.
12. Kawamorita, S.; Ohmiya, H.; Sawamura, M. *J. Org. Chem.* **2010**, 75, 3855.
13. Kawamorita, S.; Murakami, R.; Iwai, T.; Sawamura, M. *J. Am. Chem. Soc.* **2013**, 135, 2947.
14. Kawamorita, S.; Miyazaki, T.; Ohmiya, H.; Iwai, T.; Sawamura, M. *J. Am. Chem. Soc.* **2011**, 133, 19310.
15. Recently, threefold cross-linked polystyrene-triphenylphosphane hybrid systems have been developed. Their synthesis is simpler and initial studies indicate that these function similar to silica-supported monophosphines.: Iwai, T.; Harada, T.; Hara, K.; Sawamura, M. *Angew. Chem. Int. Ed.* **2013**, 52, 12322.

16. Fang, H.; Choe, Y.-K.; Li, Y.; Shimada, S. *Chem. Asian J.* **2011**, 6, 2512.
17. Vanchura, B. A.; Preshlock, S. M.; Roosen, P. C.; Kallepalli, V. A.; Staples, R. J.; Maleczka, R. E., Jr.; Singleton, D. A.; Smith, M. R., III *Chem. Commun.* **2010**, 46, 7724.
18. Zhang, F.; Wang, L.; Chang, S.-H.; Huang, K.-L.; Chi, Y.; Hung, W.-Y.; Chen, C.-M.; Lee, G.-H.; Chou, P.-T. *Dalton Trans.* **2013**, 42, 7111.
19. Preshlock, S. M.; Ghaffari, B.; Maligres, P. E.; Krska, S. W.; Maleczka, R. E., Jr.; Smith, M. R., III *J. Am. Chem. Soc.* **2013**, 135, 7572.
20. Stradiotto, M.; Fajdala, K. L.; Tilley, T. D. *Chem. Commun.* **2001**, 1200.
21. Sangtrirutnugul, P.; Tilley, T. D. *Organometallics* **2007**, 26, 5557.
22. Some of this work was previously partially presented in a) Sean Micheal Preshlock, STOICHIOMETRIC AND CATALYTIC C–H BORYLATIONS OF ARENES, Michigan State University, Ph.D dissertation, **2013** b) Donald Plattner, THE IRIIDIUM CATALYZED ORTHO BORYLATION OF AROMATICS, Michigan State University, Msc dissertation, **2014**.
23. This work was previously published as a journal publication. Ghaffari, B.; Preshlock, S. M.; Plattner, D. L.; Staples, R. J.; Maligres, P. E.; Krska, S. W.; Maleczka, R. E.; Smith, M. R. *J. Am. Chem. Soc.* **2014**, 136, 14345.

CHAPTER 4 – EXPERIMENTAL

General Procedures

All commercially available chemicals were used as received unless otherwise indicated. Pinacolborane (HBpin containing 1% NEt₃) and was generously supplied by BoroPharm, Inc. (η^6 -mesitylene)Ir(Bpin)₃ and compound **5** were prepared per the literature procedures.¹ Solvents were refluxed over sodium benzophenone ketyl, distilled, and degassed. All the experiments were carried out in a glove box under a nitrogen atmosphere or by using standard Schlenk techniques.

Analytical Methods

¹H NMR spectra were recorded on a Varian VXR-500 or Varian Unity-500-Plus spectrometer (499.74 MHz) and referenced to residual solvent signals. ¹¹B NMR spectra were recorded on Varian VXR-500 operating at 160.41 MHz. ³¹P NMR spectra were recorded on Varian Unity-500-Plus operating at 202.29 MHz. ¹¹B and ³¹P NMR spectra were indirectly referenced relative to SiMe₄ according to IUPAC standard using VnmrJ software. All coupling constants are apparent *J* values measured at the indicated field strengths. Melting points were measured on a MEL-TEMP or Thomas Hoover capillary melting apparatus and are uncorrected. Note: Because all of the compounds are in equilibrium with each other, it was not possible to isolate bulk samples containing one species for combustion analysis.

X-ray Crystallography Details

Crystal Structures of compounds **6**, **8**, **9**, and **10** were performed using a Bruker CCD x-ray diffractometer and associated software applying standard crystallographic

techniques. Specifics for compound **6** include a disorder model for on boryl group, modeled at a 50:50 population. No restraints or constraints were performed to keep the groups together, although the thermal parameters were large for oxygen atoms on one of the boryls. Compounds **8**, and **9** were solved without incident, and the hydride atoms were found and refined isotropically. Compound **10** was solved without a problem, but the hydride atoms on the Ir atom could not be located. These were then modeled as riding atoms based on calculated positions generated in theoretical calculations (red, M06//SDD/6-31G*).

Computational Methods

DFT quantum chemical calculations were carried out using the Gaussian 09 software suite (Revision D.01)² using the M06 functional.³ A split basis set was employed with an SDD basis and core potential on Ir, and a 6-31G* basis set on the other atoms. Structures were minimized until program default convergence limits were reached.

Synthesis of compounds

Synthesis of (dippe)IrH(Bpin)₂(=BOCMe₂CMe₂OBpin) (6)

HBpin (8.7 μ L, 0.06 mmol, 1 equiv) was added to a pentane solution (1.0 ml) of compound **5** (50 mg, 0.06 mmol, 1 equiv) in a 20 mL scintillation vial. The initially yellow solution lightened upon addition of the HBpin. The resulting solution was stirred for approximately 2 minutes when a white precipitate began forming. The vial was placed in a freezer at $-35\text{ }^{\circ}\text{C}$ and allowed to sit overnight. The next day the mother liquor was pipetted from the vial, leaving a white solid on the sides of the vial. Nitrogen was blown from a pipette to dry the white solid (43 mg, 75%, mp $151\text{--}153\text{ }^{\circ}\text{C}$).

When the solid was placed back into solution for NMR characterization, the yellow color of the initial reaction solution reappeared. ^1H NMR (benzene- d_6 , 500 MHz): δ 2.37-2.30 (m, 2 H), 1.97 (s, 6 H), 1.80-1.72 (m, 2 H), 1.68 (s, 6 H), 1.29 (s, 28 H), 1.19-1.12 (m, 6 H), 1.12-1.06 (m, 6 H), 1.06-1.00 (m, 18 H, boryl singlet 1.05 ppm), 0.94-0.89 (m, 6 H), -11.05 (t, $J = 19.3$ Hz); ^{11}B NMR (benzene- d_6 , 160 MHz): δ 22.0, 38.8, 54.5; ^{31}P NMR (benzene- d_6 , 202 MHz): δ 67.24

Calculation of the equilibrium constant between compound **5, HBpin, and compound **6****

0.01 mmol of compound **6** was weighed in a test tube and then transferred to a J. Young tube after dissolution in benzene- d_6 (500 μ L). When recording the ^{31}P {Borreguero, #105} and ^1H NMR spectra, peaks for compounds **6** (67.24 ppm) and **5** (86.35 ppm) were observed in a roughly 3:1 ratio. The equilibrium constant was calculated from molar ratios determined by integrating resonances in the ^1H NMR

spectrum for the HBpin hydride and the methine protons in compounds **5** and **6** (compound **6** has two sets methine peaks), which gave $K_{eq} = 0.00165 \text{ mol} \cdot \text{L}^{-1}$

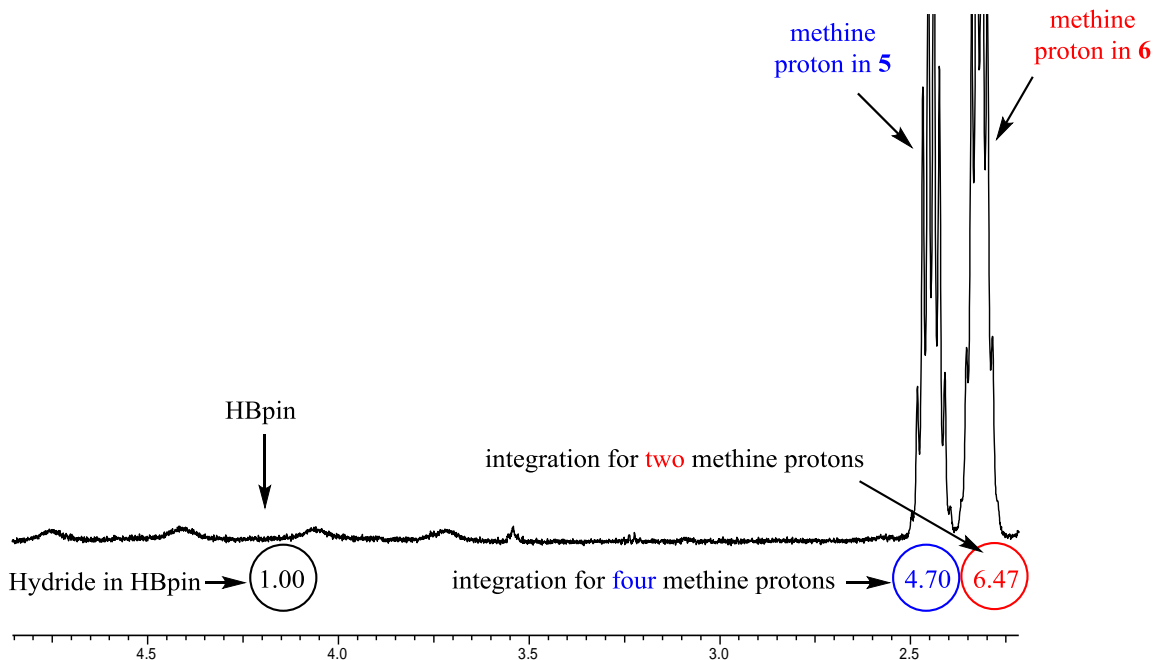


Figure 50. Expansion of ^1H NMR in benzene- d_6 for calculation of equilibrium constant

$$4.70 \div 4 = 1.175 \quad \text{Normalized value for one methine hydrogen in compound } \mathbf{5}$$

$$6.47 \div 2 = 3.235 \quad \text{Normalized value for one methine hydrogen in compound } \mathbf{6}$$

$$1.175 + 3.235 = 4.41 \quad \text{Total normalized value for one methine hydrogen in compound } \mathbf{5} \text{ and } \mathbf{6}$$

$$1.175 \div 4.41 = 0.26643991 \quad \text{Fraction of compound } \mathbf{5} \text{ in Iridium mixture}$$

$$3.235 \div 4.41 = 0.73356009 \quad \text{Fraction of compound } \mathbf{6} \text{ in Iridium mixture}$$

$$[1.000 \div 1.175] \times 0.26643991 = 0.22675737 \quad \text{Fraction of HBpin in mixture based on value for compound } \mathbf{5}$$

$$\text{Initial mmol of compound } \mathbf{6} = 0.01 \text{ mmol} \quad \text{Volume of solvent} = 0.5 \text{ mL}$$

$$0.26643991 \times 0.01 = 0.0026643991 \quad \text{mmol of compound } \mathbf{5}$$

$$0.73356009 \times 0.01 = 0.0073356009 \quad \text{mmol of compound } \mathbf{6}$$

$$0.22675737 \times 0.01 = 0.0022675737 \quad \text{mmol of HBpin}$$

$$0.002643991 \div 0.5 = 0.005287982 \quad \text{molarity of compound } \mathbf{5}$$

$$0.0073356009 \div 0.5 = 0.0146712 \quad \text{molarity of compound } \mathbf{6}$$

$$0.0022675737 \div 0.5 = 0.004535147 \quad \text{molarity of HBpin}$$

$$K_{eq} = \frac{[0.005287982][0.0045351474]}{[0.0146712]} = 0.001647$$

Catalytic borylation of 2-methylthiophene with compound **5**, using 0.5 equivalents of HBpin

Compound **5** (20.8 mg, 0.025 mmol, 0.05 equiv) was weighed in a test tube and then transferred to a J. Young NMR tube after dissolution in cyclohexane- d_{12} (150 $\mu\text{L} \times 4$). 2-methylthiophene (49 μL , 0.5 mmol, 1 equiv) and HBpin (36 μL , 0.25 mmol, 0.5 equiv) were then added to the J. Young NMR tube via syringe. The J. Young NMR tube was capped and heated in the NMR probe at 100 °C. The reaction was monitored by ^1H and $^{31}\text{P}\{^1\text{H}\}$ NMR spectroscopy every 20 minutes for conversion of starting material as well as catalyst intermediates for 4 hours which the NMR yield of 4,4,5,5-tetramethyl-2-(5-methylthiophen-2-yl)-1,3,2-dioxaborolane was showing full conversion based of limiting reagent (HBpin) see Figures 51 and 52.

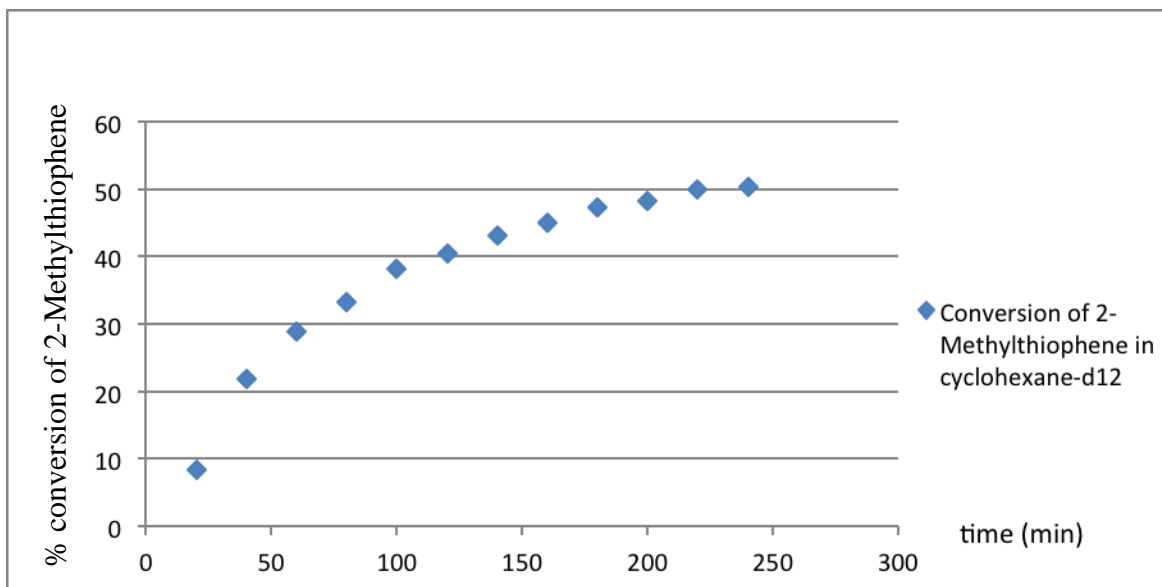


Figure 51. Catalytic conversion of 2-methylthiophene with compound **5**, using 0.5 equivalents of HBpin

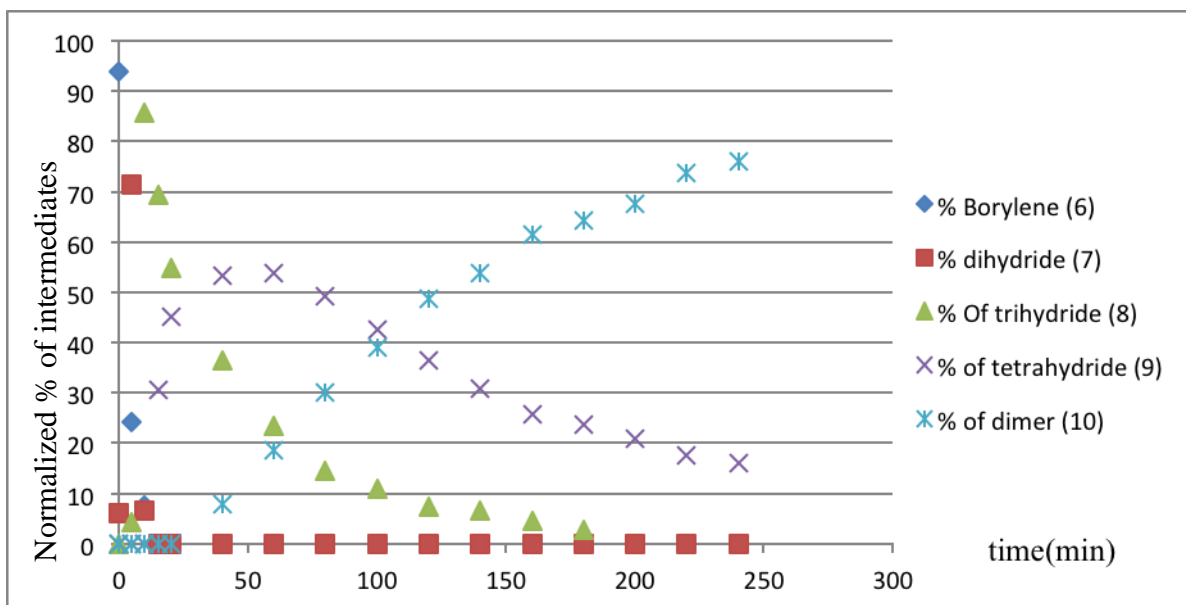


Figure 52. Catalytic intermediates for borylation of 2-methylthiophene with compound **5**, using 0.5 equivalents of HBpin.

Generation of (dippe)Ir(H)₂(Bpin)₃ (**7**)

A toluene-*d*₈ solution (0.6 mL) of compound **5** (20.8 mg, 0.025 mmol, 1 equiv) was added to a J. Young NMR tube. The tube was connected to a Schlenk line and then subjected to three freeze-pump-thaw cycles. The tube was opened to an atmosphere of H₂ gas, closed, and then placed in a precooled NMR probe, at −45 °C ³¹P{¹H} and ¹H NMR spectroscopy showed a major resonance (~ 70%) corresponding to compound **7** at 53.56 ppm and a minor one corresponding to compound **8** (~30%) at 61.22 ppm.

¹H NMR (toluene-*d*₈, 500 MHz): δ 2.15 (septet, 4 H, *J* = 7.2 Hz) 1.33 (s, 36 H), 1.21 (dd, *J* = 15.5, 7.10 Hz, 12 H), 1.02 (m, 4 H), 0.95 (dd, *J* = 13.02, 7.1 Hz, 12 H), −11.01 (t, *J* = 11.4 Hz, 2 H, 9.5 Hz FWHM); ¹¹B NMR (toluene-*d*₈, 160 MHz): δ 38.8; ³¹P NMR (toluene-*d*₈, 202 MHz): δ 53.56.

The probe was then cooled to $-60\text{ }^{\circ}\text{C}$, and a ^{31}P NMR spectrum was recorded. With selective decoupling of the aliphatic protons, the hydride coupling is preserved and the resulting triplet proves that two hydrides are bound to iridium in compound **7**.

Generation of (dippe)Ir(H)₃(Bpin)₂ (**8**)

The J. Young tube from previous experiment which contained **7** (~ 70%) and **8** (~30%) was warmed up to $-15\text{ }^{\circ}\text{C}$ while the relative ratio of **8** to **7** was increasing, the rate of conversion was slow, therefore, the NMR tube was removed from the probe and shook for 10 seconds and placed back at $-15\text{ }^{\circ}\text{C}$ probe. $^{31}\text{P}\{^1\text{H}\}$, ^1H and ^{11}B NMR showed compound **8** as the sole product (2% impurity from compound **9** was observed).

^1H NMR (toluene-*d*₈, 500 MHz): δ 1.96 (septet, 4 H, $J = 7.2\text{ Hz}$) 1.28 (s, 24 H), 1.11 (dd, $J = 15.9, 7.1\text{ Hz}$, 12 H), 1.02 (m, 4 H), 0.97 (s, 12 H), 0.89 (dd, $J = 13.0, 7.1\text{ Hz}$, 12 H), -11.21 (t, $J = 5.5\text{ Hz}$, 3 H); ^{11}B NMR (toluene-*d*₈, 160 MHz): δ 37.4; $^{31}\text{P}\{^1\text{H}\}$ NMR (toluene-*d*₈, 202 MHz): δ 61.22.

Single crystals of compound **8** were initially isolated from a pentane solution containing compounds **5**, **6**, and a 10-fold excess of HBpin. The reaction solution was placed in a $-35\text{ }^{\circ}\text{C}$ freezer to crystallize. After 1 week the crystals were analyzed and found to be compound **8**.

Generation of (dippe)Ir(H)₄(Bpin) (**9**)

The J. Young NMR tube, containing compound **8** (from the previous experiment) was warmed to room temperature and $^{31}\text{P}\{^1\text{H}\}$ and ^1H NMR spectra were recorded. A new signal appeared at 66.75 ppm in ^{31}P NMR (compound **9**); the ratio of compound **9** to compound **8** increased gradually. To facilitate the process the NMR tube was taken out of the NMR probe and shaken for 15 minutes at room temperature. ^{31}P NMR, ^1H NMR and

^{11}B NMR confirmed formation of compound **9** in 97% purity (traces of compound **8** were present).

^1H NMR (toluene- d_8 , 500 MHz): δ 1.73 (m, 4 H, $J = 7.1$ Hz) 1.15 (m, 4 H), 1.02 (dd, $J = 15.3, 7.1$ Hz, 12 H), 0.92 (dd, $J = 13.7, 7.1$ Hz, 12 H), -11.59 (t, $J = 17.0$ Hz, 4 H); ^{11}B NMR (toluene- d_8 , 160 MHz): δ 37.5; $^{31}\text{P}\{^1\text{H}\}$ NMR (toluene- d_8 , 202 MHz) δ 66.75.

When the ^{31}P NMR spectrum is recorded with selective decoupling of the aliphatic protons, the hydride coupling is preserved and the resulting pentet proves that four hydrides are bound to iridium in compound **9**.

Single crystals of compound **9** were initially isolated from a pentane solution containing compounds **5**, **6**, **8**, and a 10-fold excess of HBpin. The reaction mixture was placed in a -30 °C freezer to crystallize. After 2 weeks the crystals were analyzed and found to be **9**.

Synthesis of [(dippe)Ir(H) $_2$ (μH)] $_2$ (**10**)

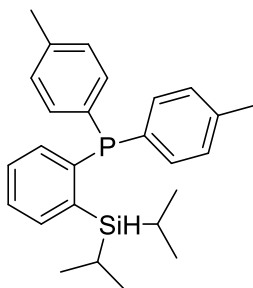
3.0 equiv of MeOH (0.075 mmol, 3.1 μL) was injected to an NMR tube containing compound **9** via a syringe and ^{31}P NMR, ^1H NMR spectra were recorded. A new broad signal starts appearing in ^{31}P NMR (compound **10**). After 12 h, $^{31}\text{P}\{^1\text{H}\}$ and ^1H NMR spectra showed a complex mixture containing $\sim 90\%$ of the desired compound. The NMR tube was taken in to the nitrogen filled glove box and solvent was removed under reduced pressure. The solid residue was then washed with pentane followed by recrystallization from mixture of toluene and pentane at -35 °C to yield compound **10** in 48% isolated yield (5.6 mg).

The crystalline solid was dissolved in toluene- d_8 and VT NMR was obtained.

Room temperature ^1H NMR: (toluene- d_8 , 500 MHz) δ 0.50-3.50 (broad features, 68 H), -3.64 (br, 2 H), -12.86 (br, 2 H), -22.56 (br, 2 H); $^{31}\text{P}\{^1\text{H}\}$ NMR (toluene- d_8 , 202 MHz) δ 77.25 (br), 75.87(br).

Upon heating the J. Young NMR tube to $85\text{ }^\circ\text{C}$, a new peak appeared at δ 88.28 in the $^{31}\text{P}\{^1\text{H}\}$ NMR spectrum, and after 30 minutes at $100\text{ }^\circ\text{C}$, compound **10** was fully converted to new species.

(2-(diisopropylsilyl)phenyl)di-*p*-tolylphosphane (15)



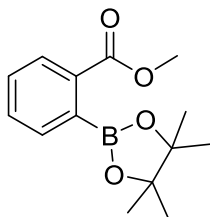
(2-bromophenyl)di-*p*-tolylphosphine was synthesized on 10 mmol scale reaction following a previously reported procedure in 95% (3.507 g) isolated yield (final work up was performed in air).⁴ (2-bromophenyl)di-*p*-tolylphosphine (3.507 g, 9.5 mmol) was added to a Schlenk flask containing a magnetic stir bar and kept under gentle stream of nitrogen through the synthesis. Dry diethyl ether (50 mL) was added via syringe, and the flask was cooled to $-78\text{ }^\circ\text{C}$. *n*-BuLi (4.0 mL, 10 mmol, 2.5 M) was added dropwise via syringe and the mixture was allowed to warm to room temperature over 1 h. The reaction mixture was cooled back to $-78\text{ }^\circ\text{C}$, and diisopropylchlorosilane (1.70 mL, 10.0 mmol) was added dropwise over 15 min. The resulting mixture was warmed to reach room temperature and stirred for 4 hours. In a nitrogen-filled glove box, the mixture was then filtered and the precipitate washed with toluene. Volatiles were removed from the filtrate under reduced pressure and the product was isolated as a white solid in 88% (3.840 g)

yield. ^1H NMR (500 MHz, C_6D_6) δ 1.01 (d, J = 7.4 Hz, 6H), 1.17 (d, J = 7.3 Hz, 6H), 1.47 (m, 2H), 1.98 (s, 6H), 4.57 (m, 1H), 6.90 (d, J = 7.8 Hz, 4H), 7.08-7.02 (m, 2H), 7.31 (d, J = 7.8 Hz, 4H), 7.36-7.33 (m, 1H), 7.62-7.58 (m, 1H); ^{13}C NMR (125 MHz, C_6D_6) 12.1 (d, J = 6.7 Hz), 19.3 (d, J = 10.5 Hz), 21.2, 127.7, 129.1 (d, J = 6.7 Hz), 133.6 (d, J = 19.1 Hz), 134.0, 134.5 (d, J = 10.5 Hz), 136.7 (d, J = 15.3 Hz), 138.1, 142.9, 143.2, 144.3 (d, J = 10.4 Hz); ^{31}P NMR (202 MHz, C_6D_6) δ -9.82. (s). HRMS (ESI) m/z calcd for $\text{C}_{26}\text{H}_{34}\text{PSi}$ $[\text{M} + \text{H}]^+$ 405.2167, found 405.2159.

General procedure for *ortho*-directed borylation of methyl benzoates.

In a nitrogen filled glovebox, $[\text{Ir}(\text{OMe})(\text{cod})]_2$ (8.3 mg, 0.0125 mmol) was dissolved in 1 mL THF in a 15 mL pressure tube containing a magnetic stir bar. To the tube, 1 equiv. B_2Pin_2 (254.0 mg), **15** (0.0250 mmol, 10.0 mg), and 1.0 mmol methyl benzoate substrate were also added, and the reaction vessel was sealed and heated at 80 $^\circ\text{C}$ for 16h. The reaction mixture was allowed to return to room temperature and was exposed to air. The volatiles were then removed under reduced pressure and the product was purified by passing it through a short plug of SiO_2 eluting with MTBE. Additional purifications were performed as described below.

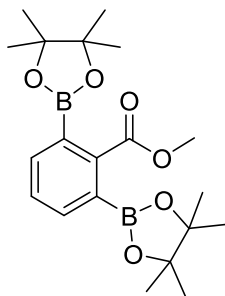
Methyl 2-(4,4,5,5-tetramethyl-1,3,2-dioxaborolan-2-yl)benzoate (**16a**)



In a glove box, $[\text{Ir}(\text{OMe})(\text{cod})]_2$ (3.3 mg, 0.0050 mmol), **15** (0.0100 mmol, 4.0 mg), and anhydrous, degassed THF (1.0 mL) were placed in a 15 mL pressure tube

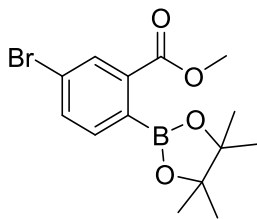
containing a magnetic stir bar, and the mixture was stirred for 1 min at room temperature. Methylbenzoate (276.0 mg, 2.0 mmol) was added to the tube and lastly bis(pinacolato)diboron (254.0 mg, 1.0 mmol) was added as a solid, the reaction vessel was sealed and heated at 60 °C. Reaction progress was monitored by GC over 1 hour intervals. After 3 hours, (100% GC conversion based on B₂pin₂) the reaction mixture was allowed to return to room temperature and was exposed to air. The volatiles were then removed under reduced pressure and the product was purified by column chromatography; hexanes: EtOAc (12:1) to hexanes: EtOAc (9:1) as a pale yellow- oil (190.0 mg, 72% yield based on B₂Pin₂ (5% diborylated product, **16b**, was observed in crude); ¹H NMR (500 MHz, CDCl₃) δ 1.42 (s, 12H), 3.91 (s, 3H), 7.42 (dt, *J* = 2.5, 8.4 Hz, 1H), 7.53-7.48 (m, 2H), 7.94 (d, *J* = 7.8 Hz, 1H).⁵

Methyl 2,6-bis(4,4,5,5-tetramethyl-1,3,2-dioxaborolan-2-yl)benzoate (16b)



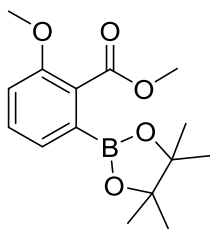
The reaction was performed using 1.0 mmol substrate (126 μl), [Ir(OMe)(cod)]₂ [Ir(OMe)(cod)]₂ (16.6 mg, 0.0250 mmol), 0.5 equiv B₂Pin₂ (254.0 mg), **15** (0.0500 mmol, 20.0 mg). The product was obtained by recrystallization from MeOH/ H₂O as a white solid (244.0 mg, 63% isolated yield); ¹H NMR (500 MHz, CDCl₃) δ 1.35 (s, 24H), 3.89 (s, 3H), 7.43 (d, *J* = 7.3 Hz, 1H), 7.70 (d, *J* = 7.4 Hz, 2H); ¹³C NMR (125 MHz, CDCl₃) δ 24.8, 52.0, 84.0, 128.9, 135.4, 141.7, 170.6; ¹¹B NMR (160 MHz, CDCl₃) δ 31.0 (br s); HRMS (ESI) *m/z* calcd for C₂₀H₃₁B₂O₆ [*M* + *H*]⁺ 389.2307, found 389.2307.

Methyl 5-bromo-2-(4,4,5,5-tetramethyl-1,3,2-dioxaborolan-2-yl)benzoate (16c)



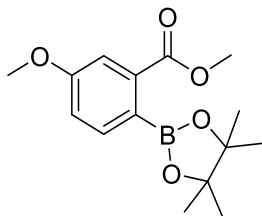
The reaction was performed using 0.5 mmol substrate (107.5 mg), $[\text{Ir}(\text{OMe})(\text{cod})]_2$ (16.6 mg, 0.0250 mmol), 2 equiv B_2Pin_2 (254.0 mg), **15** (0.0500 mmol, 20.0 mg). Purified by column chromatography; hexanes: EtOAc (9:1). The product was obtained as yellow oil (139 mg, 60% yield (95% assay yield by ^1H NMR); ^1H NMR (500 MHz, CDCl_3) δ 1.40 (s, 12H), 3.91 (s, 3H), 7.37 (d, $J = 7.8$ Hz, 1H), 7.64 (dd, $J = 2.0, 7.8$ Hz, 1H), 8.07 (s, $J = 1.5$ Hz, 1H).⁶

Methyl 2-methoxy-6-(4,4,5,5-tetramethyl-1,3,2-dioxaborolan-2-yl)benzoate (16d)



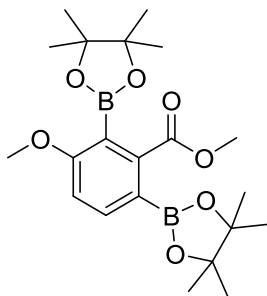
The reaction was performed using 1.0 mmol substrate (166.0 mg), $[\text{Ir}(\text{OMe})(\text{cod})]_2$ (8.3 mg, 0.0125 mmol), 1.25 equiv B_2Pin_2 (317.0 mg), **15** (0.0250 mmol, 10.0 mg). The product was obtained by recrystallization from MeOH/ H_2O as brown crystals (240.0 mg, 82% yield); ^1H NMR (500 MHz, CDCl_3) δ 1.32 (s, 12H), 3.83 (s, 3H), 3.88 (s, 3H), 7.02 (d, $J = 8.3$ Hz, 1H), 7.32 (d, $J = 6.4$ Hz, 1H), 7.38 (t, $J = 7.3$ Hz, 1H).⁷

Methyl 5-methoxy-2-(4,4,5,5-tetramethyl-1,3,2-dioxaborolan-2-yl)benzoate (16e)



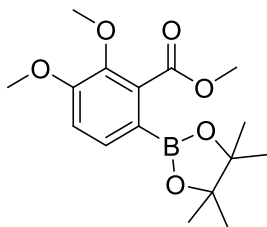
Purified by column chromatography; hexanes: EtOAc (9:1). The product was obtained as yellow oil (193.0 mg, 66% yield) Spectrum contains minor amounts of methyl 3-methoxy-2-(4,4,5,5-tetramethyl-1,3,2-dioxaborolan-2-yl)benzoate ^1H NMR (500 MHz, CDCl_3) δ 1.39 (s, 12H), 3.83 (s, 3H), 3.89 (s, 3H), 7.05 (dd, $J = 2.4, 8.3$ Hz, 1H), 7.45-7.42 (m, 2H).⁴

Methyl 3-methoxy-2,6-bis(4,4,5,5-tetramethyl-1,3,2-dioxaborolan-2-yl)benzoate (16e')



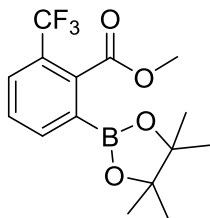
Purified by column chromatography; hexanes: EtOAc (9: 1). The product was obtained as yellow powder (20.0 mg, 5% yield); ^1H NMR (500 MHz, CDCl_3) δ 1.34 (s, 12H), 1.39 (s, 12H), 3.79 (s, 3H), 3.87 (s, 3H), 6.93 (d, $J = 8.3$ Hz, 1H), 7.50 (d, $J = 7.9$ Hz, 1H); ^{13}C NMR (125 MHz, CDCl_3) δ 24.8, 24.9, 52.1, 55.6, 83.6, 83.8, 112.3, 135.4, 139.0, 163.6, 169.3; ^{11}B NMR (160 MHz, CDCl_3) δ 31.0 (br, s); HRMS (ESI) m/z calcd for $\text{C}_{21}\text{H}_{33}\text{B}_2\text{O}_7$ $[\text{M} + \text{H}]^+$ 419.2420, found 419.2434.

Methyl 2,3-dimethoxy-6-(4,4,5,5-tetramethyl-1,3,2-dioxaborolan-2-yl)benzoate (16f)



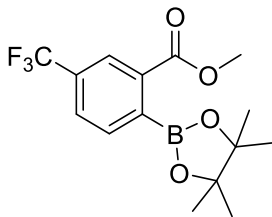
The compound was obtained via recrystallization with MeOH/H₂O as white crystals (227.0 mg, 70% yield); ¹H NMR (500 MHz, CDCl₃) δ 1.30 (s, 12H), 3.85 (s, 3H), 3.88 (s, 3H), 3.89 (s, 3H), 6.94 (d, *J* = 8.3 Hz, 1H), 7.51 (d, *J* = 7.8 Hz, 1H); ¹³C NMR (125 MHz, CDCl₃) δ 24.8, 52.2, 55.8, 61.6, 83.8, 112.6, 131.8, 134.6, 145.4, 155.0, 168.7; ¹¹B NMR (160 MHz, CDCl₃) δ 30.0 (br, s); HRMS (ESI) *m/z* calcd for C₁₆H₂₄BO₆ [M + H]⁺ 323.1669, found 323.1677. Structure determination was done by single crystal X-ray diffraction studies.

Methyl 2-(4,4,5,5-tetramethyl-1,3,2-dioxaborolan-2-yl)-6-(trifluoromethyl)benzoate (6g)



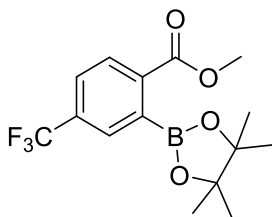
The compound was obtained via recrystallization with MeOH/H₂O, as black crystals (270.0 mg, 82% yield); ¹H NMR (500 MHz, CDCl₃) δ 1.34 (s, 12H), 3.92 (s, 3H), 7.55 (t, *J* = 7.8 Hz, 1H), 7.76 (d, *J* = 8.3 Hz, 1H), 7.99 (d, *J* = 7.9 Hz, 1H).⁷

Methyl 2-(4,4,5,5-tetramethyl-1,3,2-dioxaborolan-2-yl)-5-(trifluoromethyl)benzoate
(16h)



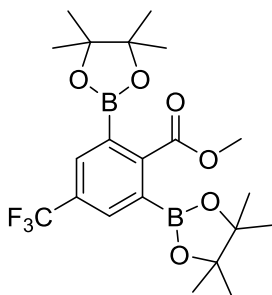
The compound was obtained via recrystallization with MeOH/H₂O, as brown powder (266.0 mg, 81% yield); ¹H NMR (500 MHz, CDCl₃) δ 1.42 (s, 12H), 3.95 (s, 3H), 7.62 (d, *J* = 7.8 Hz, 1H), 7.76 (dd, *J* = 1.0, 7.8 Hz, 1H), 8.19 (s, 1H).⁷

Methyl 2-(4,4,5,5-tetramethyl-1,3,2-dioxaborolan-2-yl)-4-(trifluoromethyl)benzoate
(16i)



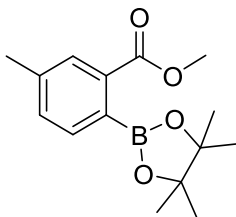
The compound purified by column chromatography; hexanes: EtOAc (9:1), and obtained as yellow oil (163.0 mg, 49% yield); ¹H NMR (500 MHz, CDCl₃) δ 1.43 (s, 12H), 3.95 (s, 3H), 7.69 (dd, *J* = 7.8, 0.9 Hz, 1H), 7.74 (s, 1H), 8.04 (d, *J* = 8.3 Hz, 1H).⁷

Methyl 2,6-bis(4,4,5,5-tetramethyl-1,3,2-dioxaborolan-2-yl)-4-(trifluoromethyl)benzoate (16i')



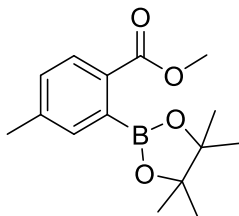
The compound purified by column chromatography; hexanes: EtOAc (9:1), and was obtained as brown crystals (77.0 mg, 17% yield); ¹H NMR (500 MHz, CDCl₃) δ 1.34 (s, 24H), 3.89 (s, 3H), 7.93 (s, 2H); ¹³C NMR (125 MHz, CDCl₃) δ 24.7, 52.3, 84.5, 124.9 (*J* = 272.7 Hz), 130.7 (*J* = 32.4 Hz), 132.6 (*J* = 3.8 Hz), 145.9, 169.8; ¹⁹F NMR (470 MHz, CDCl₃) δ -62.8 (s); ¹¹B NMR (160 MHz, CDCl₃) δ 31.0 (br, s); HRMS (ESI) *m/z* calcd for C₂₁H₃₀B₂F₃O₆ [M + H]⁺ 457.2188, found 457.2198.

Methyl 5-methyl-2-(4,4,5,5-tetramethyl-1,3,2-dioxaborolan-2-yl)benzoate (16j)



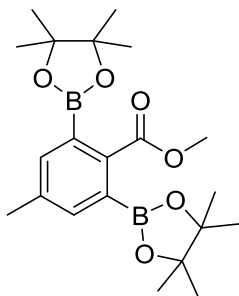
The compound purified by column chromatography; hexanes: EtOAc (9:1) and was obtained as yellow oil (227.0 mg, 82% yield); ¹H NMR (500 MHz, CDCl₃) δ 1.42 (s, 12H), 2.38 (s, 3H), 3.91 (s, 3H), 7.34 (d, *J* = 7.4 Hz, 1H), 7.41 (d, *J* = 7.3 Hz, 1H), 7.76 (s, 1H).⁶

Methyl 4-methyl-2-(4,4,5,5-tetramethyl-1,3,2-dioxaborolan-2-yl)benzoate (16k)



The product was obtained via column chromatography; hexanes: EtOAc (9:1), as white powder (135.0 mg, 49% yield); ^1H NMR (500 MHz, CDCl_3) δ 1.43 (s, 12H), 2.38 (s, 3H), 3.90 (s, 3H), 7.22 (dd, $J = 1.0, 7.9$ Hz, 1H), 7.29 (s, 1H), 7.85 (d, $J = 7.8$ Hz, 1H).⁶

Methyl 4-methyl-2,6-bis(4,4,5,5-tetramethyl-1,3,2-dioxaborolan-2-yl)benzoate (16k')

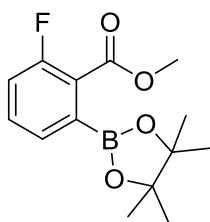


The product was obtained by column chromatography; hexanes: EtOAc (9:1), as brown crystals (54.0 mg, 13% yield); ^1H NMR (500 MHz, CDCl_3) δ 1.36 (s, 24H), 2.35 (s, 3H), 3.87 (s, 3H), 7.45 (s, 2H); ^{13}C NMR (125 MHz, CDCl_3) δ 21.2, 24.8, 51.9, 83.9, 135.4, 137.7, 139.3, 170.3; ^{11}B NMR (160 MHz, CDCl_3) δ 30.0 (br, s); HRMS (ESI) m/z calcd for $\text{C}_{21}\text{H}_{33}\text{B}_2\text{O}_6$ $[\text{M} + \text{H}]^+$ 403.2471, found 403.2462.

Reaction optimization for catalyst loading, temperature and time

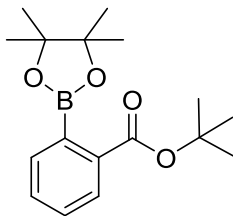
In a glove box, [Ir(OMe)(cod)]₂ (3.3 mg, 0.0050 mmol), **15** (0.0100 mmol, 4.0 mg), and anhydrous, degassed THF (1.0 mL) were placed in a 15 mL pressure tube containing a magnetic stir bar, and the mixture was stirred for 1 min at room temperature. Methyl 4-methylbenzoate (150.2 mg, 1.0 mmol) was added to the tube and lastly bis(pinacolato)diboron (254.0 mg, 1.0 mmol) was added as solid, the reaction vessel was sealed and heated at 60 °C. Reaction progress was monitored by GC over 1 hour intervals. After 3 hours, (100% GC conversion based on B₂pin₂) the reaction mixture was allowed to return to room temperature and was exposed to air. The volatiles were then removed under reduced pressure and the product was purified by column chromatography; hexanes: EtOAc (9:1). **16K** and **16K'** were obtained in 55% (152.0 mg) and 10% (41.2 mg) isolated yield.

Methyl 2-fluoro-6-(4,4,5,5-tetramethyl-1,3,2-dioxaborolan-2-yl)benzoate (**16l**)



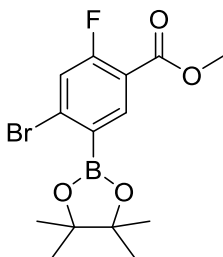
Product was purified by column chromatography; hexanes: EtOAc (9:1) as yellow oil (281.0 mg, 84% yield); ¹H NMR (500 MHz, CDCl₃) δ 1.36 (s, 12H), 3.92 (s, 3H), 7.16 (m, 1H), 7.46 (m, 2H); ¹³C NMR (125 MHz, DMSO-d₆) δ 24.9, 53.0, 84.6, 118.8 (*J* = 21.0 Hz), 124.9 (*J* = 13.3 Hz), 130.1 (*J* = 3.8 Hz), 133.2 (*J* = 8.6 Hz), 160.3 (*J* = 251.8 Hz), 166.1; ¹⁹F NMR 470 MHz, CDCl₃) δ -115.0 (s); ¹¹B NMR (160 MHz, CDCl₃) δ 31.0 (br, s); HRMS (ESI) *m/z* calcd for C₁₄H₁₉BF₄ [M + H]⁺ 281.1363, found 281.1371.

tert-Butyl 2-(4,4,5,5-tetramethyl-1,3,2-dioxaborolan-2-yl)benzoate (16m)



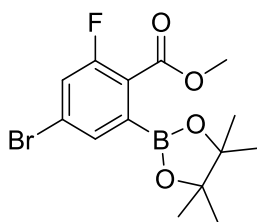
In a glove box, $[\text{Ir}(\text{OMe})(\text{cod})]_2$ (3.3 mg, 0.0050 mmol), **15** (0.0100 mmol, 4.0 mg), and anhydrous, degassed THF (1.0 mL) were placed in a 15 mL pressure tube containing a magnetic stir bar, and the mixture was stirred for 1 min at room temperature. tert-Butyl benzoate (178.2 mg, 1.0 mmol) was added to the tube and lastly bis(pinacolato)diboron (254.0 mg, 1.0 mmol) was added as solid, the reaction vessel was sealed and heated at 80 °C. Reaction progress was monitored by GC over 2 hour intervals. After 16 hours, (80% GC conversion based on B_2pin_2) the reaction mixture was allowed to return to room temperature and was exposed to air. The volatiles were then removed under reduced pressure and the product was purified by column chromatography; hexanes: Et_2O (4:1) as a white solid (192.0 mg, 63% yield). No diborylated product was observed in crude; ^1H NMR (500 MHz, CDCl_3) δ 1.42 (s, 12H), 1.58 (s, 9H), 7.34 (m, 1H), 7.43-7.49 (m, 2H), 7.82 (d, $J = 7.8$ Hz, 1H).⁷

Methyl 4-bromo-2-fluoro-5-(4,4,5,5-tetramethyl-1,3,2-dioxaborolan-2-yl)benzoate (16n)



The reaction was performed using 1.0 mmol substrate (233.0 mg), [Ir(OMe)(cod)]₂ (8.3 mg, 0.0125 mmol), 1 equiv B₂pin₂ (254.0 mg), 4,4'-di-tert-butyl bipyridine (6.7 mg, 0.0250 mmol), 1 mL hexanes. Product was obtained via recrystallization with MeOH/H₂O as a pale white powder (370 mg, 80% yield) Spectrum contains minor amounts of 4-bromo-2-fluoro-3-(4,4,5,5-tetramethyl-1,3,2-dioxaborolan-2-yl)benzoate; ¹H NMR (500 MHz, CDCl₃) δ 1.38 (s, 12H), 3.97 (s, 3H), 7.40 (d, *J* = 10.3 Hz, 1H), 8.23 (d, *J* = 8.3 Hz, 1H), Aromatic couplings are due to H-F couplings; ¹³C NMR (125 MHz, CDCl₃) δ 24.8 (*J* = 10.5 Hz), 52.4, 84.6, 117.1 (*J* = 8.6 Hz), 121.8 (*J* = 24.8 Hz), 133.7 (*J* = 9.5 Hz), 140.2 (*J* = 1.9 Hz), 163.6 (*J* = 268), 164.2; ¹⁹F NMR 470 MHz, CDCl₃) δ – 104.6 (s); ¹¹B NMR (160 MHz, CDCl₃) δ 30.0 (br, s); HRMS (ESI) *m/z* calcd for C₁₃H₁₄BBrFO₄ [M - CH₃ + H]⁺ 343.0155, found 343.0160.

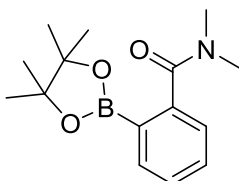
Methyl 4-bromo-2-fluoro-6-(4,4,5,5-tetramethyl-1,3,2-dioxaborolan-2-yl)benzoate (160)



Purified by column chromatography; hexanes: EtOAc (8.5: 1). Yellow Oil (255.0 mg, 70% yield); ¹H NMR (500 MHz, CDCl₃) δ 1.38 (s, *J*=0.9 Hz, 12H), 3.93 (s, *J* = 1.5 Hz, 3H), 7.35 (d, *J*= 9.3 Hz, 1H), 7.53 (s, 1H); ¹³C NMR (125 MHz, CDCl₃) δ 24.7, 52.8, 84.6, 121.4 (*J* = 24.8 Hz), 122.7 (*J* = 12.4 Hz), 126.1 (*J* = 8.6 Hz), 132.0 (*J* = 3.8 Hz), 160.9 (*J* = 261.3 Hz), 166.2; ¹⁹F NMR (470 MHz, CDCl₃) δ -109.7 (s); ¹¹B NMR (160

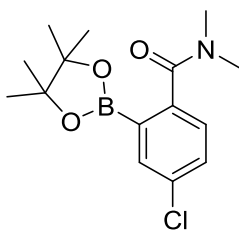
MHz, CDCl₃) δ 30.0 (br, s); HRMS (ESI) m/z calcd for C₁₃H₁₄BBrFO₄ [M - CH₃ + H]⁺ 343.0155, found 343.0150.

***N,N*-Dimethyl-2-(4,4,5,5-tetramethyl-1,3,2-dioxaborolan-2-yl)benzamide (18a)**



In a glove box, [Ir(OMe)(cod)]₂ (8.3 mg, 0.0125 mmol), **15** (0.0250 mmol, 10.0 mg), bis(pinacolato)diboron (254.0 mg, 1 mmol) and anhydrous, degassed THF (4.5 mL) were placed in a 15 mL pressure tube containing a magnetic stir bar, and the mixture was stirred for 1 min at room temperature. *N,N*-Dimethyl benzamide (149.0 mg, 1.0 mmol) was added to the tube, the reaction vessel was sealed and heated at 80 °C. Reaction progress was monitored by GC over 4 hour intervals. After 16 hours, (86% GC conversion) the reaction mixture was allowed to return to room temperature and was exposed to air. The volatiles were then removed under reduced pressure and the product was purified by passing it through a short plug of SiO₂ eluting (hexane/EtOAc = 1/1). The product was isolated by precipitation from hexane. White solid (206.2 mg) in 75% isolated yield. ¹H NMR (500 MHz, CDCl₃) δ 1.31 (s, 12H), 2.97 (br s, 6H), 7.30 (dd, J = 7.5, 0.6 Hz, 1H), 7.37 (dt, J = 7.5, 1.5 Hz, 1H), 7.45 (dt, J = 7.5, 1.5 Hz, 1H), 7.80 (dd, J = 7.5, 0.6 Hz, 1H).⁷

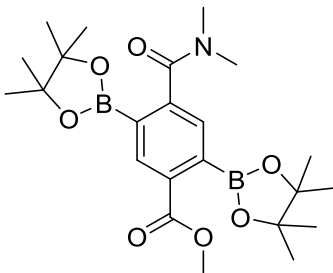
4-chloro-N,N-dimethyl-2-(4,4,5,5-tetramethyl-1,3,2-dioxaborolan-2-yl)benzamide
(18b)



In a glove box, $[\text{Ir}(\text{OMe})(\text{cod})]_2$ (8.3 mg, 0.0125 mmol), **15** (0.0250 mmol, 10.0 mg), bis(pinacolato)diboron (254.0 mg, 1.0 mmol) and anhydrous, degassed THF (4.5 mL) were placed in a 15 mL pressure tube containing a magnetic stir bar, and the mixture was stirred for 1 min at room temperature. 4-Chloro *N,N*-dimethyl benzamide (183.6 mg, 1.0 mmol) was added to the tube, the reaction vessel was sealed and heated at 80 °C. Reaction progress was monitored by GC over 4 hour intervals. After 16 hours, 95% conversion was observed. The reaction was stopped and mixture was allowed to return to room temperature and was exposed to air. The volatiles were then removed under reduced pressure and the product was purified by passing it through a short plug of SiO_2 eluting with (hexane/EtOAc = 1/1). The product was isolated by precipitation from hexane. White solid (263.1 mg) in 85% isolated yield was obtained.

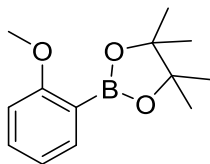
^1H NMR (500 MHz, CDCl_3) δ ppm 1.31 (s, 12 H) 3.00 (br. s., 6 H) 7.26 (d, $J=8.3$, 1 H) 7.40 (d, $J=8.3$ Hz, 1 H) 7.76 (s, 1 H); ^{13}C NMR (125 MHz, CDCl_3) δ ppm 24.9, 83.6, 127.1, 130.6, 134.5, 135.1, 139.7, 171.5; ^{11}B NMR (160 MHz, CDCl_3) δ ppm 27.3 (s); HRMS (ESI) m/z calcd for $\text{C}_{15}\text{H}_{22}\text{BClINO}_3$ $[\text{M} + \text{H}]^+$ 310.1384, found 310.1386.

Methyl 4-(dimethylcarbamoyl)-2,5-bis(4,4,5,5-tetramethyl-1,3,2-dioxaborolan-2-yl)benzoate (18c)



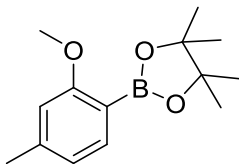
In a glove box, $[\text{Ir}(\text{OMe})(\text{cod})]_2$ (8.3 mg, 0.0125 mmol), **15** (0.0250 mmol, 10.0 mg), bis(pinacolato)diboron (508.0 mg, 2 mmol) and anhydrous, degassed THF (4.5 mL) were placed in a 15 mL pressure tube containing a magnetic stir bar, and the mixture was stirred for 1 min at room temperature. Methyl 4-(dimethylcarbamoyl)benzoate (207.0 mg, 1.0 mmol) was added to the tube, the reaction vessel was sealed and heated at 100 °C. Reaction progress was monitored by GC over 4 hour's intervals. After 16 hours the reaction mixture was allowed to return to room temperature and was exposed to air. The volatiles were then removed under reduced pressure and the product was purified by passing it through a short plug of SiO_2 eluting with (hexane/EtOAc = 1/1). The product was isolated by precipitation from hexane. White solid (436.0 mg) in 95% isolated yield. ^1H NMR (500 MHz, CDCl_3) δ ppm 1.31 (s, 12 H) 1.41 (s, 12 H) 2.75 (br. s., 3 H) 3.09 (br. s., 3 H) 3.93 (s, 3 H) 7.42 (s, 1 H) 8.37 (s, 1 H); ^{13}C NMR (125 MHz, CDCl_3) δ ppm 24.8, 24.9, 52.4, 84.0, 84.2, 129.5, 132.8, 135.3, 146.0, 168.0, 171.7; ^{11}B NMR (160 MHz, CDCl_3) δ ppm 30.2 (s); HRMS (ESI) m/z calcd for $\text{C}_{23}\text{H}_{36}\text{B}_2\text{NO}_7$ $[\text{M} + \text{H}]^+$ 460.2686, found 460.2684.

2-(2-methoxyphenyl)-4,4,5,5-tetramethyl-1,3,2-dioxaborolane (18d)



In a glove box, $[\text{Ir}(\text{OMe})(\text{cod})]_2$ (8.3 mg, 0.0125 mmol), **15** (0.0250 mmol, 10.0 mg), bis(pinacolato)diboron (254.0 mg, 1 mmol) and anhydrous, degassed THF (3 mL) were placed in a 15 mL pressure tube containing a magnetic stir bar, and the mixture was stirred for 1 min at room temperature. Anisole (108.0 mg, 1.0 mmol) was added to the tube; the reaction vessel was sealed and heated at 100 °C. Reaction progress was monitored by GC over 4 hour intervals. After 12 hours all of bis(pinacolato)diboron was consumed and no further conversion was observed, the reaction mixture was allowed to return to room temperature and was exposed to air. The volatiles were then removed under reduced pressure and the product was characterized as mixture of 6:1:2 (ortho: meta+para: diborylation) with 55% total GC conversion, (for better clarity of isomeric ratio on ^1H NMR of crude material, some starting material was removed under vacuum).⁸

2-(2-methoxy-4-methylphenyl)-4,4,5,5-tetramethyl-1,3,2-dioxaborolane (18e)

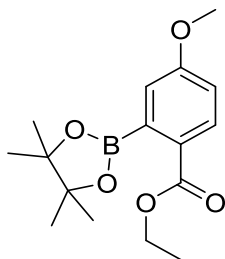


In a glove box, $[\text{Ir}(\text{OMe})(\text{cod})]_2$ (8.3 mg, 0.0125 mmol), **15** (0.0250 mmol, 10.0 mg), bis(pinacolato)diboron (254.0 mg, 1 mmol) and anhydrous degassed THF (3 mL) were placed in a 15 mL pressure tube containing a magnetic stir bar, and the mixture was stirred for 1 min at room temperature. 3-Methyl anisole (122.0 mg, 1.0 mmol) was added

to the tube; the reaction vessel was sealed and heated at 100 °C. Reaction progress was monitored by GC over 4 hour intervals. After 12 hours, all bis(pinacolato)diboron was consumed and 46% GC conversion based on substrate and no further was observed (crude mixture contained 7% of the meta isomer). The reaction mixture was allowed to return to room temperature and was exposed to air. The volatiles were then removed under reduced pressure and product was purified by Kugelrohr distillation. The product was isolated as white solid (86.0 mg) in 35 % isolated yield.

¹H NMR (500 MHz, CDCl₃) δ ppm 1.32 (s, 12 H) 2.33 (s, 3 H) 3.8 (s, 3 H) 6.65 (s, 1 H) 6.74 (d, *J*=7.4 Hz, 1 H) 7.55 (d, *J*=7.5 Hz, 1 H).⁹

Ethyl 4-methoxy-2-(4,4,5,5-tetramethyl-1,3,2-dioxaborolan-2-yl)benzoate (18f)

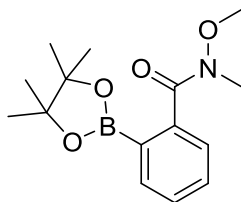


In a glove box, [Ir(OMe)(cod)]₂ (8.3 mg, 0.0125 mmol), **15** (0.0250 mmol, 10.0 mg), bis(pinacolato)diboron (254.0 mg, 1.0 mmol) and anhydrous, degassed *n*-hexane (1 mL) were placed in a 15 mL pressure tube containing a magnetic stir bar, and the mixture was stirred for 1 min at room temperature. Ethyl 4-methoxybenzoate (180.0 mg, 1.0 mmol) was added to the tube, the reaction vessel was sealed and heated at 80 °C, and reaction progress was monitored by GC. After 12 hours 90% conversion was observed and reaction mixture was allowed to return to room temperature and was exposed to air. Purification with column chromatography (gradient from hexane/EtOAc = 9/1 to

hexane/EtOAc = 4/1) resulted in ethyl 4-methoxy-2-(4,4,5,5-tetramethyl-1,3,2-dioxaborolan-2-yl)benzoate (226.0 mg) as oil with 77% isolated yield. (5% conversion to ethyl 4-methoxy-2,6-bis(4,4,5,5-tetramethyl-1,3,2-dioxaborolan-2-yl)benzoate was observed by ¹H NMR of the crude reaction mixture and by GC). ¹H NMR (500 MHz, CDCl₃) δ ppm 1.37 (t, *J*=7.1 Hz, 3H) 1.43 (s, 12 H) 3.86 (s, 3 H) 4.36 (q, *J*=7.3 Hz, 2 H) 6.88 (dd, *J*=8.8, 2.5 Hz, 1 H) 6.95 (d, *J*=2.5 Hz, 1 H) 7.91 (d, *J*=8.8 Hz, 1 H); ¹³C NMR (125 MHz, CDCl₃) δ ppm 14.4, 24.9, 55.4, 60.9, 84.0, 114.1, 116.8, 126.0, 130.7, 162.4, 167.7; ¹¹B NMR (160 MHz, CDCl₃) δ ppm 31.1 (s); HRMS (ESI) *m/z* calcd for C₁₆H₂₄BO₅ [M + H]⁺ 307.1720, found 307.1726.

N-Methoxy-N-methyl-2-(4,4,5,5-tetramethyl-1,3,2-dioxaborolan-2-yl)benzamide

(18g)

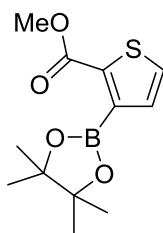


In a glove box, [Ir(OMe)(cod)]₂ (8.3 mg, 0.0125 mmol), **15** (0.0250 mmol, 10.0 mg), bis(pinacolato)diboron (254.0 mg, 1.0 mmol) and anhydrous, degassed THF (4.5 mL) were placed in a 15 mL pressure tube containing a magnetic stir bar, and the mixture was stirred for 1 min at room temperature. *N*-Methoxy-*N*-methylbenzamide (165.0 mg, 1.0 mmol) was added to the tube; the reaction vessel was sealed and heated at 80 °C. Reaction progress was monitored by GC over 4 hour intervals. After 12 hours the reaction mixture was allowed to return to room temperature and was exposed to air. The volatiles were then removed under reduced pressure and the product was purified by

silica column chromatography (gradient from CHCl_3 to 2% MeOH: 98% CHCl_3). Colorless viscose oil (244.4 mg) was obtained in 84% isolated yield.

^1H NMR (500 MHz, CDCl_3) δ ppm 1.32 (s, 12 H) 3.34 (br. s., 3 H) 3.50 (br. s., 3 H) 7.38 - 7.46 (m, 2 H) 7.49 - 7.55 (m, 1 H) 7.72 - 7.77 (m, 1 H); ^{13}C NMR (125 MHz, CDCl_3) δ ppm 25.0, 34.03, 61.0, 83.32, 126.5, 128.0, 128.1, 128.7, 129.5, 130.03, 130.6, 132.2, 133.6 (br); (Presumably, due to interaction of NOME group with pinacol group some peaks in ^1H NMR and ^{13}C NMR are broad). ^{11}B NMR (160 MHz, CDCl_3) δ ppm 27.8 (br,s) ; HRMS (ESI) m/z calcd for $\text{C}_{15}\text{H}_{23}\text{BNO}_4$ $[\text{M} + \text{H}]^+$ 292.1723, found 292.1728.

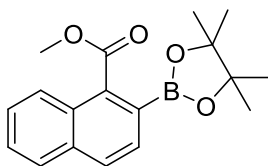
Methyl 3-(4,4,5,5-tetramethyl-1,3,2-dioxaborolan-2-yl)thiophene-2-carboxylate (18h)



In a glove box, $[\text{Ir}(\text{OMe})(\text{cod})]_2$ (8.3 mg, 0.0125 mmol), **15** (0.0250 mmol, 10.0 mg), bis(pinacolato)diboron (254.0 mg, 1.0 mmol) and anhydrous, degassed *n*-hexane (2 mL) were placed in a 15 mL pressure tube containing a magnetic stir bar, and the mixture was stirred for 1 min at room temperature. Thiophene-2-carboxylic acid methyl ester (142.0 mg, 1.0 mmol) was added to the tube; the reaction vessel was sealed and heated at 80 °C. Reaction progress was monitored by GC over 1 h interval. After 1h, the reaction mixture was allowed to return to room temperature and was exposed to air. 85% GC conversion was observed (ratio 3 position: 5 position: diborylated: 14:1:1). The volatiles were then removed under reduced pressure and Kugelrohr distillation resulted in a white solid

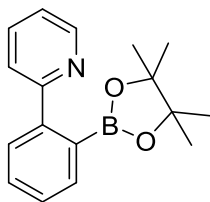
(174.2 mg) in 65% isolated yield. ^1H NMR (500 MHz, CDCl_3) δ 1.42 (s, 12H), 3.9 (s, 3H), 7.19 (d, $J = 4.9$ Hz, 1H), 7.5 (d, $J = 4.9$ Hz, 1H).¹⁰

Methyl 2-(4,4,5,5-tetramethyl-1,3,2-dioxaborolan-2-yl)-1-naphthoate (18i)



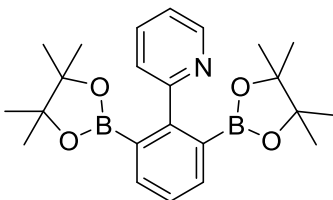
In a glove box, $[\text{Ir}(\text{OMe})(\text{cod})]_2$ (8.3 mg, 0.0125 mmol), **15** (0.025 mmol, 10.0 mg), bis(pinacolato)diboron (254.0 mg, 1.0 mmol) and anhydrous, degassed *n*-hexane (1 mL) were placed in a 15 mL pressure tube containing a magnetic stir bar, and the mixture was stirred for 1 min at room temperature. Methyl 1-naphthoate (186.0 mg, 1.0 mmol) was added to the tube, the reaction vessel was sealed and heated at 80 °C, Reaction progress was monitored by GC. After 8h full conversion was observed and the reaction mixture was allowed to return to room temperature and was exposed to air. Purification with column chromatography (dichloromethane) resulted in colorless oil (265.0 mg) in 85% isolated yield. ^1H NMR (500 MHz, CDCl_3) δ ppm 1.39 (s, 12 H) 4.03 (s, 3 H) 7.50 - 7.58 (m, 2 H), 7.78 (d, $J=8.3$ Hz, 1 H) 7.83 - 7.89 (m, 1 H) 7.9 (d, $J=8.3$ Hz, 1 H) 8.1 (d, $J=8.3$ Hz, 1 H); ^{13}C NMR (125 MHz, CDCl_3) δ ppm 24.9, 52.4, 84.2, 125.5, 127.0, 127.0, 128.1, 129.4, 129.5, 134.4, 137.0, 170.5; ^1H NMR (500 MHz, C_6D_6) δ ppm 1.12 (s, 12 H) 3.77 (s, 3 H) 7.17 - 7.21 (m, 1 H) 7.25 (ddd, $J=8.3, 6.9, 1.5$ Hz, 1 H) 7.51 (d, $J=8.3$ Hz, 1 H) 7.59 (d, $J=7.8$ Hz, 1 H) 8.01 (d, $J=8.3$ Hz, 1 H) 8.35 (d, $J=8.3$ Hz, 1 H); ^{13}C NMR (125 MHz C_6D_6) δ ppm 24.5, 51.6, 83.7, 125.7, 126.8, 126.9, 128.1, 129.1, 129.8, 129.9, 134.7, 138.4, 169.7; ^{11}B NMR (160 MHz, CDCl_3) δ ppm 31.1 (s); HRMS (ESI) m/z calcd for $\text{C}_{18}\text{H}_{22}\text{BO}_4$ $[\text{M} + \text{H}]^+$ 313.1614, found 313.1612.

2-(2-(4,4,5,5-tetramethyl-1,3,2-dioxaborolan-2-yl)phenyl)pyridine (18j**)**



In a glove box, $[\text{Ir}(\text{OMe})(\text{cod})]_2$ (8.3 mg, 0.0125 mmol), **15** (0.0250 mmol, 10.0 mg), bis(pinacolato)diboron (254.0 mg, 1.0 mmol) and anhydrous, degassed THF (2 mL) were placed in a 15 mL pressure tube containing a magnetic stir bar, and the mixture was stirred for 1 min at room temperature. 2-Phenyl pyridine (202.0 mg, 1.3 mmol) was added to the tube, the reaction vessel was sealed and heated at 60 °C, and reaction progress was monitored by GC. After 2h the reaction mixture was allowed to return to room temperature and was exposed to air. After removal of solvent, purification using silica column chromatography (hexane/EtOAc = 1/3) resulted in a white solid (182 mg) 65% isolated yield. (15% of diborylated material was observed in crude reaction mixture by GC, which was characterized as **18j'** by independent synthesis, see below). ^1H NMR (500 MHz, CDCl_3) δ ppm 1.45 (s, 12H), 7.27–7.44 (m, 3H), 7.68 (d, J = 7.8 Hz, 1H), 7.75 (d, J = 7.3 Hz, 1H), 7.83 (d, J = 8.3 Hz, 1H), 7.99 (td, J = 7.8, 1.5 Hz, 1H), 8.70 (d, J = 5.4 Hz, 1H).¹¹

2-(2,6-bis(4,4,5,5-tetramethyl-1,3,2-dioxaborolan-2-yl)phenyl)pyridine (18j'**)**



In a glove box, $[\text{Ir}(\text{OMe})(\text{cod})]_2$ (8.3 mg, 0.0125 mmol), **15** (0.0250 mmol, 10.0 mg), bis(pinacolato)diboron 508.0 mg, 2.0 mmol) and anhydrous, degassed THF (2 mL) were

placed in a 15 mL pressure tube containing a magnetic stir bar, and the mixture was stirred for 1 min at room temperature. 2-phenyl pyridine (155.2 mg, 1.0 mmol) was added to the tube, the reaction vessel was sealed and heated at 60 °C, and reaction progress was monitored by GC. After 24 hours the reaction mixture was allowed to return to room temperature and was exposed to air. Solvent was removed under reduced pressure. Upon addition of hexane to the mixture white solid precipitate. White solid (264.4 mg) with 65 % isolated yield (15% of monoborylated material was observed in GC of crude reaction mixture). ¹H NMR (500 MHz, CDCl₃) δ ppm 1.42 (s, 24 H) 7.37 (m, 2 H) 7.79 (d, *J*=7.34 Hz, 2 H) 7.91 - 7.96 (t, *J*=7.83 Hz, 1 H) 8.68 (d, *J*=5.4 Hz, 1 H) 8.81 (d, *J*=7.8 Hz, 1 H); ¹³C NMR (125 MHz, CDCl₃) δ ppm 26.1, 82.0, 121.6, 122.4, 129.9, 134.9, 141.6, 142.6, 157.7; ¹¹B NMR (160 MHz, CDCl₃) δ ppm 21.6 (s); HRMS (ESI) *m/z* calcd for C₂₃H₃₂B₂NO₄ [M + H]⁺ 408.2517, found 408.2526

Borylation of Chlorobenzene

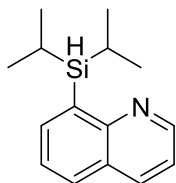
In a glove box, [Ir(OMe)(cod)]₂ (8.3 mg, 0.0125 mmol), **15** (0.0250 mmol, 10.0 mg), bis(pinacolato)diboron (127.0 mg, 0.5 mmol) and anhydrous, degassed THF (1 mL) were placed in a 15 mL pressure tube containing a magnetic stir bar, and the mixture was stirred for 1 min at room temperature. Chlorobenzene (56.0 mg, 0.5 mmol) was added to the tube; the reaction vessel was sealed and heated at 80 °C. The reaction was stopped after 16 hours, and the mixture was allowed to return to room temperature and was exposed to air. The volatiles were then removed under reduced pressure and the product was characterized as mixture of isomers, with ortho: (meta+para) being 1:3 after 55% conversion.

IrCODSiPBz (19)

In a nitrogen filled glove box, [Ir(OMe)(cod)]₂ (100.0 mg, 0.151 mmol) was fully dissolved in a minimum amount of *n*-hexane (30 mL) in a 100 mL flask, **15** (121.0 mg, 0.302 mmol) was added to the flask as a solid. Upon addition of SiPBz, the solution turned a deep red color. After 15 minutes, ³¹P NMR showed full consumption of free phosphine. Then the solvent was fully removed under vacuum and the crude was dissolved in a minimal amount of pentane and stored in a -30 °C freezer. Dark red crystals were obtained after 2 days (100.1 mg, 47% isolated yield).

Structure determination was made by single crystal X-ray diffraction studies. ¹H NMR (500 MHz, C₄D₈O, d₈-THF) δ ppm 0.97 (d, *J*=7.4 Hz, 6 H), 1.02 (d, *J*=7.4 Hz, 6 H), 1.55 - 1.63 (m, 2 H), 1.63 - 1.70 (m, 2 H), 1.75 - 1.85 (m, 2 H), 1.97 - 2.07 (m, 2 H), 2.07 - 2.18 (m, 2 H), 2.26 - 2.40 (s, 6 H), 3.77 (m, 2 H), 5.38 (m, 2 H), 7.10 - 7.23 (m, 5 H), 7.28 (td, *J*=7.24, 1.77 Hz, 1 H), 7.38 - 7.53 (m, 5 H), 7.71 (d, *J*=7.1 Hz, 1 H); ¹³C NMR (125 MHz, C₄D₈O, d₈-THF) δ ppm 19.7, 21.2 (d, *J*=2.8 Hz), 21.5 (d, *J*=2.3 Hz), 30.3 (d, *J*=2.9 Hz), 34.3 (d, *J*=2.9 Hz), 77.7 (d, *J*=12.4 Hz), 81.3, 129.2, 129.3, 129.76, 129.84, 130.1, 132.3 (d, *J*=5.7 Hz), 133.6, 133.9, 134.2, 134.3, 135.2 (d, *J*=22.7 Hz), 140.69, 140.71, 148.6, 157.2, 157.6; ³¹P NMR (202 MHz, C₄D₈O, d₈-THF) δ ppm 52.8 (s)

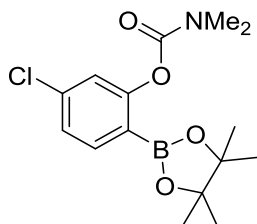
8-(diisopropylsilyl)quinolone (QSi) (20)



sec-Butyllithium (1.3 M in cyclohexane, 7.25 mL, 9.45 mmol) was added dropwise *via* syringe to a magnetically stirred solution of 8-bromoquinoline (1.955 g, 9.4 mmol) in

35.00 mL of Tetrahydrofuran at -78°C over 5 min, followed by stirring for an additional 15 min at this temperature. Diisopropylchlorosilane (1.59 mL, 9.3 mmol), was then added dropwise *via* syringe over 10 min, and the resulting mixture was allowed to warm to ambient temperature over 2 h. After removal of the solvent and volatiles, the crude mixture was subjected to silica column using hexane. Product was obtained as colorless liquid (1.970 g), in 87% yield. ¹H NMR (500 MHz, C₆D₆) δ ppm 1.14 (d, *J*=7.3 Hz, 6 H), 1.30 (d, *J*=7.3 Hz, 6 H) 1.82 (m, 2 H) 4.50 (t, *J*=3.9 Hz, 1 H) 6.75 (dd, *J*=8.3, 3.9 Hz, 1 H) 7.23 (dd, *J*=8.1, 6.6 Hz, 1 H) 7.42 (dd, *J*=8.3, 1.5 Hz, 1 H) 7.52 (dd, *J*=8.3, 2.0 Hz, 1 H) 8.02 (dd, *J*=6.8, 1.5 Hz, 1 H) 8.67 (dd, *J*=4.4, 2.0 Hz, 1 H); ¹³C NMR (125 MHz, C₆D₆) δ ppm 12.7, 20.17, 20.22, 121.3, 126.7, 129.9, 136.4, 138.9, 139.7, 149.9, 153.4; HRMS (ESI) *m/z* calcd for C₁₅H₂₂NSi [M + H]⁺ 244.1521, found 244.1527.

5-chloro-2-(4,4,5,5-tetramethyl-1,3,2-dioxaborolan-2-yl)phenyl dimethylcarbamate
(**22a**)



In a glove box, [Ir(OMe)(cod)]₂ (8.3 mg, 0.0125 mmol), **20** (0.0250 mmol, 6.1 mg), bis(pinacolato)diboron (254.0 mg, 1.0 mmol) and anhydrous, degassed THF (1 mL) were placed in a 15 mL pressure tube containing a magnetic stir bar, and the mixture was stirred for 1 min at room temperature. 3-Chlorophenyl dimethylcarbamate (200.0 mg, 1.0 mmol) was added to the tube; the reaction vessel was sealed and heated at 80 °C. Reaction progress was monitored by GC. After 4h, 93% conversion was observed and the reaction mixture was allowed to return to room temperature and was exposed to air.

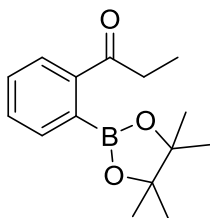
Purification with column chromatography (gradient from dichloromethane to dichloromethane/EtOAc, 98/2) resulted in pale yellow oil (195.0 mg) with 60% isolated yield.

^1H NMR (500 MHz, CDCl_3) δ ppm 1.30 (s, 12 H) 3.00 (s, 3 H) 3.12 (s, 3 H) 7.11 (d, $J=1.5$ Hz, 1 H) 7.18 (dd, $J=7.8, 2.0$ Hz, 1 H) 7.69 (d, $J=8.3$ Hz, 1 H); ^{13}C NMR (125 MHz, CDCl_3) δ ppm 24.9, 36.5, 36.7, 83.6, 122.8, 125.2, 137.0, 137.6, 155.1, 156.8; ^{11}B NMR (160 MHz, CDCl_3) δ 30.0 (br, s); HRMS (ESI) m/z calcd for $\text{C}_{15}\text{H}_{22}\text{BClNO}_4$ [$\text{M} + \text{H}$] $^+$ 326.1333 found 326.1324.

Method B

The reaction was performed using 0.5 mmol substrate (99.5 mg), $[\text{Ir}(\text{OMe})(\text{cod})]_2$ (8.3 mg, 0.0125 mmol), 2 equiv B_2pin_2 (254.0 mg), **15** (0.0250 mmol, 10.0 mg) (5.0 mol %), 1.5 ml THF. Purified by column chromatography; hexanes: EtOAc (8.5:1) using Alizarin as an indicator. The compound was isolated as a clear gel (26.0 mg, 12 % yield).

1-(2-(4,4,5,5-tetramethyl-1,3,2-dioxaborolan-2-yl)phenyl)propan-1-one (**22b**)



In a glove box, $[\text{Ir}(\text{OMe})(\text{cod})]_2$ (8.3 mg, 0.0125 mmol), **20** (0.0250 mmol, 6.1 mg), bis(pinacolato)diboron (254.0 mg, 1 mmol) and anhydrous, degassed THF (1 mL) were placed in a 15 mL pressure tube containing a magnetic stir bar, and the mixture was stirred for 1 min at room temperature. propiophenone (134.0 mg, 1.0 mmol) was added to the tube, the reaction vessel was sealed and heated at 80 °C. Reaction progress was

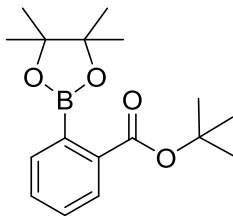
monitored by GC. After 1h the reaction mixture was allowed to return to room temperature and was exposed to air (82% GC conversion). Purification with column chromatography (hexane/EtOAc) resulted in a white solid (182.2 mg) with 70% isolated yield (NMR shows 3% starting material).

^1H NMR (500 MHz, CDCl_3) δ ppm 1.24 (t, $J=7.3$ Hz, 3 H) 1.45 (s, 12 H) 3.01 (q, $J=7.3$ Hz, 2 H) 7.43 (ddd, $J=7.9, 5.3, 2.9$ Hz, 1 H) 7.52 - 7.55 (m, 2 H) 7.82 (d, $J=7.8$ Hz, 1 H).¹²

Borylation of anisole using **20**

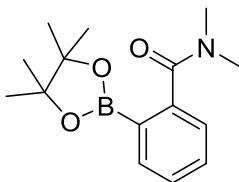
In a glove box, $[\text{Ir}(\text{OMe})(\text{cod})]_2$ (8.3 mg, 0.0125 mmol), **20** (0.0250 mmol, 6.1 mg), and anhydrous, degassed THF (3 mL) were placed in a 15 mL pressure tube containing a magnetic stir bar, and the mixture was stirred for 1 min at room temperature. Anisole (108.0 mg, 1.0 mmol) was added to the tube and lastly, bis(pinacolato)diboron (254.0 mg, 1.0 mmol) was added as a solid; the reaction vessel was sealed and heated at 80 °C. Reaction progress was monitored by GC over 4 hour intervals. After 12 hours no further conversion was observed, the reaction mixture was allowed to return to room temperature and was exposed to air. The volatiles were then removed under reduced pressure and the product was characterized as mixture of 1.6:4.2:1.0 (ortho: meta+para: diborylation) with 40% total GC conversion.

Borylation of tert-Butyl benzoate using (**20**)



In a glove box, $[\text{Ir}(\text{OMe})(\text{cod})]_2$ (3.3 mg, 0.0050 mmol), **20** (0.0100 mmol, 3.0 mg), and anhydrous, degassed THF (1.0 mL) were placed in a 15 mL pressure tube containing a magnetic stir bar, and the mixture was stirred for 1 min at room temperature. *tert*-Butyl benzoate (178.2 mg, 1.0 mmol) was added to the tube and lastly bis(pinacolato)diboron (254.0 mg, 1.0 mmol) was added as a solid, the reaction vessel was sealed and heated at 80 °C. Reaction progress was monitored by GC over 1 hour intervals. After 3 hours, (91% GC conversion based on benzoate) the reaction mixture was allowed to return to room temperature and was exposed to air. The volatiles were then removed under reduced pressure and the product was purified by column chromatography; hexanes: Et₂O (4:1) to afford a white solid (238.0 mg, 78% yield). No diborylated product was observed in the crude reaction; ¹H NMR was identical to the previous report.⁷

Borylation of *N,N*-dimethylbenzamide using (**20**)



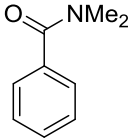
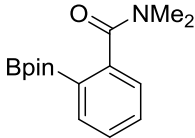
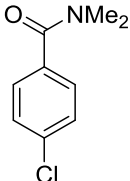
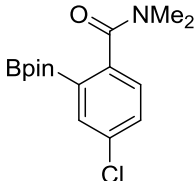
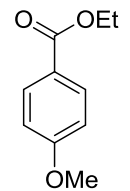
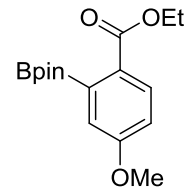
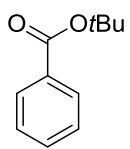
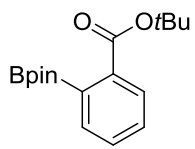
In a glove box, $[\text{Ir}(\text{OMe})(\text{cod})]_2$ (8.3 mg, 0.0125 mmol), **20** (0.0250 mmol, 6.1 mg), bis(pinacolato)diboron (254.0 mg, 1.0 mmol) and anhydrous, degassed THF (4.5 mL) were placed in a 15 mL pressure tube containing a magnetic stir bar, and the mixture was stirred for 1 min at room temperature. *N,N*-Dimethyl benzamide (149.0 mg, 1.0 mmol) was added to the tube, the reaction vessel was sealed and heated at 80 °C. Reaction progress was monitored by GC over 1 hour intervals. After 4 hours, (90% GC conversion) the reaction mixture was allowed to return to room temperature and was

exposed to air. The volatiles were then removed under reduced pressure and the product was purified by passing it through a short plug of SiO₂ eluting (hexane/EtOAc = 1/1). The product was isolated by precipitation from hexane. A white solid (220.2 mg) was isolated in 80% yield. ¹H NMR was identical to the previous report.⁷

Borylation of benzamides (17a and 18a) and benzoates (17f and tert-butyl benzoate) using (20) vs (15)

Reactions were performed under identical conditions as described for analogues reaction using (15).

Table 5. Comparing reactivity of Ir-catalyzed CHB using ligand **15** and **20**

$\text{Ar-H} \xrightarrow[\text{80 } ^\circ\text{C, Time, Solvent}]{\begin{array}{c} 1.25 \text{ mol } \% [\text{Ir}(\text{OMe})(\text{cod})]_2 \\ 2.5 \text{ mol } \% \text{ ligand} \\ 1 \text{ equiv B}_2\text{pin}_2 \end{array}} \text{Ar-Bpin}$						
Entry	Substrate	Product	Ligand	Solvent	Time (h)	% yield
1			15	THF	16	75
			20	THF	4	80
2			15	THF	16	85
			20	THF	2	85
3			15	Hex	12	77 ^a
			20	Hex	2	75 ^b
4 ^c			15	THF	16	63
			20	THF	3	78

^a5% diborylation was obtained. ^b15% diborylation was obtained. ^c 0.5 mol % [Ir(OMe)(cod)]₂ and 1.0 mol % ligand was used.

REFERENCES

REFERENCES

1. Chotana, G. A.; Vanchura, B. A., II; Tse, M. K.; Staples, R. J.; Maleczka, R. E., Jr.; Smith, M. R., III *Chem. Commun.* **2009**, 5731.
2. Frisch, M. J.; Trucks, G. W.; Schlegel, H. B.; Scuseria, G. E.; Robb, M. A.; Cheeseman, J. R.; Scalmani, G.; Barone, V.; Mennucci, B.; Petersson, G. A.; Nakatsuji, H.; Caricato, M.; Li, X.; Hratchian, H. P.; Izmaylov, A. F.; Bloino, J.; Zheng, G.; Sonnenberg, J. L.; Hada, M.; Ehara, M.; Toyota, K.; Fukuda, R.; Hasegawa, J.; Ishida, M.; Nakajima, T.; Honda, Y.; Kitao, O.; Nakai, H.; Vreven, T.; Montgomery Jr., J. A.; Peralta, J. E.; Ogliaro, F.; Bearpark, M. J.; Heyd, J.; Brothers, E. N.; Kudin, K. N.; Staroverov, V. N.; Kobayashi, R.; Normand, J.; Raghavachari, K.; Rendell, A. P.; Burant, J. C.; Iyengar, S. S.; Tomasi, J.; Cossi, M.; Rega, N.; Millam, N. J.; Klene, M.; Knox, J. E.; Cross, J. B.; Bakken, V.; Adamo, C.; Jaramillo, J.; Gomperts, R.; Stratmann, R. E.; Yazyev, O.; Austin, A. J.; Cammi, R.; Pomelli, C.; Ochterski, J. W.; Martin, R. L.; Morokuma, K.; Zakrzewski, V. G.; Voth, G. A.; Salvador, P.; Dannenberg, J. J.; Dapprich, S.; Daniels, A. D.; Farkas, Ö.; Foresman, J. B.; Ortiz, J. V.; Cioslowski, J.; Fox, D. J.; Gaussian, Inc.: Wallingford, CT, USA, 2009.
3. Zhao, Y.; Truhlar, D. *Theor. Chem. Acc.* **2008**, *120*, 215.
4. Conifer, C. M.; Law, D. J.; Sunley, G. J.; White, A. J. P.; Britovsek, G. J. *Organometallics* **2011**, *30*, 4060.
5. Wolan, A.; Zaidlewicz, M. *Org. Biomol. Chem.* **2003**, *1*, 3274.
6. Ishiyama, T.; Isou, H.; Kikuchi, T.; Miyaoura, N. *Chem. Commun.* **2010**, *46*, 159.
7. Kawamorita, S.; Ohmiya, H.; Hara, K.; Fukuoka, A.; Sawamura, M. *J. Am. Chem. Soc.* **2009**, *131*, 5058.
8. **a)** Chotana, G. A.; Rak, M. A.; Smith, M. R., III. *J. Am. Chem. Soc.* **2005**, *127*, 10539. **b)** Tajuddin, H.; Harrisson, P.; Bitterlich, B.; Collings, J. C.; Sim, N.; Batsanov, A. S.; Cheung, M. S.; Kawamorita, S.; Maxwell, A. C.; Shukla, L.; Morris, J.; Lin, Z.; Marder, T. B.; Steel, P. G. *Chem. Sci.* **2012**, *3*, 3505.
9. Iwashita, M.; Fujii, S.; Ito, S.; Hirano, T.; Kagechika, H. *Tetrahedron* **2011**, *67*, 6073.
10. Kawamorita, S.; Ohmiya, H.; Sawamura, M. *J. Org. Chem.* **2010**, *75*, 3855.
11. **a)** Kawamorita, S.; Miyzaki, T.; Ohmiya, H.; Iwai, T.; Sawamura, M. *J. Am. Chem. Soc.* **2011**, *133*, 19310. **b)** Ros, A.; Estepa, B.; Lopez-Rodriguez, R.; Alvarez, E.; Fernandez, R.; Lassaletta, J. M. *Angew. Chem.-Int. Edit.* **2011**, *50*, 11724.

12. Itoh, H.; Kikuchi, T.; Ishiyama, T.; Miyaura, N. *Chem. Lett.* **2011**, *40*, 1007.

APPENDICES

APPENDIX A, NMR Spectra

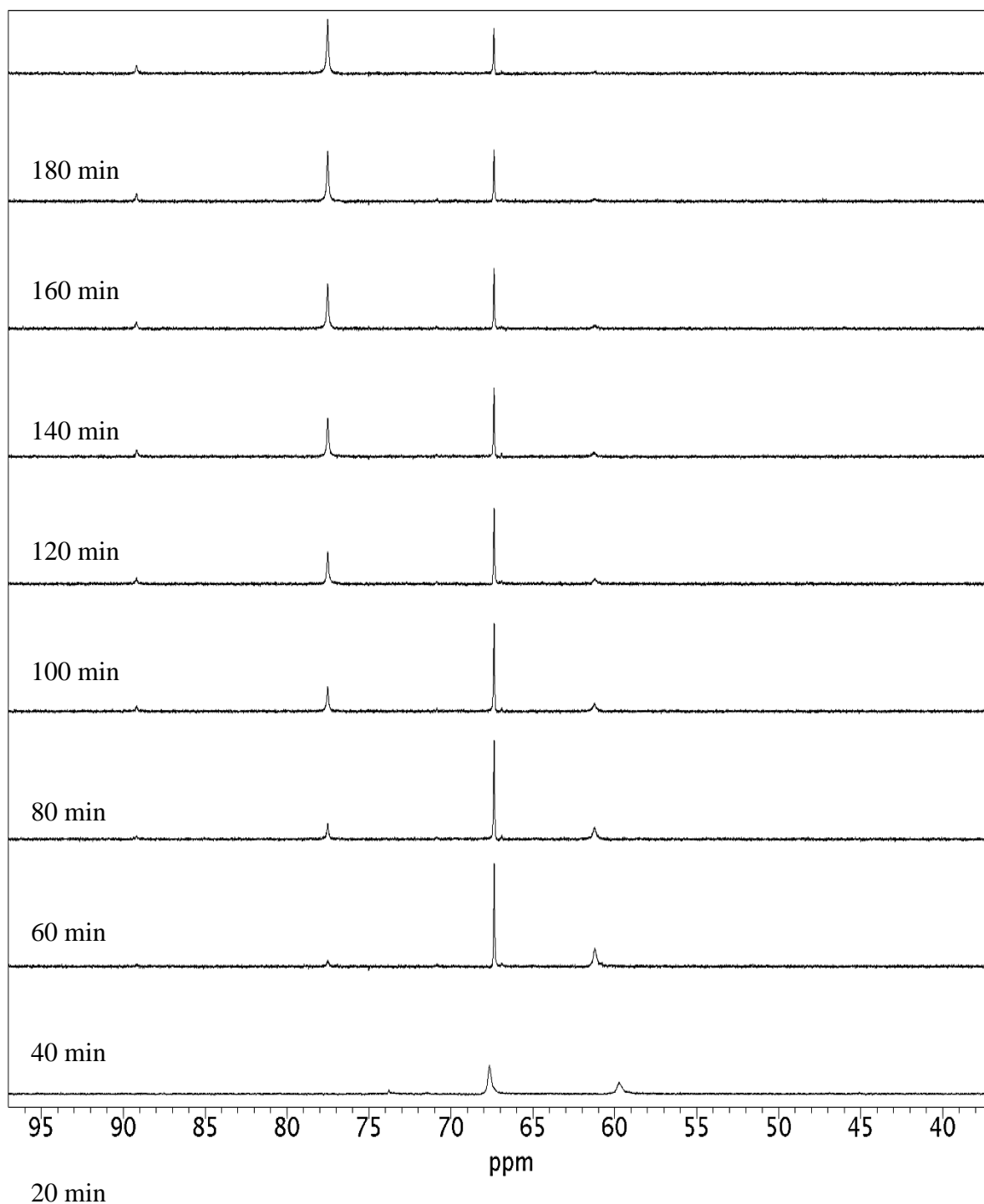


Figure A 1. $^{31}\text{P}\{^1\text{H}\}$ NMR of reaction intermediates for catalytic borylation of 2-methylthiophene with compound **5**, using 0.5 equivalents of HBpin in cyclohexane- d_{12}

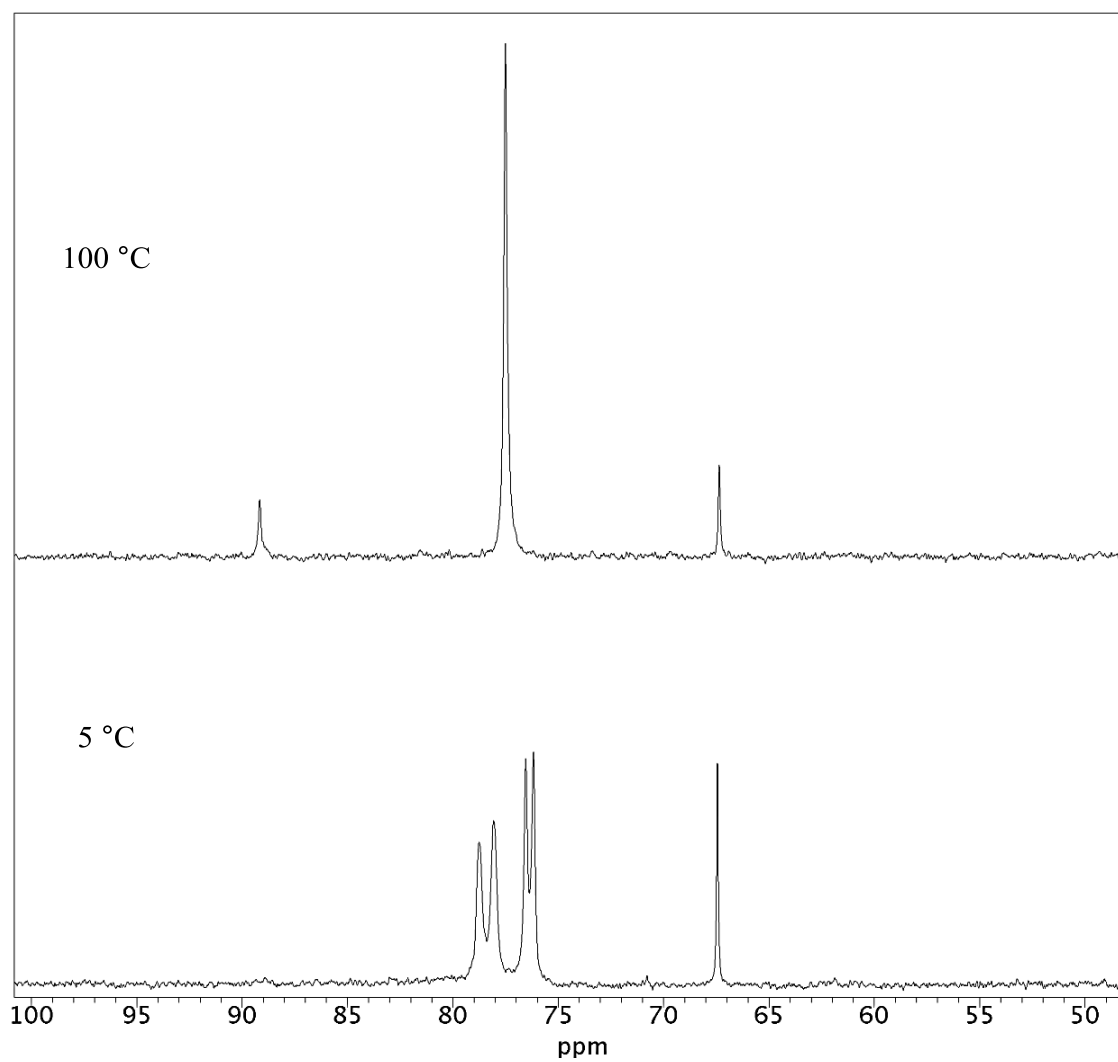


Figure A 2. $^{31}\text{P}\{^1\text{H}\}$ NMR spectra in cyclohexane- d_{12} at the end of catalytic borylation run of 2-methylthiophene with 0.5 equivalents of HBpin, mainly shows compound **10**

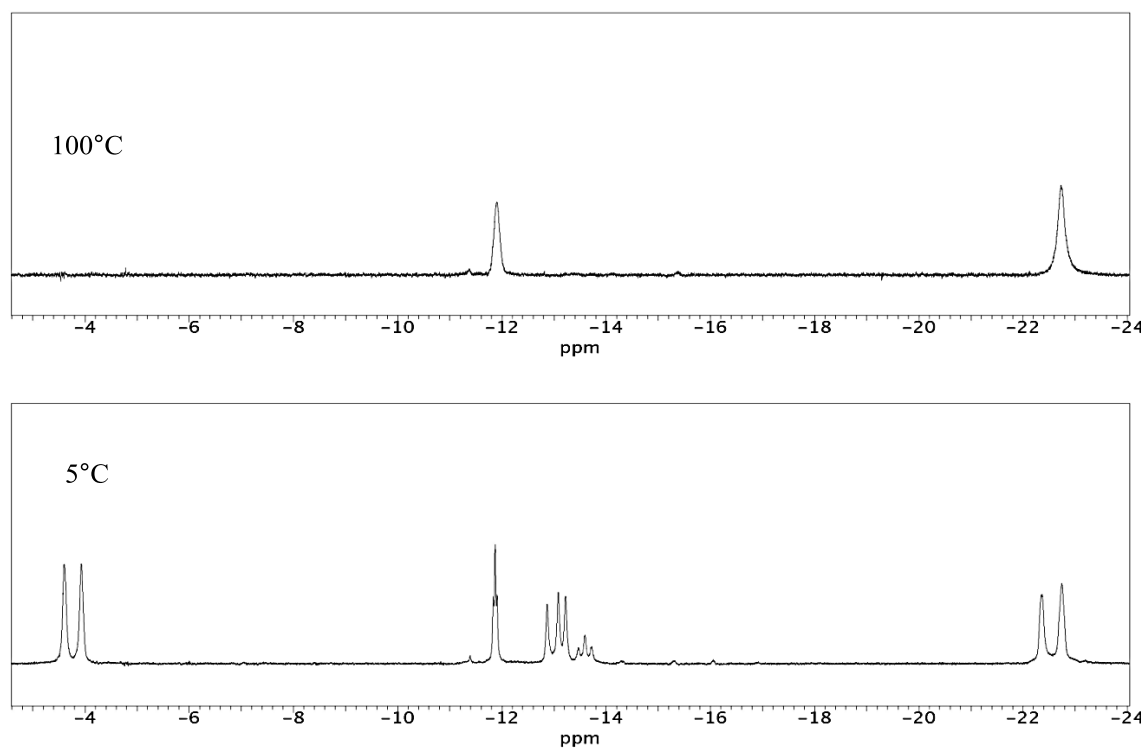


Figure A 3. ¹H NMR spectra of hydride region in cyclohexane-*d*₁₂ at the end of catalytic run of 2-methylthiophene with 0.5 equivalents of HBpin, mainly shows compound **10**

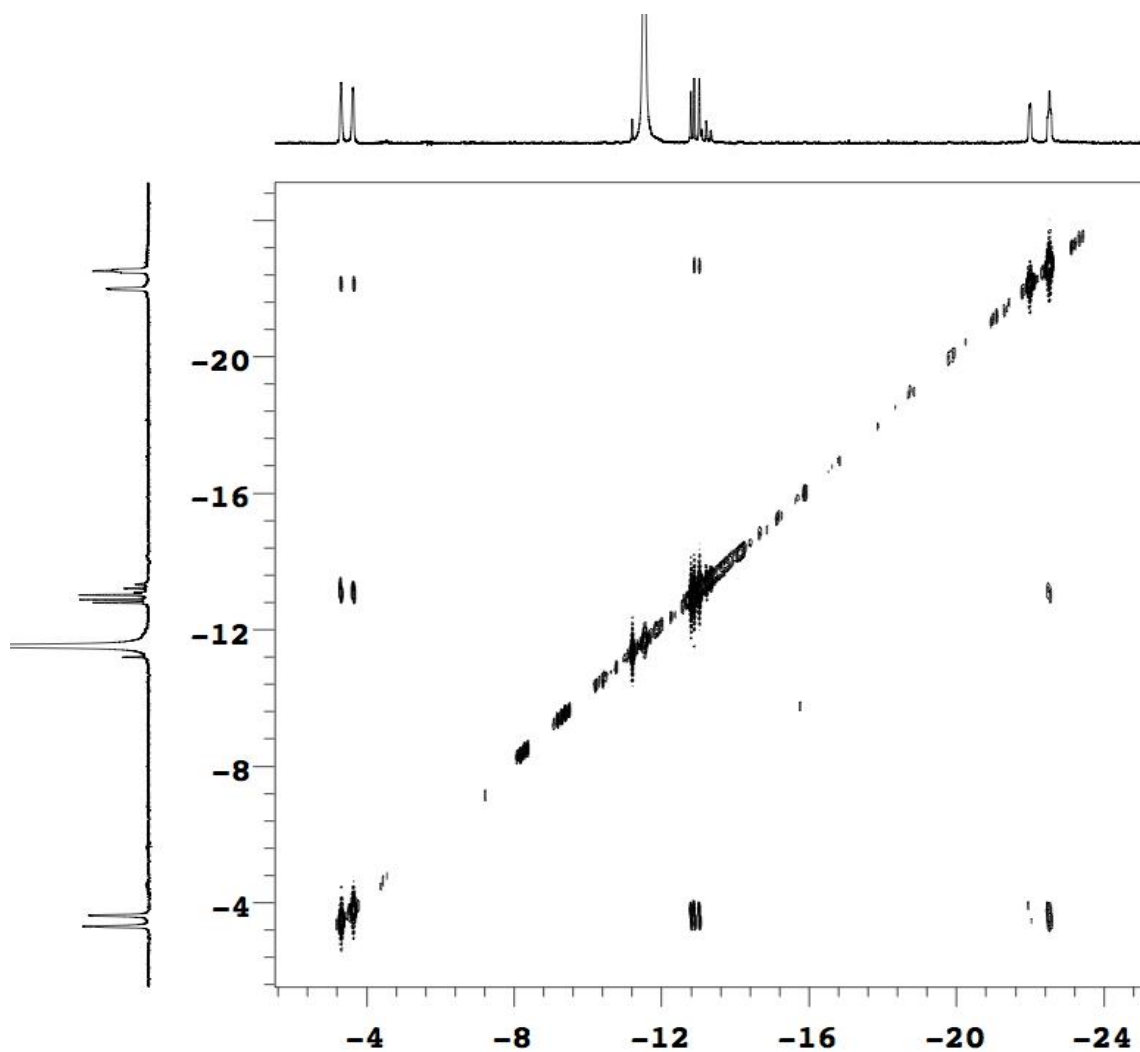


Figure A 4. gCOSY spectrum of hydride region in cyclohexane- d_{12} at the end of catalytic run of 2-methylthiophene with 0.5 equivalents of HBpin, mainly shows compound **10**

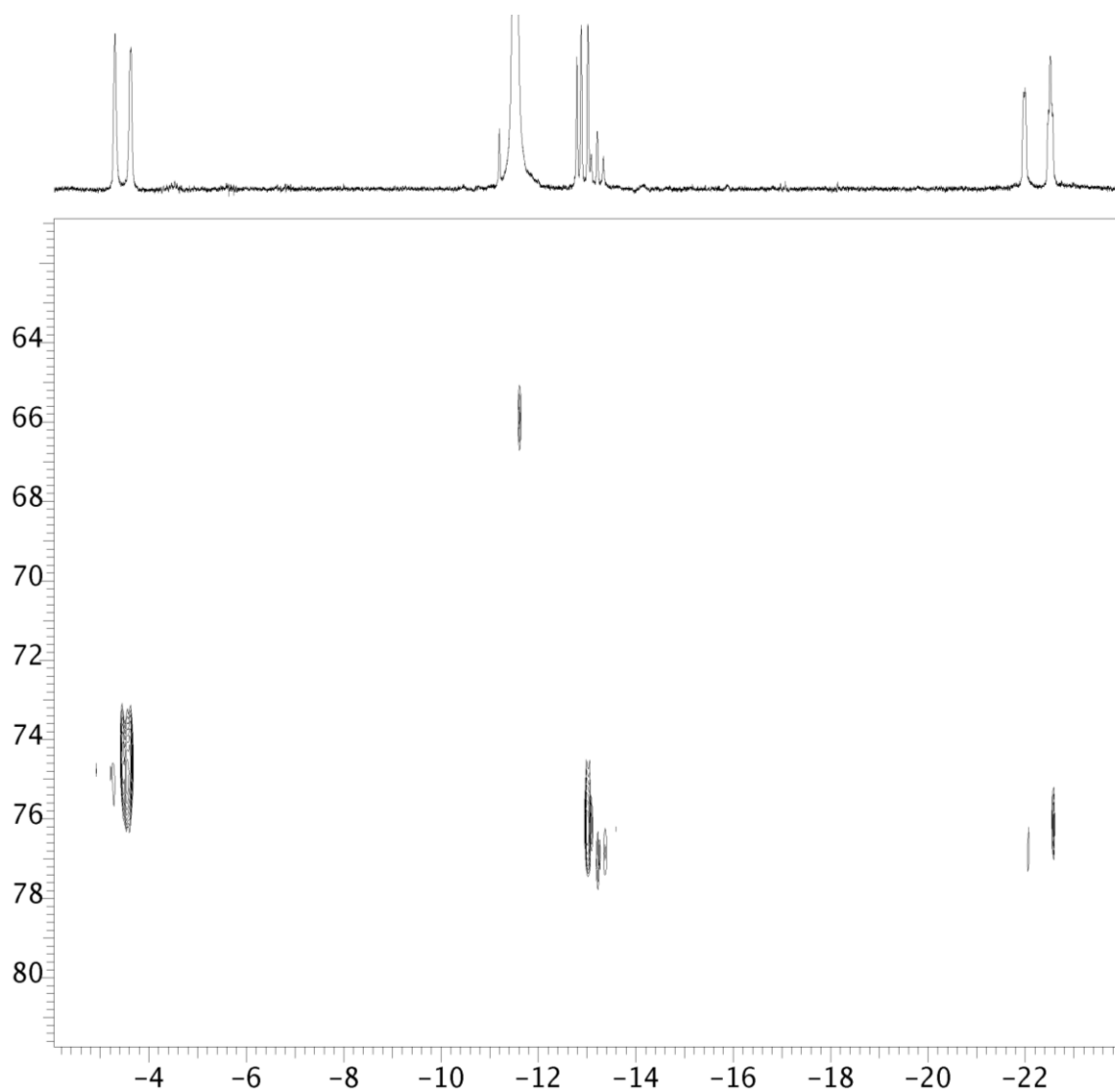


Figure A 5. ^1H - ^{31}P HMQC spectrum of hydride region in cyclohexane- d_{12} at the end of catalytic run of 2-methylthiophene with 0.5 equivalents of HBpin, mainly shows compound **10**

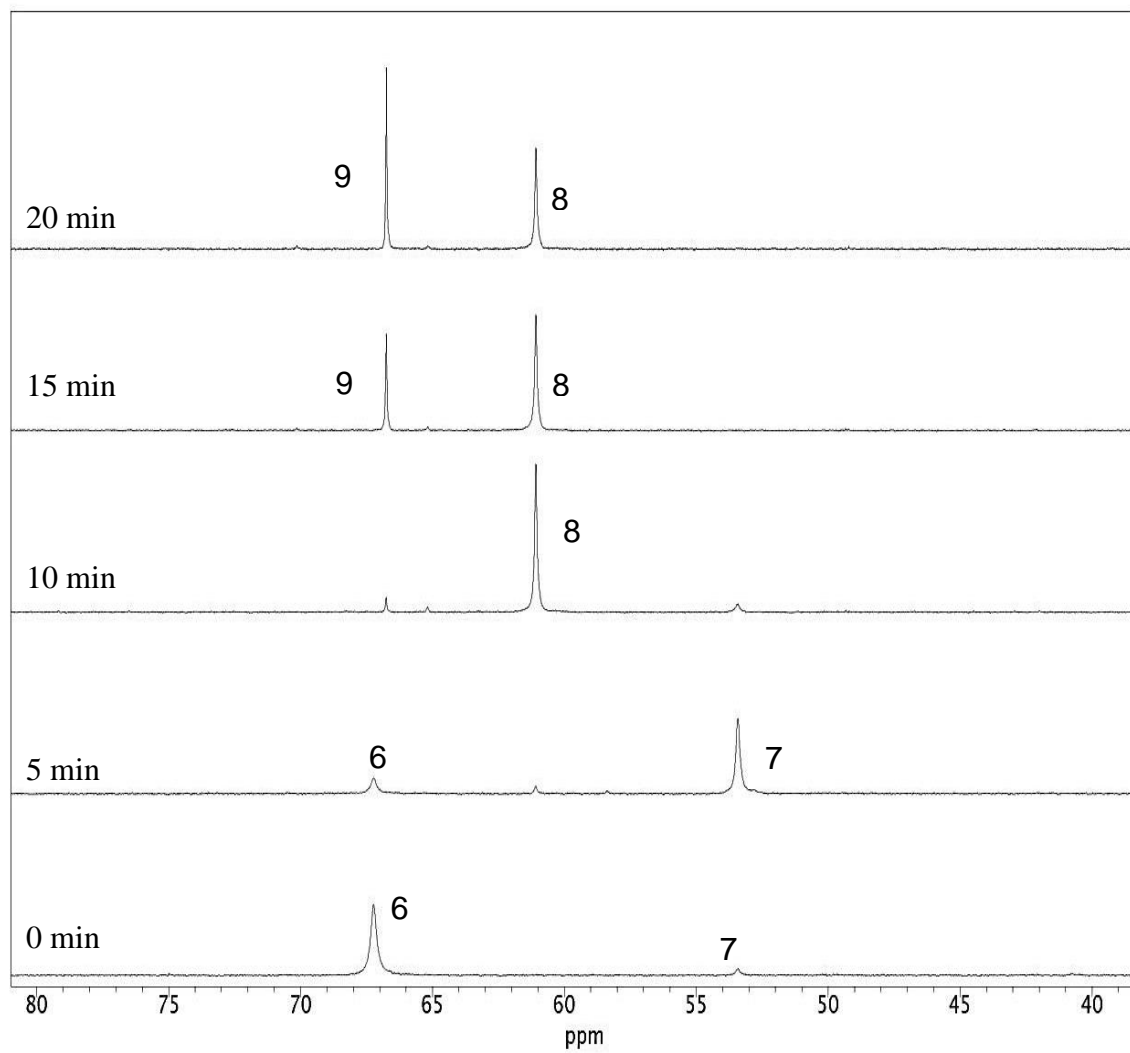


Figure A 6. $^{31}\text{P}\{^1\text{H}\}$ NMR of reaction intermediates for early stage of catalytic conversion of 2-methylthiophene with compound **5**, using 0.5 equivalents of HBpin

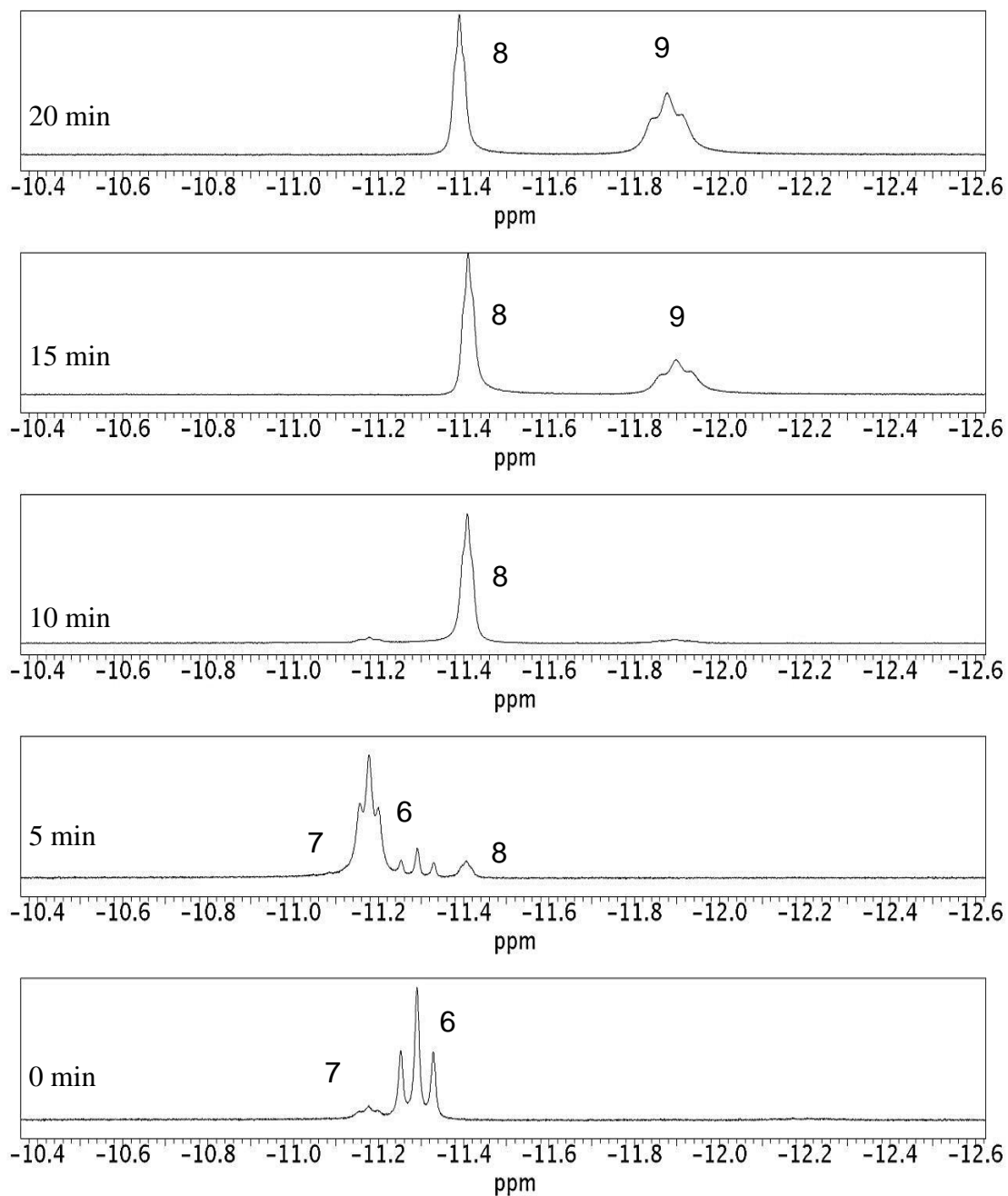


Figure A 7. Hydride region in ^1H NMR spectra of reaction intermediates for early stage of catalytic borylation of 2-methylthiophene with compound **5**, using 0.5 equivalents of HBpin in toluene- d_8 .

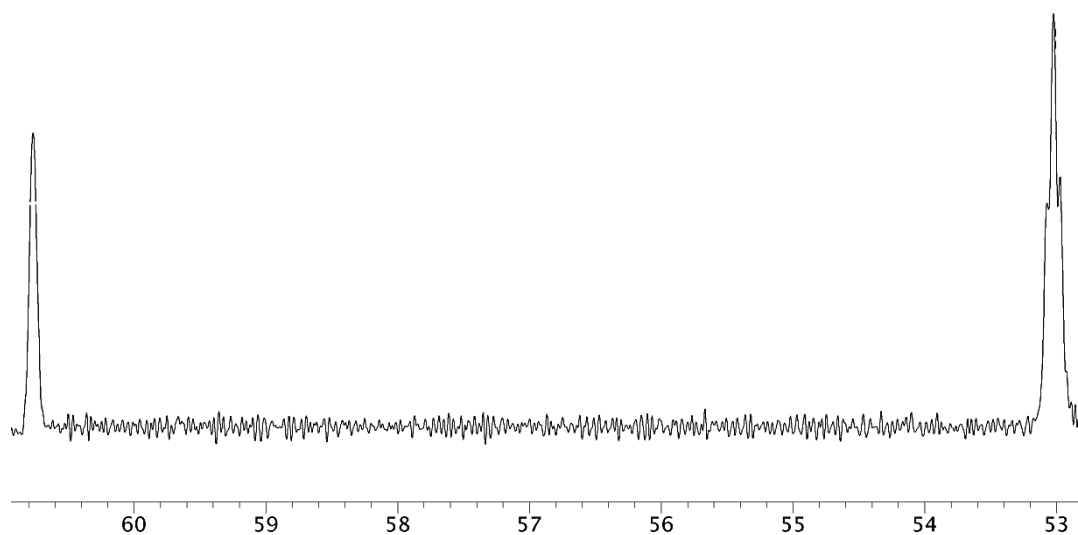


Figure A 8. ^{31}P NMR spectrum with selective decoupling of aliphatic protons for compound **7** at $-45\text{ }^{\circ}\text{C}$, ($J=9.9\text{ Hz}$)

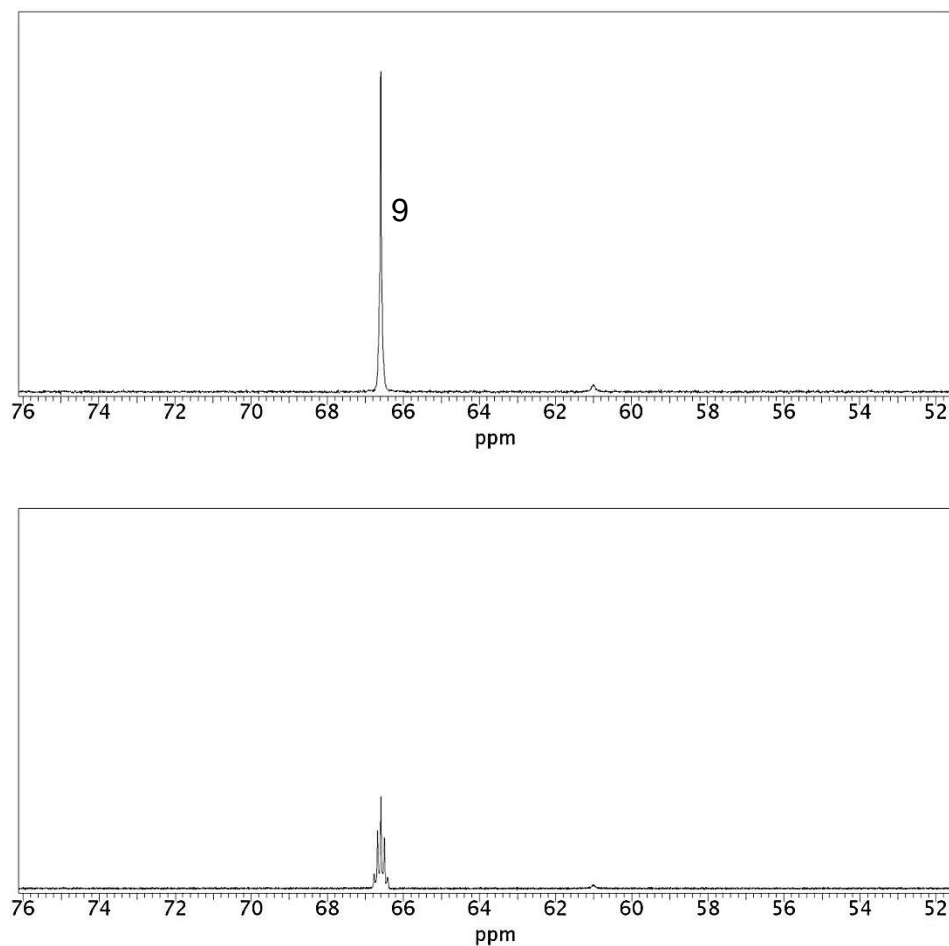


Figure A 9. ^{31}P NMR spectrum with selective decoupling of aliphatic protons for compound **9** ($J= 18.3$ Hz)

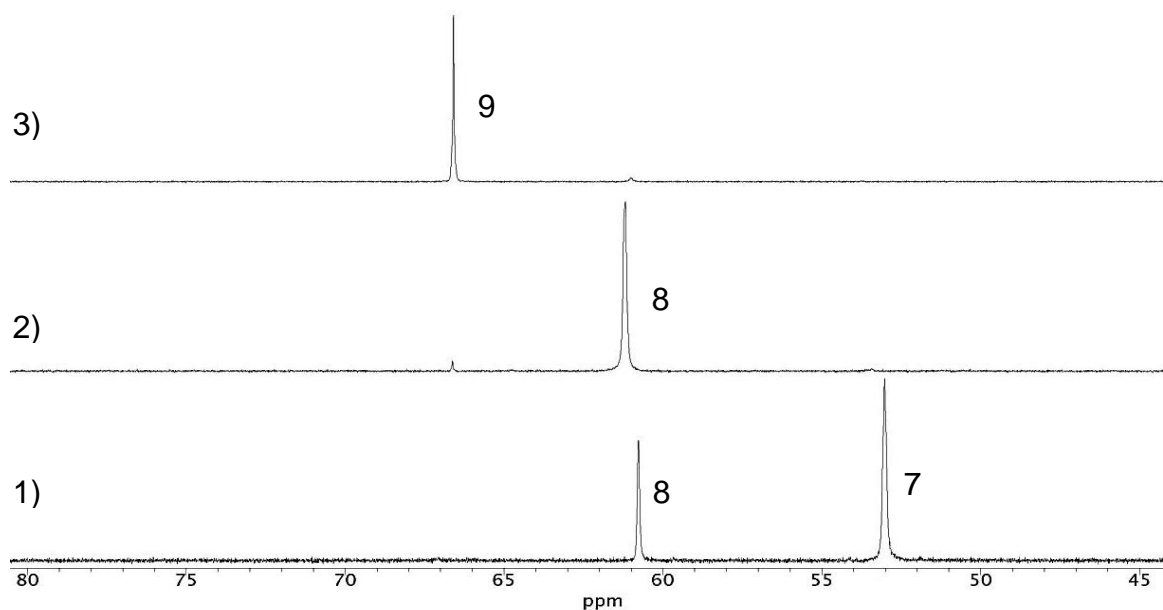


Figure A 10. $^{31}\text{P}\{^1\text{H}\}$ NMR of reaction of H_2 with compound **5**. 1) Initial spectrum at -45 °C, 2) At -15 °C after 10 sec of shaking the tube, 3) At rt after 15 minutes of shaking the tube

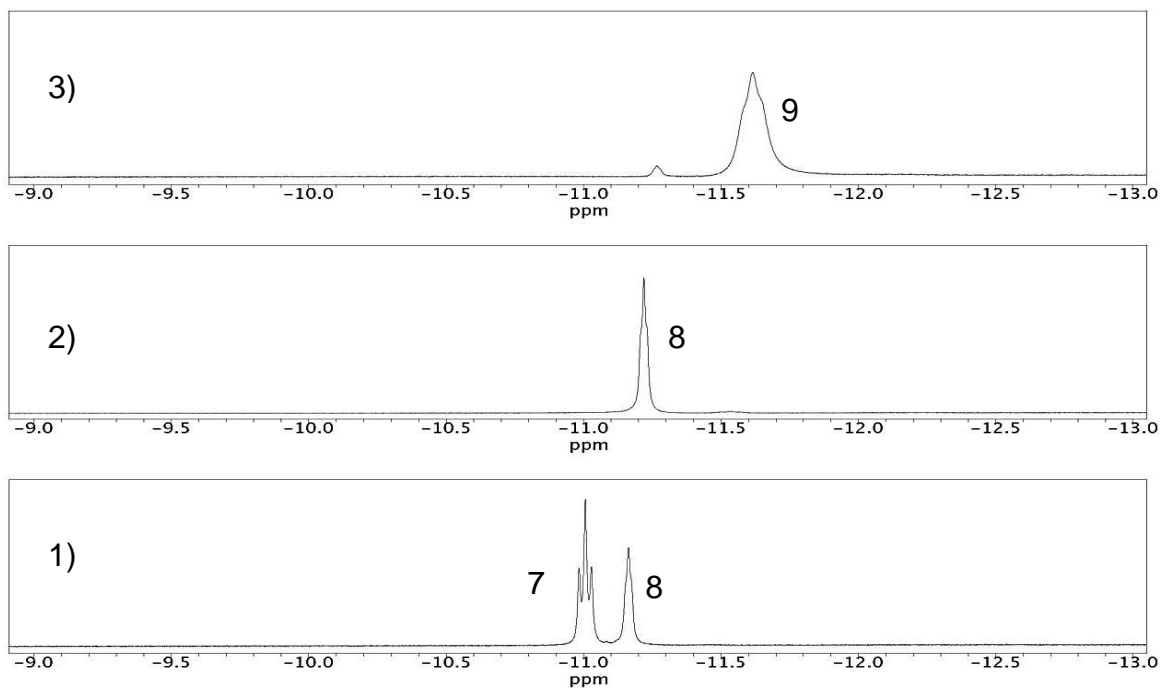


Figure A 11. Hydride region in ^1H NMR spectra of reaction of H_2 with compound **5** 1) Initial ^1H NMR at $-45\text{ }^\circ\text{C}$, 2) At $-15\text{ }^\circ\text{C}$ after 10 sec of shaking the tube, 3) At rt after 15 minutes of shaking the mixture

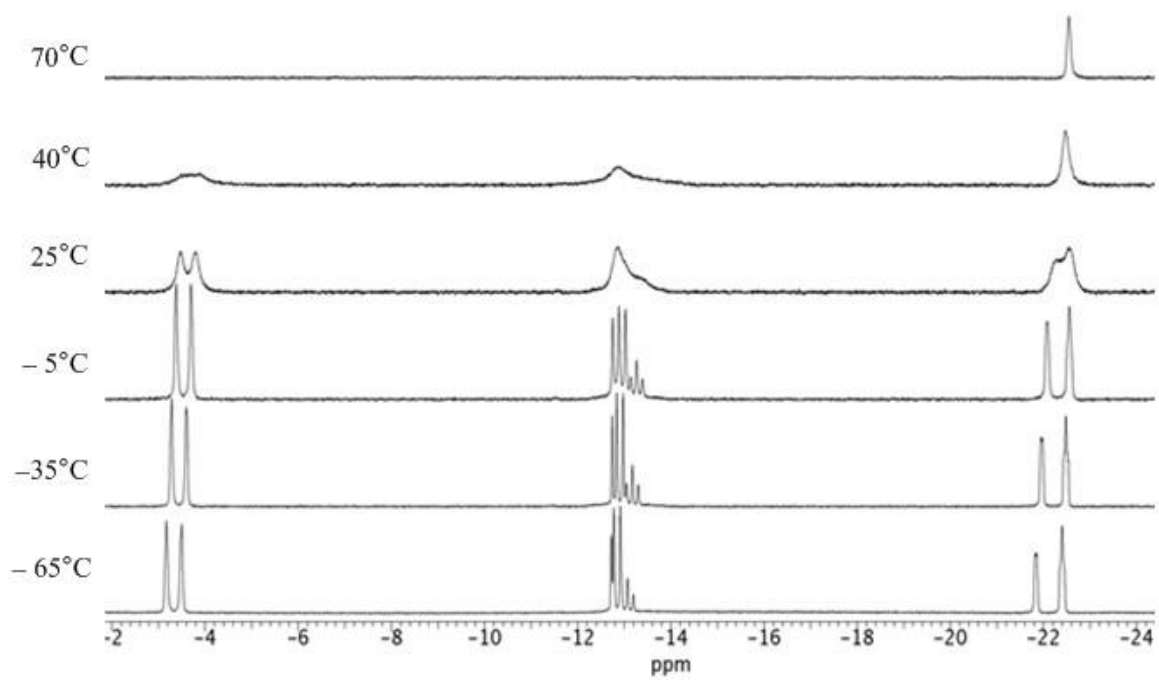


Figure A 12. Hydride region in ^1H NMR spectra of compound **10** in $\text{toluene-}d_8$ at different temperatures

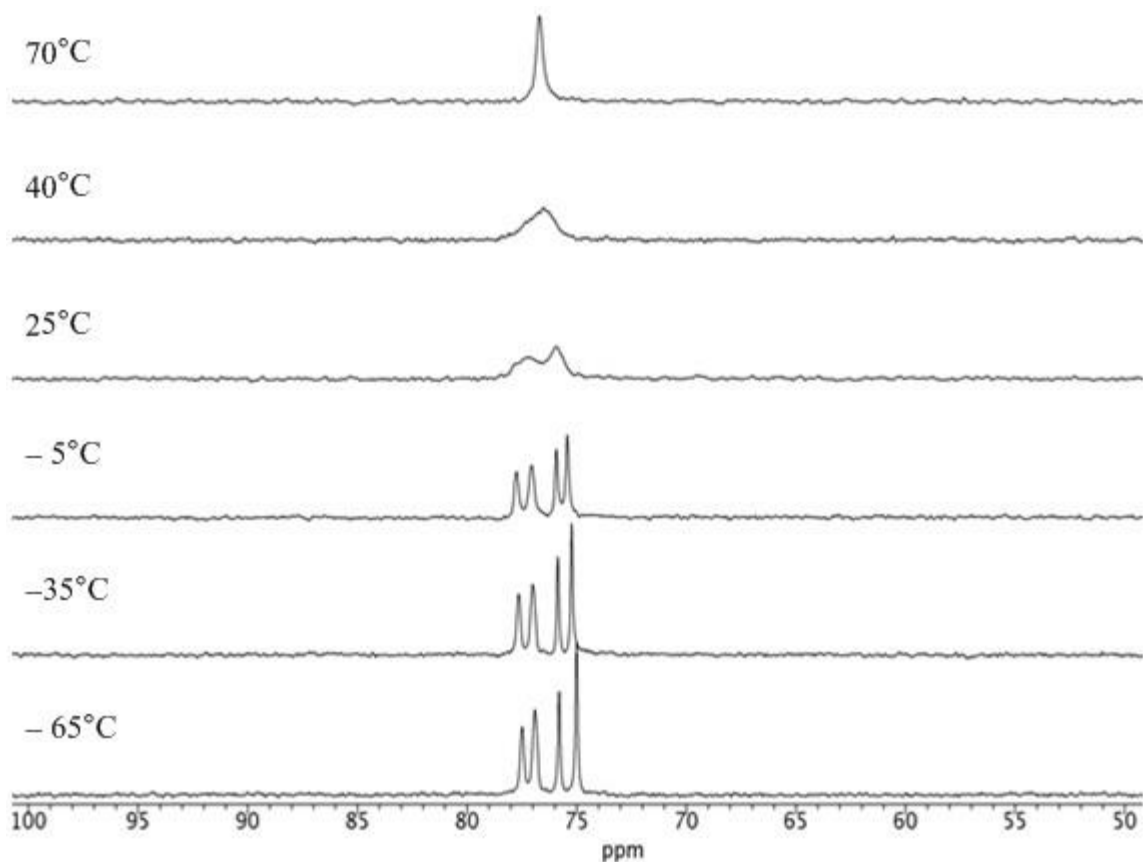


Figure A 13. $^{31}\text{P}\{^1\text{H}\}$ NMR spectra of compound **10** in toluene d_8 at different temperatures

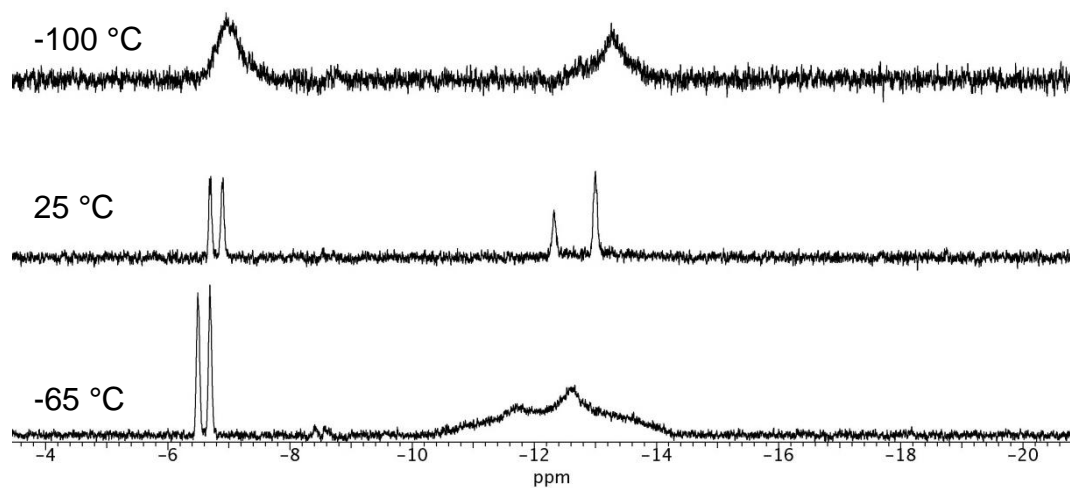


Figure A 14. ^1H NMR spectra of thermolysis of compound **10**, in toluene d_8 at different temperatures

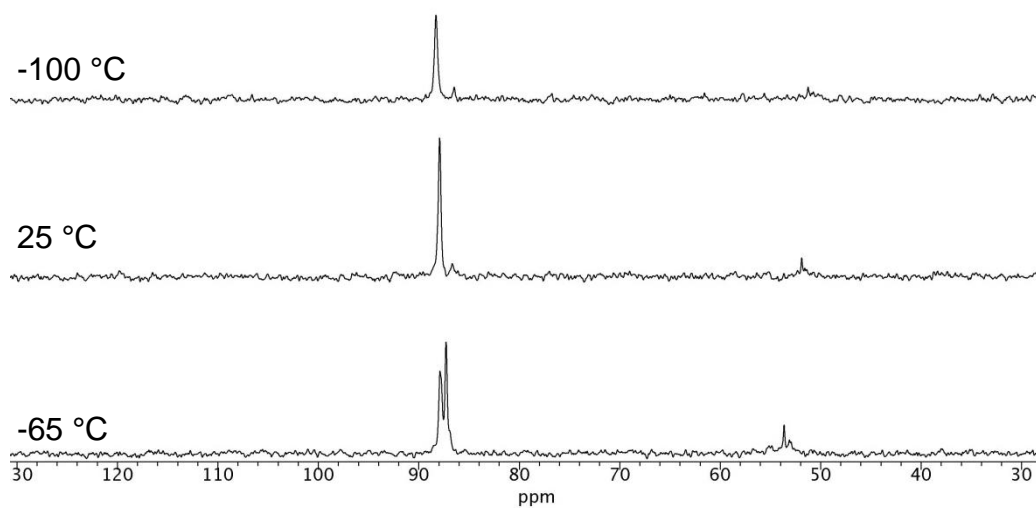


Figure A 15. $^{31}\text{P}\{^1\text{H}\}$ NMR spectra of thermolysis of compound 10, in $\text{toluene-}d_8$ at different temperatures

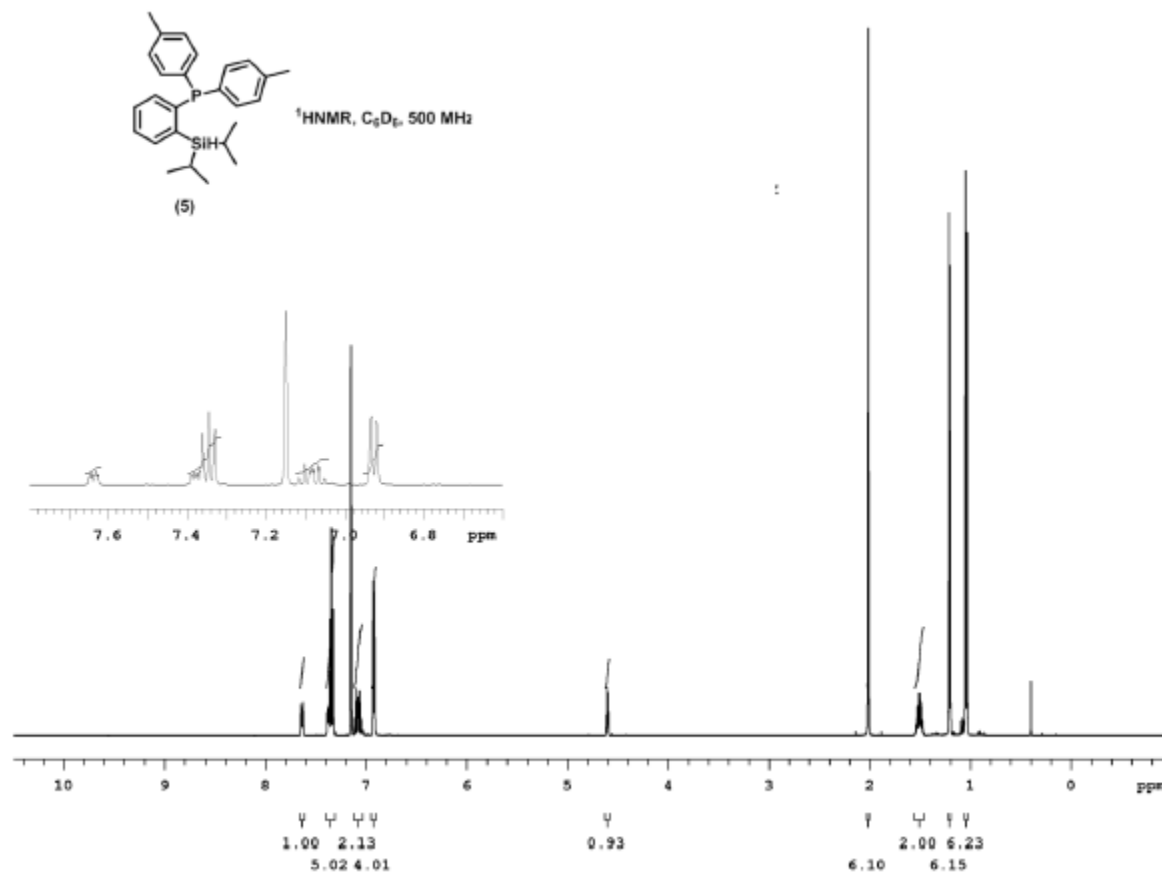


Figure A 16. ^1H NMR of compound **15**

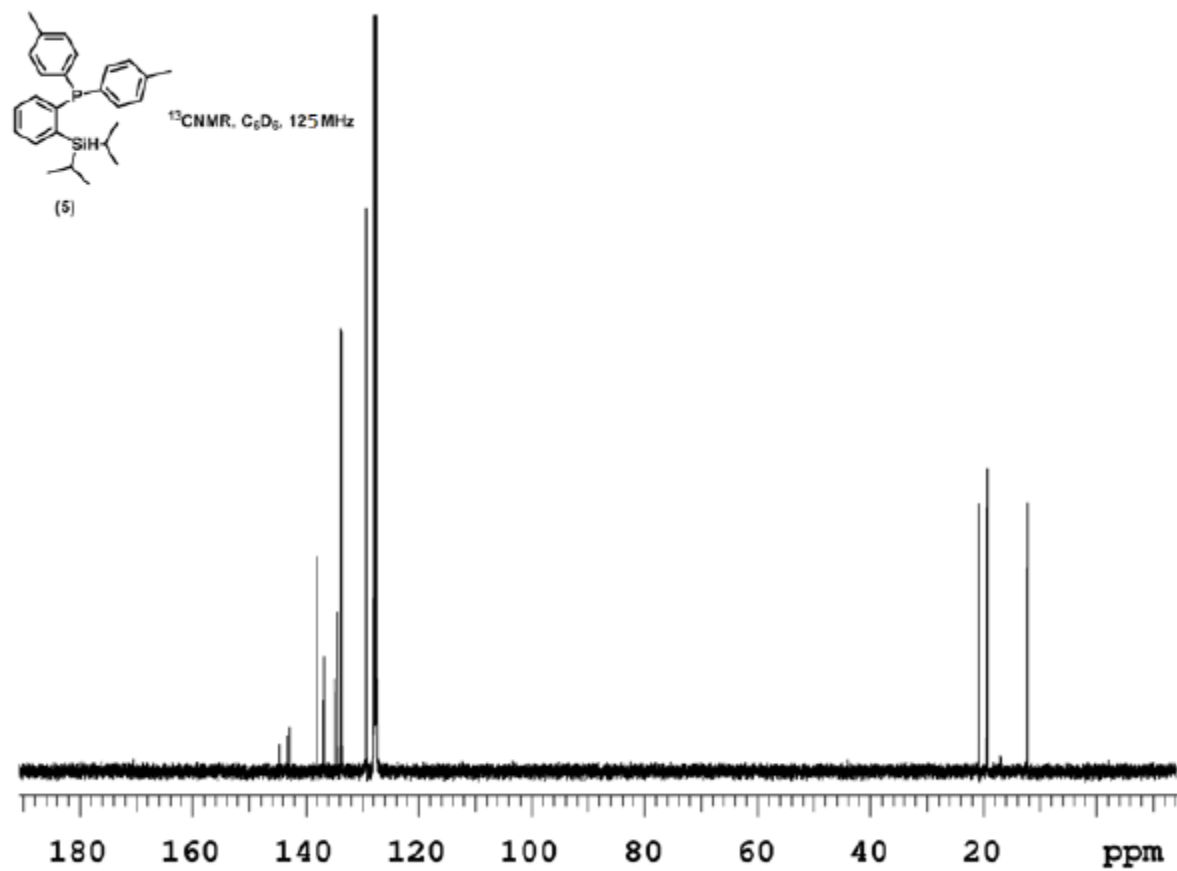


Figure A 17. ^{13}C NMR of compound **15**

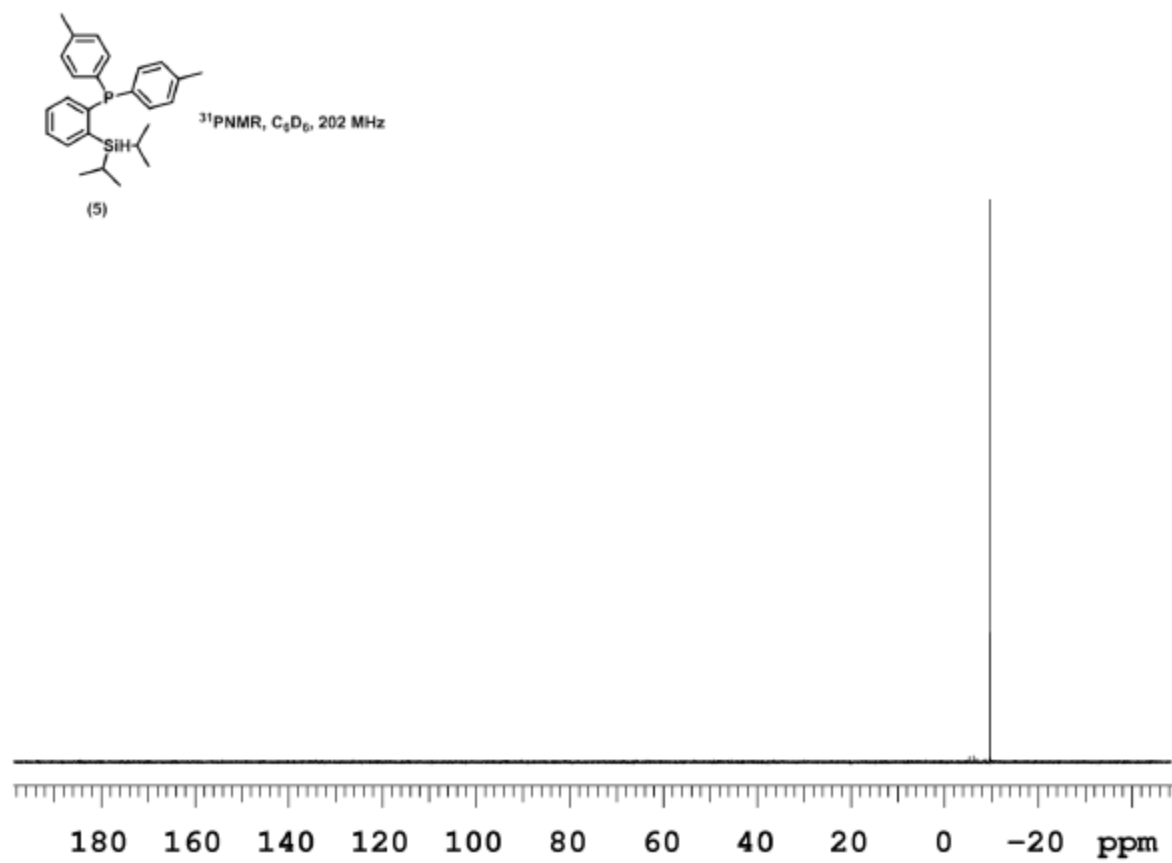


Figure A 18. ³¹P NMR of compound **15**

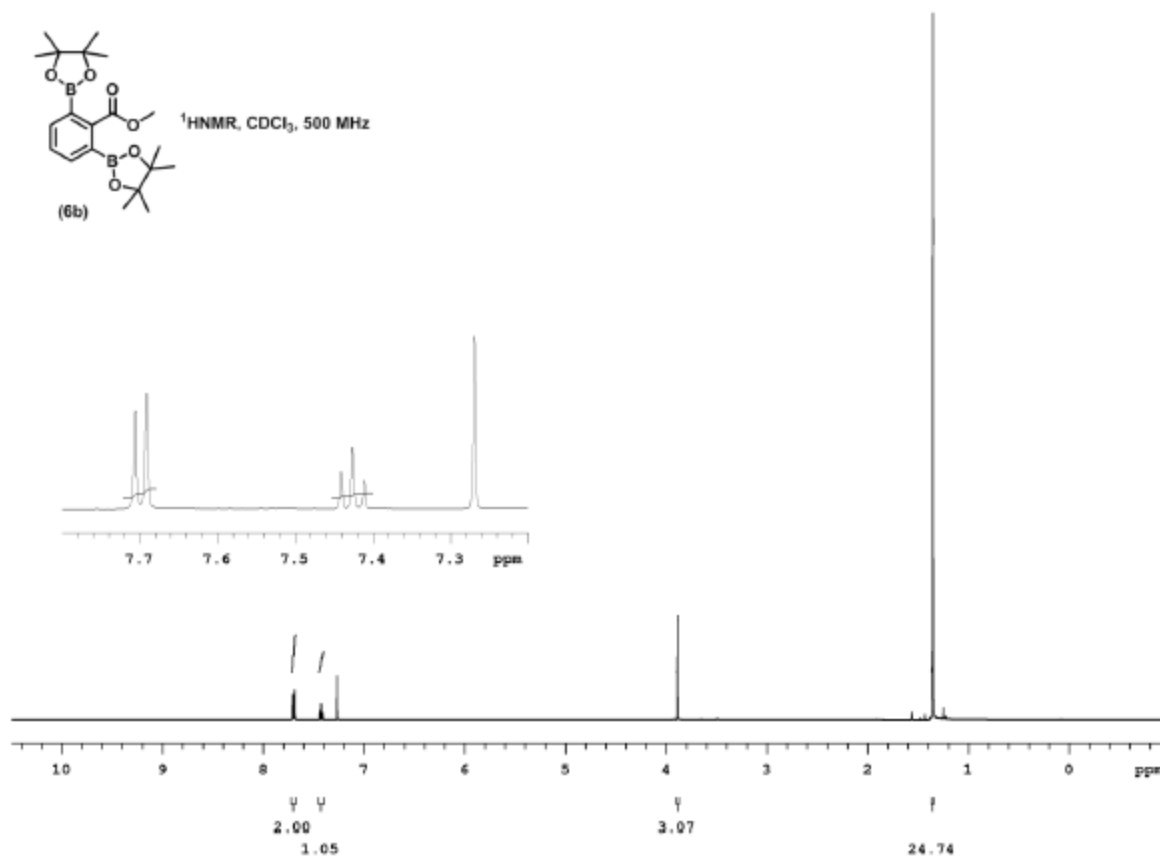


Figure A 19. ^1H NMR of compound **16b**

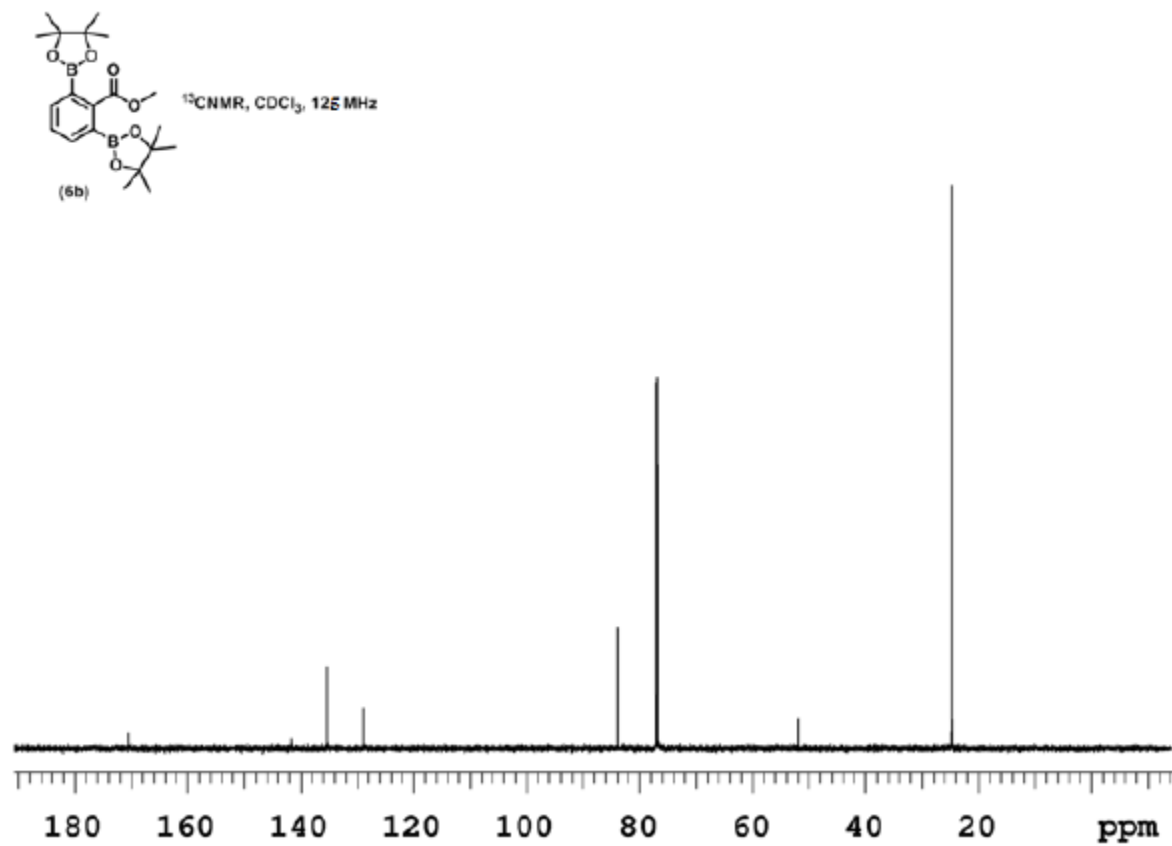


Figure A 20. ^{13}C NMR of compound **16b**

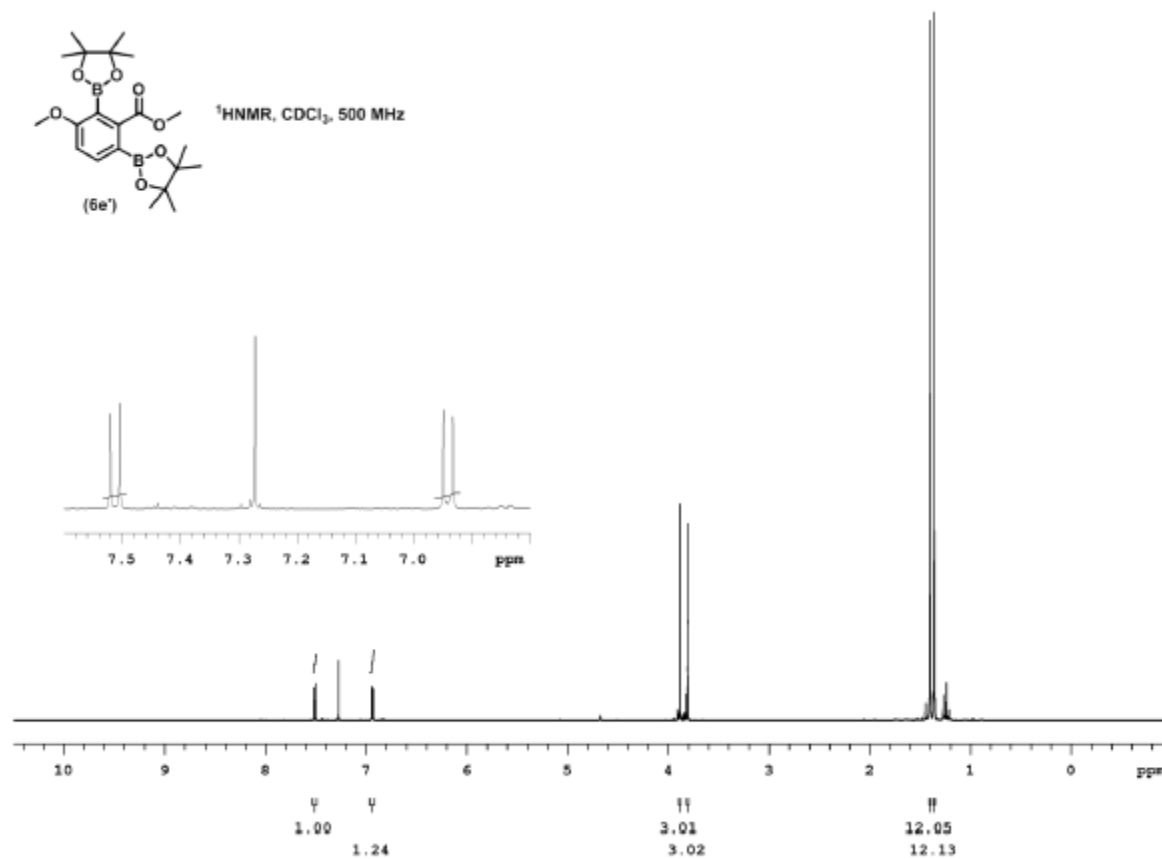


Figure A 21. ¹H NMR of compound **16e'**

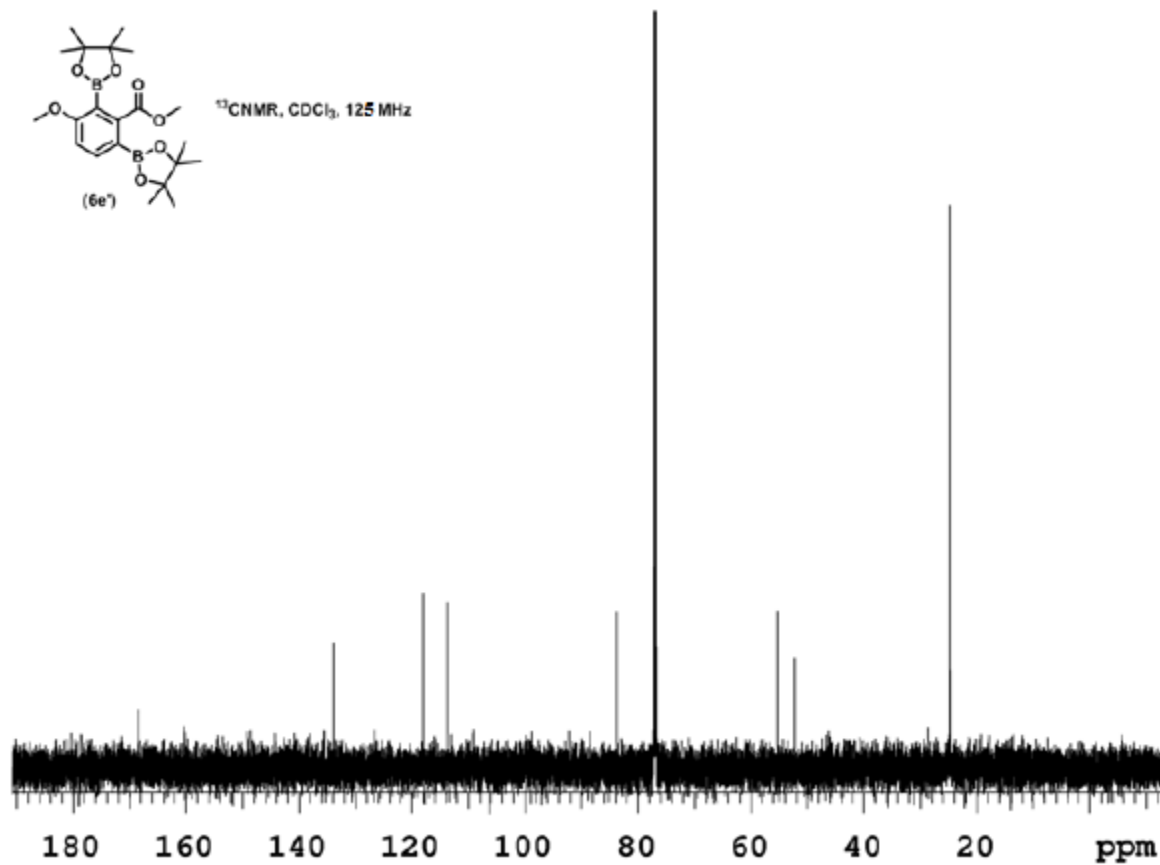


Figure A 22. ^{13}C NMR of compound **16e'**

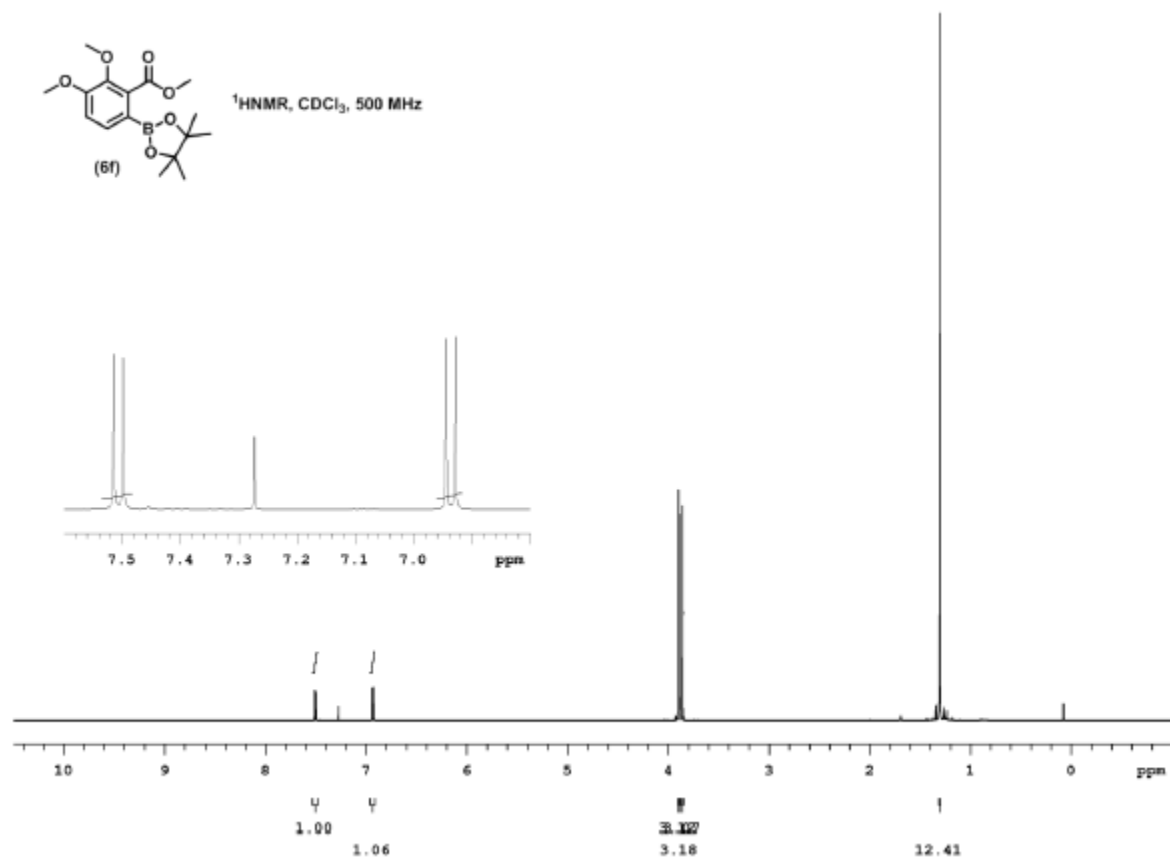


Figure A 23. ¹H NMR of compound **16f**

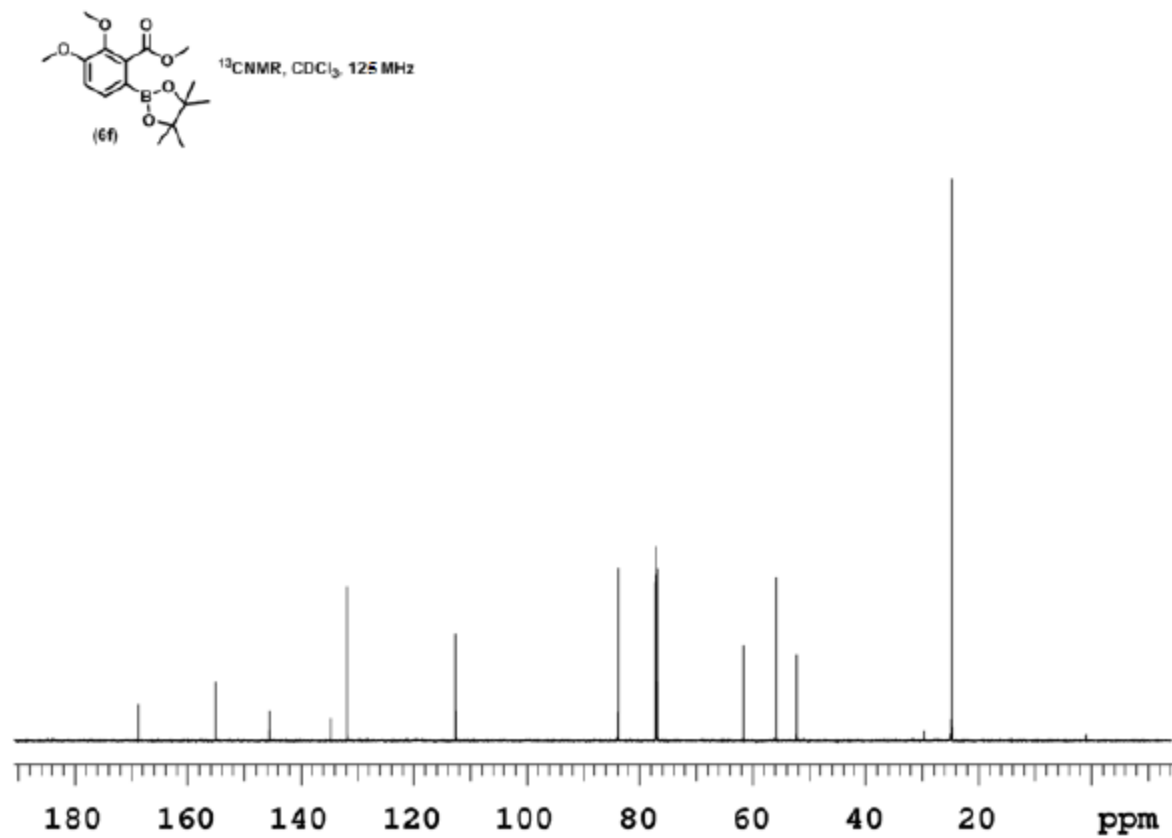


Figure A 24. ^{13}C NMR of compound **16f**

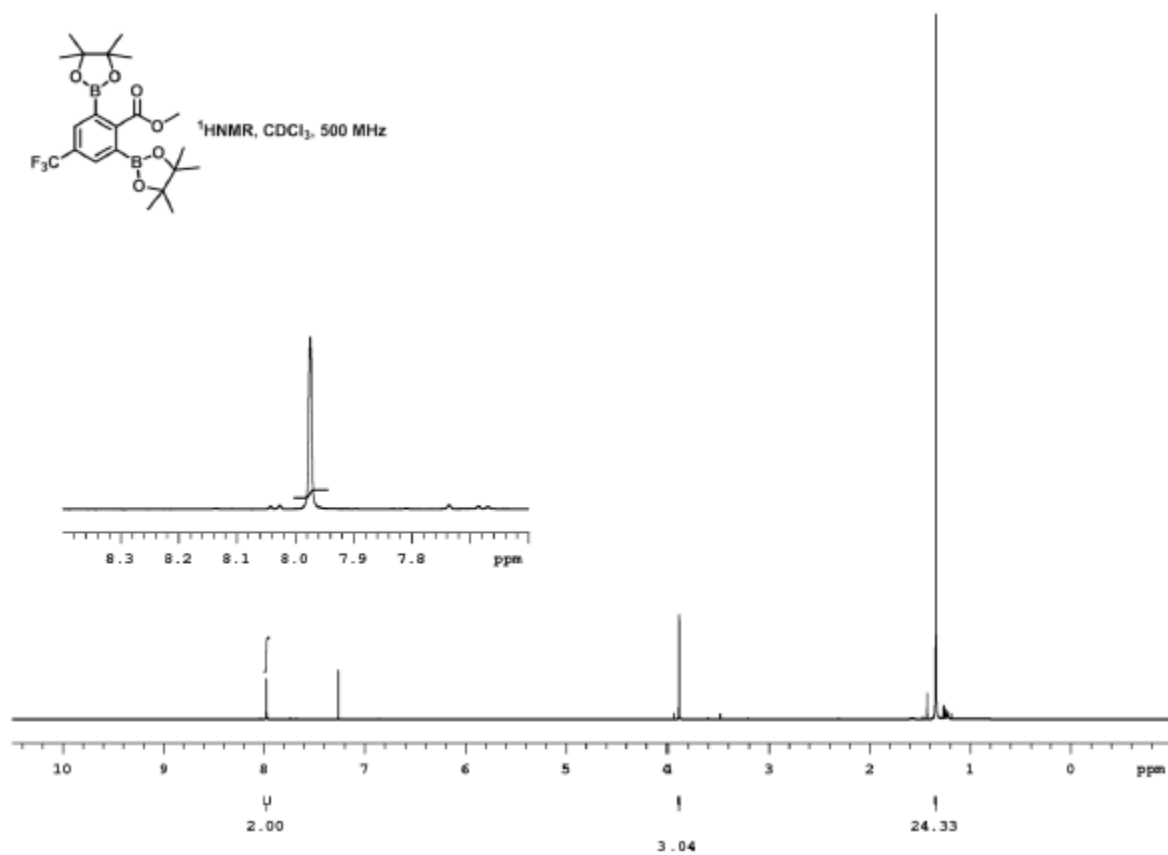


Figure A 25. ¹H NMR of compound **16i**

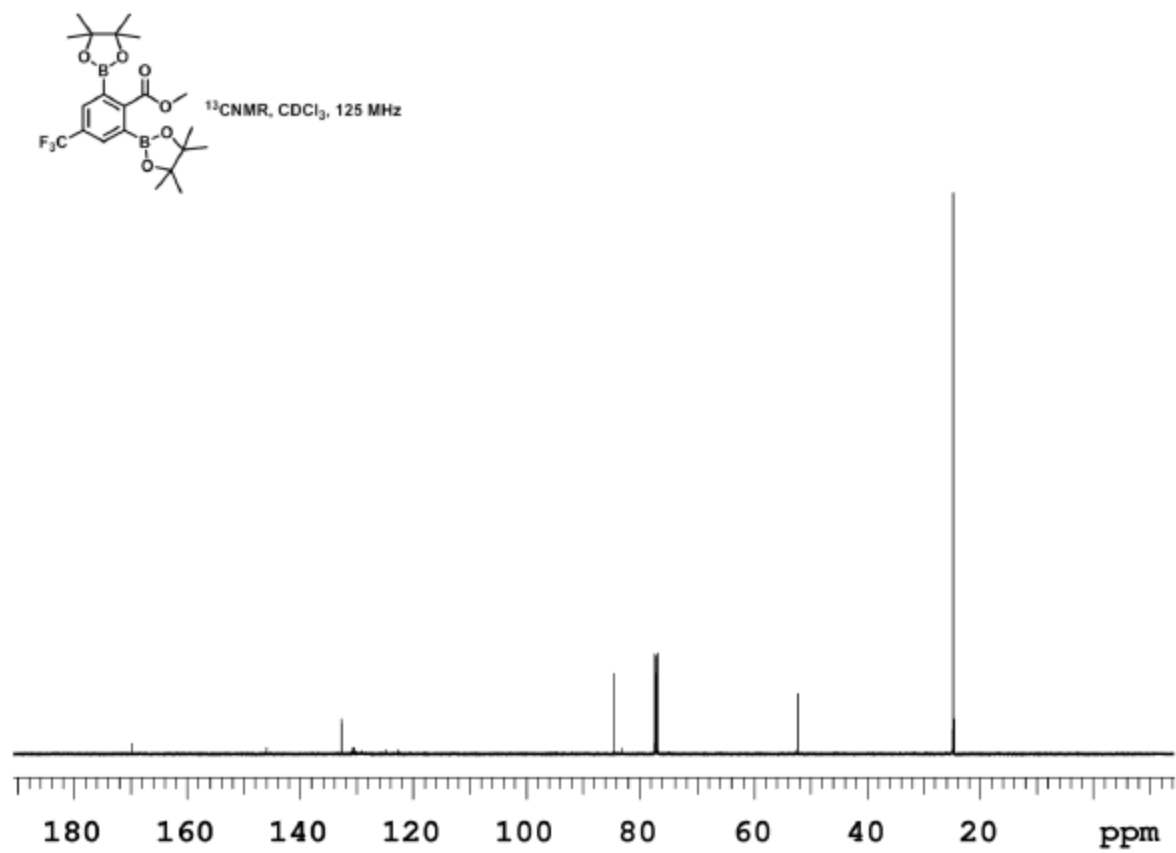


Figure A 26. ¹³C NMR of compound **16i**

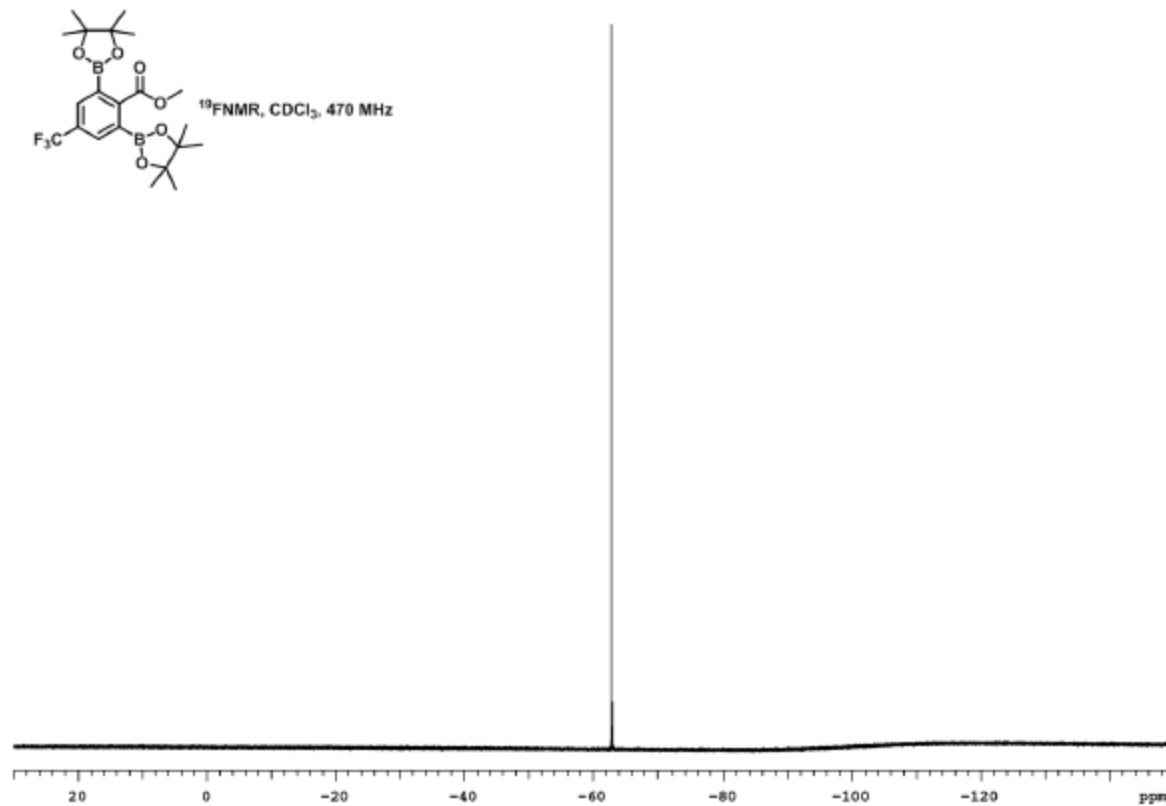


Figure A 27. ^{19}F NMR of compound **16i**

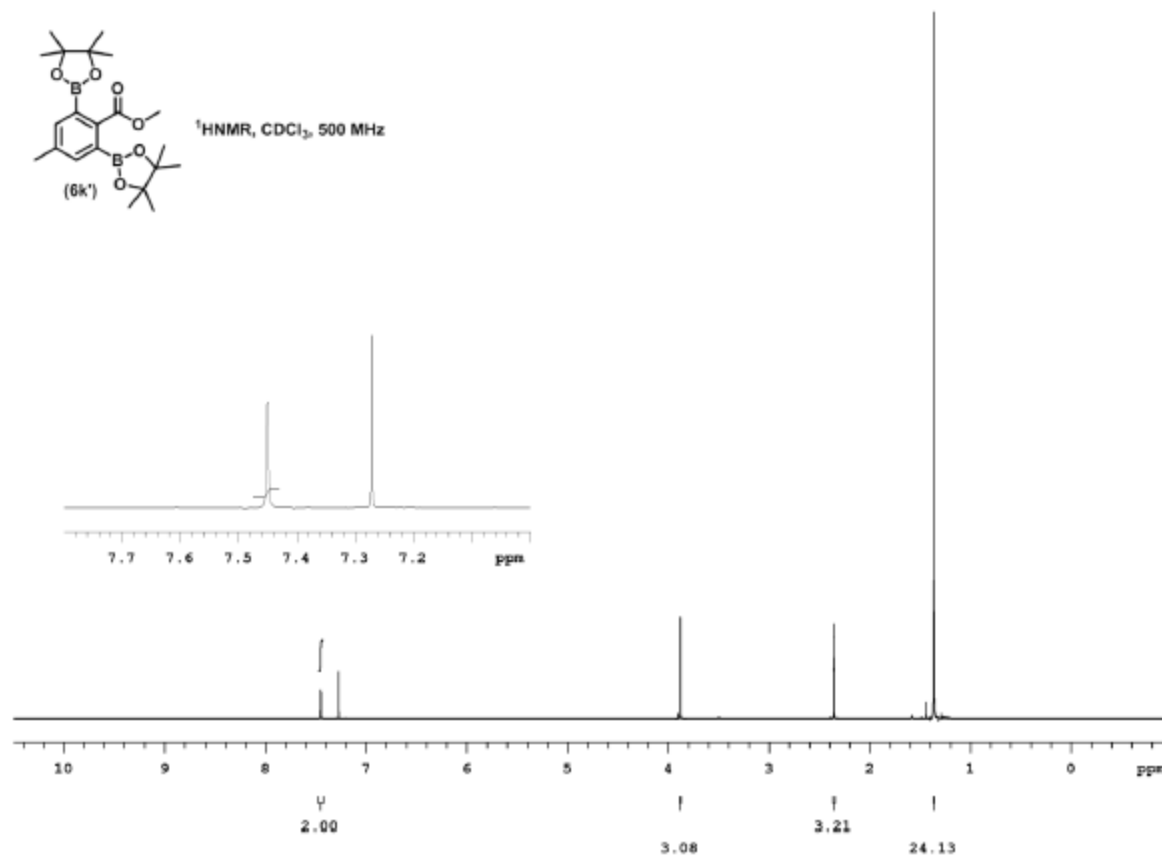
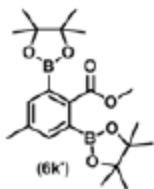


Figure A 28. ¹H NMR of compound **16k'**



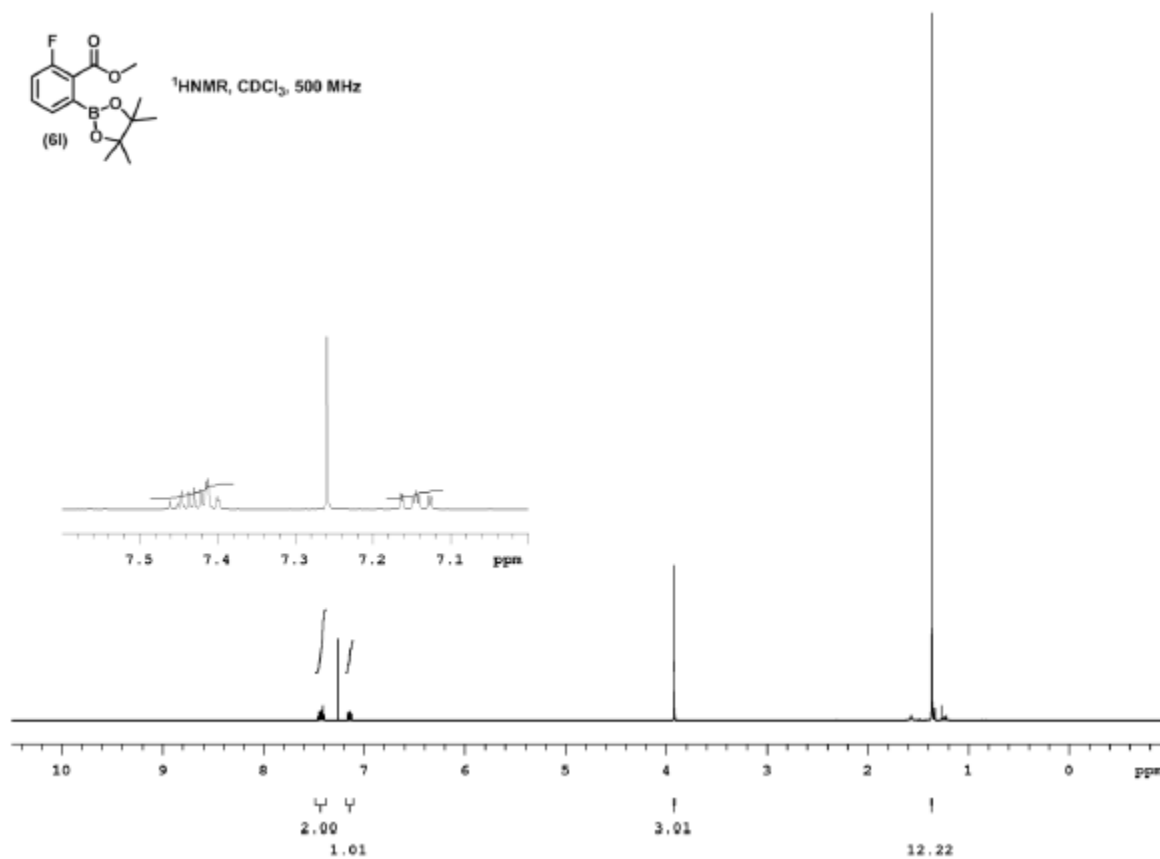


Figure A 30. $^1\text{H NMR}$ of compound **16l**

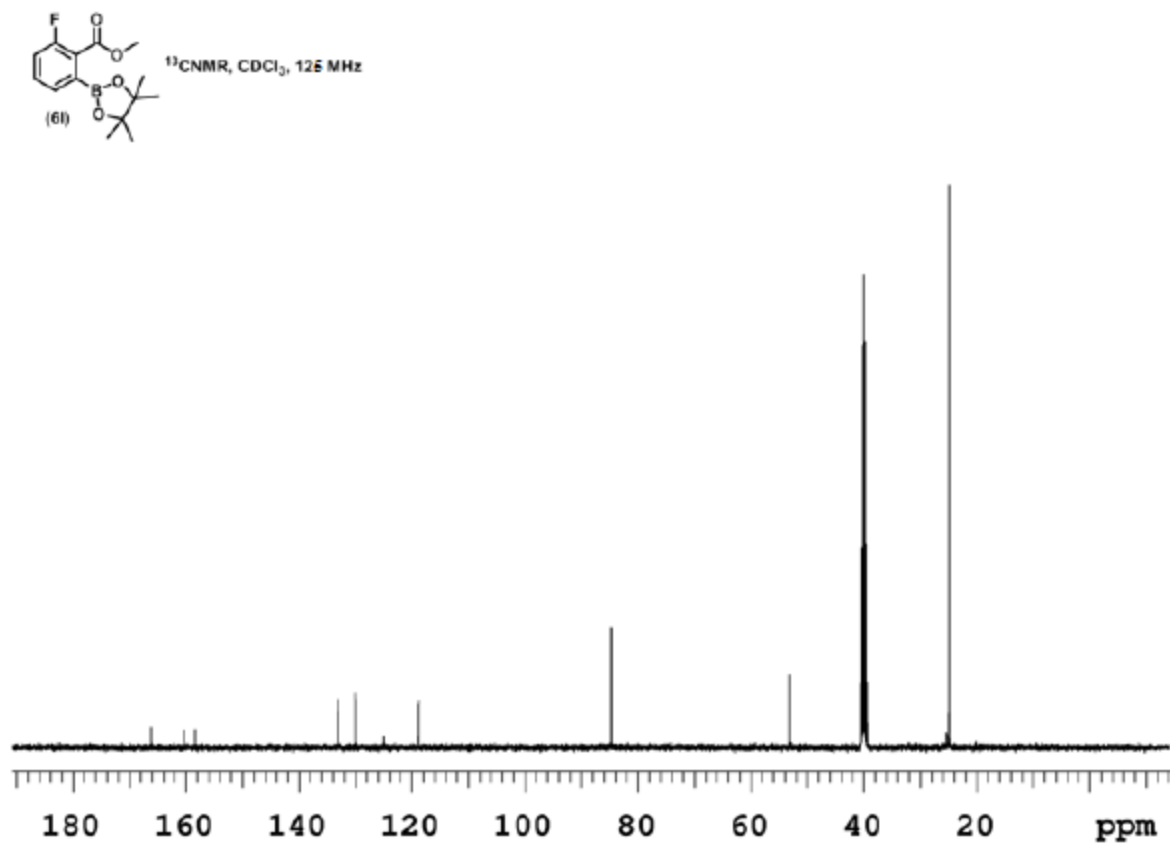


Figure A 31. ^{13}C NMR of compound **16l**

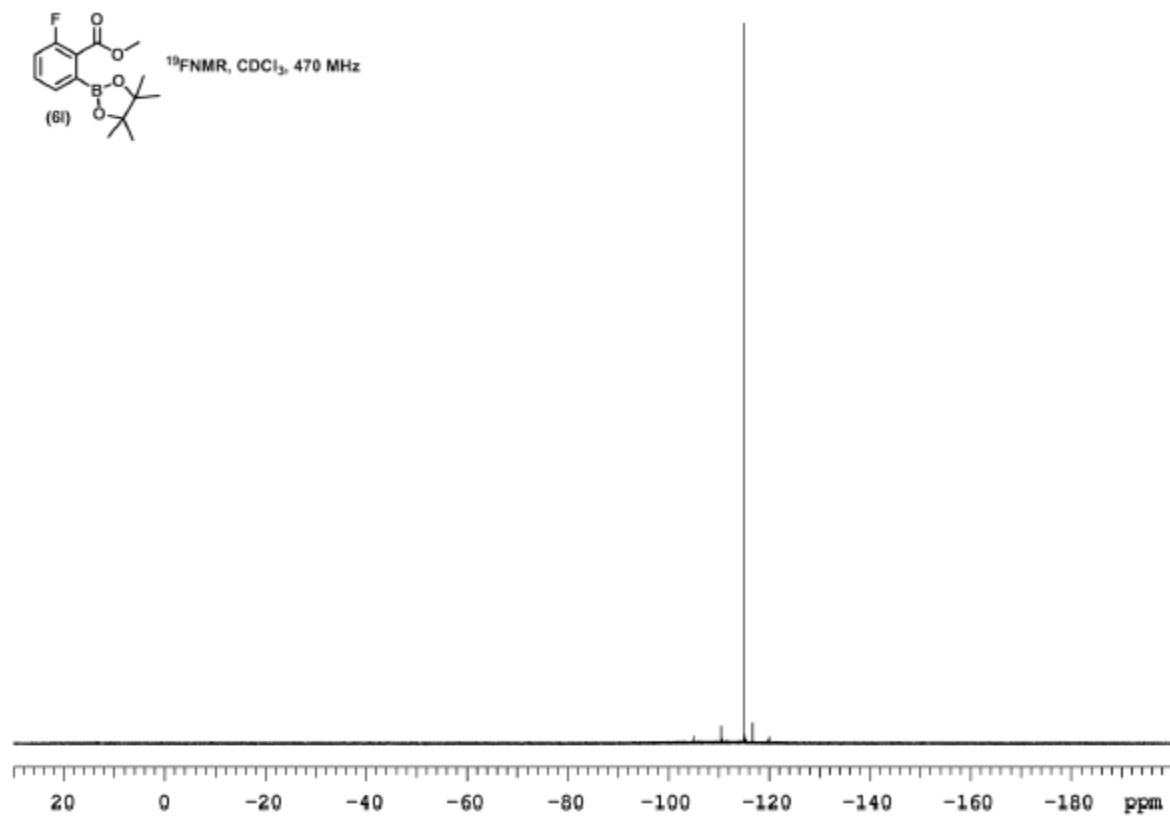


Figure A 32 ^{19}F NMR of compound **16l**

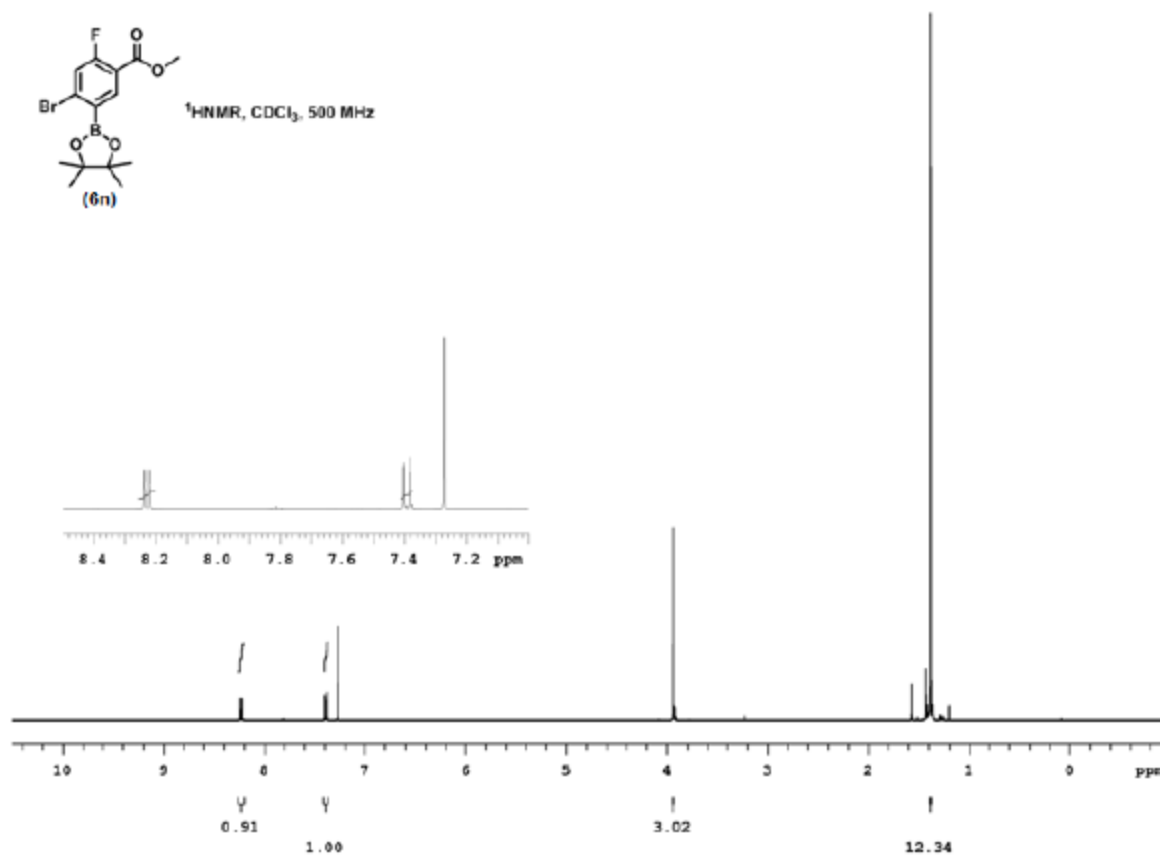


Figure A 33. ^1H NMR of compound **16n**

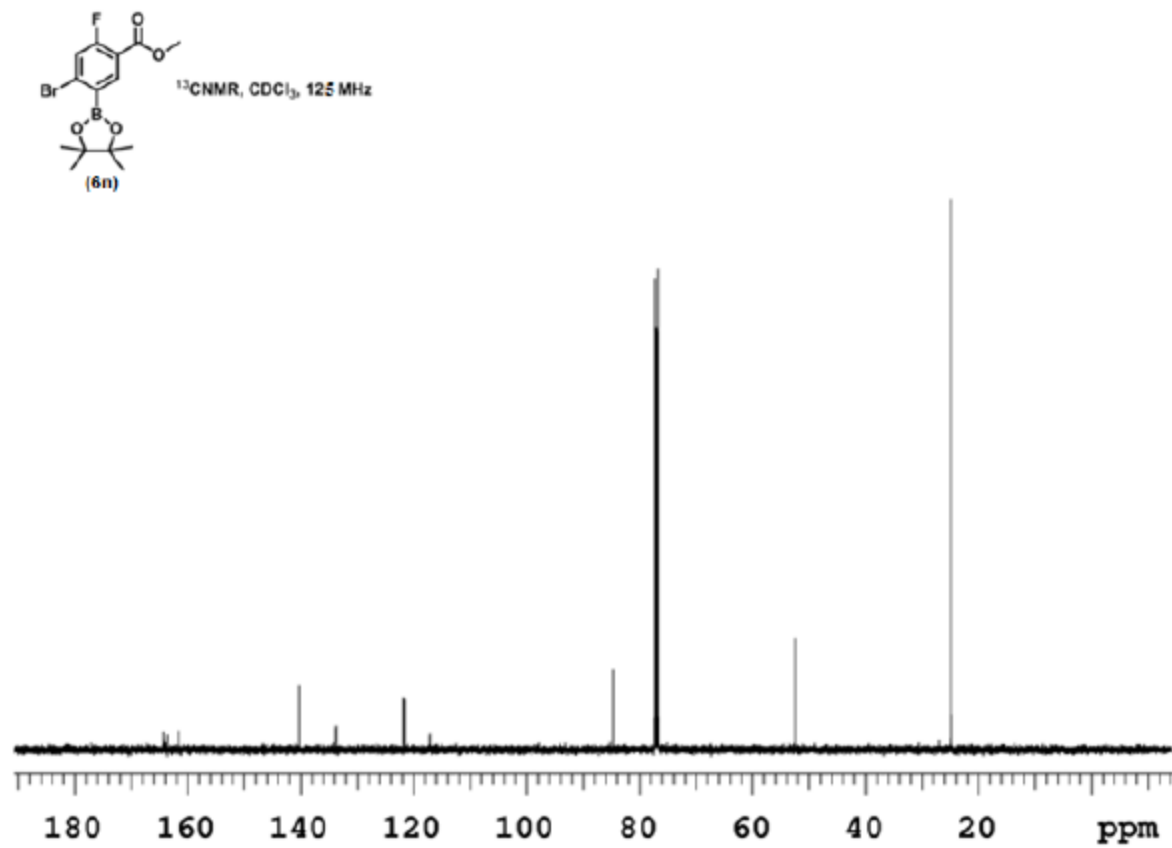


Figure A 34. ^{13}C NMR of compound **16n**

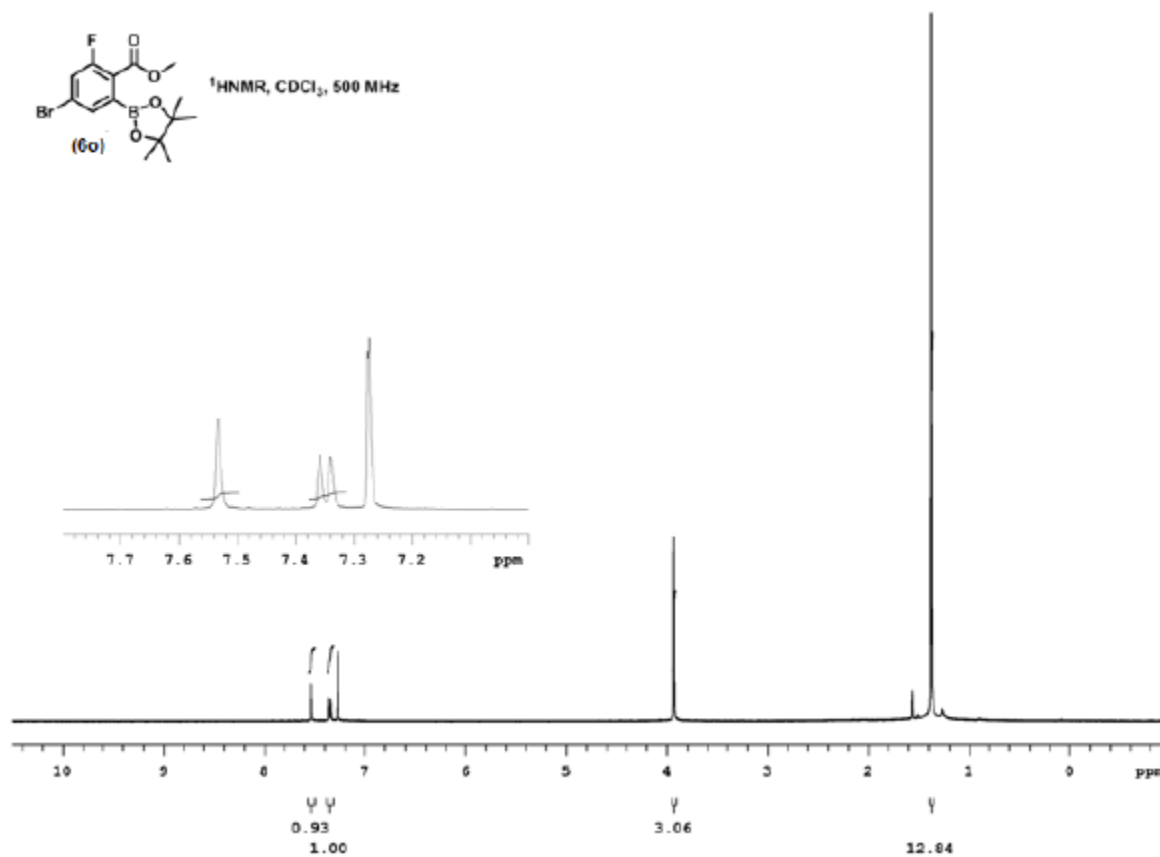


Figure A 35. $^1\text{H NMR}$ of compound **160**

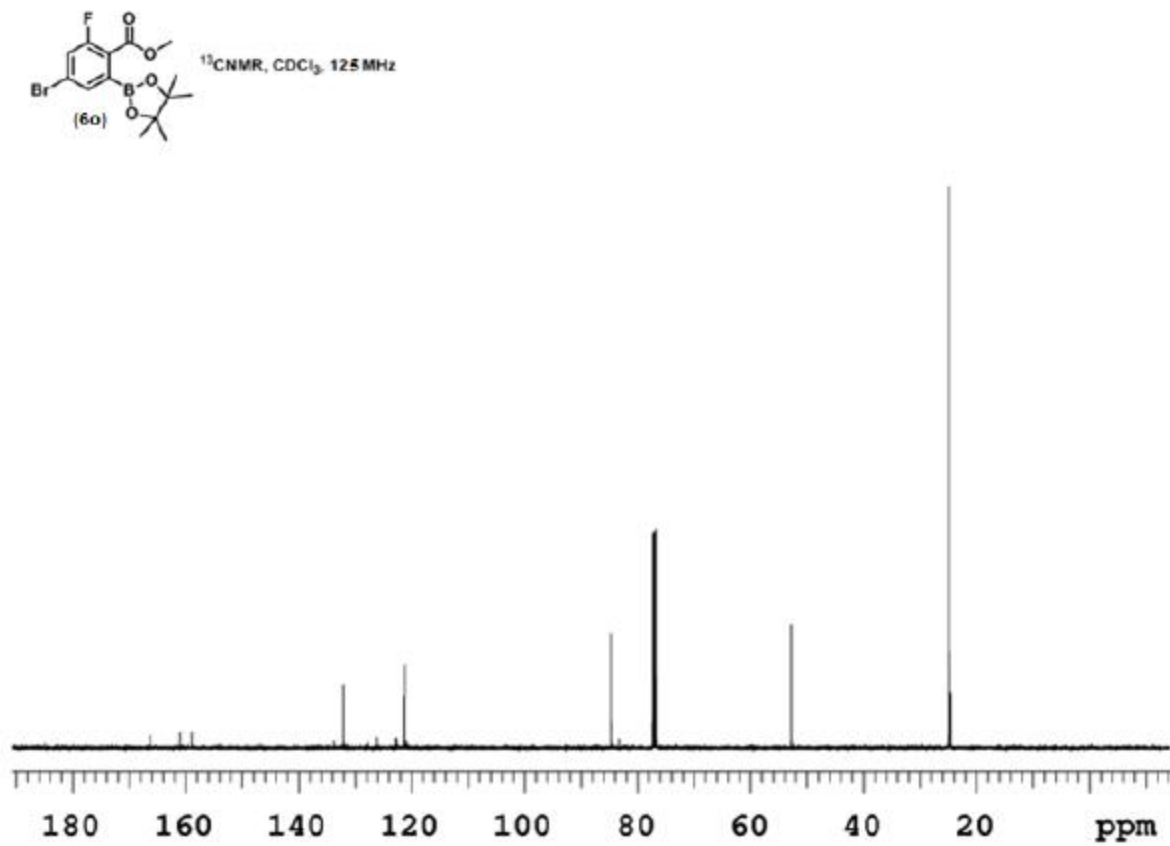


Figure A 36. ^{13}C NMR of compound **160**

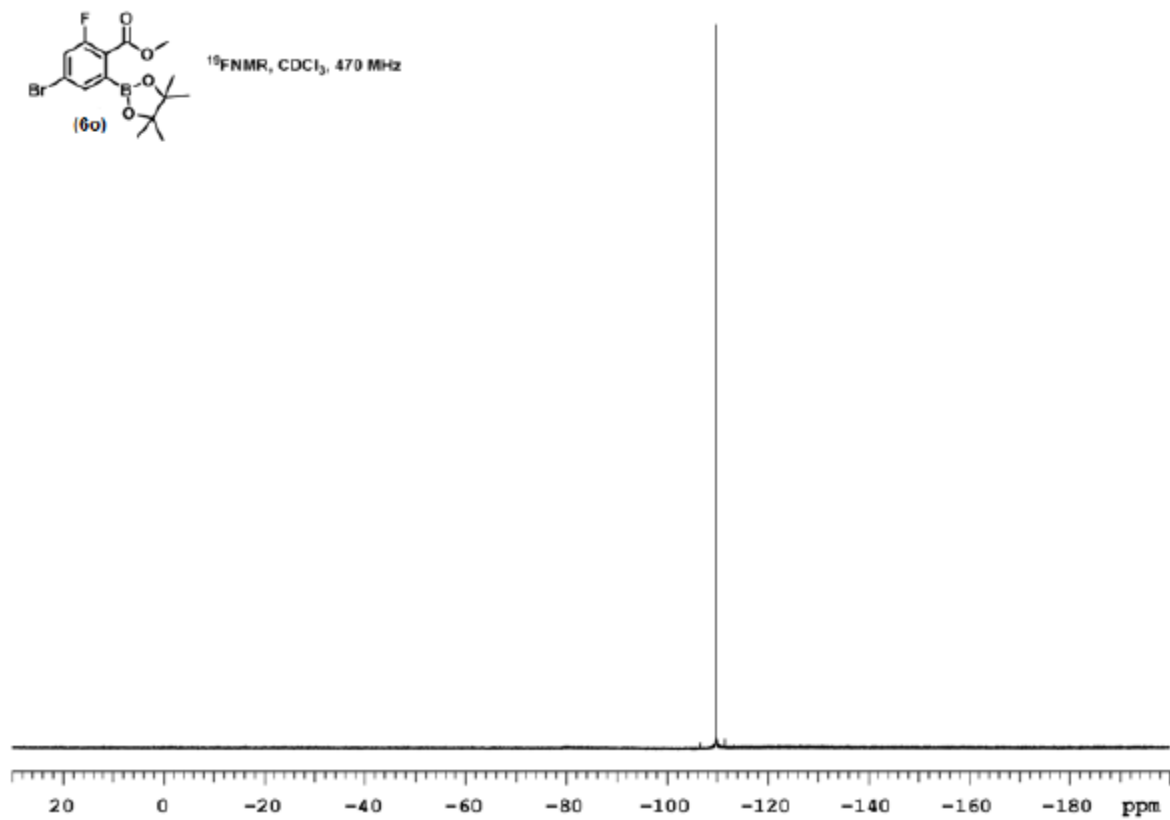


Figure A 37. ^{19}F NMR of compound **16o**

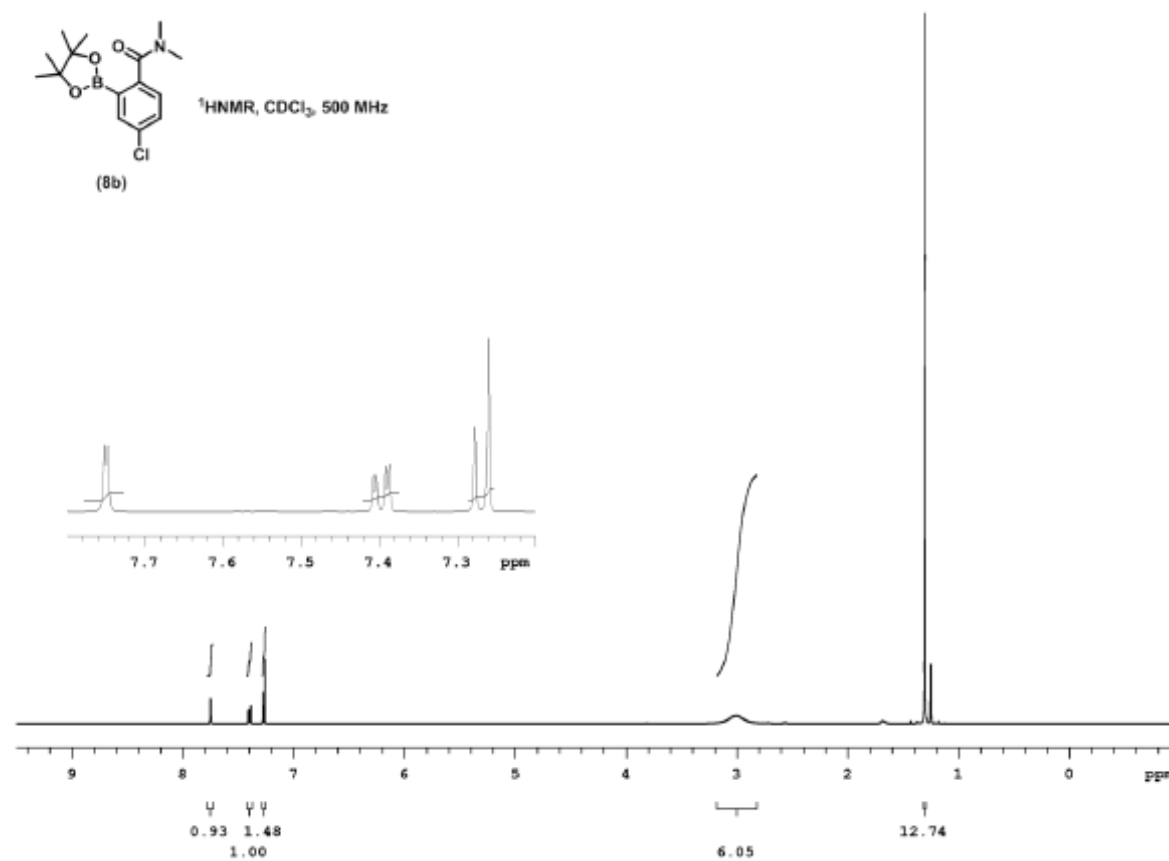


Figure A 38. $^1\text{H NMR}$ of compound **18a**

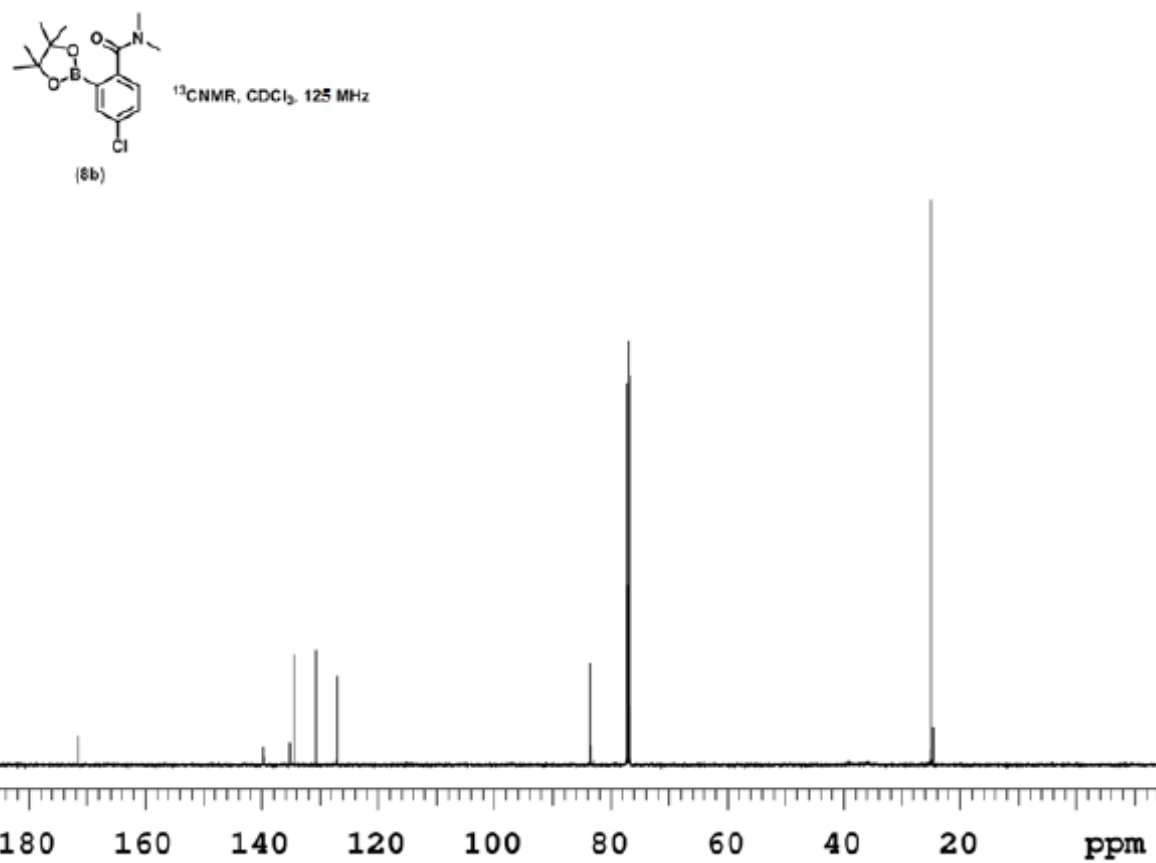


Figure A 39. ^{13}C NMR of compound **18a**

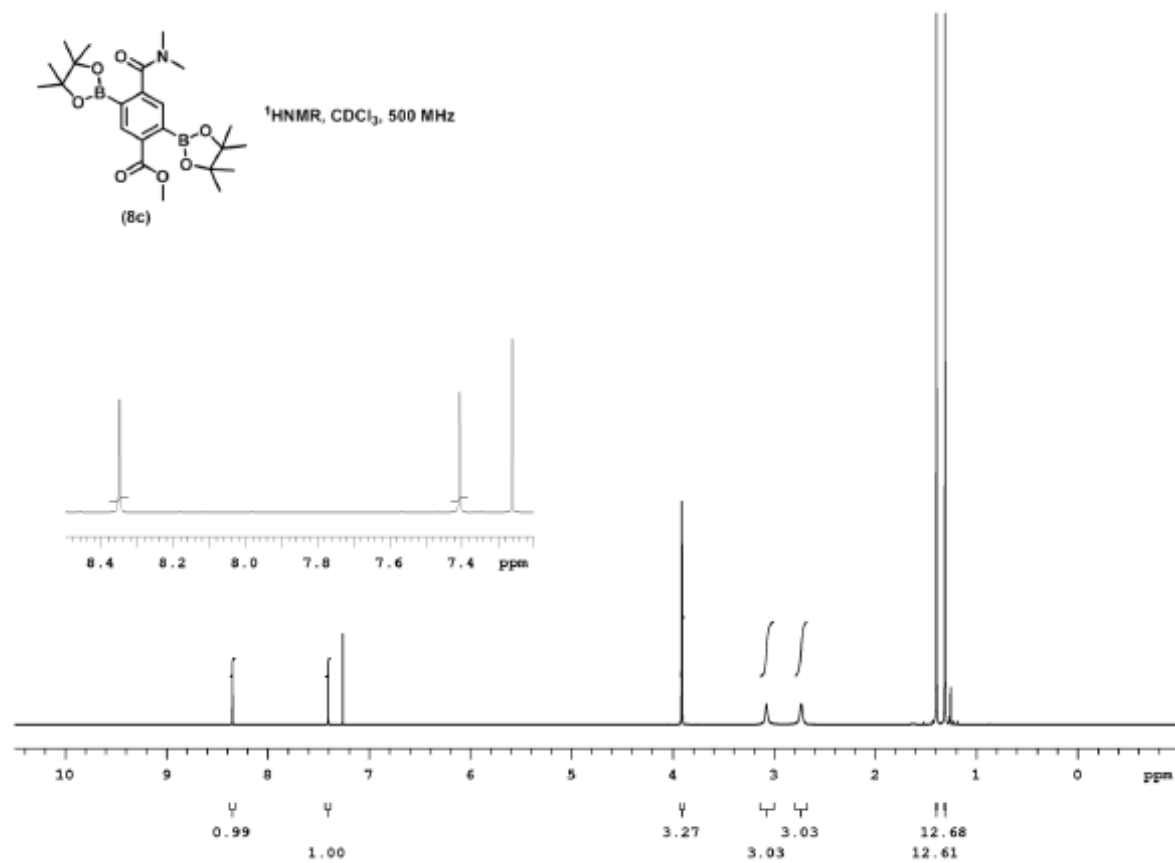


Figure A 40. ¹H NMR of compound **18c**

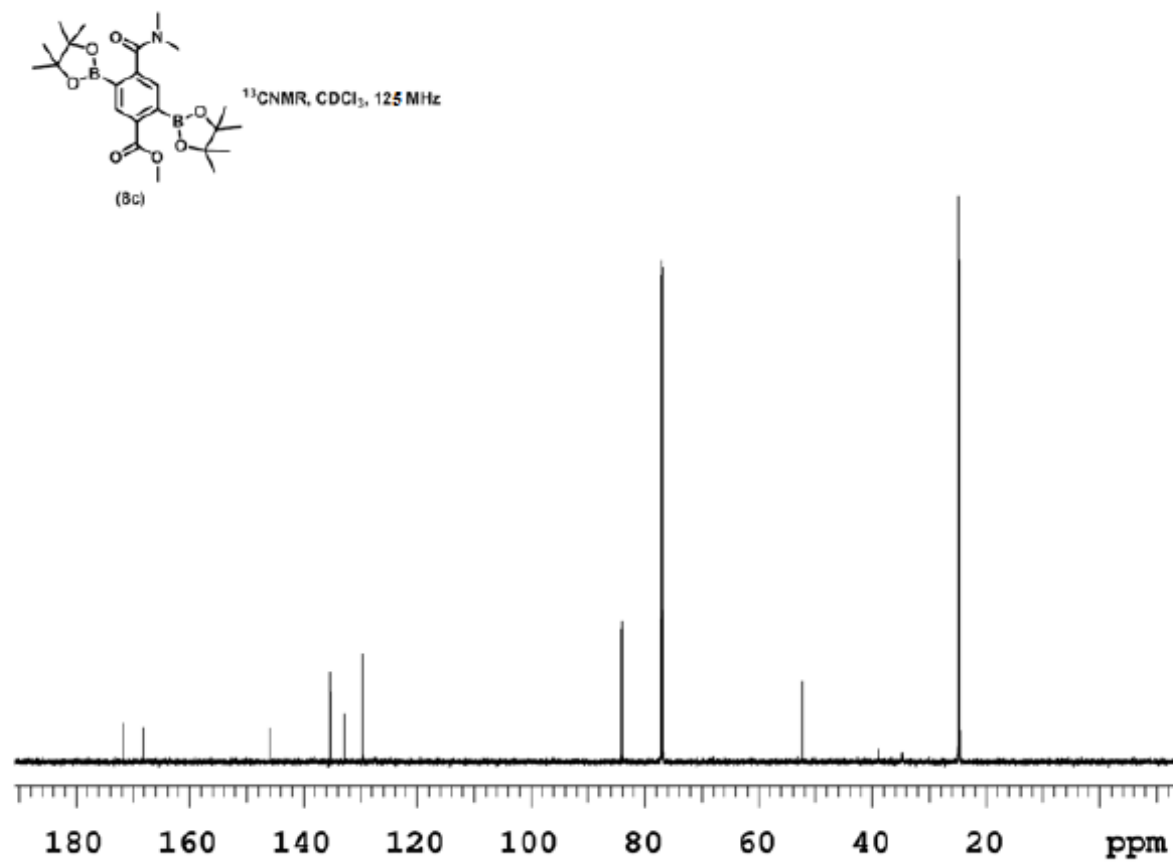


Figure A 41. ¹³C NMR of compound **18c**

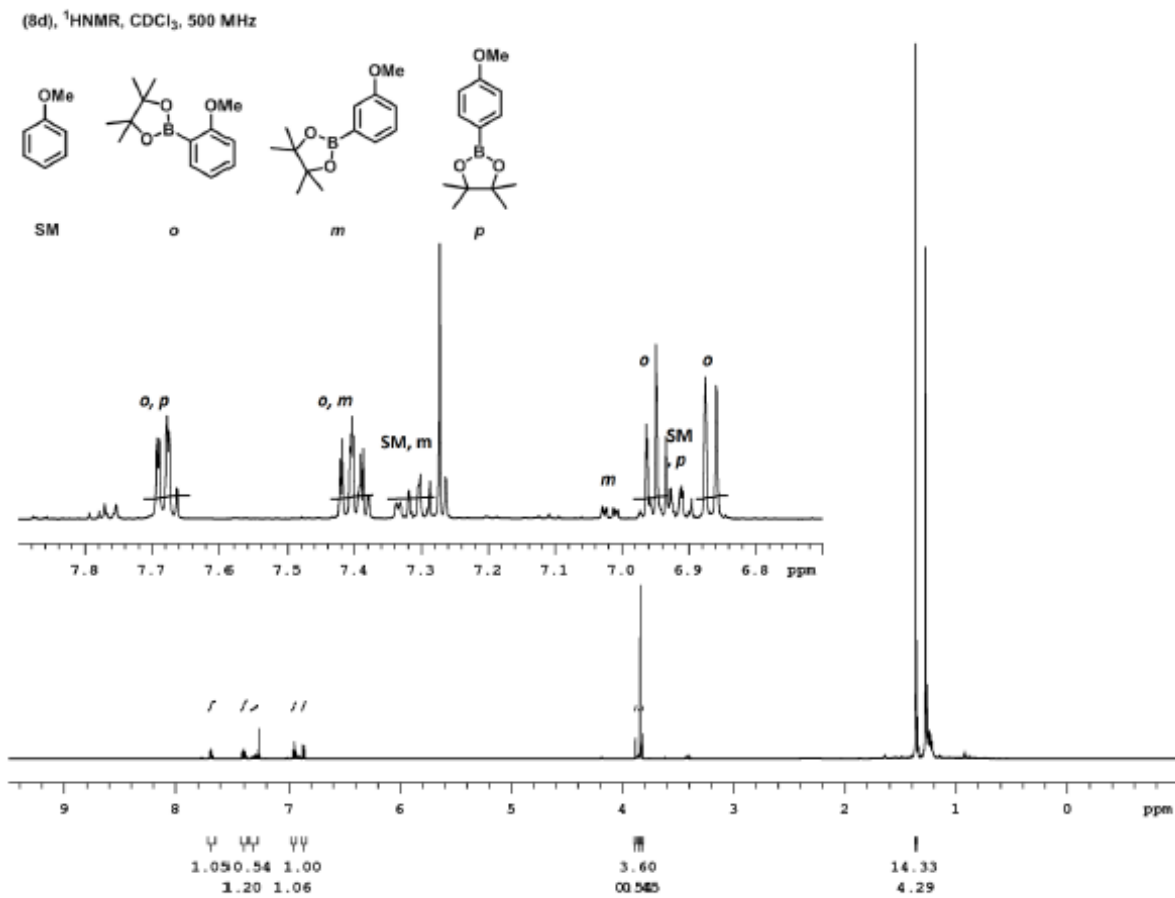


Figure A 42. ^1H NMR of compound **18d**

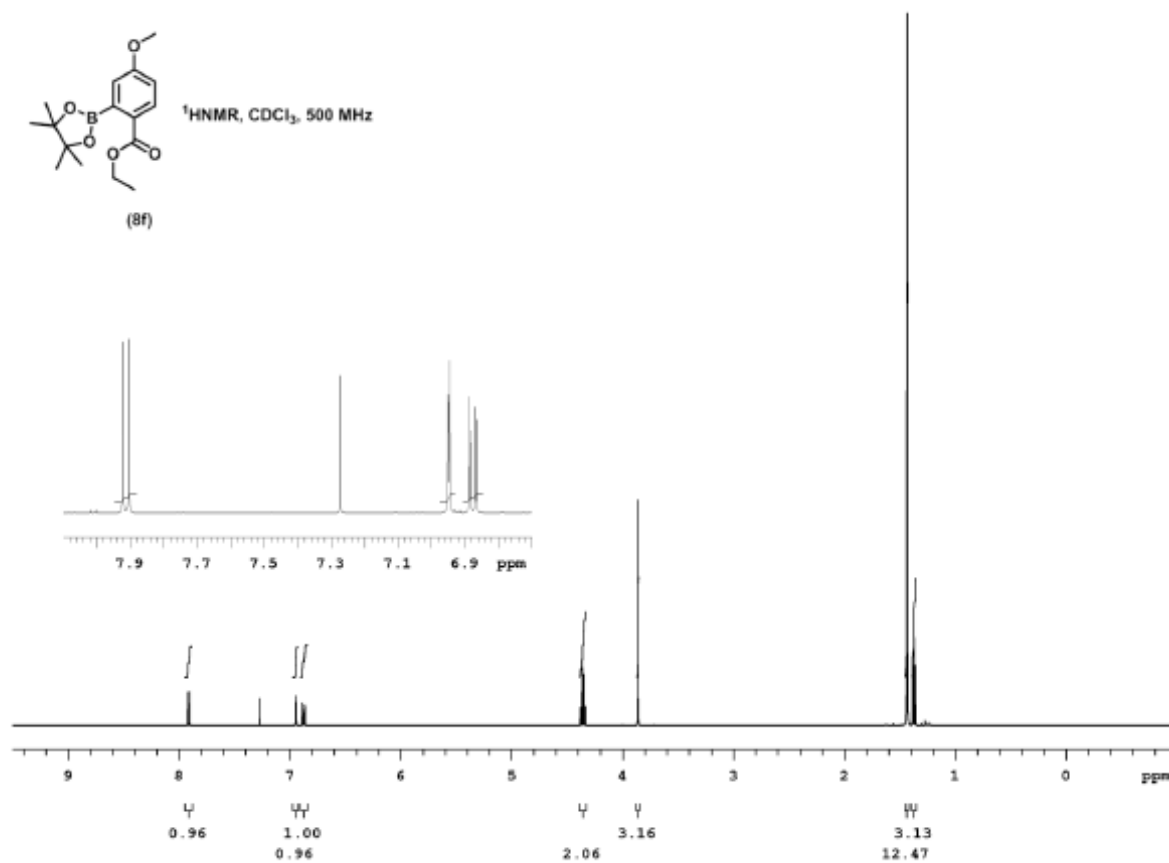


Figure A 43. ^1H NMR of compound **18f**

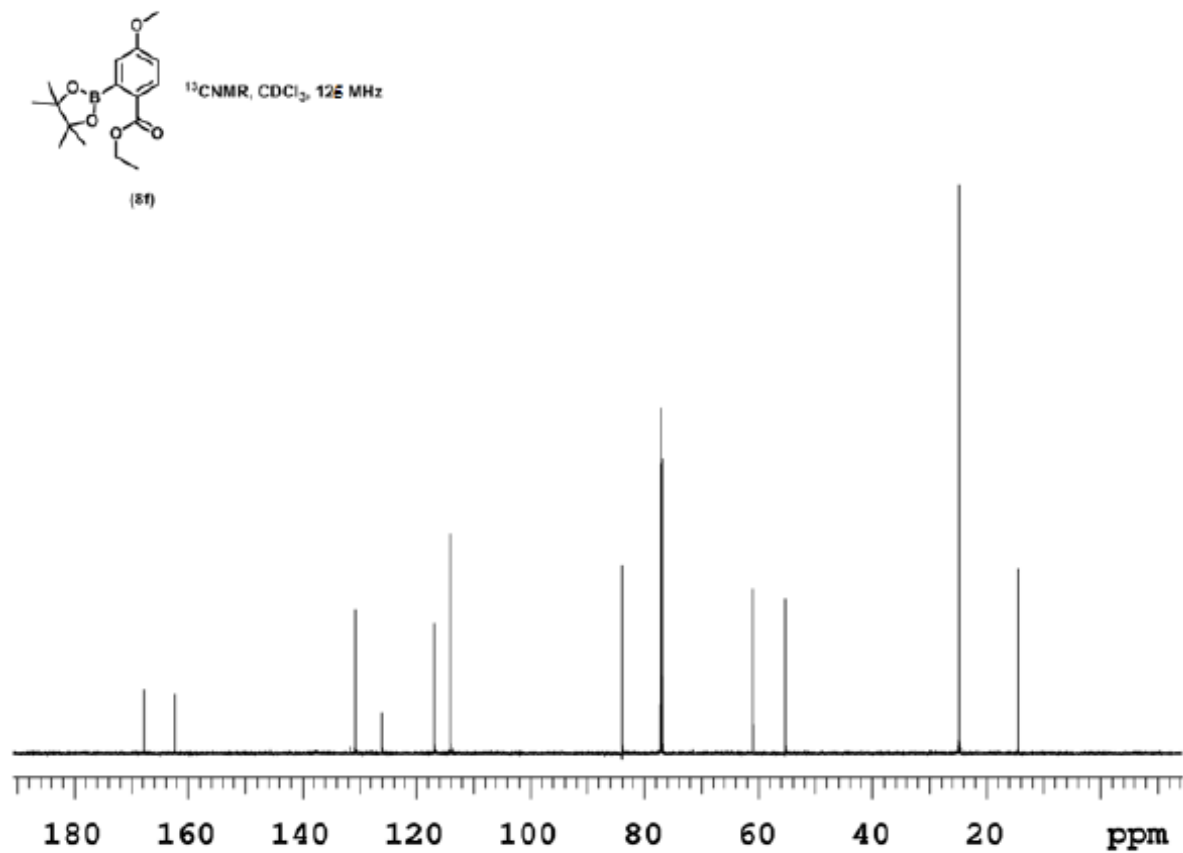


Figure A 44. ^{13}C NMR of compound **18f**

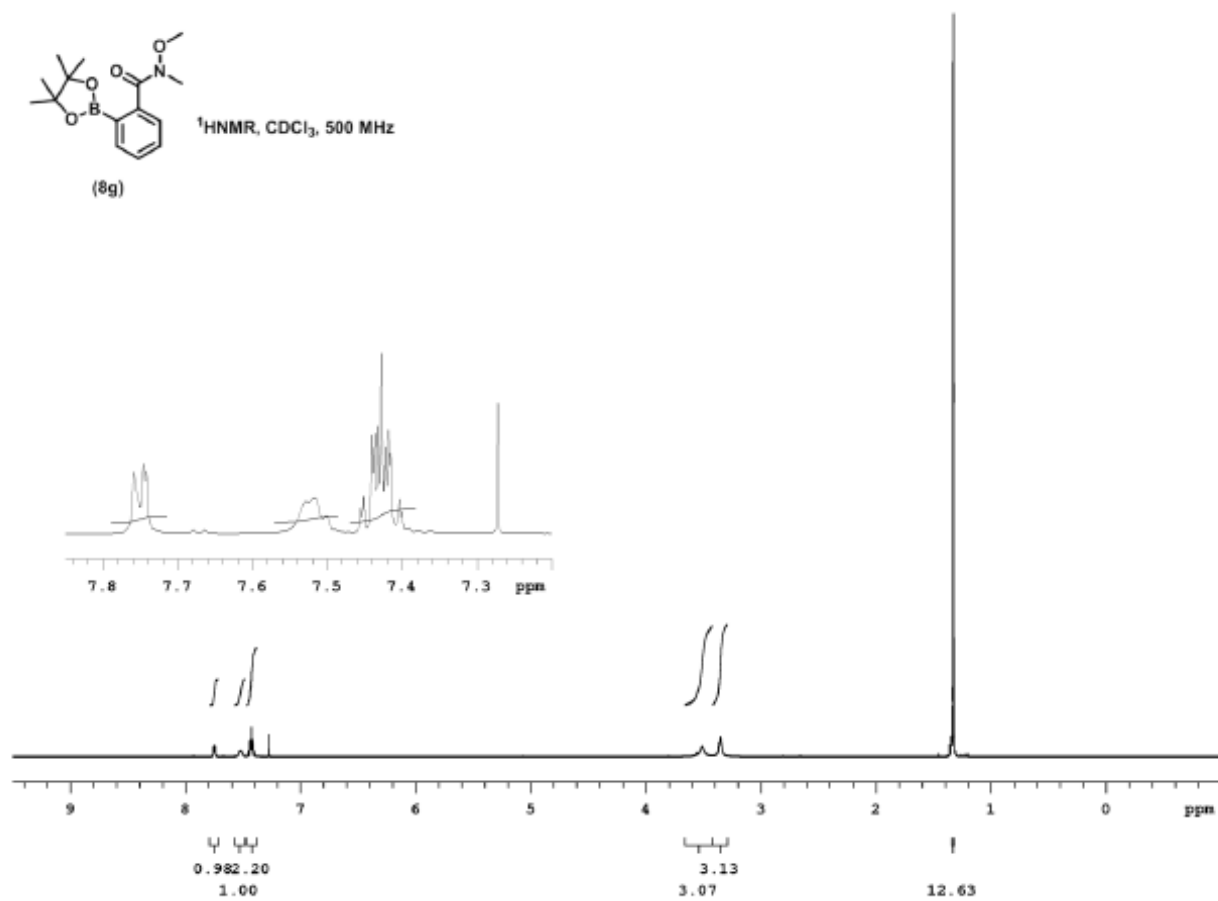


Figure A 45. ¹H NMR of compound **18g**

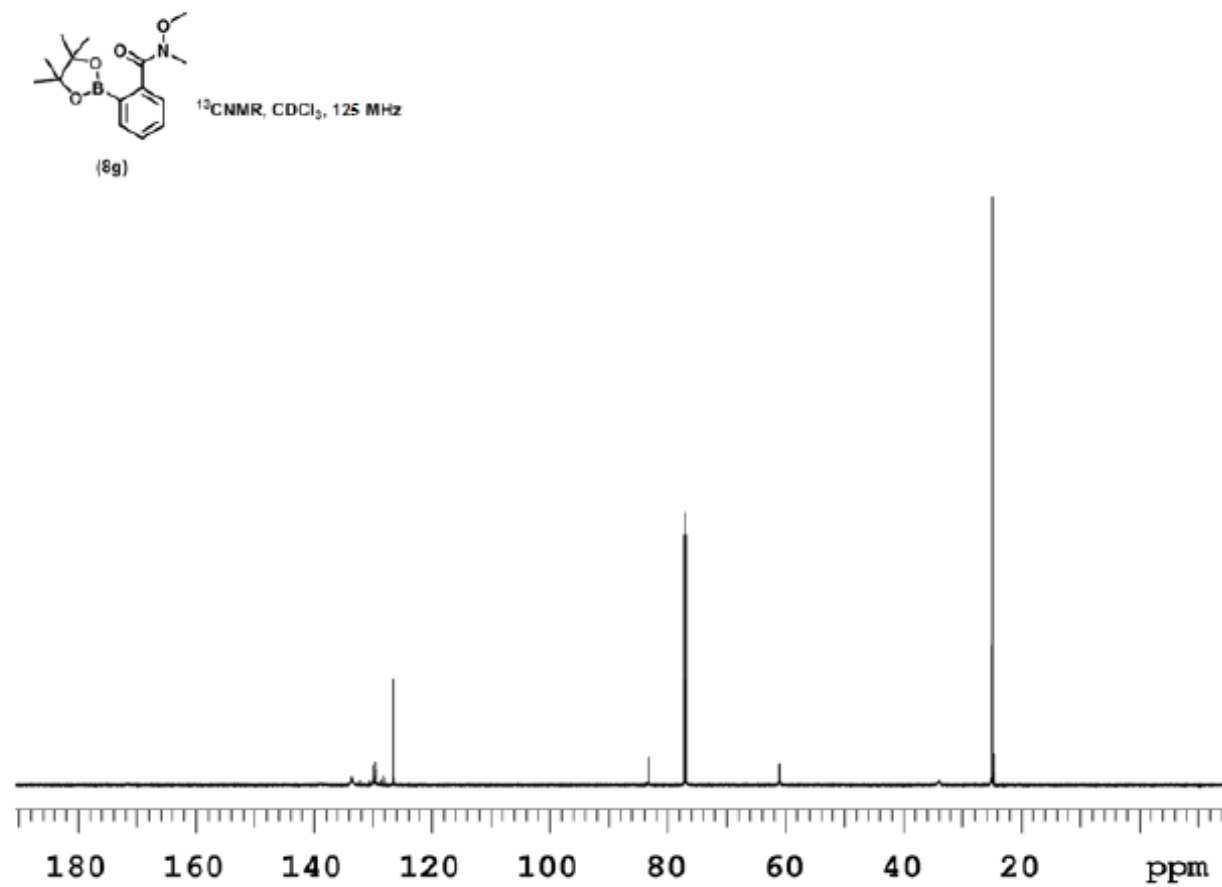


Figure A 46. ^{13}C NMR of compound **18g**

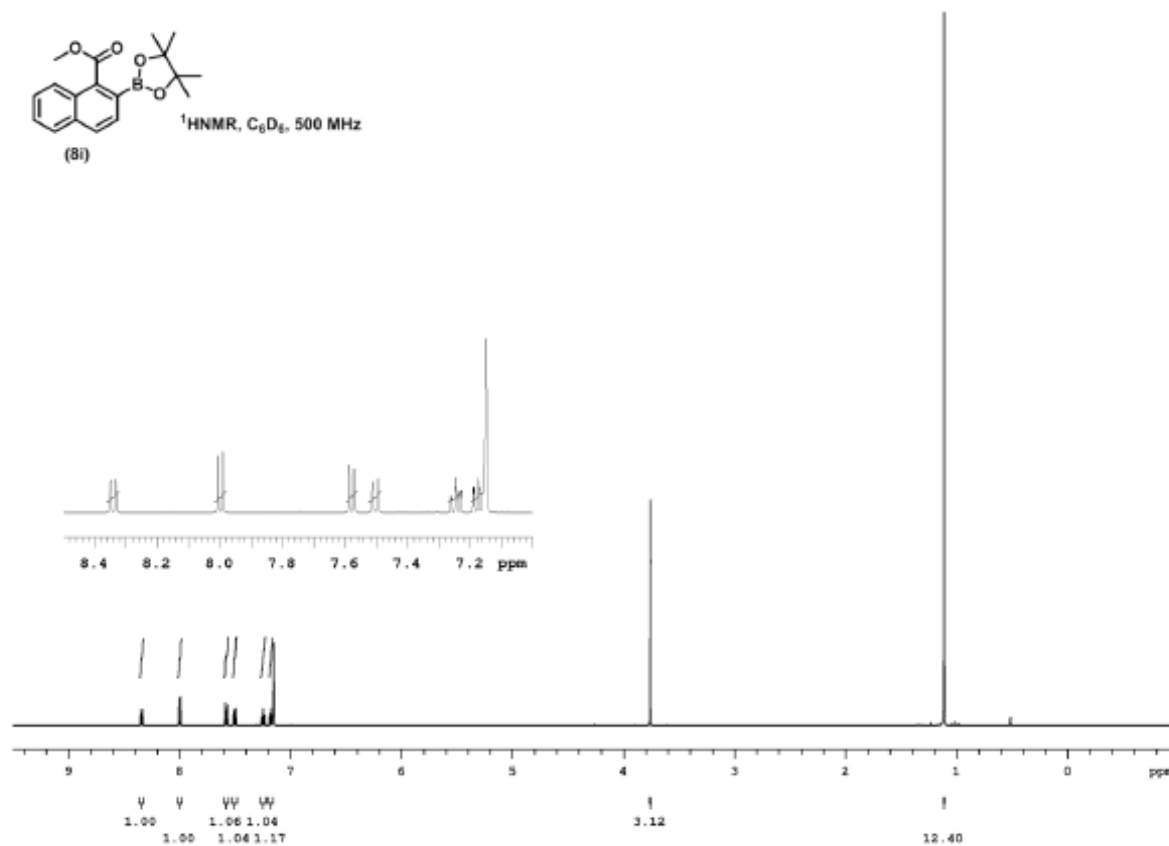


Figure A 47. ¹H NMR of compound **18i**

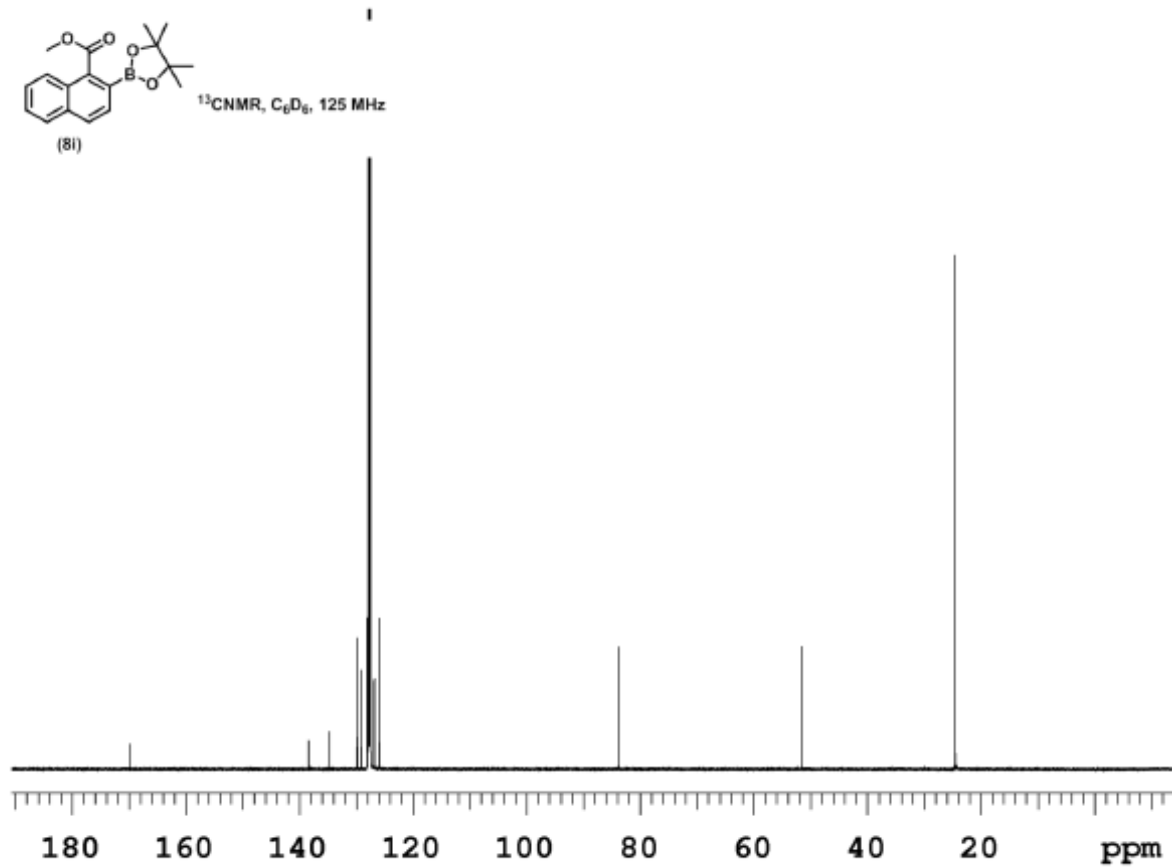


Figure A 48. ^{13}C NMR of compound **18i**

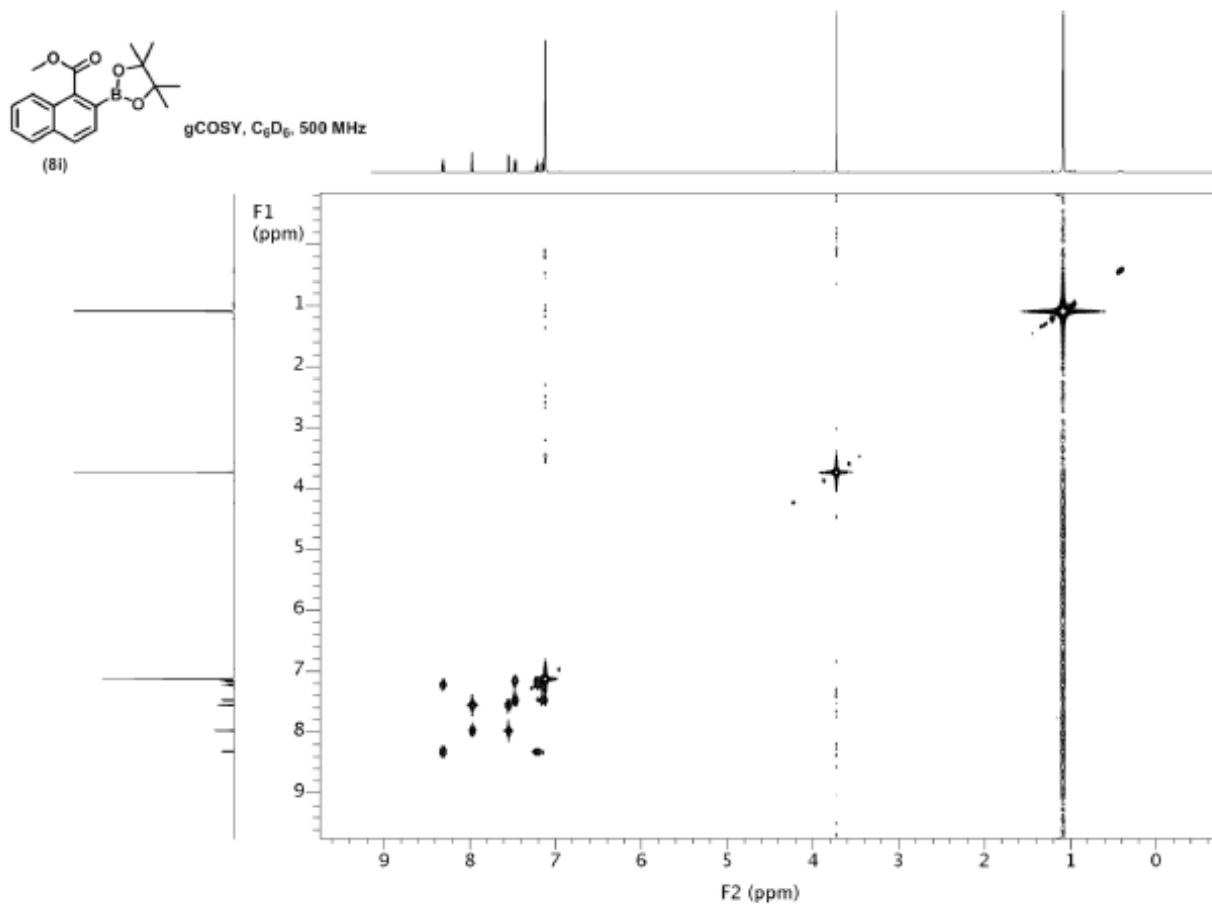


Figure A 49. gCOSY NMR of compound **18i**

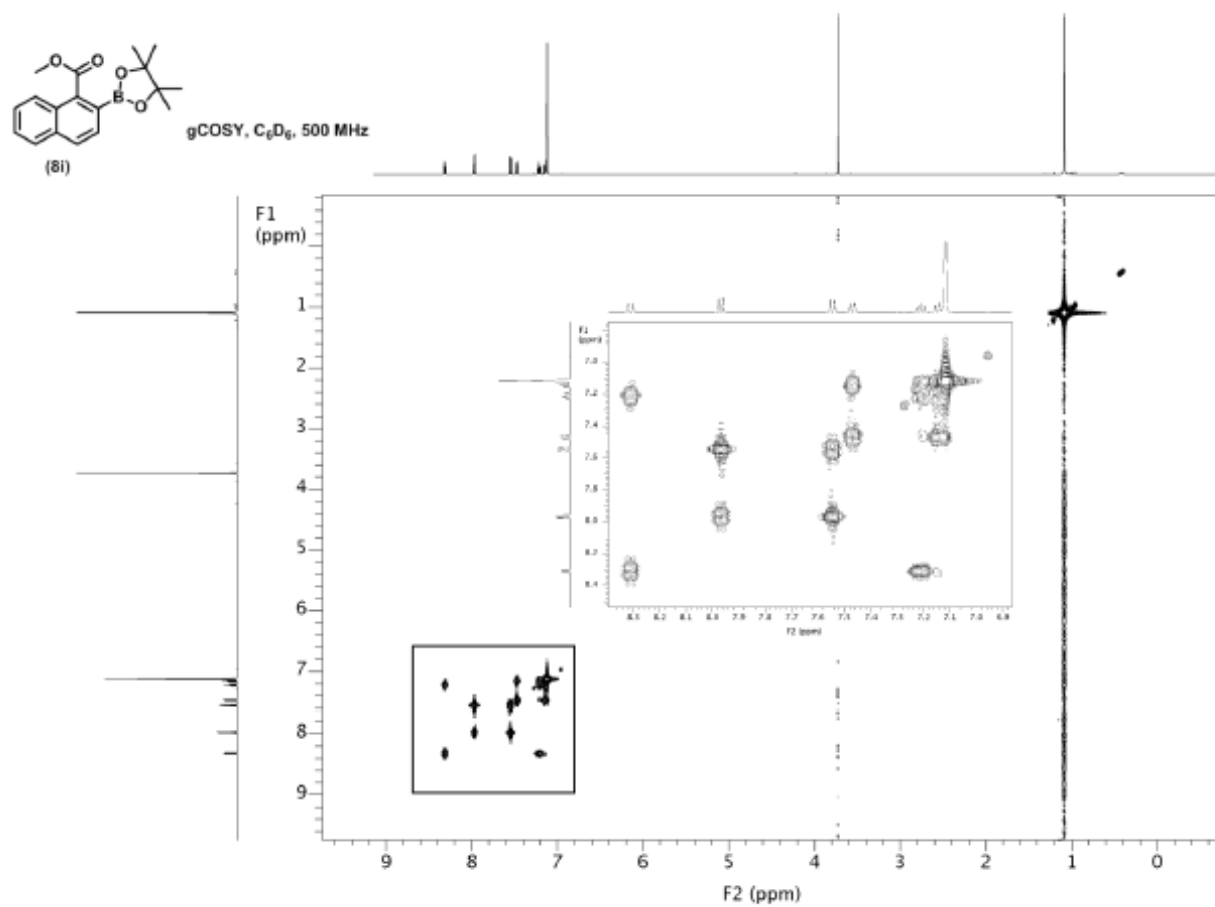


Figure A 50. Expansion of gCOSY NMR of compound 18i

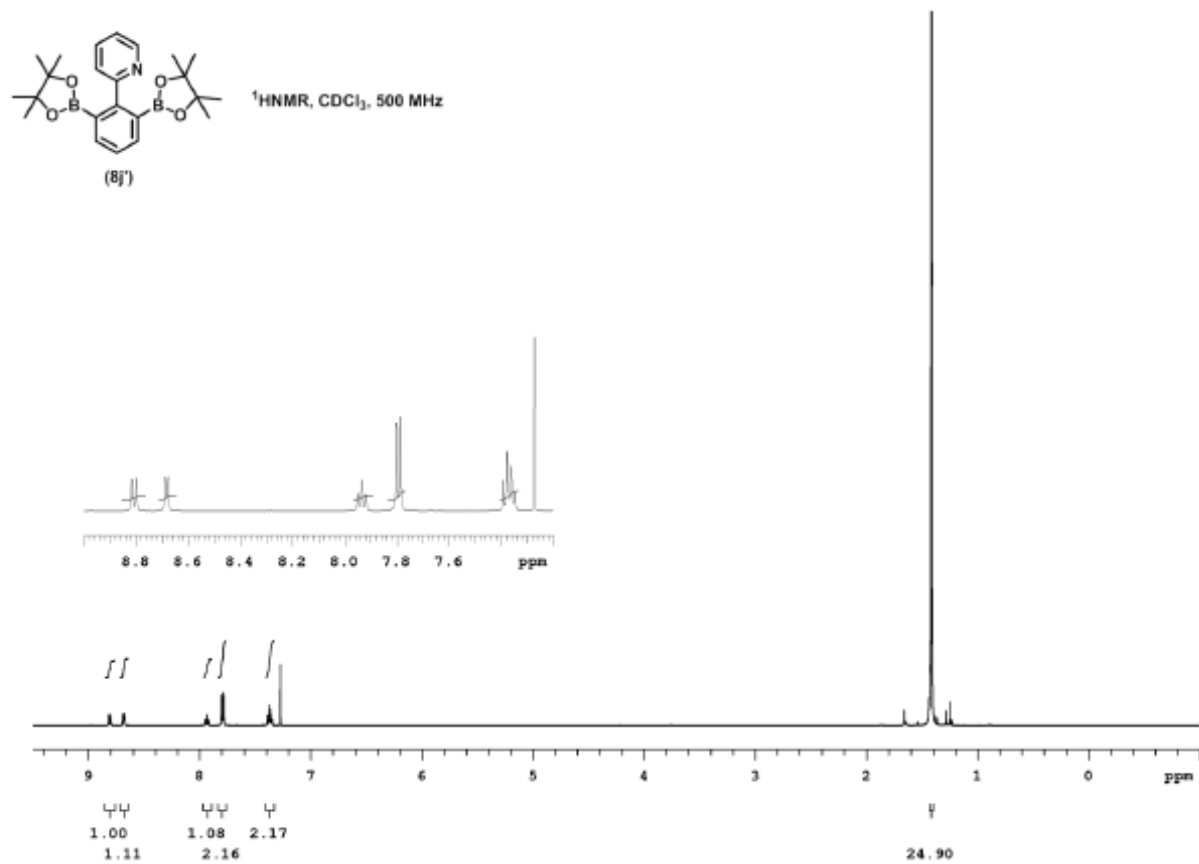


Figure A 51. ¹H NMR of compound **18j'**

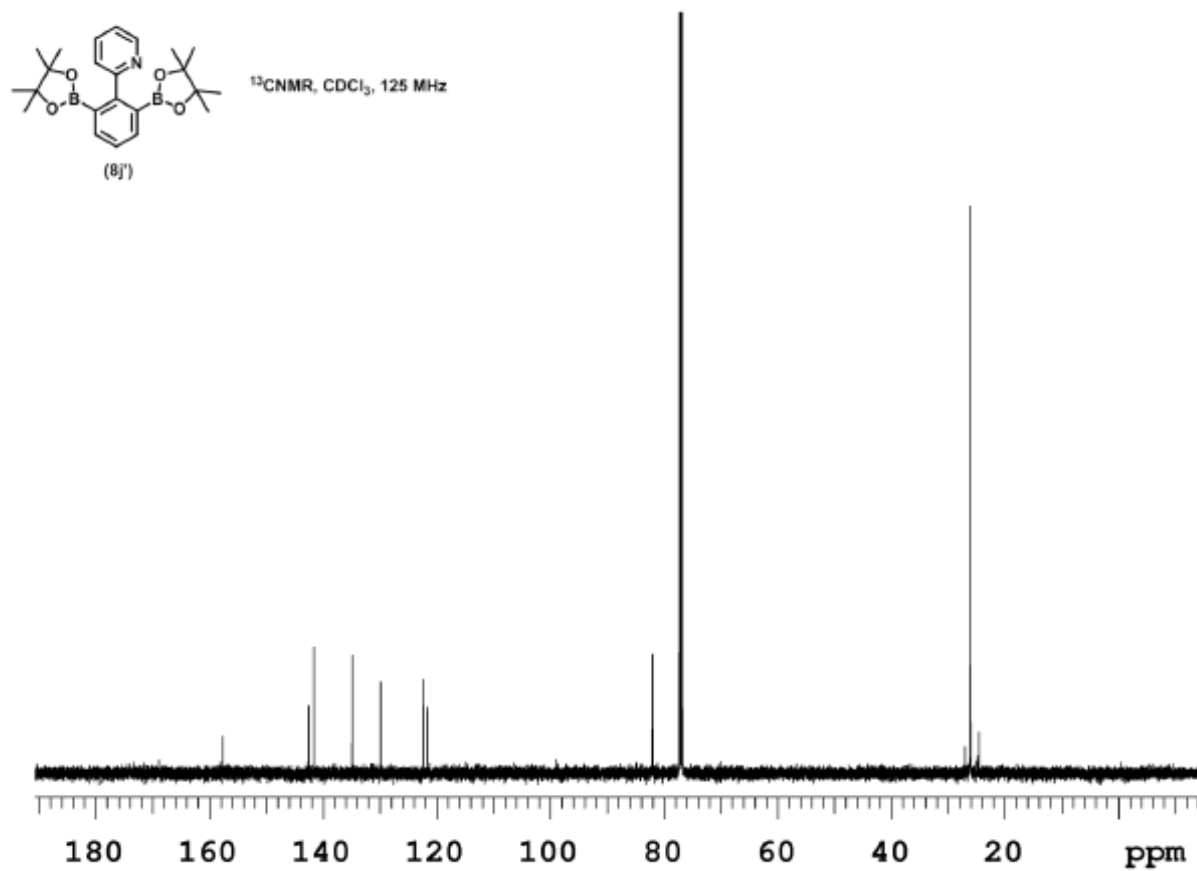


Figure A 52. ^{13}C NMR of compound **18j'**

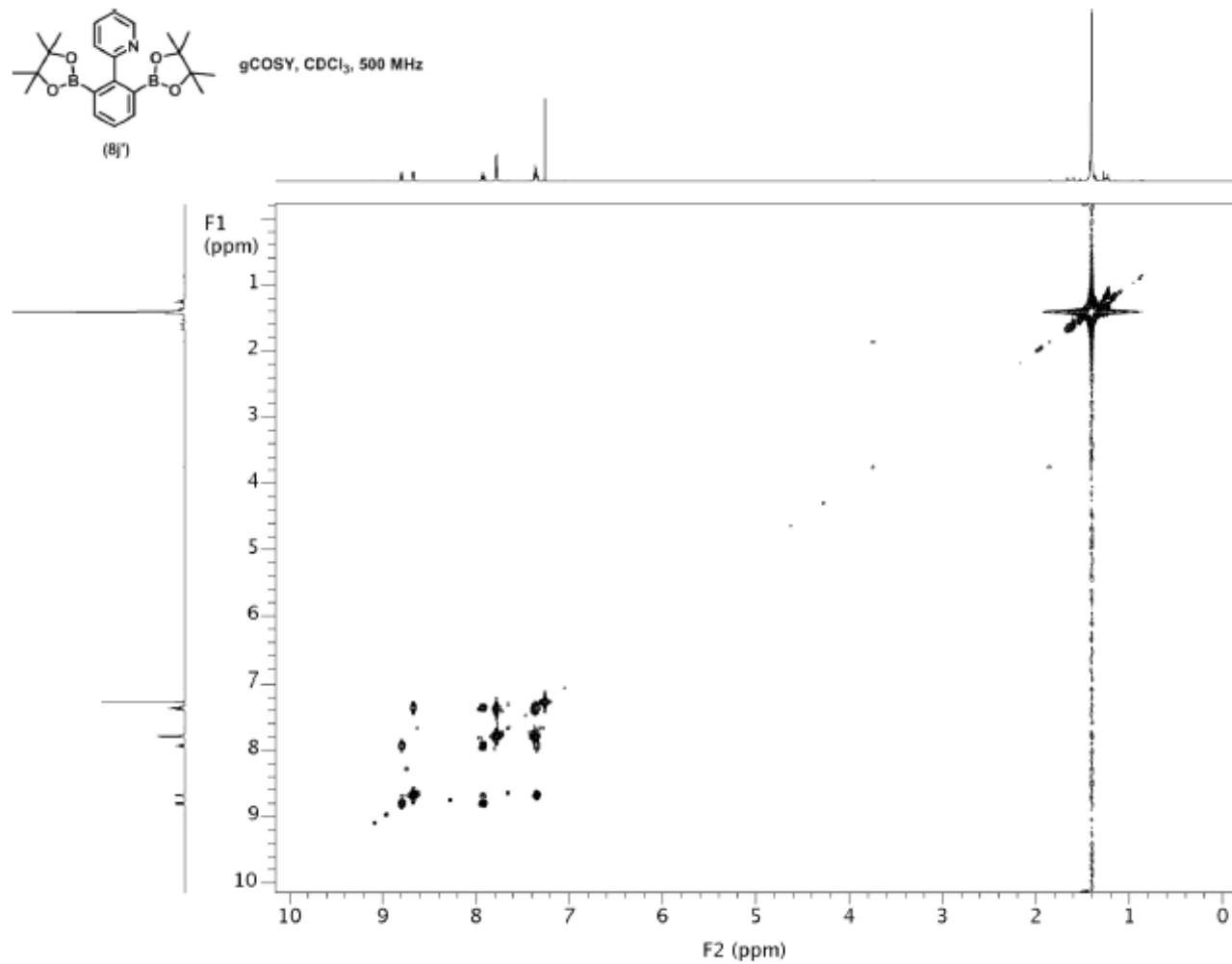


Figure A 53. gCOSY NMR of compound **18j'**

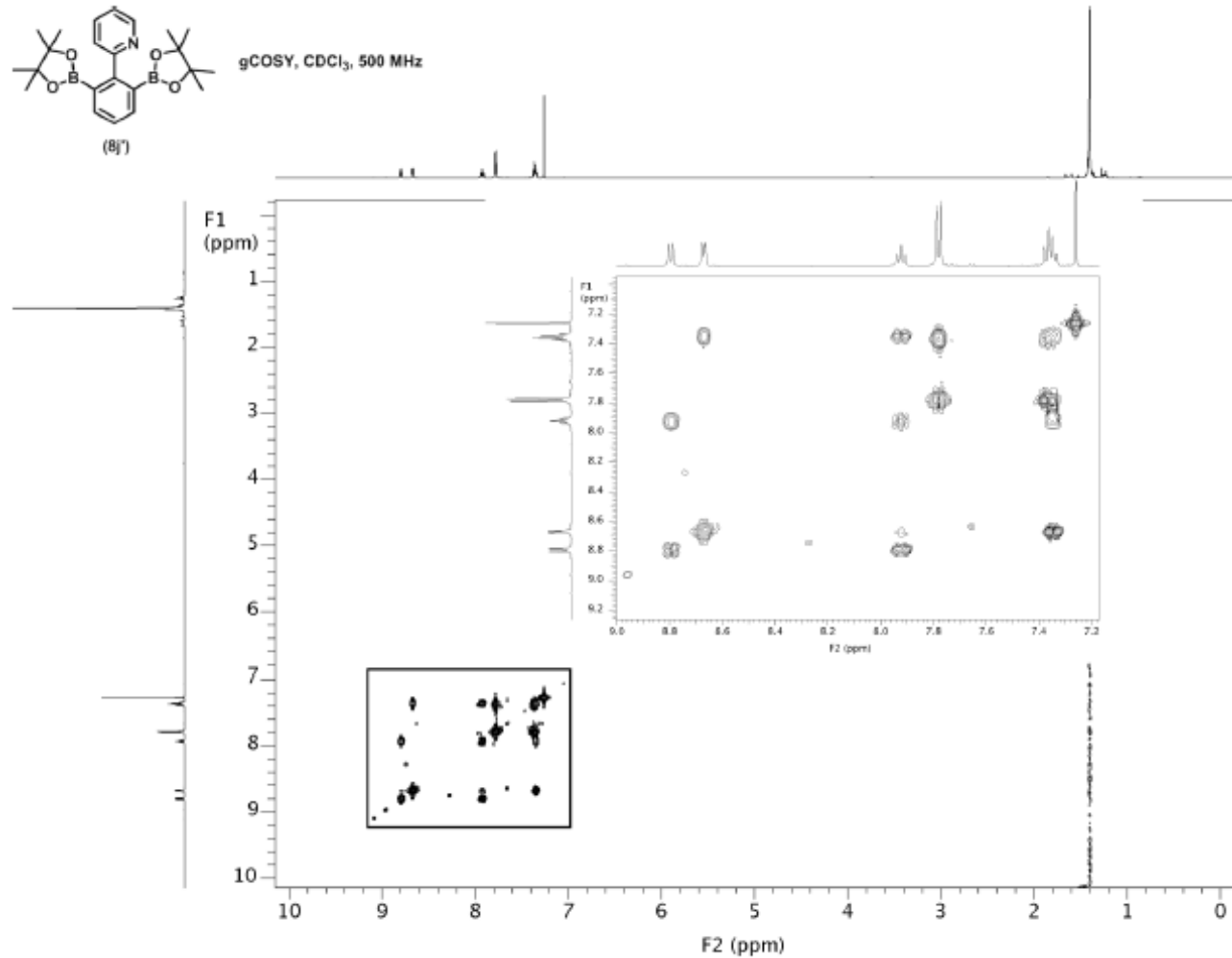


Figure A 54. Expansion of gCOSY NMR of compound **18j'**

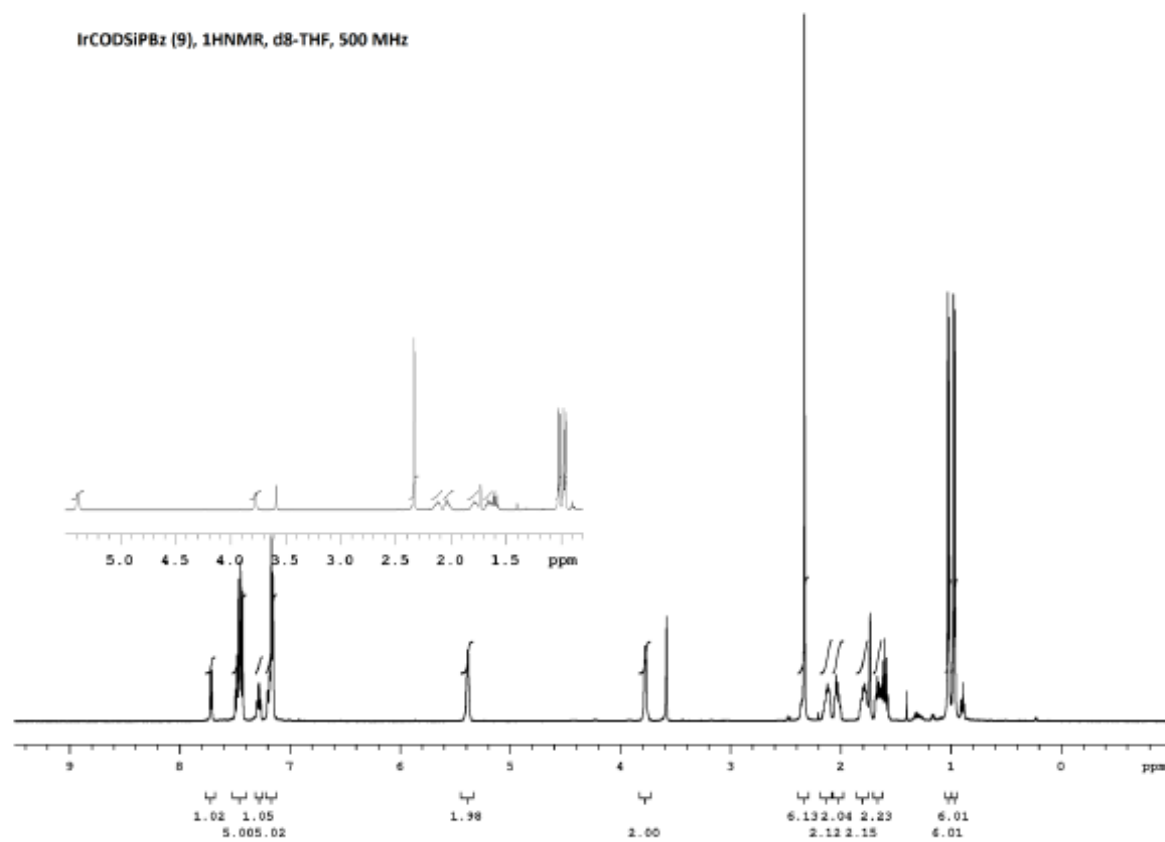


Figure A 55. ^1H NMR of compound **19**

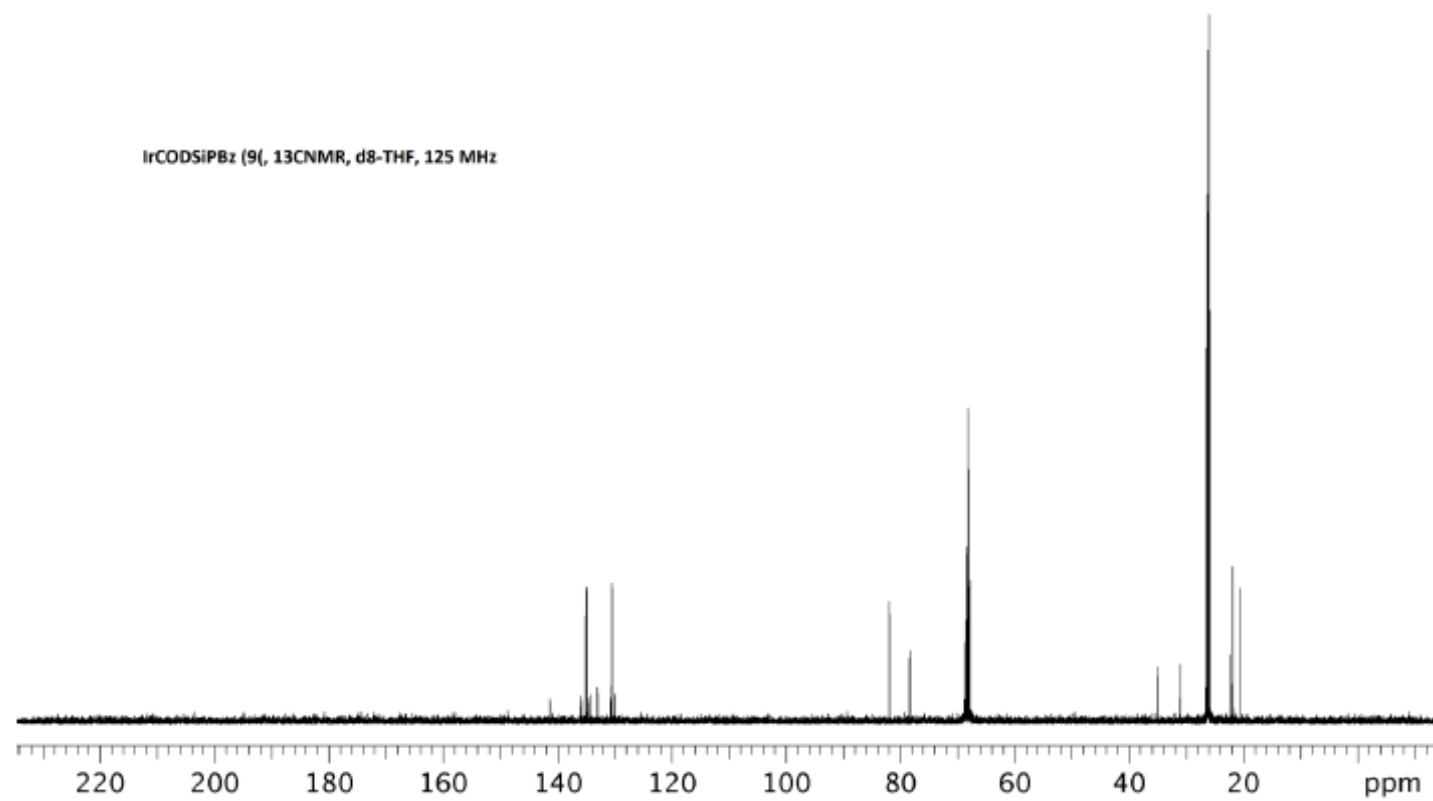


Figure A 56. ^{13}C NMR of compound **19**

IrCODSiPBz (9), ^{31}P NMR, d8-THF, 202 MHz

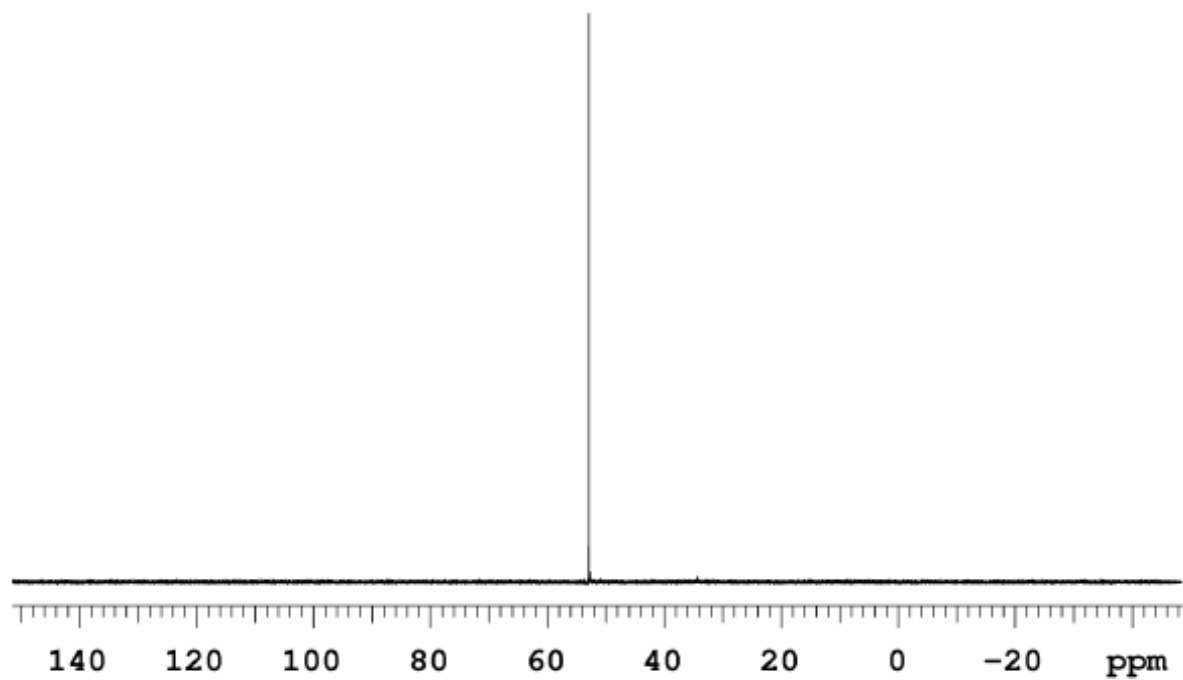


Figure A 57. ^{31}P NMR of compound **19**

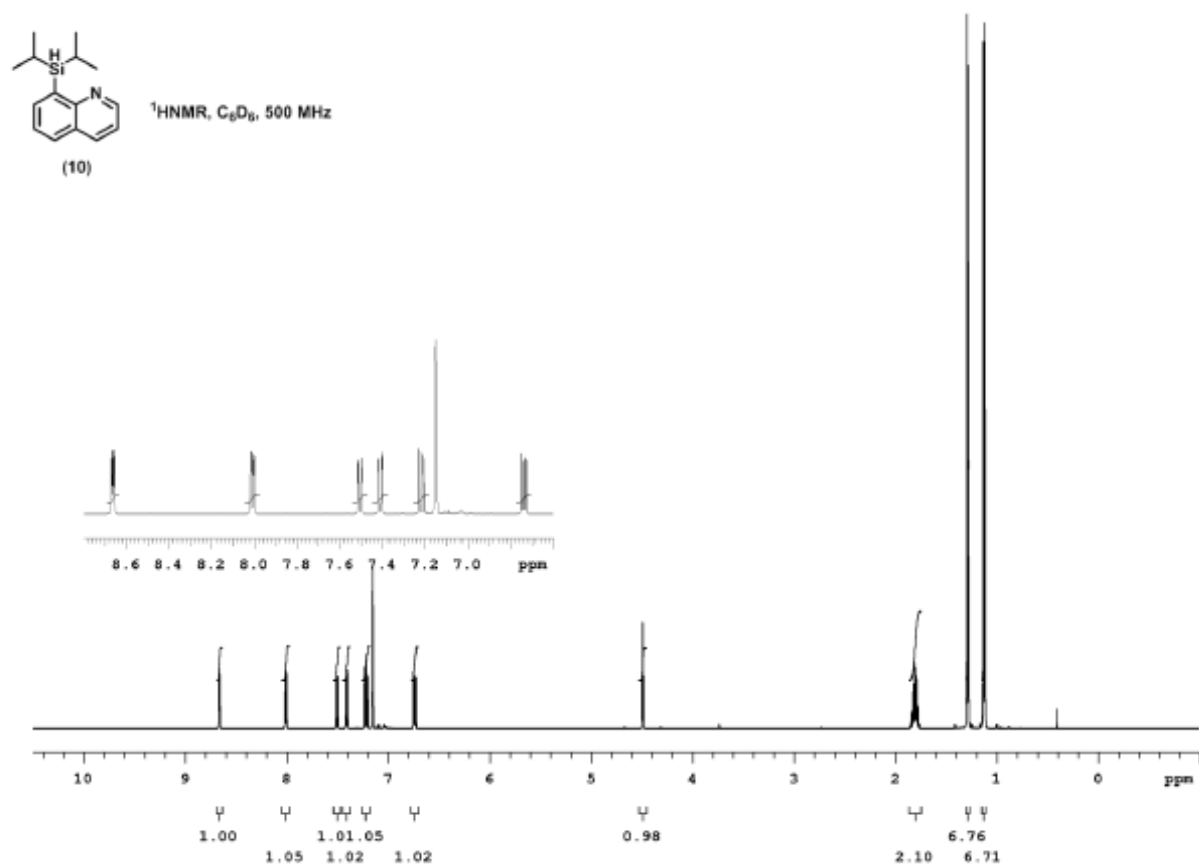


Figure A 58. ^1H NMR of compound **20**



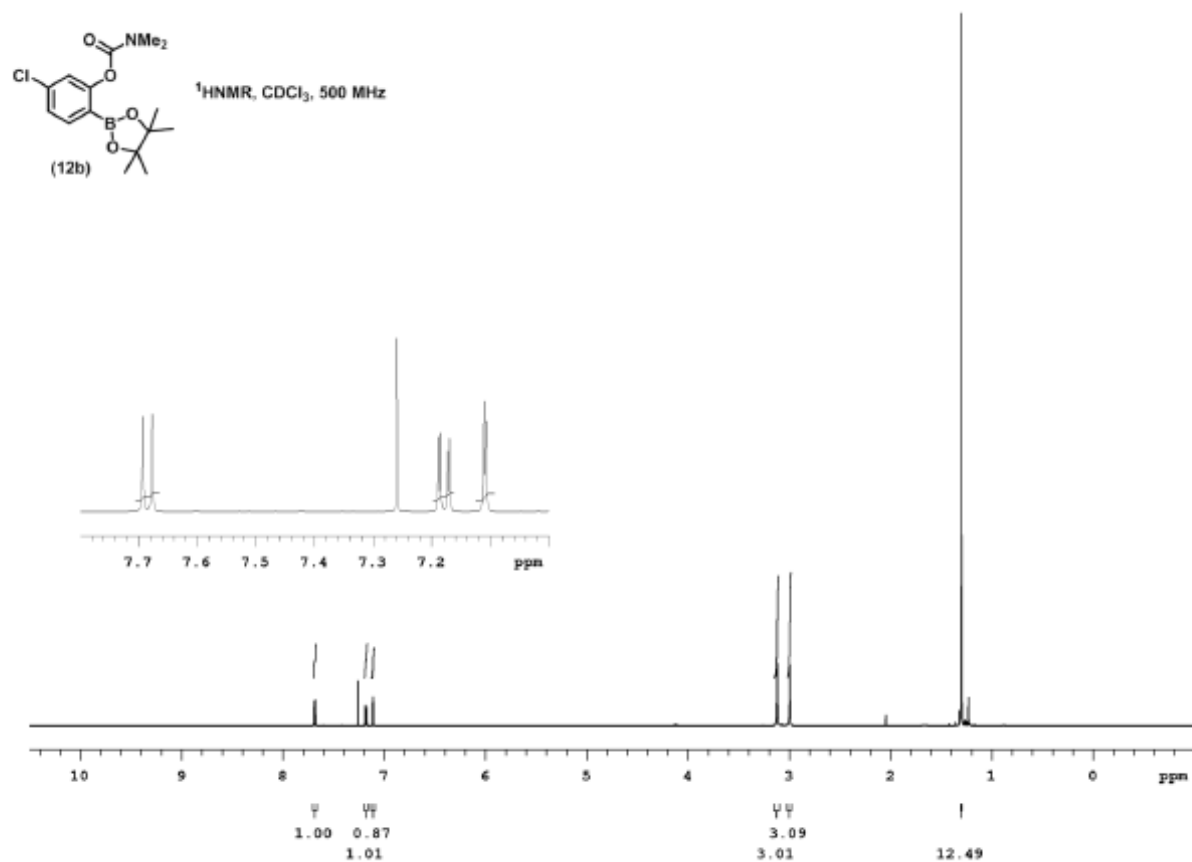


Figure A 60. $^1\text{H NMR}$ of compound 22a

APPENDIX B, Crystal Data and Structure

Crystal data and structure refinement for **6**•(CF₃)₂C₆H₄.

Identification code	(dippe)IrH(BPin) ₂ (=BPinBPin)
Empirical formula	C ₄₆ H ₈₅ B ₄ F ₆ Ir O ₈ P ₂
Formula weight	1177.52
Temperature	173(2) K
Wavelength	0.71073 Å
Crystal system	Monoclinic
Space group	P2(1)/n
Unit cell dimensions	a = 12.6467(15) Å α = 90°. b = 11.3423(13) Å β = 93.481(2)°. c = 39.579(5) Å γ = 90°.
Volume	5666.9(11) Å ³
Z	4
Density (calculated)	1.380 Mg/m ³
Absorption coefficient	2.477 mm ⁻¹
F(000)	2424
Crystal size	0.035 x 0.013 x 0.003 mm ³
Theta range for data collection	1.66 to 29.20°.
Index ranges	-16 ≤ h ≤ 17, -15 ≤ k ≤ 15, -52 ≤ l ≤ 51
Reflections collected	67440
Independent reflections	14253 [R(int) = 0.1050]
Completeness to theta = 25.00°	100.0 %
Absorption correction	Semi-empirical from equivalents
Max. and min. transmission	1.00 and 0.8286
Refinement method	Full-matrix least-squares on F ²
Data / restraints / parameters	14253 / 354 / 697
Goodness-of-fit on F ²	1.074
Final R indices [I > 2σ(I)]	R1 = 0.0587, wR2 = 0.1184
R indices (all data)	R1 = 0.1192, wR2 = 0.1411
Largest diff. peak and hole	1.457 and -1.949 e.Å ⁻³

Crystal data and structure refinement for **8**.

Identification code	(dippe)Ir(H) ₃ (BPin) ₂	
Empirical formula	C ₂₆ H ₅₉ B ₂ Ir O ₄ P ₂	
Formula weight	711.49	
Temperature	173(2) K	
Wavelength	0.71073 Å	
Crystal system	Triclinic	
Space group	P-1	
Unit cell dimensions	a = 11.6009(5) Å	α = 100.827(3)°.
	b = 14.7110(7) Å	β = 92.604(3)°.
	c = 20.1115(11) Å	γ = 96.944(3)°.
Volume	3338.2(3) Å ³	
Z	4	
Density (calculated)	1.416 Mg/m ³	
Absorption coefficient	4.122 mm ⁻¹	
F(000)	1456	
Crystal size	0.450 x 0.252 x 0.17 mm ³	
Theta range for data collection	1.59 to 27.13°.	
Index ranges	-14 ≤ h ≤ 14, -18 ≤ k ≤ 18, -25 ≤ l ≤ 25	
Reflections collected	53994	
Independent reflections	14567 [R(int) = 0.0238]	
Completeness to theta = 25.00°	99.6 %	
Absorption correction	Semi-empirical from equivalents	
Max. and min. transmission	0.7455 and 0.5592	
Refinement method	Full-matrix least-squares on F ²	
Data / restraints / parameters	14567 / 0 / 1103	
Goodness-of-fit on F ²	1.081	
Final R indices [I > 2σ(I)]	R1 = 0.0187, wR2 = 0.0422	
R indices (all data)	R1 = 0.0242, wR2 = 0.0440	
Largest diff. peak and hole	0.941 and -0.454 e.Å ⁻³	

Crystal data and structure refinement for **9**.

Identification code	(dippe)Ir(H) ₄ (BPin)	
Empirical formula	C ₂₀ H ₄₈ B Ir O ₂ P ₂	
Formula weight	585.53	
Temperature	173(2) K	
Wavelength	0.71073 Å	
Crystal system	Monoclinic	
Space group	P2(1)/n	
Unit cell dimensions	a = 14.309(2) Å	$\alpha = 90^\circ$.
	b = 10.9786(16) Å	$\beta = 93.976(2)^\circ$.
	c = 16.258(2) Å	$\gamma = 90^\circ$.
Volume	2547.8(6) Å ³	
Z	4	
Density (calculated)	1.526 Mg/m ³	
Absorption coefficient	5.377 mm ⁻¹	
F(000)	1184	
Crystal size	0.23 x 0.16 x 0.06 mm ³	
Theta range for data collection	1.83 to 28.11°.	
Index ranges	-18 ≤ h ≤ 17, -13 ≤ k ≤ 13, -20 ≤ l ≤ 20	
Reflections collected	19742	
Independent reflections	5676 [R(int) = 0.0256]	
Completeness to theta = 25.00°	99.8 %	
Absorption correction	Semi-empirical from equivalents	
Max. and min. transmission	0.7385 and 0.3710	
Refinement method	Full-matrix least-squares on F ²	
Data / restraints / parameters	5676 / 0 / 427	
Goodness-of-fit on F ²	0.989	
Final R indices [I > 2sigma(I)]	R1 = 0.0191, wR2 = 0.0400	
R indices (all data)	R1 = 0.0304, wR2 = 0.0436	
Largest diff. peak and hole	0.647 and -0.875 e.Å ⁻³	

Crystal data and structure refinement for **10**.

Empirical formula	C ₂₈ H ₇₀ Ir ₂ P ₄
Formula weight	915.12
Temperature/K	173.15
Crystal system	monoclinic
Space group	P2 ₁ /c
a/Å	10.2844(8)
b/Å	14.0396(10)
c/Å	12.9636(10)
α /°	90
β /°	108.7800(10)
γ /°	90
Volume/Å ³	1772.1(2)
Z	2
$\rho_{\text{calc}}/\text{cm}^3$	1.715
μ/mm^{-1}	7.698
F(000)	904.0
Crystal size/mm ³	0.138 × 0.084 × 0.043
Radiation	MoK α (λ = 0.71073)
2 θ range for data collection/°	4.184 to 50.728
Index ranges	-12 ≤ h ≤ 12, -16 ≤ k ≤ 16, -15 ≤ l ≤ 15
Reflections collected	14563
Independent reflections	3249 [R_{int} = 0.0386, R_{sigma} = 0.0327]
Data/restraints/parameters	3249/0/162
Goodness-of-fit on F ²	1.054
Final R indexes [$I \geq 2\sigma(I)$]	R_1 = 0.0315, wR_2 = 0.0762
Final R indexes [all data]	R_1 = 0.0414, wR_2 = 0.0815

Crystal data and structure refinement for **19**.

Empirical formula	C ₃₄ H ₄₄ IrPSi
Formula weight	703.95
Temperature/K	173.15
Crystal system	triclinic
Space group	P-1
a/Å	9.9128(11)
b/Å	10.2416(11)
c/Å	16.4821(18)
α /°	77.3150(10)
β /°	86.7650(10)
γ /°	69.1190(10)
Volume/Å ³	1524.8(3)
Z	2
ρ_{calc} /mg/mm ³	1.533
m/mm ⁻¹	4.491
F(000)	708.0
Crystal size/mm ³	0.10 × 0.092 × 0.073
Radiation	MoK α (λ = 0.71073)
2 Θ range for data collection	4.358 to 50.38°
Index ranges	-11 ≤ h ≤ 11, -12 ≤ k ≤ 12, -19 ≤ l ≤ 19
Reflections collected	28194
Independent reflections	5481[R(int) = 0.0621]
Data/restraints/parameters	5481/48/340
Goodness-of-fit on F ²	1.060
Final R indexes [I ≥ 2 σ (I)]	R ₁ = 0.0395, wR ₂ = 0.0819
Final R indexes [all data]	R ₁ = 0.0519, wR ₂ = 0.0884
Largest diff. peak/hole / e Å ⁻³	1.19/-0.95

APPENDIX C, Computational Results

Calculated coordinates for (dmpe)Ir(H)(Bpin)₂(=BOCMe₂CMe₂OBpin)

C	4.352864	-3.165203	-0.985134
P	3.196543	-1.995913	-1.791029
C	4.254386	-1.312454	-3.165059
C	3.654219	-0.036103	-3.747299
P	3.196312	1.135964	-2.375665
C	2.163172	2.381393	-3.239384
Ir	2.318999	-0.139202	-0.579493
B	1.831203	-1.330285	1.076850
O	1.946502	-2.727298	1.065414
C	1.367637	-3.244240	2.273267
C	1.478388	-2.023954	3.230726
O	1.379223	-0.917647	2.323204
B	2.055971	1.585770	0.574596
O	2.983764	2.629915	0.657391
C	2.392139	3.715349	1.391178
C	1.311215	2.984383	2.234132
O	0.954273	1.900924	1.366987
B	0.385117	-0.224263	-0.788612
O	-0.910164	-0.370799	-0.771478
C	-1.983816	0.343262	-0.097642
C	-3.289824	-0.292651	-0.662742
O	-4.331940	0.409664	0.029926
B	-5.655175	0.225597	-0.155540
O	-6.571818	1.103211	0.374837
C	-7.871206	0.514785	0.180054
C	-7.629140	-0.429414	-1.039681
O	-6.245666	-0.801669	-0.864125
C	2.061174	-3.145718	-2.664344
C	4.745004	2.074613	-2.094395
H	3.801996	-3.710410	-0.210896
H	2.602703	-3.928416	-3.211508
H	2.721322	-0.259188	-4.287500
H	4.337776	0.448910	-4.459742
H	5.231722	-1.094464	-2.707720
H	4.420962	-2.078324	-3.936599
H	4.558964	2.788031	-1.282507
H	2.673743	2.806999	-4.113248
H	3.829405	-0.080463	0.197922
C	2.839511	-1.917191	3.909711
C	0.373949	-1.912721	4.263433
C	2.143405	-4.473705	2.703651
C	-0.072507	-3.624167	1.949303
H	1.929246	3.185627	-2.531136

H	1.221107	1.914421	-3.548302
H	5.078702	2.598740	-2.999285
H	5.523437	1.383175	-1.752974
H	1.409233	-3.607067	-1.913208
H	1.429885	-2.577667	-3.356982
H	4.786460	-3.867467	-1.709115
H	5.148068	-2.590988	-0.496791
C	0.069786	3.795300	2.549793
C	1.862667	2.362014	3.512522
C	1.802958	4.677752	0.366183
C	3.466904	4.413308	2.200148
C	-1.853137	1.819569	-0.437251
C	-1.835906	0.131722	1.400234
C	-3.434207	-0.053692	-2.161591
C	-3.366677	-1.784443	-0.359879
C	-7.723272	0.287801	-2.380473
C	-8.481077	-1.680406	-1.058160
C	-8.878578	1.619731	-0.062224
C	-8.220553	-0.237344	1.456968
H	3.028310	5.182252	2.850688
H	4.024429	3.704155	2.818926
H	4.178518	4.904560	1.525631
H	1.413188	5.592848	0.830239
H	2.594843	4.961805	-0.338904
H	0.993469	4.201718	-0.202727
H	2.061235	3.115036	4.286180
H	1.119018	1.648344	3.890065
H	2.782581	1.797556	3.315123
H	0.315862	4.666799	3.171378
H	-0.437559	4.145124	1.644888
H	-0.638289	3.169140	3.107632
H	1.780677	-4.852919	3.668740
H	2.013063	-5.268323	1.958455
H	3.214555	-4.264316	2.788526
H	-0.582699	-4.081952	2.806385
H	-0.645608	-2.747091	1.621907
H	-0.066776	-4.345934	1.123450
H	0.369138	-2.783867	4.932857
H	0.535758	-1.016209	4.874038
H	-0.610742	-1.823622	3.793159
H	2.979043	-2.683209	4.683212
H	3.653809	-1.994832	3.178269
H	2.912365	-0.930606	4.382945
H	-2.667688	0.615758	1.923174
H	-1.831275	-0.932811	1.656624
H	-0.888674	0.563383	1.744491

H	-2.730454	2.364658	-0.072834
H	-0.955774	2.215824	0.051812
H	-1.756630	1.976899	-1.517681
H	-2.559539	-0.436738	-2.697917
H	-4.325154	-0.570910	-2.534776
H	-3.542682	1.013995	-2.382066
H	-2.468711	-2.293738	-0.725991
H	-3.457221	-1.967104	0.716355
H	-4.242789	-2.219439	-0.850228
H	-8.758442	0.548049	-2.631923
H	-7.121222	1.205091	-2.390551
H	-7.337645	-0.378638	-3.160870
H	-9.547167	-1.421088	-1.092487
H	-8.247561	-2.272171	-1.950562
H	-8.299547	-2.307484	-0.180619
H	-9.864833	1.202026	-0.303756
H	-8.980120	2.225551	0.845200
H	-8.567174	2.283162	-0.874222
H	-9.237878	-0.645205	1.424152
H	-7.519429	-1.059062	1.645070
H	-8.156900	0.459918	2.299517

Calculated coordinates for 8a.

Ir	0.565159	-0.145103	-0.454983
O	-1.571512	2.031756	-0.090300
O	-2.183568	0.624488	-1.769791
O	-2.039556	-1.181019	1.015243
O	-1.407608	-2.560905	-0.694554
C	-4.396513	1.401529	-2.316737
C	1.525265	3.763342	2.636735
C	-2.355037	2.634400	-3.023944
C	0.370610	-0.644004	3.503849
C	-1.062700	1.367036	3.192634
C	2.870835	-3.342846	-1.126668
C	-3.876080	1.923596	0.495772
C	3.065515	-2.726619	1.295756
C	-2.902921	3.979682	-0.505646
C	5.265008	-0.668282	-2.185771
C	3.590727	1.137857	-2.648741
C	-2.303067	-3.223910	2.203619
C	1.095985	3.030177	1.371435
C	3.453544	-2.349932	-0.127887
C	-4.285341	-1.919322	1.467144
C	-3.697279	-2.388086	-1.342190
C	0.368175	0.839501	3.156649
C	-2.991625	1.803797	-1.916236
C	-2.802672	-4.483382	-0.353434
C	2.951032	0.804122	1.876212
C	3.806418	0.458803	0.656972
C	3.784895	-0.301155	-2.186155
C	-2.871513	2.463652	-0.512841
C	-2.878837	-2.344989	1.099258
C	-2.729025	-2.968495	-0.320730
P	2.906719	-0.622436	-0.566925
P	1.147794	1.161647	1.488230
C	1.890831	3.527815	0.170674
B	-1.074797	-1.427462	0.034008
B	-1.242909	0.869097	-0.781073
H	4.073503	1.377188	0.114840
H	3.395177	1.643005	2.432569
H	0.986236	1.377949	3.895911
H	0.033714	3.232584	1.176379
H	-0.265979	-1.197468	2.801791
H	2.572385	3.551441	2.899588
H	4.553932	-2.356236	-0.196499
H	1.975612	-2.677476	1.435828

H	3.167632	-4.367799	-0.863373
H	5.442249	-1.736657	-2.010895
H	3.247545	-0.953205	-2.894563
H	4.115595	1.849315	-1.993187
H	-2.276254	-2.646045	3.137269
H	-4.276475	-1.424158	2.447621
H	-2.011088	-4.946119	0.246189
H	-4.733178	-2.695102	-1.142136
H	-3.413570	-2.754039	-2.336742
H	-3.635006	-1.293438	-1.371775
H	-4.952721	-2.790885	1.530552
H	-2.908861	-4.124111	2.372514
H	-1.275537	-3.535856	1.967880
H	-3.776651	-4.835953	0.015888
H	2.935338	-0.048940	2.568541
H	4.752492	-0.012828	0.965159
H	1.372341	-1.095073	3.491310
H	3.383766	-3.756536	1.509670
H	3.536400	-2.076092	2.045966
H	1.772310	-3.294270	-1.124074
H	5.712995	-0.420294	-3.158248
H	5.820903	-0.102867	-1.423166
H	-4.904239	2.226217	0.256195
H	-3.822823	0.828507	0.553265
H	-3.624923	2.317215	1.489368
H	-2.086658	4.407808	-1.098610
H	-2.792300	4.340943	0.526243
H	-2.284427	2.015718	-3.926976
H	-1.336990	2.944888	-2.751236
H	0.334082	-0.931029	-1.859324
H	-2.686729	-4.833302	-1.386840
H	-4.374200	0.914351	-3.300172
H	-5.050192	2.283131	-2.387551
H	-3.858576	4.359177	-0.895315
H	1.451893	4.849109	2.479879
H	4.007150	1.264005	-3.657629
H	2.530530	1.415490	-2.675551
H	-0.040172	-0.788834	4.513753
H	-1.127780	2.445524	2.996365
H	-1.505561	1.179710	4.181695
H	-1.672337	0.847891	2.440673
H	2.971916	3.364751	0.306355
H	1.745159	4.610033	0.044227
H	1.579524	3.030586	-0.756771
H	0.318708	-1.564036	0.508252
H	0.835413	1.126550	-1.457438

H	-4.840177	0.697290	-1.603114
H	-2.945286	3.529528	-3.263407
H	0.903794	3.516887	3.506493
H	3.209507	-3.154017	-2.154231
H	-4.704948	-1.217855	0.736886

Calculated coordinates for 8b.

Ir	0.212321	-0.287193	-0.404395
O	-2.741007	-0.622737	0.459185
O	1.393952	2.559571	0.288776
O	-2.574594	0.538849	-1.492145
O	-0.898512	2.608466	0.283811
C	-4.500781	-0.701465	-2.137555
C	-4.014208	1.243076	1.199409
C	-5.115737	-0.928987	0.680025
C	-4.657750	1.718573	-1.569002
C	-0.727824	-3.870561	2.941807
C	5.155951	0.070074	0.821110
C	3.698610	0.938498	-2.354527
C	1.967245	4.784318	0.981408
C	0.391711	-4.118467	-1.545512
C	1.072811	4.317388	-1.295448
C	-0.526371	-1.382921	3.198233
C	2.949304	-1.349542	-3.018322
C	-0.512410	3.901764	2.246237
C	3.126546	0.249394	2.282386
C	-1.381354	4.953669	0.161150
C	-1.943132	-3.658523	-0.785883
C	-4.009946	0.027724	0.279782
C	1.823587	-2.911757	1.147587
C	-3.977555	0.405088	-1.232008
C	-0.867269	-2.521317	2.244929
C	3.663743	0.372849	0.860904
C	3.600670	-0.520833	-1.917951
C	2.911460	-2.390254	0.208664
C	-0.453458	3.895708	0.722337
C	1.003263	3.935169	0.178080
C	-0.498693	-3.841077	-0.340264
P	2.623645	-0.624424	-0.334647
P	0.101021	-2.381598	0.653514
B	0.226883	1.793213	0.183053
B	-1.866132	-0.127093	-0.510525
H	-5.053542	-1.877036	0.134010
H	-4.167823	2.558446	-1.062570
H	-2.016444	-2.828995	-1.502861
H	-2.623319	-3.444089	0.048634
H	-2.297258	-4.569377	-1.289004
H	0.417396	-3.250037	-2.218672
H	-0.006206	-4.971748	-2.112288
H	-0.436256	-4.705409	0.341274

H	3.484689	1.408030	0.538218
H	3.646262	0.957285	2.943285
H	2.051439	0.467565	2.334975
H	3.297715	-0.757781	2.692898
H	5.685928	0.690947	1.557543
H	5.366738	-0.978220	1.080140
H	4.609262	-0.920388	-1.715948
H	2.863353	-2.413489	-2.757979
H	4.206761	1.013153	-3.325993
H	-1.908478	-2.371660	1.920752
H	0.528431	-1.408995	3.513624
H	-1.137916	-1.463755	4.107571
H	-0.259332	4.885450	2.664192
H	-1.532067	3.644381	2.561192
H	-1.496133	4.854294	-0.923528
H	-1.009837	5.963105	0.388686
H	-2.376260	4.849424	0.615426
H	0.367122	3.726579	-1.894122
H	2.086132	4.109513	-1.663627
H	2.962851	4.748891	0.519543
H	1.869207	-4.008519	1.232746
H	1.981873	-2.511775	2.160150
H	2.930064	-2.988569	-0.713124
H	3.904677	-2.499105	0.669758
H	0.065251	-1.117551	-1.799217
H	0.204669	0.696461	1.065093
H	-1.335386	-3.881513	3.857374
H	0.311164	-4.067204	3.243524
H	-1.065931	-4.710714	2.322515
H	-4.240727	-0.458899	-3.175276
H	-5.592388	-0.807743	-2.069800
H	-3.842143	0.900076	2.228664
H	2.061127	4.424762	2.012372
H	1.641962	5.834114	1.001799
H	0.860796	5.383455	-1.452903
H	0.171691	3.153877	2.670780
H	2.693476	1.372605	-2.467088
H	4.251180	1.561677	-1.639410
H	3.544356	-1.284795	-3.940170
H	1.938649	-0.976461	-3.234358
H	5.607235	0.270164	-0.159205
H	1.423427	-4.366820	-1.261677
H	-0.723069	-0.405333	2.742035
H	0.233230	1.059468	-1.388974
H	-5.719898	1.700192	-1.285074
H	-4.599792	1.897013	-2.650001

H	-4.971487	1.780964	1.169958
H	-6.105740	-0.486836	0.497011
H	-5.039131	-1.150065	1.753018
H	-4.041421	-1.666917	-1.890341
H	-3.201768	1.932763	0.934729

Calculated coordinates for 9.

O	-2.655405	0.232489	0.289665
Ir	0.279392	-0.468332	-0.625993
P	0.449381	1.811428	0.069668
P	2.403551	-0.719103	0.305378
C	2.055539	2.007383	1.015317
C	3.116952	0.975507	0.630234
O	-2.544107	-1.963870	-0.362686
C	-3.924849	-1.585076	-0.404234
C	-0.794953	2.595073	1.233207
C	-3.946911	-0.341475	0.529264
B	-1.809364	-0.811533	-0.109818
C	3.724136	-1.534678	-0.723375
C	1.789384	2.833079	-2.189160
C	-4.268096	-1.240773	-1.848422
C	0.594630	3.090466	-1.281451
C	2.527705	-1.614587	1.942855
C	3.869595	-0.895093	-2.099104
C	-0.960135	1.766389	2.501336
C	1.711087	-0.898889	3.011635
C	-4.770628	-2.751711	0.064432
C	3.946336	-1.859432	2.444121
C	-0.699617	3.131519	-2.086299
C	3.423944	-3.022647	-0.875832
C	-5.010463	0.688939	0.207684
C	-4.012700	-0.711141	2.006627
C	-0.512935	4.052725	1.579173
H	-1.095410	-0.287557	-1.552137
H	0.313670	-1.981150	-1.239560
H	3.909541	0.923385	1.392049
H	1.823236	3.587478	-2.988092
H	0.747586	4.061639	-0.783012
H	2.441503	-3.165300	-1.347863
H	4.085558	0.180769	-2.055586
H	3.913418	-2.365857	3.419139
H	1.720567	1.843448	-2.660038
H	-0.056187	1.783423	3.129109
H	-4.935381	1.527477	0.913152
H	2.041632	-2.582668	1.736406
H	2.447379	3.028883	0.896561
H	-1.744708	2.519803	0.681231
H	-4.437513	-3.128003	1.037821
H	-0.558930	4.717239	0.707783
H	0.685845	-0.695932	2.678295
H	2.745032	2.889433	-1.649507
H	-1.574348	3.372792	-1.466944

H	-3.814015	0.188216	2.604589
H	1.794489	1.890712	2.077445
H	-4.893219	1.089239	-0.805397
H	4.696799	-1.374421	-2.641138
H	4.490689	-0.915712	2.595182
H	-3.250683	-1.460967	2.259281
H	-4.015514	-2.098619	-2.483638
H	4.542400	-2.487368	1.771737
H	-6.017241	0.257543	0.302206
H	-1.778989	2.179501	3.108055
H	2.952089	-1.029078	-2.685970
H	-4.693861	-3.575011	-0.656953
H	-5.336711	-1.018227	-1.973319
H	-1.257882	4.416672	2.301304
H	2.179498	0.056499	3.294627
H	3.608099	1.272546	-0.307456
H	1.658055	-1.512141	3.921595
H	3.416319	-3.560258	0.080814
H	4.179919	-3.497277	-1.516574
H	4.670571	-1.399071	-0.172181
H	-5.828947	-2.462860	0.139064
H	-1.212235	0.724901	2.271035
H	-0.887139	2.158235	-2.561426
H	-0.633691	3.889444	-2.879589
H	0.474443	4.176955	2.048356
H	-3.686699	-0.378461	-2.200493
H	-4.998238	-1.103779	2.290642
H	1.075961	-0.103525	-1.989551
H	-0.719114	-1.081041	0.719926

Calculated coordinates for 10.

Ir	0.205474	-0.218043	1.385189
P	1.318376	-1.565169	2.831900
P	-1.704417	-1.558113	1.835549
C	0.221615	-2.976498	3.382460
H	0.435504	-3.820041	2.709546
H	0.507572	-3.303079	4.394241
C	-1.263844	-2.617483	3.320762
H	-1.541035	-2.025417	4.204757
H	-1.882869	-3.526714	3.351042
C	-3.271921	-0.725641	2.416390
H	-3.935565	-1.518267	2.802825
C	-3.946159	-0.014838	1.246385
H	-4.211595	-0.692274	0.423718
H	-3.274876	0.753980	0.836617
H	-4.867292	0.482180	1.583407
C	-3.003944	0.275766	3.532937
H	-2.557998	-0.184767	4.424635
H	-3.946081	0.748832	3.845803
H	-2.321423	1.064191	3.187419
C	-2.354327	-2.804857	0.597039
H	-2.590117	-2.184774	-0.282425
C	-3.601008	-3.568248	1.024530
H	-3.433242	-4.149073	1.944084
H	-3.885193	-4.287085	0.242315
H	-4.465341	-2.914338	1.195977
C	-1.243083	-3.761327	0.187275
H	-0.961611	-4.430736	1.015287
H	-0.351274	-3.215792	-0.146104
H	-1.577455	-4.400427	-0.642291
C	1.915771	-0.853580	4.449781
H	2.400483	-1.687685	4.984044
C	2.932707	0.254969	4.211963
H	3.820692	-0.095970	3.669475
H	3.273406	0.671785	5.170440
H	2.481197	1.066199	3.624467
C	0.767200	-0.347126	5.312370
H	0.041030	-1.135533	5.554470
H	0.230506	0.468755	4.809059
H	1.157088	0.041751	6.263917
C	2.854686	-2.415935	2.180793
H	3.508144	-1.570789	1.905409
C	3.575726	-3.293479	3.198971
H	2.917091	-4.084591	3.587302

H	3.964770	-2.726966	4.054013
H	4.430981	-3.794116	2.723065
C	2.563479	-3.205837	0.910191
H	1.986162	-4.117889	1.124814
H	3.506602	-3.527686	0.446160
H	2.003226	-2.612696	0.175269
H	1.538874	0.724070	1.242605
H	0.636170	-0.977456	-0.333584
Ir	-0.205474	0.218043	-1.385189
P	-1.318376	1.565169	-2.831900
P	1.704417	1.558113	-1.835549
C	-0.221615	2.976498	-3.382460
H	-0.435504	3.820041	-2.709546
H	-0.507572	3.303079	-4.394241
C	1.263844	2.617483	-3.320762
H	1.541035	2.025417	-4.204757
H	1.882869	3.526714	-3.351042
C	3.271921	0.725641	-2.416390
H	3.935565	1.518267	-2.802825
C	3.946159	0.014838	-1.246385
H	4.211595	0.692274	-0.423718
H	3.274876	-0.753980	-0.836617
H	4.867292	-0.482180	-1.583407
C	3.003944	-0.275766	-3.532937
H	2.557998	0.184767	-4.424635
H	3.946081	-0.748832	-3.845803
H	2.321423	-1.064191	-3.187419
C	2.354327	2.804857	-0.597039
H	2.590117	2.184774	0.282425
C	3.601008	3.568248	-1.024530
H	3.433242	4.149073	-1.944084
H	3.885193	4.287085	-0.242315
H	4.465341	2.914338	-1.195977
C	1.243083	3.761327	-0.187275
H	0.961611	4.430736	-1.015287
H	0.351274	3.215792	0.146104
H	1.577455	4.400427	0.642291
C	-1.915771	0.853580	-4.449781
H	-2.400483	1.687685	-4.984044
C	-2.932707	-0.254969	-4.211963
H	-3.820692	0.095970	-3.669475
H	-3.273406	-0.671785	-5.170440
H	-2.481197	-1.066199	-3.624467
C	-0.767200	0.347126	-5.312370
H	-0.041030	1.135533	-5.554470
H	-0.230506	-0.468755	-4.809059

H	-1.157088	-0.041751	-6.263917
C	-2.854686	2.415935	-2.180793
H	-3.508144	1.570789	-1.905409
C	-3.575726	3.293479	-3.198971
H	-2.917091	4.084591	-3.587302
H	-3.964770	2.726966	-4.054013
H	-4.430981	3.794116	-2.723065
C	-2.563479	3.205837	-0.910191
H	-1.986162	4.117889	-1.124814
H	-3.506602	3.527686	-0.446160
H	-2.003226	2.612696	-0.175269
H	-1.538874	-0.724070	-1.242605
H	-0.636170	0.977456	0.333584
H	-0.074481	0.682969	2.685061
H	0.074481	-0.682969	-2.685061

Calculated coordinates for [(dippe)IrH(μ -H)]₂.

Ir	0.443634	-0.506442	1.307177
P	1.437788	-1.757278	2.945249
P	-1.532150	-1.677717	1.809910
C	0.278576	-3.122816	3.488554
H	0.501373	-3.989544	2.847550
H	0.501994	-3.430152	4.522187
C	-1.190085	-2.727307	3.336481
H	-1.501262	-2.114970	4.195882
H	-1.836284	-3.617620	3.347405
C	-3.043744	-0.735145	2.394938
H	-3.671784	-1.446680	2.960617
C	-3.846485	-0.160955	1.232270
H	-4.261587	-0.935370	0.574045
H	-3.212453	0.483770	0.607305
H	-4.684579	0.439865	1.615083
C	-2.613173	0.391732	3.327347
H	-2.045102	0.032180	4.195807
H	-3.492919	0.932462	3.705887
H	-1.975271	1.109276	2.789314
C	-2.242146	-2.900462	0.586704
H	-2.533012	-2.257966	-0.260226
C	-3.451416	-3.687361	1.073291
H	-3.189664	-4.357363	1.905804
H	-3.838323	-4.324274	0.264443
H	-4.276637	-3.046540	1.408892
C	-1.143436	-3.836674	0.101796
H	-0.759573	-4.461283	0.924302
H	-0.302528	-3.274954	-0.324516
H	-1.530492	-4.519132	-0.668725
C	1.960396	-0.960971	4.550426
H	2.280492	-1.771441	5.227462
C	3.120179	0.001342	4.323045
H	4.037470	-0.509893	4.004119
H	3.350886	0.543532	5.251128
H	2.860776	0.739843	3.550783
C	0.783767	-0.227988	5.182873
H	-0.058601	-0.896669	5.408557
H	0.417499	0.564090	4.512409
H	1.091290	0.243172	6.127449
C	2.980114	-2.660987	2.405328
H	3.689771	-1.840678	2.206770
C	3.564591	-3.595719	3.457639
H	2.870636	-4.415010	3.695902
H	3.813476	-3.081790	4.395142
H	4.488759	-4.057891	3.082071

C	2.748221	-3.392083	1.088213
H	2.066647	-4.246714	1.212684
H	3.698397	-3.790631	0.704663
H	2.315442	-2.721890	0.333137
H	1.877346	0.297043	1.067853
H	0.387359	-0.824954	-0.399368
Ir	-0.443634	0.506442	-1.307177
P	-1.437788	1.757278	-2.945249
P	1.532150	1.677717	-1.809910
C	-0.278576	3.122816	-3.488554
H	-0.501373	3.989544	-2.847550
H	-0.501994	3.430152	-4.522187
C	1.190085	2.727307	-3.336481
H	1.501262	2.114970	-4.195882
H	1.836284	3.617620	-3.347405
C	3.043744	0.735145	-2.394938
H	3.671784	1.446680	-2.960617
C	3.846485	0.160955	-1.232270
H	4.261587	0.935370	-0.574045
H	3.212453	-0.483770	-0.607305
H	4.684579	-0.439865	-1.615083
C	2.613173	-0.391732	-3.327347
H	2.045102	-0.032180	-4.195807
H	3.492919	-0.932462	-3.705887
H	1.975271	-1.109276	-2.789314
C	2.242146	2.900462	-0.586704
H	2.533012	2.257966	0.260226
C	3.451416	3.687361	-1.073291
H	3.189664	4.357363	-1.905804
H	3.838323	4.324274	-0.264443
H	4.276637	3.046540	-1.408892
C	1.143436	3.836674	-0.101796
H	0.759573	4.461283	-0.924302
H	0.302528	3.274954	0.324516
H	1.530492	4.519132	0.668725
C	-1.960396	0.960971	-4.550426
H	-2.280492	1.771441	-5.227462
C	-3.120179	-0.001342	-4.323045
H	-4.037470	0.509893	-4.004119
H	-3.350886	-0.543532	-5.251128
H	-2.860776	-0.739843	-3.550783
C	-0.783767	0.227988	-5.182873
H	0.058601	0.896669	-5.408557
H	-0.417499	-0.564090	-4.512409
H	-1.091290	-0.243172	-6.127449
C	-2.980114	2.660987	-2.405328

H	-3.689771	1.840678	-2.206770
C	-3.564591	3.595719	-3.457639
H	-2.870636	4.415010	-3.695902
H	-3.813476	3.081790	-4.395142
H	-4.488759	4.057891	-3.082071
C	-2.748221	3.392083	-1.088213
H	-2.066647	4.246714	-1.212684
H	-3.698397	3.790631	-0.704663
H	-2.315442	2.721890	-0.333137
H	-1.877346	-0.297043	-1.067853
H	-0.387359	0.824954	0.399368